SPATIAL STABILITY OF DEVELOPING FLOW IN A TWO DIMENSIONAL CHANNEL AND IN A CIRCULAR PIPE

By

S. C. GUPTA

DEPARTMENT OF MECHANICAL ENGINEERING

INDIAN INSTITUTE OF TECHNOLOGY, KANPUR

FEBRUARY, 1980

SPATIAL STABILITY OF DEVELOPING FLOW IN A TWO DIMENSIONAL CHANNEL AND IN A CIRCULAR PIPE

A Thesis Submitted
in Partial Fulfilment of the Requirements
for the Degree of

DOCTOR OF PHILOSOPHY

By

S. C. GUPTA

to the

DEPARTMENT OF MECHANICAL ENGINEERING

INDIAN INSTITUTE OF TECHNOLOGY, KANPUR

FEBRUARY, 1980

DEDICATED

TO

MY PARENTS

ME-1980-D-GUP-SPA

CERTIFICATE

This is to certify that this thesis entitled, 'Spatial Stability of Developing Flow in a Two Dimensional Channel and in a Circular Pipe', by S.C. Gupta is a record of work carried out under my supervision and has not been submitted elsewhere for a degree.

February, 1980.

(V.K. Garg)
Assistant Professor
Department of Mechanical Engineering
Indian Institute of Technology
Kanpur.

ACKNOWLEDGEMENTS

I wish to express my deep sense of gratitude to Professor V.K. Garg for his valuable guidance and constructive criticism thrcughout the present investigation. I also extend my sincere thanks to Professor M.M. Oberai for his encouragement throughout my stay at IIT, Kanpur.

I feel highly grateful to Professor S.C. Goyal, Ex-Vice Chancellor, to Professor S. Divakaran, Ex-Dean, Faculty of Engineering and to Professor M.L. Mathur, Head, Department of Mechanical Engineering, University of Jodhpur, for encouraging me to join IIT, Kanpur.

My sincere thanks are also due to Professor B.L. Dhoopar, Head, Department of Mechanical Engineering and Professors V. Rajaraman and R. Sankar, successive Heads, Computer Center at IIT, Kanpur.

I must also thank Messers R.N. Srivastava for a careful typing, B.L. Arora and S.S. Kushwaha for preparing the figures and A. Goyal, A. Agrawal, G. Bagaria and other N.S.S. volunteers for proof checking. Help in various forms was also available to me from several other friends and I must thankfully acknowledge the same.

I am indebted to my wife S. Gupta who through much self-sacrifice provided a home environment conducive to concentrated study and also to our children Ashwani, Himanshu and Sudhanshu who, though young, understood the need to leave their dad alone during his study periods and hence contributed immeasurably.

Financial aid was provided by the Ministry of Education, Government of India and University of Jodhpur, I sincerely acknowledge the same.

S.C. GUPTA

TABLE OF CONTENTS

Page

Appendices

LIST OF TABLES

LIST OF FIGURES

NOMENCLATURE

a	Half width of channel or radius of pipe
A	Function of X_1 defined in eqn. (3.7)
A_1, A_2	Coefficients defined in eqns. (3.9)
b	Number of Gram-Schmidt orthonormalizations
b_{ij}	Elements of matrix $\underset{\sim}{B}^i$ defined in eqns. (5.4)
B_1 to B_7	Coefficients defined in eqns. (2.22)
$\underset{\sim}{B}^i$	Transformation matrix (eqn. (5.3))
c	Number of orthonormalizations for Davey's method (Section 5.1)
C	Variable defined in eqn. (4.9)
D	Determinant defined in eqn. (5.1)
E	Disturbance kinetic energy density defined in eqn. (4.8)
F	Variable defined in eqn. (3.15)
g_E	Growth rate of disturbance kinetic energy density
g_u	Growth rate of streamwise component of disturbance velocity
g_ψ	Growth rate of disturbance stream function
G	Disturbance property (complex)
H	Variable defined in eqns. (2.14)
i	$= \sqrt{-1}$
k_o	Complex eigenvalue for parallel flow stability
k_1	Complex function of X_1 defined in eqn. (3.6)
k_{oi}	Imaginary part of k_o (spatial growth rate)
k_{or}	Real part of k_o (wavenumber)

K	Constant used in eqn. (5.9)
L	Order of the integration method
m	Integer whose value is 0 for channel and 1 for pipe
M	Coefficient defined in eqns. (3.2); number of eigenvalues enclosed by a certain region in the k_o-plane
n	(Number of mesh points along Y direction) -(2 or 1)
N	Variable defined in eqn. (5.11); number of zeros of the determinant within a closed region
N_o	Constant used in eqn. (5.12)
p	Dimensionless disturbance pressure
$\bar{p}$	Complex eigenfunction for disturbance pressure
$\tilde{p}$	Disturbance pressure
$\hat{p}$	Resultant pressure in the flow
P	Number of poles of the determinant within a closed region
$\bar{P}$	Pressure in the mainflow
$\tilde{P}$	Dimensionless pressure in the mainflow
$\bar{P}_o$	Pressure in the mainflow at the inlet section
$\underset{\sim}{q}^1, \underset{\sim}{q}^2$	Column vectors of the matrix $\underset{\sim}{Q}$
$\underset{\sim}{Q}$	Solution matrix during integration (eqn. (5.5))
R	Reynolds number ($= u_a a/\nu$)
$\underset{\sim}{s}^1, \underset{\sim}{s}^2$	Column vectors of the matrix $\underset{\sim}{S}$
s_{jj}	Diagonal elements of the matrix $\underset{\sim}{S}$
$\underset{\sim}{S}$	Solution matrix
$\underset{\sim}{S}_1, \underset{\sim}{S}_2$	Submatrices of $\underset{\sim}{S}$; $\underset{\sim}{S}_1$ being a null matrix
t	Time

T	Dimensionless time
u	Dimensionless streamwise component of disturbance velocity
$\bar{u}$	Complex eigenfunction for streamwise component of disturbance velocity
$\tilde{u}$	Streamwise component of disturbance velocity
$\hat{u}$	Resultant velocity of flow in the x direction
u_a	Average velocity of the mainflow
U	Dimensionless mainflow velocity in the x direction
$\bar{U}$	Mainflow velocity in the x direction
v	Dimensionless y-component of disturbance velocity
$\bar{v}$	Complex eigenfunction for y-component of disturbance velocity
$\tilde{v}$	y-component of disturbance velocity
$\hat{v}$	Resultant velocity of flow in the y direction
V	Dimensionless mainflow velocity in the y direction
$\bar{V}$	Mainflow velocity in the y direction
$\tilde{V}$	= RV
$\underset{\sim}{w}$	Vector defined in eqns. (5.4)
WN	Wavenumber for nonparallel flow stability
x	Streamwise distance measured from the inlet section
X	Dimensionless streamwise distance (= x/a)
$\bar{X}$	Dimensionless streamwise coordinate (= X/R)
X^*	Stretched streamwise coordinate defined in eqn. (A.11)
X_1	Slow streamwise scale (eqn. (2.16))
y	Transverse or radial distance measured from the channel centre line or pipe axis respectively

Y	Dimensionless y coordinate (= y/a)
$\underset{\sim}{z}_1, \underset{\sim}{z}_2$	Column vectors of the matrix $\underset{\sim}{Z}$
$\underset{\sim}{Z}$	Orthogonalized solution matrix (eqn. (5.3))
α	$= k_o + \varepsilon k_1$
α_i	Imaginary part of α
β	Complex eigenfunction for the disturbance stream function
$\underset{\sim}{\gamma}$	Matrix relating the matrices $\underset{\sim}{S}$ and $\underset{\sim}{Q}$ (Section 5.2.2)
δ	Constant used in eqn. (5.15)
$\Delta\bar{X}$	Axial spacing used in Bodoia and Osterle's method
ΔY	Step size of integration (= 1/(n + 1))
ε	Parameter characterising nonparallelism of the flow
ε^*	Weighting function defined in eqn. (A.18)
η	Variable defined in eqns. (2.14)
θ	Variable defined in eqn. (2.18)
λ	Roots of characteristic eqns. (A.15) and (A.17)
Λ	Function of $\bar{X}$ defined in eqn. (A.10)
ν	Kinematic viscosity of the fluid
π	The constant 3.1415926535897932.....
$\prod_{i=1}^{b}$	Multiplication over i from 1 to b
ρ	Density of the fluid
ϕ_o, ϕ_1	Amplitude of zeroth and first order dimensionless disturbance stream function
ψ	Dimensionless disturbance stream function
ω	Dimensionless frequency of the disturbance

Subscript

c	Critical value

Superscripts

*	Eigenfunctions for the adjoint problem except for X^* and ε^*
'	Derivative with respect to Y

SYNOPSIS

The present study describes the linear spatial stability characteristics of the developing flow in a two dimensional parallel plate channel and in a rigid circular pipe while accounting for all non-parallel effects. It also compares the parallel-flow stability characteristics of the developing velocity profiles obtained from the linearization and finite difference methods. Both symmetric and antisymmetric disturbances are considered for the parallel flow stability characteristics of the developing flow in a channel while only symmetric disturbances are considered when determining the non-parallel effects on the stability characteristics since they are more unstable. For the developing flow in a pipe, only axisymmetric disturbances are considered.

The method of multiple scales has been used for studying the stability characteristics of the non-parallel developing flow in these ducts. This method leads to a sequence of ordinary differential equations, the lowest (zeroth) order of which is the familiar Orr-Sommerfeld equation describing the parallel flow stability problem. The present study restricts itself to the first order non-parallel effects only since the higher order effects are expected to be negligible owing to the large Reynolds number involved for both the flows. Instead of integrating Orr-Sommerfeld equation for the parallel flow stability characteristics,

this analysis integrates the continuity and momentum equations separately for the disturbance velocity components and pressure since this method is found to be both economical and more accurate. The fourth order Runge-Kutta method is used along with a selective application of the Gram-Schmidt orthonormalization technique in order to remove the parasitic growth of error during integration. Muller's iteration has been used for finding the eigenvalues.

Results for parallel flow stability are summarized below.

(i) The developing flow in a channel is more unstable and has lower critical Reynolds numbers for symmetric disturbances as compared to antisymmetric disturbances. There are, however, some eigenstates that lie close to the lower branch of the neutral curve and correspond to Reynolds numbers much greater than the critical value for which the antisymmetric disturbances are more unstable. For the antisymmetric disturbance, the critical Reynolds number R_c first decreases to about 12100 at $\bar{X} \simeq 0.005$ and then increases rapidly so that the fully developed flow seems to be stable to such disturbances. Here $\bar{X} = x/aR$; a being half width of the channel (or radius of the pipe), x being the streamwise distance from the entry section and R being the Reynolds number based on a and the average velocity of flow.

(ii) For the channel flow the critical Reynolds number, wavenumber and frequency ~~and wavenumber~~ for symmetric disturbances decrease with increasing $\bar{X}$ and approach asymptotically the corresponding values of 3848.1, 1.0198 and 0.40369 respectively for the fully developed flow. For pipe flow, however, the critical frequency and wavenumber decrease continuously with $\bar{X}$ but the critical Reynolds number decreases to a value of about 11700 at $\bar{X} \simeq$ 0.0035 and then increases monotonically to infinity.

(iii) The stability characteristics are very sensitive to the velocity field description of both the flows; the velocity field obtained from the finite-difference method being more unstable than that obtained by the linearization method. In the near-entry region of both the flows, the critical Reynolds number for the velocity obtained by the finite-difference method is about half of that for the velocity field determined by the linearization method.

Results for the actual non-parallel flow stability are summarized below.

(i) The actual developing flow in both geometries becomes unstable at lower Reynolds numbers and over a wider range of frequencies as compared to its parallel flow approximate.

(ii) The growth rate and wavenumber of the disturbance become functions of $\bar{X}$, Y (the transverse coordinate),

and the disturbance property for the non-parallel flow. While the non-parallel effects on the growth rate of any disturbance property are substantial, they are negligible for the wavenumber obtained from the parallel flow theory. The growth rate of the disturbance stream function is found to be maximum at $Y = 0$ (the channel centreline or the pipe axis) for all values of $\bar{X}$, Reynolds number and frequency.

(iii) For both the flows neutral curves at various $\bar{X}$ are provided for the stream function, the streamwise component of velocity and the energy density of the disturbance. Neutral curves obtained from $g_{\psi}(\bar{X}, 0)$, the growth rate of the disturbance stream function at $Y = 0$, give the minimum R_c and encompass the maximum unstable region.

(iv) In comparison to the results for the parallel flow theory, the critical frequency is larger whereas R_c is smaller for all disturbance properties at all $\bar{X}$ for both the flows; however, the behaviour remains similar. In comparison to the value obtained for $g_{\psi}(\bar{X}, 0)$ by the non-parallel flow theory, the parallel flow theory overpredicts R_c by 23% for the channel flow and by 27% for the pipe flow at $\bar{X} = 0.001$. Based on $g_{\psi}(\bar{X}, 0)$, the first instability of the developing flow in a pipe appears at $x/a \simeq 33$ while the parallel flow theory yields a value of $x/a \simeq 37$.

(v) For the pipe flow, the R_c vs. $\overline{X}$ curve obtained on the basis of $g_\psi(\overline{X}, 0)$ is closest to the experimental data of Sarpkaya. Such a comparison for the channel flow is not possible since no experimental work is available for the same.

Chapter 1

INTRODUCTION

Following Reynolds experimental observation [1], several attempts have been made to investigate the stability of laminar flows to small disturbances. This stability analysis may be either temporal or spatial. In the temporal stability analysis, disturbances which are periodic in the downstream direction are assumed to be applied at an initial instant everywhere in the fluid and are observed as time elapses. In the spatial stability analysis, disturbances which are periodic in time are imposed at a specific location in the fluid and are observed during their propagation downstream. The flow is considered to be stable, neutrally stable, or unstable depending on whether these disturbances decay, remain unchanged, or amplify with respect to time for the temporal case or with respect to the downstream distance for the spatial case.

1.1. Literature Survey

The following four sub-sections critically discuss the available literature for the flow and its stability in a two dimensional parallel plate channel and in a circular pipe.

1.1.1. Parallel Plate Channel

The plane Poiseuille flow has been found to exhibit instability at Reynolds number, based on half width of the channel and average velocity of flow, of about 3850 as obtained theoretically by Lin [2], Thomas [3], Hains [4], Orszag [5], Chock and Schechter [6], and Davey [7] from the linear stability theory. Experiments conducted by Nishioka et al. [8] and Karnitz et al. [9] support the predicted results of the linear theory. However, Sherlin [10], Narayanan and Narayana [11], Patel and Head [12], and Breslin [13] found the critical Reynolds number to be 3000 or less in their experiment probably because the disturbance level in the upstream flow was reasonably high.

The temporal stability characteristics of the hydrodynamically developing flow in the entrance region of the channel have been investigated by Hahneman et al. [14] and by Chen and Sparrow [15]. Hahneman et al. computed the critical Reynolds numbers by applying the approximate formulae deduced by Lin [16] from the zeroth-order asymptotic solution of the disturbance equations. These formulae do not provide accurate results in the developing region because conditions postulated in their derivation are not fulfilled. Moreover, they used Schlichting's [17] velocity profile for the mainflow which does not give accurate values of the velocity gradients. As is well known, such gradients play a significant role in the behaviour of the stability characteristics.

This probably explains the large scatter among the calculated points in the plot of critical Reynolds number versus axial location shown by Hahneman et al.

Chen and Sparrow [15] used each of the three viscous solutions (singular, regular, and composite), obtained by asymptotic method, along with the inviscid solution to provide the critical Reynolds numbers and neutral stability curves by taking the basic flow velocity as (i) channel velocity profile, and (ii) a boundary layer velocity profile. As is demonstrated later, none of these solutions give accurate neutral stability curves. They also used two numerical methods to obtain critical Reynolds numbers. While Nachtsheim's method [18] was found by them to be quite involved and it also failed at high Reynolds numbers, the finite difference method [3] was used for computing only the critical Reynolds numbers. Therefore, the neutral stability curves reported by them are not accurate. Further they used the linearization method of Sparrow et al. [19] to calculate the channel velocity profile, hereafter, referred to as the Sparrow profile. However, it has now generally been accepted (cf. Section 1.1.4) that the Bodoia and Osterle method [20] gives better velocity field description. Nevertheless no attempt has heretofore been made to study the stability of the velocity profile (hereafter referred to as the B-O profile) obtained by the Bodoia and Osterle method. It is also well known [21-23] that the stability of parallel

flow is very sensitive to changes in the basic velocity profile. Even a little change in the velocity profile may change the neutral stability characteristics to a large extent. Therefore, it becomes all the more important to study the stability characteristics of the developing flow in a channel for the B-O profile.

Moreover, Chen and Sparrow's parallel flow approximation of the developing flow in the channel is not correct since the flow is actually nonparallel. Shen [24] has shown that the effect of nonparallelism of the flow is to widen the unstable region and to reduce the critical Reynolds number. In the case of a channel, one expects the effect of nonparallelism of the flow in the near entry region to be of the order of that for the boundary layer flow over a flat plate since the flow in this region of the channel can be treated as one of boundary layer type. This is expected since thickness of the boundary layer is much less than that of the central core in this region. Experiments of Schubauer and Skramstad [25] and Ross et al. [26] for the boundary layer flow over a flat plate show that the parallel flow theory predicts about 30% higher critical Reynolds number. The effects of nonparallelism of the flow should, therefore, necessarily be considered while studying the stability characteristics of the developing flow in the channel.

1.1.2. Rigid Circular Pipe

The temporal stability of Hagen-Poiseuille flow to infinitesimal, axisymmetric disturbances was, perhaps, first analysed by Sexl [27] and later by Pretsch [28], Pekeris [29], Corcos and Sellars [30], Schensted [31], and Davey and Drazin [32] while for the non-axisymmetric disturbances the analysis has been done by Lessen, Saddler and Liu [33], Burridge [34], Graebel [35], and Salwen and Grosch [36]. For the linear spatial stability characteristics, theoretical analyses by Gill [37,38] and Davey and Drazin [32] and experimental study by Leite [39] for the axisymmetric disturbances, and theoretical analyses by Garg and Rouleau [40] and Gill [38] and experimental study by Lessen et al. [41] for the non-axisymmetric disturbances are available. Except for the work of Graebel [35] and Lessen et al. [41], all these studies reveal that the Hagen-Poiseuille flow is stable to all infinitesimal disturbances. While Graebel's analysis has errors [36], Lessen et al. had too large a disturbance level for the linear stability results to hold.

The temporal stability behaviour of the hydrodynamically developing flow in the entrance region of the pipe to the infinitesimal, axisymmetric disturbances was first studied by Tatsumi [42,43]. He used an asymptotic series solution and showed that instability of the flow exists in the entrance region of a circular tube. Tatsumi found that the critical Reynolds number decreases from infinity at the

tube inlet to a minimum at some location within the entrance length and then increases monotonically to infinity further downstream. However, Tatsumi obtained the mainflow velocity profile by considering the developing flow as an almost similar flow. This velocity field description is inferior to the one obtained by more recent methods (cf. Section 1.1.4). It has also been pointed out by Chen [44] that there is an error in Tatsumi's calculation of the velocity field. Besides, Tatsumi used an essentially boundary layer model for the stability calculations in the entrance region of the pipe. Chen and Sparrow [15] have shown that the boundary layer model does not provide accurate stability results. Therefore, Tatsumi's results are not reliable.

Huang and Chen [45,46] also analysed this problem on temporal basis while using Sparrow's profile, the velocity profile obtained from the linearization method of Sparrow et al. [19]. They considered both axisymmetric and non-axisymmetric disturbances and found that in the near entry region axisymmetric disturbances are more unstable than the non-axisymmetric disturbances. However, their choice of Sparrow's profile for the mainflow is open to question as literature survey shows that the Hornbeck method [47] is more accurate. No attempt has heretofore been made to study the stability of the velocity profile (hereafter referred to as the Hornbeck profile) obtained by the Hornbeck method. This is important in view of the fact that the critical

Reynolds numbers found by Huang and Chen are much larger than the experimental values obtained by Sarpkaya [48] in the developing region.

Except for an extension of Huang and Chen's work [45] by Shen et al. [49], no other work is available for the stability characteristics of the actual (nonparallel) developing flow in a pipe. However, they considered only the effect of the radial component of velocity on the otherwise parallel flow temporal stability analysis and found that the minimum critical Reynolds number dropped to 19670 from the value of 19900 for the parallel flow theory. They did not consider such nonparallel effects as the effect of streamwise variation of the wavenumber, eigenfunctions and growth rate.

1.1.3. Nonparallel Effects

The idealization of a given flow by a parallel or quasi-parallel flow for the purpose of studying its linear stability characteristics is very common. In reality, only fully developed, two dimensional flows are exactly parallel. The shear layers such as jets and wakes, all boundary-layer type flows including developing flow through ducts have velocity components that are functions of both the streamwise and transverse coordinates. The parallel flow hydrodynamic stability theory has had only qualitative success in such cases. Experiments of Sato and Sakao [50], Ross et al. [26], Scotti and Corcos [51], and Mattingly and Criminale [52] on the stability characteristics of the jet flow, boundary

layer flow over a flat plate, stratified shear layer and two dimensional wake, respectively, show systematic differences from the quasi-parallel flow theory.

The difficulty in solving for the stability characteristics of a nonparallel flow lies in the evaluation of the eigenvalue of a set of partial differential equations. The basic problem is that the equations for linear stability of the two dimensional flows are nonseparable. To overcome this difficulty it is generally assumed that the nonparallel effects are of high order. Benney and Rosenblat [53] were perhaps the first to suggest that the method of slowly varying approximation be applied to flow stability problems. Lanchon and Eckhaus [54] considered the stability of nonparallel flows by using straightforward expansion about the parallel flow solution. However, they did not present any quantitative results. Barry and Ross [55], Boehman [56], Haaland [57], Wazzan et al. [58], Bajaj and Garg [59] and Shen et al. [49] accounted for some nonparallel effects by retaining only the transverse (or radial) component of velocity. In this model, the governing equations are separable and they reduce to a modified Orr-Sommerfeld equation.

Joseph [60] used the modified Orr-Sommerfeld equation as the zeroth-order term in his perturbation scheme to study the nonlinear stability of nearly parallel flows. Voldin [61] presented an expansion procedure which accounts for all nonparallel effects. However, he assumed the lowest

order problem to be separable. Ling and Reynolds [62] also presented a perturbation scheme that accounts for all non-parallel effects. However, they considered the temporal rather than the more realistic spatial stability problem, and expanded the stream functions of the basic flow and of the disturbance along with the eigenvalues in a power series about a given streamwise location. Their analysis is, therefore, valid only for a small neighbourhood of that streamwise location. It also neglects the vertical structure of Orr-Sommerfeld solutions [63].

Bouthier [64,65] developed the method of multiple scales for steady, spatially dependent shear flows and applied it to the stability of the boundary layer on a flat plate. Other studies that consider all nonparallel effects are by Nayfeh, Saric and Mook [66], Gaster [63], Saric and Nayfeh [67], and Smith [68] for the Blasius boundary layer, by Drazin [69] for the flow in a channel whose width is a slowly varying function of time and streamwise coordinate, by Eagles and Weissman [70] for divergent channel flow, by Crighton and Gaster [71] for developing axisymmetric jet, by Eagles [72] for slowly varying flow between concentric cylinders, and by Garg and Round [73], and Garg [74] for the Bickley jet. Some criticism of the work by Nayfeh et al. and by Drazin is also available in Eagles and Weissman. For the present study of nonparallel effects, we essentially use the approach of Eagles and Weissman.

1.1.4. Velocity Field

The developing flows in the channel and pipe, because of their practical importance, have been widely studied in the past and are still attracting many researchers. The methods used so far for calculating the velocity and pressure fields can be classified broadly as (i) finite difference solution of the boundary layer equations [20,47, 75,76], (ii) linearization of inertia terms [19,77-80], (iii) integral methods [81-84], and (iv) series expansions [85-87]. Series expansions do not provide velocity gradients with good accuracy [14] and one does not expect very accurate results from integral methods in comparison to those obtained from direct integration of the differential equations. The closed form expression for velocity and its derivatives obtained by Sparrow et al. [19] using linearization technique is definitely easier to use but the literature survey reveals that the velocity profiles obtained by Bodoia and Osterle [20] for the channel and by Hornbeck [47] for the pipe are more accurate. Bodoia and Osterle devised a finite difference method for obtaining the velocity field for the developing flow in a channel and Hornbeck extended it to the case of developing flow in a pipe.

Sparrow et al. also agree that the solution obtained by the finite difference method is likely to be more accurate. The work of Crane and Burley [88], Schmidt and Zeldin [89] and Shah [90] clearly reveals that the Hornbeck

method gives more accurate velocity description, length of entrance region, and pressure drop in the developing region of the pipe. For the channel flow van Dyke [91] considers the B-O profile to be more accurate. This view has also been supported by Morihara and Cheng [92]. Shah [90], on the basis of data reported in [93], concludes that the B-O profile is the most accurate one. Schmidt and Zeldin's [89] comparison of the pressure drop coefficient obtained by various methods supports further the view that the Bodoia and Osterle method is superior.

1.2. Present Investigation

From the above survey it is found that the stability analysis of the developing flow in a channel and pipe has not been made for the velocity profile obtained by the finite difference method which describes the velocity field in these two domains more accurately in comparison to that obtained by other methods. Since the stability characteristics of the flow are sensitive to the velocity field description [21-23], it is important to carry out the above analysis. Also, except for the work of Shen et al. [49] in which they considered only the effects of radial component of the mainflow velocity on the stability characteristics of the developing flow in a pipe, no study has heretofore been made for determining the extent to which the nonparallelism of the developing flow affects the stability behaviour of the flows. The above

literature survey reveals that these effects may be as much as 30%. Moreover, only the temporal stability of the developing flow in a channel and pipe has heretofore been investigated whereas the spatial stability analysis is more realistic.

The present work, therefore, aims to study the linear, spatial stability of the developing flow in a two dimensional channel and in a circular pipe for the velocity profile obtained by the finite difference method. While all nonparallel effects on the stability characteristics of both the flows are studied, the infinitesimal disturbance is assumed to be axisymmetric for the pipe flow stability and symmetric for the channel flow stability. A comparative study of the parallel flow stability of the velocity profile obtained for both the flows by the finite difference and linearization methods has also been carried out for these types of disturbances. Moreover, in order to check Grohne's conclusions that only the symmetric mode is likely to lead to instability of the plane Poiseuille flow [94], the velocity profile obtained for the channel flow by the finite difference method has also been investigated for its parallel flow stability to antisymmetric disturbances.

For the pipe flow stability, main consideration is given to the wall mode since for developing flow this is found to be more unstable than the central mode [46]. This is true because the developing flow is of the boundary

layer type and the instability of the flow, if it exists, should originate near the pipe wall as in the boundary layer flow. For the sake of completeness, however, the central modes are also studied for the parallel flow stability.

Chapter 2

THEORETICAL ANALYSIS

In this chapter stability equations which include all nonparallel effects have been obtained for the developing flow in a circular pipe and in a two dimensional channel. This is followed by a discussion on the appropriate boundary conditions.

2.1. Development of the Stability Equations

The stability equations for infinitesimal, two dimensional disturbances are formulated under the conventional assumption that the fluid motion can be decomposed into a mean flow (whose stability constitutes the subject of the investigation) and a disturbance having pressure $\tilde{p}$ and velocity components $\tilde{u}$ and $\tilde{v}$ in the streamwise and transverse (or radial) direction respectively. Thus in the resultant motion, the velocity field is

$$\hat{u} = \bar{U} + \tilde{u} , \qquad \hat{v} = \bar{V} + \tilde{v} , \tag{2.1}$$

and the pressure field is

$$\hat{p} = \bar{P} + \tilde{p} , \tag{2.2}$$

where $\bar{U}$ and $\bar{V}$ are the mainflow velocity components in the streamwise and transverse (or radial) direction respectively and $\bar{P}$ is the pressure at any point in the mainflow. The

mainflow velocity field is obtained either by the finite difference method or by the linearization method both of which are described in Appendix A.

In formulating the disturbance equations, the following assumptions are made:

(i) the fluid is incompressible and Newtonian with constant properties;

(ii) the mainflow is steady and laminar;

(iii) the (duct) walls are rigid and impermeable;

(iv) there are no body forces; and

(v) the streamwise velocity component $\bar{U}$ is a slowly varying function of the streamwise coordinate x.

For such a fluid the equations of motion expressed in terms of the coordinate system shown in Figure A-1 are:

$$\frac{\partial \hat{u}}{\partial x} + \frac{m\hat{v}}{y} + \frac{\partial \hat{v}}{\partial y} = 0 , \tag{2.3}$$

$$\frac{\partial \hat{u}}{\partial t} + \hat{u}\frac{\partial \hat{u}}{\partial x} + \hat{v}\frac{\partial \hat{u}}{\partial y} = -\frac{1}{\rho}\frac{\partial \hat{p}}{\partial x} + \nu\left(\frac{\partial^2 \hat{u}}{\partial x^2} + \frac{m}{y}\frac{\partial \hat{u}}{\partial y} + \frac{\partial^2 \hat{u}}{\partial y^2}\right) , \tag{2.4}$$

$$\frac{\partial \hat{v}}{\partial t} + \hat{u}\frac{\partial \hat{v}}{\partial x} + \hat{v}\frac{\partial \hat{v}}{\partial y} = -\frac{1}{\rho}\frac{\partial \hat{p}}{\partial y} + \nu\left(\frac{\partial^2 \hat{v}}{\partial x^2} + \frac{m}{y}\frac{\partial \hat{v}}{\partial y} - \frac{m\hat{v}}{y^2} + \frac{\partial^2 \hat{v}}{\partial y^2}\right), \tag{2.5}$$

where x is the streamwise coordinate measured from the inlet section and y is the transverse (or radial) coordinate measured from the channel centre line (or pipe axis), ρ is the density and ν the kinematic viscosity of the fluid, t is the time, and m = 0 for the channel flow while m = 1 for the pipe flow.

If we now substitute eqns. (2.1) and (2.2) in eqns. (2.3) through (2.5), make use of equations of motion for the mainflow which are similar to eqns. (2.3) through (2.5) and neglect the product terms of disturbance velocity components with their spatial derivatives, we obtain the following set of linearized hydrodynamic equations for the disturbance velocity components and pressure

$$\frac{\partial \tilde{u}}{\partial x} + \frac{m\tilde{v}}{y} + \frac{\partial \tilde{v}}{\partial y} = 0 , \tag{2.6}$$

$$\frac{\partial \tilde{u}}{\partial t} + \bar{U}\frac{\partial \tilde{u}}{\partial x} + \bar{V}\frac{\partial \tilde{u}}{\partial y} + \tilde{u}\frac{\partial \bar{U}}{\partial x} + \tilde{v}\frac{\partial \bar{U}}{\partial y} + \frac{1}{\rho}\frac{\partial \tilde{p}}{\partial x}$$
$$= \nu\left(\frac{\partial^2 \tilde{u}}{\partial x^2} + \frac{m}{y}\frac{\partial \tilde{u}}{\partial y} + \frac{\partial^2 \tilde{u}}{\partial y^2}\right) , \tag{2.7}$$

$$\frac{\partial \tilde{v}}{\partial t} + \bar{U}\frac{\partial \tilde{v}}{\partial x} + \bar{V}\frac{\partial \tilde{v}}{\partial y} + \tilde{u}\frac{\partial \bar{V}}{\partial x} + \tilde{v}\frac{\partial \bar{V}}{\partial y} + \frac{1}{\rho}\frac{\partial \tilde{p}}{\partial y}$$
$$= \nu\left(\frac{\partial^2 \tilde{v}}{\partial x^2} + \frac{m}{y}\frac{\partial \tilde{v}}{\partial y} - \frac{m\tilde{v}}{y^2} + \frac{\partial^2 \tilde{v}}{\partial y^2}\right) . \tag{2.8}$$

Equations (2.6) through (2.8) can be made dimensionless by choosing the half width a of the channel (or radius a of the pipe) and the average velocity u_a of the mainflow as the characteristic length and velocity respectively and introducing the following dimensionless variables:

$$u = \frac{\tilde{u}}{u_a} , \qquad U = \frac{\bar{U}}{u_a} , \qquad X = \frac{x}{a}$$
$$v = \frac{\tilde{v}}{u_a} , \qquad V = \frac{\bar{V}}{u_a} , \qquad Y = \frac{y}{a} \tag{2.9}$$
$$p = \frac{\tilde{p}}{\rho u_a^2} , \qquad T = \frac{t u_a}{a} , \qquad R = \frac{u_a a}{\nu} .$$

Substituting these in eqns. (2.6) through (2.8), dividing eqns. (2.7) and (2.8) by u_a^2/a and eqn. (2.6) by u_a/a, we get the following set of linear, partial differential equations for the disturbance properties in nondimensional form:

$$\frac{\partial u}{\partial X} + \frac{mv}{Y} + \frac{\partial v}{\partial Y} = 0 , \tag{2.10}$$

$$\frac{\partial u}{\partial T} + U\frac{\partial u}{\partial X} + V\frac{\partial u}{\partial Y} + u\frac{\partial U}{\partial X} + v\frac{\partial U}{\partial Y} + \frac{\partial p}{\partial X}$$

$$= \frac{1}{R}\left(\frac{\partial^2 u}{\partial X^2} + \frac{m}{Y}\frac{\partial u}{\partial Y} + \frac{\partial^2 u}{\partial Y^2}\right) , \tag{2.11}$$

$$\frac{\partial v}{\partial T} + U\frac{\partial v}{\partial X} + V\frac{\partial v}{\partial Y} + u\frac{\partial V}{\partial X} + v\frac{\partial V}{\partial Y} + \frac{\partial p}{\partial Y}$$

$$= \frac{1}{R}\left(\frac{\partial^2 v}{\partial X^2} + \frac{m}{Y}\frac{\partial v}{\partial Y} - \frac{mv}{Y^2} + \frac{\partial^2 v}{\partial Y^2}\right) . \tag{2.12}$$

Equations (2.10) through (2.12) are combined into a single equation by differentiating eqn. (2.11) with respect to Y and eqn. (2.12) with respect to X, subtracting the latter from the former and using eqn. (2.10). This yields

$$\frac{\partial \eta}{\partial T} + U\frac{\partial \eta}{\partial X} + V\frac{\partial \eta}{\partial Y} + u\frac{\partial H}{\partial X} + v\frac{\partial H}{\partial Y}$$

$$= \frac{1}{R}\left[\frac{\partial^2 \eta}{\partial Y^2} + \frac{3m}{Y}\frac{\partial \eta}{\partial Y} + \frac{2m(m-1)\eta}{Y^2} + \frac{\partial^2 \eta}{\partial X^2}\right] , \tag{2.13}$$

where

$$\eta = \frac{1}{Y^m}\left(\frac{\partial u}{\partial Y} - \frac{\partial v}{\partial X}\right) \quad \text{and} \quad H = \frac{1}{Y^m}\left(\frac{\partial U}{\partial Y} - \frac{\partial V}{\partial X}\right) . \tag{2.14}$$

The term having the coefficient m(m-1) is always zero for m = 0 or 1. Henceforth such terms will be deleted.

Also, the constant coefficient of m, if any, will henceforth utilize the fact that m = 0 or 1. Equation (2.13) thus reduces to

$$\frac{\partial \eta}{\partial T} + U \frac{\partial \eta}{\partial X} + V \frac{\partial \eta}{\partial Y} + u \frac{\partial H}{\partial X} + v \frac{\partial H}{\partial Y}$$

$$= \frac{1}{R} \left[\frac{\partial^2 \eta}{\partial Y^2} + \frac{3m}{Y} \frac{\partial \eta}{\partial Y} + \frac{\partial^2 \eta}{\partial X^2} \right] . \qquad (2.15)$$

It is well known that for the developing flow in a pipe or channel, U(X, Y) and V(X, Y) are slowly varying functions of X. To express this slow variation we introduce another independent variable X_1 along X direction such that

$$X_1 = \varepsilon X , \qquad (2.16)$$

where ε is a small dimensionless parameter which characterizes the nonparallelism of the flow; $\varepsilon = 0$ implies a truly parallel flow. The value of ε depends on the type of flow and the Reynolds number. Bouthier [65] determined it from the order of the terms expressing the boundary layer effect on the velocity field and Gaster [63] obtained it in an iteration process. For the boundary layer flow on a flat plate, Gaster as well as Bouthier take $\varepsilon = R^{-1/2}$. Smith [68], on the basis of comparison of Gaster's [63] results with the experimental results of Ross et al. [26] and Schubauer and Skramstad [25], points out that the choice of $\varepsilon = R^{-3/8}$ gives results which are in closer agreement with the experimental ones. Unfortunately no experimental results for the developing flow in a channel are available and those for the developing flow

in a pipe, obtained by Sarpkaya [48], are, as Sarpkaya himself admits, not free from the effects of non-axisymmetric disturbances and of finite level amplitude of the disturbances. Therefore, the experimental data of Sarpkaya cannot be used to estimate the value of ε. Since the developing flow in these ducts, particularly in the near entry region, can be treated as one of boundary layer type, we take $\varepsilon = R^{-1/2}$ for these cases. This choice of ε is further supported by the expressions given by Schlichting [17] and Goldstein [85] for the velocity at the channel centre line and at the pipe axis respectively.

Though ε and R are related, we may treat them as independent in the expansions that follow. By doing this we are, in effect, solving the problem on an ε-R plane instead of on a single curve and thus the real solution is contained in the family of fictitious extensions over all ε and R.

Now coming back to the eqns. (2.10) through (2.12), we note that the coefficients of u, v and their derivatives are functions of X_1 and Y only. Therefore, the disturbance stream function can be taken as

$$\psi(X_1, Y, T) = [\phi_o(X_1, Y) + \varepsilon\phi_1(X_1, Y) + \ldots] e^{i\theta} , \qquad (2.17)$$

where

$$\frac{\partial \theta}{\partial T} = -\omega , \quad \frac{\partial \theta}{\partial X} = k_o(X_1) , \qquad (2.18)$$

with ω being real. Here, ω is the dimensionless frequency of the disturbance, the real part, k_{or}, of k_o is the

wavenumber, and its imaginary part, k_{oi}, is the spatial growth rate. Using the following transformation relations

$$\frac{\partial}{\partial T} = -\omega \frac{\partial}{\partial \Theta}, \qquad \frac{\partial}{\partial X} = k_o \frac{\partial}{\partial \Theta} + \varepsilon \frac{\partial}{\partial X_1} \tag{2.19}$$

between (X, T) and (X_1, Θ) planes and denoting Y derivative with a prime, we get

$$v = -\frac{1}{Y^m}\frac{\partial \psi}{\partial X} = -\frac{e^{i\Theta}}{Y^m}\left[ik_o\phi_o + \varepsilon\left(ik_o\phi_1 + \frac{\partial \phi_o}{\partial X_1}\right)\right] + O(\varepsilon^2),$$

$$u = \frac{1}{Y^m}\frac{\partial \psi}{\partial Y} = \frac{1}{Y^m}\left[\phi_o' + \varepsilon\,\phi_1'\right] + O(\varepsilon^2),$$

$$\eta = \frac{e^{i\Theta}}{Y^{2m}}\left[\left(\phi_o'' - k_o^2\phi_o - \frac{m\phi_o'}{Y}\right)\right.$$

$$+ \varepsilon\left\{\left(\phi_1'' - k_o^2\phi_1 - \frac{m\phi_1'}{Y}\right) + i\left(2k_o\frac{\partial \phi_o}{\partial X_1} + \phi_o\frac{dk_o}{dX_1}\right)\right\}\Bigg]$$

$$+ O(\varepsilon^2),$$

$$\frac{\partial \eta}{\partial T} = \frac{\omega e^{i\Theta}}{Y^{2m}}\left[i\left(k_o^2\phi_o - \phi_o'' + \frac{m\phi_o'}{Y}\right)\right.$$

$$+ \varepsilon\left\{\left(2k_o\frac{\partial \phi_o}{\partial X_1} + \phi_o\frac{dk_o}{dX_1}\right) + i\left(k_o^2\phi_1 - \phi_1'' + \frac{m\phi_1'}{Y}\right)\right\}\Bigg]$$

$$+ O(\varepsilon^2),$$

$$\frac{\partial \eta}{\partial X} = \frac{e^{i\Theta}}{Y^{2m}}\left[ik_o\left(\phi_o'' - k_o^2\phi_o - \frac{m\phi_o'}{Y}\right)\right.$$

$$+ \varepsilon\left\{ik_o\left(\phi_1'' - k_o^2\phi_1 - \frac{m\phi_1'}{Y} + 3ik_o\frac{\partial \phi_o}{\partial X_1} + 3i\frac{dk_o}{dX_1}\phi_o\right)\right.$$

$$\left.\left. + \left(\frac{\partial \phi_o''}{\partial X_1} - \frac{m}{Y}\frac{\partial \phi_o'}{\partial X_1}\right)\right\}\right] + O(\varepsilon^2),$$

$$\frac{\partial \eta}{\partial Y} = \frac{e^{i\Theta}}{Y^{2m}}\Big[\{ \phi_o''' - \frac{3m}{Y}\phi_o'' + (\frac{3m}{Y^2} - k_o^2)\phi_o' + \frac{2m}{Y}k_o^2\phi_o \}$$

$$+ \varepsilon\{ \phi_1''' - \frac{3m}{Y}\phi_1'' + (\frac{3m}{Y^2} - k_o^2)\phi_1' + \frac{2m}{Y}k_o^2\phi_1$$

$$+ 2ik_o(\frac{\partial \phi_o'}{\partial X_1} - \frac{2m}{Y}\frac{\partial \phi_o}{\partial X_1}) + i\frac{dk_o}{dX_1}(\phi_o' - \frac{2m}{Y}\phi_o)\}\Big]$$

$$+ O(\varepsilon^2) ,$$

$$\frac{\partial^2 \eta}{\partial Y^2} = \frac{e^{i\Theta}}{Y^{2m}}\Big[\{ \phi_o^{iv} - \frac{5m}{Y}\phi_o''' + \frac{12m}{Y^2}\phi_o'' - k_o^2\phi_o''$$

$$- \frac{12m}{Y^3}\phi_o' + \frac{4mk_o^2}{Y}\phi_o' - \frac{6k_o^2m}{Y^2}\phi_o \}$$

$$+ \varepsilon\{ \phi_1^{iv} - \frac{5m\phi_1'''}{Y} + \frac{12m\phi_1''}{Y^2} - k_o^2\phi_1'' - \frac{12m}{Y^3}\phi_1' + \frac{4mk_o^2}{Y}\phi_1'$$

$$- \frac{6k_o^2m}{Y^2}\phi_1 + 2ik_o(\frac{\partial \phi_o''}{\partial X_1} - \frac{4m}{Y}\frac{\partial \phi_o'}{\partial X_1} + \frac{6m}{Y^2}\frac{\partial \phi_o}{\partial X_1})$$

$$+ i\frac{dk_o}{dX_1}(\phi_o'' - \frac{4m}{Y}\phi_o' + \frac{6m}{Y^2}\phi_o)\}\Big] + O(\varepsilon^2) ,$$

$$\frac{\partial^2 \eta}{\partial X^2} = \frac{e^{i\Theta}}{Y^{2m}}\Big[- k_o^2(\phi_o'' - k_o^2\phi_o - \frac{m\phi_o'}{Y})$$

$$+ \varepsilon\{ - k_o^2(\phi_1'' - k_o^2\phi_1 - \frac{m\phi_1'}{Y}) + i\frac{dk_o}{dX_1}(\phi_o'' - 6k_o^2\phi_o - \frac{m\phi_o'}{Y})$$

$$+ ik_o(2\frac{\partial \phi_o''}{\partial X_1} - 4k_o^2\frac{\partial \phi_o}{\partial X_1} - \frac{2m}{Y}\frac{\partial \phi_o'}{\partial X_1})\}\Big] + O(\varepsilon^2) ,$$

$$\frac{\partial H}{\partial X} = \frac{\varepsilon}{Y^m}\frac{\partial U'}{\partial X_1} ,$$

$$\frac{\partial H}{\partial Y} = \frac{1}{Y^m}\left[\left(\frac{\partial^2 U}{\partial Y^2} - \frac{m}{Y}\frac{\partial U}{\partial Y}\right)\right].$$

Substituting these transformed relations into eqn. (2.15) and equating coefficients of like powers of ε we obtain order ε^o:

$$L(\phi_o) \equiv \phi_o^{iv} - \frac{2m}{Y}\phi_o''' + \frac{3m}{Y^2}\phi_o'' - 2k_o^2\phi_o'' - \frac{3m}{Y^3}\phi_o' + \frac{2mk_o^2}{Y}\phi_o' + k_o^4\phi_o$$

$$- iR\left[(\phi_o'' - k_o^2\phi_o - \frac{m}{Y}\phi_o')(k_oU - \omega) - k_o(U'' - \frac{m}{Y}U')\phi_o\right]$$

$$= 0 \qquad (2.20)$$

order ε:

$$L(\phi_1) = R\left[B_1\frac{\partial \phi_o}{\partial X_1} + B_2\frac{\partial}{\partial X_1}(\phi_o'' - \frac{m}{Y}\phi_o') + \{B_3\phi_o + B_4(\phi_o'' - \frac{m}{Y}\phi_o')\}\frac{dk_o}{dX_1}\right.$$

$$\left. + B_5\phi_o + B_6\phi_o' + B_7\phi_o'' + V\phi_o'''\right] \qquad (2.21)$$

where

$$B_1 = 2\omega k_o - 3k_o^2U - U'' + \frac{m}{Y}U' + \frac{4ik_o^3}{R},$$

$$B_2 = U - 4ik_o/R,$$

$$B_3 = \omega - 3Uk_o + 6ik_o^2/R,$$

$$B_4 = -2i/R, \qquad (2.22)$$

$$B_5 = \frac{2mk_o^2}{Y}V,$$

$$B_6 = -\frac{\partial^2 V}{\partial Y^2} - \frac{m}{Y}\frac{\partial V}{\partial Y} - k_o^2V + \frac{4m}{Y^2}V, \text{ and}$$

$$B_7 = -\frac{3m}{Y}V.$$

The eigenvalue problems defined by eqns. (2.20) and (2.23) or (2.24) or (2.26) are the familiar Orr-Sommerfeld problems for the parallel flow. In eqn. (2.21), which gives first order corrections over the parallel flow theory, we note that the first two terms on the right hand side represent the effects of the streamwise variation of the amplitude of the disturbance stream function, the third accounts for the streamwise variation of the wavenumber and of the spatial growth rate, and the remaining four terms represent the effects of the transverse or radial velocity component of the main flow; the last being the only effect considered by Shen et al. [49] for the developing flow in a pipe.

2.2. Boundary Conditions

Physical considerations such as no slip at the walls or boundedness of the eigenfunctions within the flow region determine the necessary boundary conditions for eqns. (2.20) and (2.21). We now derive them for the channel and pipe flows separately.

2.2.1. Parallel Plate Channel

The boundary conditions for eqn. (2.20) at $Y = \pm 1$ are provided by the 'no slip' requirement at the channel walls. However, since the velocity profile of the mainflow in the channel is symmetric about the centre line, eqn. (2.20) with $m = 0$ admits eigenfunctions which are either symmetric

(even mode) or antisymmetric (odd mode). In such cases, it is sufficient to consider the stability of the flow confined between the centre line and any of the walls, say the upper one (Y = 1). Then the boundary conditions at Y = -1 are replaced by the appropriate boundary conditions at Y = 0. The boundary conditions, therefore, are

$$\begin{aligned} \phi_o' &= \phi_o''' = 0 \quad \text{at} \quad Y = 0 , \\ \phi_o &= \phi_o' = 0 \quad \text{at} \quad Y = 1 \quad \text{(no slip condition)} \end{aligned} \tag{2.23}$$

for symmetric disturbances, and

$$\begin{aligned} \phi_o &= \phi_o'' = 0 \quad \text{at} \quad Y = 0 , \\ \phi_o &= \phi_o' = 0 \quad \text{at} \quad Y = 1 \end{aligned} \tag{2.24}$$

for antisymmetric disturbances.

The work of Grohne [94] suggests that for plane Poiseuille flow only symmetric disturbances are likely to lead to instability. Accordingly, Chen and Sparrow [15] studied the temporal stability of only symmetric disturbances for the developing flow in a channel. In the present analysis both symmetric and antisymmetric disturbances have been considered for the parallel flow stability analysis, but only symmetric disturbances have been considered for evaluating the effects of nonparallelism of the flow on the stability characteristics. The boundary conditions for eqn. (2.21) which are similar to those for eqn. (2.20) are

$$\phi_1' = \phi_1''' = 0 \quad \text{at} \quad Y = 0 ,$$
$$\text{and} \quad \phi_1 = \phi_1' = 0 \quad \text{at} \quad Y = 1 . \tag{2.25}$$

2.2.2. Circular Pipe

Boundary conditions at the pipe wall are determined by the no slip requirement and at the pipe axis by the requirement that the velocity components and pressure for the disturbance be bounded and continuous. Thus we can write the following boundary conditions for axisymmetric disturbances

$$\lim_{Y \to 0} \frac{\phi_o}{Y} = 0 , \qquad \lim_{Y \to 0} \frac{\phi_o'}{Y} = \text{finite} ,$$
$$\text{or} \quad \phi_o = \phi_o' = 0 \quad \text{at} \quad Y = 0 ,$$
$$\text{and} \quad \phi_o = \phi_o' = 0 \quad \text{at} \quad Y = 1 \tag{2.26}$$

for eqn. (2.20) with m = 1.

Similarly the boundary conditions for eqn. (2.21) are

$$\phi_1 = \phi_1' = 0 \quad \text{at} \quad Y = 0 ,$$
$$\text{and} \quad \phi_1 = \phi_1' = 0 \quad \text{at} \quad Y = 1 . \tag{2.27}$$

Chapter 3

SOLUTION OF DISTURBANCE EQUATIONS

Equation (2.20) together with the appropriate boundary conditions depending upon the type of disturbance and the flow govern the propagation of an arbitrary, infinitesimal disturbance through an incompressible, viscous, parallel flow in a channel or pipe. The variable X_1 appears implicitely in this equation. For given values of ω, R and $U(X_1, Y)$, this problem can be solved numerically to determine the eigenvalue $k_o(X_1)$ and the eigenfunction $\beta(Y; X_1)$. The solution can be expressed as

$$\phi_o(X_1, Y) = A(X_1)\ \beta(Y; X_1)\ , \qquad (3.1)$$

where $A(X_1)$ is still an undetermined function. It will be determined from eqn. (2.21). If the mainflow is assumed to be parallel, A is constant and we have the complete solution in eqn. (3.1).

Substituting for ϕ_o from eqn. (3.1) into eqn. (2.21), we get

$$L(\phi_1) = RM(A, \beta, U, V, k_o)\ ,$$

where

$$M = \left[B_1\beta + B_2\left(\beta'' - \frac{m\beta'}{Y}\right)\right]\frac{dA}{dX_1} + \left[B_1\frac{\partial\beta}{\partial X_1} + B_2\frac{\partial}{\partial X_1}\left(\beta'' - \frac{m\beta'}{Y}\right)\right]A$$

$$+\left[\left\{B_3\beta + \left(\beta'' - \frac{m\beta'}{Y}\right)B_4\right\}\frac{dk_o}{dX_1} + B_5\beta + B_6\beta' + B_7\beta'' + V\beta'''\right]A\,. \tag{3.2}$$

The inhomogeneous problem consisting of eqns. (3.2) and (2.25) or (2.27) has a solution if, and only if, the following solvability condition

$$\int_o^1 M\,\beta^*\,dY = 0 \tag{3.3}$$

is satisfied. Here β^* is the eigenfunction corresponding to the eigenvalue k_o of the adjoint homogeneous problem

$$L^*(\beta^*) = \beta^{*iv} - 2k_o^2\beta^{*''} + k_o^4\beta^* + \frac{2m\beta^{*'''}}{Y} - \frac{3m}{Y^2}\beta^{*''} - \left(\frac{2m}{Y}k_o^2 - \frac{3m}{Y^3}\right)\beta^{*'}$$

$$+\left(\frac{2mk_o^2}{Y^2} - \frac{3m}{Y^4}\right)\beta^* - iR\left[(Uk_o - \omega)\left(\beta^{*''} - k_o^2\beta^* - \frac{m}{Y^2}\beta^* + \frac{m\beta^{*'}}{Y}\right)\right.$$

$$\left.+\left(2U'\beta^{*'} + \frac{2mU'}{Y}\beta^*\right)k_o\right] = 0 \tag{3.4}$$

With the boundary conditions

$$\begin{aligned}&\beta^{*'} = \beta^{*'''} = 0 \quad \text{at} \quad Y = 0\,,\\ &\beta^{*} = \beta^{*'} = 0 \quad \text{at} \quad Y = 1\end{aligned} \tag{3.5a}$$

for the channel flow (symmetric disturbances) and

$$\beta^{*} = \beta^{*'} = 0 \quad \text{at} \quad Y = 0 \text{ and } 1 \tag{3.5b}$$

for the pipe flow. Substituting for M from eqn. (3.2) into eqn. (3.3) and noting that

$$\int_0^1 B_2 \frac{\partial}{\partial X_1} (\beta'' - \frac{m}{Y}\beta') \beta^* \, dY$$

$$= \int_0^1 [B_2\beta^{*''} + (2B_2' + \frac{mB_2}{Y})\beta^{*'} + (B_2'' + \frac{mB_2'}{Y} - \frac{mB_2}{Y^2})\beta^*] \frac{\partial \beta}{\partial X_1} dY ,$$

obtained by evaluating the integral by parts and using the appropriate boundary conditions, we get on simplification

$$\frac{dA}{dX_1} = ik_1(X_1)A , \qquad (3.6)$$

where $ik_1 = b_2(X_1)/b_1(X_1)$,

$b_2(X_1)$ =

$$\int_0^1 [(B_2'' + \frac{mB_2'}{Y} - \frac{mB_2}{Y^2} + B_1)\beta^* + (2B_2' + \frac{mB_2}{Y})\beta^{*'} + B_2\beta^{*''}] \frac{\partial \beta}{\partial X_1} dY$$

$$+ \int_0^1 [(B_4\beta'' - \frac{mB_4}{Y}\beta' + B_3\beta) \frac{dk_o}{dX_1} + B_5\beta + B_6\beta' + B_7\beta'' + V\beta'''']\beta^* dY ,$$

$$b_1(X_1) = - \int_0^1 [B_1\beta + B_2(\beta'' - \frac{m\beta'}{Y})] \beta^* \, dY .$$

The solution of eqn. (3.6) is

$$A(X_1) = A_o \exp[i \int k_1(X_1)dX_1] = A_o \exp[i\varepsilon \int k_1(X_1)dX] , \qquad (3.7)$$

where A_o is an arbitrary constant of integration. Thus, to the first approximation

$$\psi(X_1, Y, T) = A_o\beta(Y; X_1) \exp[i \int (k_o + \varepsilon k_1)dX - i\omega T] , \qquad (3.8)$$

where β and k_o are calculated at each axial location as if the basic flow were parallel, and k_1 contains the effects of the streamwise variation of the mainflow, the eigenfunction β, and the eigenvalue k_o. To determine $b_2(X_1)$, we need to evaluate $\partial\beta/\partial X_1$ and dk_o/dX_1. To do this, we replace ϕ_o by β in eqn. (2.20) and the corresponding boundary conditions and differentiate the result with respect to X_1 to obtain

$$L\left(\frac{\partial \beta}{\partial X_1}\right) = A_1 + A_2 \frac{dk_o}{dX_1}, \tag{3.9a}$$

with boundary conditions

$$\left.\begin{aligned} \left(\frac{\partial \beta}{\partial X_1}\right)' = \left(\frac{\partial \beta}{\partial X_1}\right)''' = 0 \quad \text{at} \quad Y = 0 \\ \text{and} \quad \frac{\partial \beta}{\partial X_1} = \left(\frac{\partial \beta}{\partial X_1}\right)' = 0 \quad \text{at} \quad Y = 1 \end{aligned}\right\} \text{(for channel)}, \tag{3.9b}$$

$$\text{and} \quad \frac{\partial \beta}{\partial X_1} = \left(\frac{\partial \beta}{\partial X_1}\right)' = 0 \quad \text{at} \quad Y = 0 \text{ and } 1 \text{ (for pipe)},$$

where

$$A_1 = \frac{iRk_o}{1}\left[\left(V''' - \frac{3m}{Y^2}V' + \frac{3mV}{Y^3} + k_o^2 V'\right)\beta - \left(\beta'' - \frac{m\beta'}{Y}\right)\left(V' + \frac{mV}{Y}\right)\right], \tag{3.9c}$$

$$\text{and} \quad A_2 = 4k_o\left(\beta'' - k_o^2\beta - \frac{m\beta'}{Y}\right)$$

$$+ iR\left[U\left(\beta'' - \frac{m\beta'}{Y}\right) + \beta\left(2\omega k_o - 3Uk_o^2 - U'' + \frac{mU'}{Y}\right)\right]. \tag{3.9d}$$

Equations (3.9) have a solution if, and only if, the solvability condition (eqn. (3.3)) with M replaced by the terms on the right hand side of eqn. (3.9a) is satisfied. This yields

$$\frac{dk_o}{dX_1} = -\left[\int_o^1 A_1 \beta^* \, dY\right] / \left[\int_o^1 A_2 \beta^* \, dY\right] . \qquad (3.10)$$

Knowing dk_o/dX_1 from eqn. (3.10), $\partial\beta/\partial X_1$ can be evaluated from the integration of eqns. (3.9).

For a truly parallel basic flow, β is a function of Y only, $k_1 = 0$, and k_o is a constant. Hence the growth rate of any disturbance quantity, such as the velocity, the pressure, and the kinetic energy, is given uniquely by the imaginary part of k_o. On the other hand, the effects of nonparallelism are to make k_o a function of X_1, to produce a correction $\varepsilon k_1(X_1)$ to k_o, and to make the mode shape β vary in the streamwise direction. Hence the streamwise variation of each flow quantity depends on its distance from the channel centre line or from the pipe axis. Moreover, at each distance Y, the different flow quantities vary differently in the streamwise direction. We shall discuss this point in detail in Chapter 4.

For determining the effects of nonparallelism of the flow on the wavenumber and growth rates, we need to integrate the Orr-Sommerfeld eqn. (2.20) with the boundary conditions (2.23) or (2.26). However, for reasons discussed in Section 5.1, we solve a set of three coupled, homogeneous eqns. (3.12) through (3.15) instead of eqn. (2.20). These equations are obtained for an infinitesimal disturbance of the form

$$[u,v,p] = [\bar{u}(Y), \bar{v}(Y), \bar{p}(Y)] \exp [i(k_o X - \omega T)] , \qquad (3.11)$$

by making substitutions in eqns. (2.10) through (2.12). This yields

$$\bar{v}' + \frac{m\bar{v}}{Y} + ik_o\bar{u} = 0 , \qquad (3.12)$$

$$\bar{u}'' + \frac{m\bar{u}'}{Y} - F\bar{u} - RU'\bar{v} - ik_oR\bar{p} = 0 , \qquad (3.13)$$

$$R\bar{p}' + F\bar{v} + ik_o\bar{u}' = 0 , \qquad (3.14)$$

where $F = k_o^2 + iR(k_oU - \omega)$. (3.15)

The boundary conditions on the basis of considerations given in Section 2.2 are

$$\begin{aligned} \bar{u} = \bar{p} = 0 \quad &\text{at} \quad Y = 0 , \\ \bar{u} = \bar{v} = 0 \quad &\text{at} \quad Y = 1 \end{aligned} \qquad (3.16)$$

for symmetric disturbances in the case of channel flow, and

$$\begin{aligned} \bar{u}' = \bar{v} = 0 \quad &\text{at} \quad Y = 0 , \\ \bar{u} = \bar{v} = 0 \quad &\text{at} \quad Y = 1 \end{aligned} \qquad (3.17)$$

for antisymmetric disturbances in the case of channel flow or axisymmetric disturbances for the pipe flow. Equations (3.12) through (3.15) may be integrated with proper boundary conditions by using any step-by-step integration method; the details of the procedure are given in Chapter 5. The eigenfunction β and its derivatives with Y are then determined from

$$\beta = iY^m \bar{v}/k_o , \quad \beta' = Y^m \bar{u} , \quad \beta'' = Y^m \bar{u}' + m\bar{u} ,$$
$$\beta''' = [F\bar{u} + R\bar{v}U' + ik_oR\bar{p}] Y^m + m\bar{u}' . \tag{3.18}$$

With k_o, β and its derivatives known, a procedure similar to the one above is used to solve the adjoint equations

$$v^{*'} + \frac{mv^*}{Y} + ik_ou^* = 0 , \tag{3.19}$$

$$u^{*''} + \frac{mu^{*'}}{Y} - Fu^* + ik_oRp^* - ik_o(v^{*'} + \frac{mv^*}{Y}) = 0 , \tag{3.20}$$

$$Rp^{*'} - Fv^* + RU'u^* = 0 , \tag{3.21}$$

with the boundary conditions

$$u^* = p^* = 0 \quad \text{at} \quad Y = 0 \text{ (for channel flow; symmetric disturbances)},$$
$$u^{*'} = v^* = 0 \quad \text{at} \quad Y = 0 \text{ (for pipe flow)}, \tag{3.22}$$

and $u^* = v^* = 0$ at $y = 1$ (for both flows).

The adjoint eigenfunction β^* and its derivatives with Y are obtained from

$$\beta^* = iY^m v^*/k_o, \quad \beta^{*'} = Y^m u^* , \text{ and } \beta^{*''} = Y^m u^{*'} + mu^* . \tag{3.23}$$

Since the eigenvalue for the original and adjoint problems is the same, no iteration is necessary while solving eqns. (3.19) through (3.22). This, in fact, serves as a check on the accuracy of the calculated eigenvalues.

Chapter 4

GROWTH RATES AND WAVENUMBERS

Herein, we derive the relations for the growth rate and wavenumber of the disturbance while accounting for all nonparallel effects.

To the first approximation, i.e., to $O(\varepsilon)$, the stream function of the disturbance is given by eqn. (3.8), which may be rewritten as

$$\psi = A_o \beta (Y; X_1) \exp \left[i \int \alpha \, dX - i\omega T \right] , \tag{4.1}$$

where $\alpha \equiv k_o + \varepsilon k_1$.

The amplitude of this stream function is

$$|\psi| = |A_o| |\beta (Y; X_1)| \exp(- \int \alpha_i \, dX) , \tag{4.2}$$

where α_i is the imaginary part of α. We define a growth rate based on ψ in X-space as

$$g_\psi \equiv \frac{1}{|\psi|} \frac{\partial |\psi|}{\partial X} . \tag{4.3}$$

Using eqn. (4.2), eqn. (4.3) becomes

$$g_\psi = - \alpha_i + \frac{\varepsilon}{|\beta|} \frac{\partial |\beta|}{\partial X_1} . \tag{4.4}$$

We note that the growth rate of the stream function is dependent on the streamwise as well as the transverse (or

radial) coordinate since β is a function of both X_1 and Y. Also, when $k_{oi} = 0$, i.e., at the neutral points determined by the parallel flow theory, there is still growth or decay due to the higher-order effects. Thus, the higher-order corrections are essential in determining the correct neutral points for the stability analysis of nonparallel flows.

Another surprising feature of $O(\varepsilon)$ corrections is that the growth rate is different for different flow quantities. Consider, for example, the X-component of the disturbance velocity, given by

$$u \equiv \frac{1}{Y^m}\frac{\partial \psi}{\partial Y} = \frac{A_o}{Y^m}\frac{\partial \beta}{\partial Y}\exp(i \int \alpha \, dX - i\omega T) \, . \tag{4.5}$$

The growth rate of u is then given by

$$g_u = -\alpha_i + \frac{\varepsilon}{\left|\frac{\partial \beta}{\partial Y}\right|}\frac{\partial \left|\partial \beta/\partial Y\right|}{\partial X_1} \, . \tag{4.6}$$

This, in general, is different from the growth rate of the stream function, given by eqn. (4.4). The question then arises about the "proper measure" for the growth of the disturbance. If one has experimental data to compare with the calculations, one must obviously use the same quantity as that which was observed. Unfortunately no experimental results for the stability of developing flow in a channel are available and those for the pipe flow, obtained by Sarpkaya [48], are, as Sarpkaya himself admits, not free

from the effects of non-axisymmetric disturbances and of finite level amplitude of the disturbances. Moreover, though Sarpkaya mentions that the growth rate of the streamwise component of the disturbance velocity was measured at different radii, he neither reported their magnitude nor the radii at which measurements were made. Since these details could not be obtained [95], it was decided to compute all the growth rates mentioned above as well as the growth rate g_E of the kinetic energy density of the disturbance, defined as

$$g_E(X) \equiv \frac{1}{2}E^{-1}\frac{dE}{dX} = -\alpha_i + \frac{\varepsilon}{2C}\frac{\partial C}{\partial X_1}, \tag{4.7}$$

$$\text{where} \quad E = \frac{1}{2}\int_0^1 (2\pi Y)^m (\overline{u^2} + \overline{v^2})\, dY, \tag{4.8}$$

$$\text{and} \quad C = \int_0^1 \frac{1}{Y^m}(|\beta'|^2 + |k_o|^2|\beta|^2)\, dY. \tag{4.9}$$

Here E represents the mean kinetic energy density, averaged over time and integrated across the flow domain. For the growth rate based on E, we have included a factor of half in the definition so that comparison with other growth rates is possible.

From eqn. (4.1) one notes that not only the growth rate but also the wavenumber is affected by the nonparallelism of the flow. The modified wavenumber for any disturbance property G is obtained from

$$\text{Wavenumber} = \partial[\arg(G)]/\partial X, \tag{4.10}$$

where arg(G) represents the phase of the complex quantity G. One, therefore, gets different wavenumbers for different disturbance properties. The modified wavenumbers $WN_{\psi}(X, Y)$ and $WN_u(X, Y)$ based on the stream function and streamwise component of velocity of the disturbance are respectively given by

$$WN_{\psi}(X, Y) = k_{or} + \varepsilon k_{1r} + \frac{\partial}{\partial X}\left[\arg\left(\frac{i\bar{v}}{k_o}\right)\right], \tag{4.11}$$

$$WN_u(X, Y) = k_{or} + \varepsilon k_{1r} + \frac{\partial}{\partial X}\left[\arg(\bar{u})\right], \tag{4.12}$$

where k_{1r} is the real part of k_1. It was found that the effect of nonparallelism of the flow on the parallel flow wavenumber, k_{or}, is insignificant since k_{or} is much larger than εk_{1r} and the terms representing the effect of streamwise variation of the argument of the eigenfunction. Therefore, the modified wavenumbers, though computed, are not reported here.

Chapter 5

COMPUTATIONAL PROCEDURE AND DETAILS

In this chapter we first describe a comparison of the various methods available for controlling the parasitic errors accruing during numerical integration. This is followed by details of the method found to be most efficient and economical and a brief outline of a technique to search for eigenvalues on the complex k_o-plane. The chapter is closed with computational details.

5.1. Comparison of Various Methods to Control the Parasitic Error

Equations (3.12) through (3.14) with (3.16) or (3.17) can be integrated by any of the suitable integration schemes available. In the case of pipe flow, L'Hospital rule is used to simplify the terms involving Y in the denominator for starting the integration of these equations. One can take advantage of the linearity of the equations to change the two point boundary value problem to an initial value problem using complementary functions [96]. Since two boundary conditions are provided at Y = 0 as well as at Y = 1, we get two solution vectors irrespective of the end from which integration may start. If we start integration from Y = 0 for given values of R, ω and an initial guess for k_o with the

initial linearly independent and orthonormal solution vectors, (1, 0, 0, 0) and (0, 0, 1, 0) for the channel or (0, 1, 0, 0) and (0, 0, 0, 1) for the pipe flow stability corresponding to $(\bar{v}, \bar{u}, \bar{u}', \bar{p})$, we get two solutions which may be represented by the subscripts 1 and 2. The boundary conditions on the wall demand that the determinant

$$D \equiv \begin{vmatrix} \bar{u}_1(1) & \bar{u}_2(1) \\ \bar{v}_1(1) & \bar{v}_2(1) \end{vmatrix} \tag{5.1}$$

must vanish. This condition determines the eigenvalue k_o.

The above method, though mathematically exact, fails to give any meaningful results when applied as a numerical procedure due to the parasitic growth of one of the two independent solutions, specially when the Reynolds number is large, say a few thousand, as is true in most of the hydrodynamic stability problems including the present ones. For this reason Kaplan [97] filtered out a part of the growing solution from the slowly growing solution at each step of the integration. Davey [7] cleverly circumvented the situation by dividing the integration range into a number of steps, say c, integrating the given differential equation separately for the range of each step starting everytime from the same set of linearly independent and orthonormal vectors and finally combining the solution vectors obtained at the end of each step which he called as transfer

matrices. Godunov [98] and Bellman and Kalaba [99] independently used the Gram-Schmidt orthonormalization procedure to make the solution vectors linearly independent during numerical integration. This method has also been used and discussed by Conte [100], Wazzan, Okamura and Smith [58], Roberts and Shipman [96], Scott and Watts [101], and Huang [102].

We tried all the above techniques with the fourth order Runge-Kutta integration scheme for the channel flow since this was the first flow geometry considered during computation. We also used the method described by Lee and Reynolds [103]. Table 5.1 shows the approximate time

Table 5.1. Comparison of different methods.

S. No.	Method of	Time/ iteration (second)	Upper limit of Rk_{or}
1.	Lee and Reynolds [103]	30	Not determined
2.	Davey [7]	5.5	60000 with c = 1
3.	Kaplan [97]	5.4	28000
4.	Gram-Schmidt [104] for eqns. (2.20) with (2.23)	3.3-3.5*	Convergence becomes slow at high R and ω
5.	Gram-Schmidt for eqns. (3.12) to (3.14) with (3.16)	2.5-3.2*	No limit

* Actual value depends on the number of orthonormalizations.

required by the different methods for one iteration on IBM 7044 computer in double precision mode with the step size of 0.01; eqns. (2.20) with (2.23) being integrated. Also given in this table is the time required per iteration while integrating eqns. (3.12) through (3.14) with (3.16) as a set of three simultaneous equations using the Gram-Schmidt orthonormalization procedure as well as the approximate upper limit of the product Rk_{or} upto which the different methods worked satisfactorily.

Lee and Reynolds method was used in the initial stage and was soon given up as it takes sufficiently large computation time and convergence to the eigenvalue is very poor. Davey [7] proposes that his method can be used upto very high values of Reynolds number by choosing c properly. However, in comparison to the Gram-Schmidt orthonormalization procedure, it not only takes more time but also leads to a highly involved procedure for determining the eigenfunctions. Kaplan's filter technique besides requiring more computation time suffers from two disadvantages. These are:

(i) It fails when the range of integration contains more than one region in which viscous forces are important, as pointed out by Sharma [105]. Thus in the case of pipe flow where there are two viscous regions, one near the boundary wall and one away from the wall, the integration will be inaccurate over the wide range

between the two viscous regions. Sharma suggests that whatever filter one uses in Kaplan's technique in such cases, integration through a viscous region will be inaccurate. Davey and Nguyen [106] found that for the central mode in pipe flow stability analysis, Kaplan's method did not work at all.

(ii) It cannot be used at high Reynolds numbers and it is rather cumbersome to use for a higher order differential system when a multiple filtration is required.

From Table 5.1 it is observed that the Gram-Schmidt orthonormalization procedure is the best possible method amongst the various methods available. This view is also supported by Gersting, Jr. and Jankowski [107], which came to our notice after our tests with various methods were over.

Table 5.1 also reveals that integration of eqns. (3.12) through (3.14) instead of a single Orr-Sommerfeld eqn. (2.20) is economical. It was observed that for the given values of ω, R and the same initial guess for k_o there was a significant decrease in the number of points at which orthonormalization was necessary as we switched over from the integration of Orr-Sommerfeld equation to the integration of the set of eqns. (3.12) through (3.14). This implies less number of computations, less round off error and hence better accuracy. It was also observed that for the same starting value, the number of iterations required

for convergence to the true eigenvalue is decreased, thus requiring less time to compute the eigenvalue when eqns. (3.12) through (3.14) are integrated. In a recent publication, Antia [108] points out that in hydrodynamic stability problems the elimination of variables to get higher order equations introduces singularities in the resulting equations and so the numerical treatment becomes difficult.

The results reported here for the channel as well as pipe flows were, therefore, obtained by integrating eqns. (3.12) through (3.14) using the Gram-Schmidt orthonormalization procedure described briefly in the next section along with the improvement for iteration to the eigenvalue. This enabled us to determine the eigenvalue k_o for Reynolds number upto 10^6 without any difficulty.

5.2. Gram-Schmidt Orthonormalization Procedure

The basic idea in this procedure is that during the integration the base vectors are orthonormalized each time the vectors start to lose their numerical independence as judged by a specified orthonormalization criterion. The orthonormalized solutions, defined on various subintervals, are then pieced together to obtain the desired solution. In the following sections, we discuss the procedure, determination of eigenfunctions, orthonormalization criterion and the application of the method to an eigenvalue problem.

5.2.1. Procedure

We choose n steps of uniform mesh size ΔY for the region $0 \leqslant Y \leqslant 1$ and apply any standard integration method to obtain the base solutions $\underset{\sim}{S}(Y) = [\underset{\sim}{s}^1, \underset{\sim}{s}^2]$ at the mesh points $Y_o, Y_1, \ldots, Y_n$; the superscript denoting the column number of the matrix. For example, $\underset{\sim}{s}^1$ and $\underset{\sim}{s}^2$ may be taken as

$$\underset{\sim}{s}^j = [\bar{v}_j, \bar{u}_j, \bar{u}'_j, \bar{p}_j]^T , \qquad (j = 1, 2) . \tag{5.2}$$

We examine these solutions at each mesh point as we integrate and when the base solutions exceed certain orthonormalization criterion (cf. Section 5.2.3) we orthonormalize the solutions. Let Y_i be any such point at which orthonormalization is first done. The matrix of solutions $\underset{\sim}{S}(Y_i)$ is orthonormalized to get $\underset{\sim}{Z}(Y_i)$ where $\underset{\sim}{Z}$ and $\underset{\sim}{S}$ are related by

$$\underset{\sim}{Z}(Y_i) = \underset{\sim}{S}(Y_i)\, \underset{\sim}{B}^i \quad ; \tag{5.3}$$

$\underset{\sim}{B}^i$ being a nonsingular upper triangular matrix with elements b_{ij}. Given the matrix $\underset{\sim}{S}(Y_i)$, we can obtain the matrices $\underset{\sim}{Z}$ and $\underset{\sim}{B}^i$ by applying the Gram-Schmidt recursion formulae (eqns. (5.4)) for orthonormalizing a set of vectors $[\underset{\sim}{s}^1, \underset{\sim}{s}^2]$. Using (,) as the usual notation for inner product of two vectors, we get

$$b_{11} = (\underset{\sim}{s}^1, \underset{\sim}{s}^1)^{-1/2} , \qquad \underset{\sim}{z}^1 = b_{11}\, \underset{\sim}{s}^1 ,$$

$$\underset{\sim}{w} = \underset{\sim}{s}^2 - (\underset{\sim}{s}^2, \underset{\sim}{z}^1)\underset{\sim}{z}^1, \quad b_{22} = (\underset{\sim}{w}, \underset{\sim}{w})^{-1/2}, \quad \underset{\sim}{z}^2 = b_{22}\underset{\sim}{w}, \tag{5.4}$$

$$b_{12} = -(\underset{\sim}{s}^2, \underset{\sim}{z}^1)\, b_{11}b_{22}, \quad \text{and} \quad b_{21} = 0.$$

It is clear that the elements b_{ij} are available as a byproduct during the orthonormalization process. Now we take $\underset{\sim}{Z}$ and not $\underset{\sim}{S}$ as the starting solution for the next step and continue integration.

5.2.2. Eigenfunctions

Due to orthonormalization during integration, the base solutions are changed several times. Let us use the notation $\underset{\sim}{Q}(Y) = [\underset{\sim}{q}^1, \underset{\sim}{q}^2]$ to denote the discrete solution available as a result of this process. Let us also suppose that we encounter b points at which orthonormalization is carried out and that $Y_n = 1$ is the bth orthonormalization point. Note that $b \leqslant n$. At $Y = Y_n$, orthonormalization gives

$$\underset{\sim}{Z}(Y_n) = \underset{\sim}{Q}(Y_n)\, \underset{\sim}{B}^b. \tag{5.5}$$

The function $\underset{\sim}{S}(Y_n)$ at $Y = Y_n$ is now obtained from

$$\underset{\sim}{S}(Y_n) = \underset{\sim}{Z}(Y_n)\, \underset{\sim}{\gamma}^b, \tag{5.6}$$

where $\underset{\sim}{\gamma}^b$ is the solution of the system of equations obtained from the boundary conditions at $Y = 1$. At other mesh points the function is obtained by backward transformation in the following manner. The matrices $\underset{\sim}{B}$ at all the b

orthonormalization points are stored during the forward integration. Then the function $\underset{\sim}{S}(Y_i)$ at any point i between the two consecutive orthonormalization points j and (j-1) is given by

$$\underset{\sim}{S}(Y_i) = \underset{\sim}{Q}(Y_i)\underset{\sim}{\gamma}^j , \qquad Y_{j-1} \leqslant Y_i \leqslant Y_j , \tag{5.7}$$

where $\underset{\sim}{\gamma}^j$ will be a constant vector for all Y_i between the two consecutive points of orthonormalization. As soon as the point i moves to the left of the orthonormalization point (j-1), the vector $\underset{\sim}{\gamma}^{(j-1)}$ is recomputed from

$$\underset{\sim}{\gamma}^{(j-1)} = \underset{\sim}{B}^j \underset{\sim}{\gamma}^j , \qquad j = b, b-1, \ldots, 1 . \tag{5.8}$$

The backward resolution is continued until we arrive at the initial point Y = 0, where an immediate check on the accuracy of the resolution is available by comparison with the boundary conditions at Y = 0.

5.2.3. Orthonormalization Criterion

In the method discussed above, the orthonormalization at each mesh point is neither necessary nor desirable due to loss of some accuracy by too frequent an orthonormalization. Several criteria for determining when orthonormalization is to be performed are available [100, 101]. The easiest criterion to implement and very inexpensive to compute is the one proposed by Conte [100] that requires an orthonormalization to be carried out whenever the magnitude of any vector $\underset{\sim}{S}(Y)$ exceeds a preassigned constant K, that is, whenever

$$\max_{j} (\underset{\sim}{s}^{j}, \underset{\sim}{s}^{j})^{1/2} > K , \quad (j = 1, 2) . \tag{5.9}$$

The constant K depends in some way upon the magnitude of the expected solution and is, therefore, highly problem-dependent as pointed out by Scott and Watts [101]. However, for the present problems, we found that taking K as 100 works very well.

5.2.4. Application to Eigenvalue Problems

While discussing an eigenvalue problem involving the Schrödinger equation, Conte [100] suggested that the orthonormalization be the same for all iterations to the eigenvalue. He, therefore, proposed that the set of b orthonormalization points and the corresponding matrices $\underset{\sim}{B}$ should be determined for the first choice of the eigenvalue and thereafter the same matrices at the corresponding points should be applied for all successive iterations. While this is a sound suggestion in order for the successive approximations to the eigenvalue to be consistent, it works only if the eigenvalues of the system of differential equations are not too widely separated. For hydrodynamic stability problems, it implies that Conte's above suggestion fails for relatively high values of the Reynolds number. What happens is that if the matrices $\underset{\sim}{B}$ (even at the same set of b orthonormalization points as for the first choice of the eigenvalue) are determined for successive iterations,

they are found to change from one iteration to the other. Thus, if the same matrices $\underset{\sim}{B}$ are kept for successive iterations as for the first one, proper orthonormalization of the solution during successive iterations is not possible resulting in "overflows". However, if the matrices $\underset{\sim}{B}$ are determined anew for every iteration, proper account for it will have to be kept so that successive approximations to the eigenvalue are consistent. The following method is therefore adopted.

For an eigenvalue problem, the starting value of $\underset{\sim}{S}(0)$ is taken as

$$\underset{\sim}{S}(0) = \begin{bmatrix} \underset{\sim}{S}_1 \\ \underset{\sim}{S}_2 \end{bmatrix} , \qquad (5.10)$$

where let $\underset{\sim}{S}_1$ be a (2 x 2) null matrix and $\underset{\sim}{S}_2$ be a (2 x 2) identity matrix. Every orthonormalization changes the initial matrix $\underset{\sim}{S}(0)$ by making $\underset{\sim}{S}_2$ an upper triangular matrix [99], while $\underset{\sim}{S}_1$ remains a null matrix. We are concerned only with the changes in the values of the diagonal elements s_{jj} of $\underset{\sim}{S}_2$. Clearly, s_{jj} is, in effect, multiplied by b_{jj}, (j = 1, 2), each time an orthonormalization is carried out. The boundary conditions at Y = 1 are generally satisfied, for an eigenvalue, by setting an appropriate determinant, such as D in eqn. (5.1), to zero. The value of this determinant depends on the initial values $\underset{\sim}{S}(0)$ and thus on the values of the diagonal elements s_{jj} of $\underset{\sim}{S}_2$. Therefore, for

the successive iterations to the eigenvalue to be consistent, the determinant D should take into account the changes in s_{jj} due to orthonormalization. This is achieved by dividing D by the product of all b_{jj}, (j = 1, 2), for all the b orthonormalizations during any iteration. Thus if

$$N = \prod_{i=1}^{b} \prod_{j=1}^{2} b_{jj}^{i} , \tag{5.11}$$

where the superscript on b_{jj} represents the latter's value for the ith orthonormalization, the determinant D/N will correspond, during each iteration, to $s_{jj} = 1$, (j = 1, 2), and successive iterations will be consistent.

While the above technique is mathematically correct, a practical difficulty may arise in computing the value of N since some, if not all, of the b values of b_{jj} are of order (K^{-1}). A direct use of eqn. (5.11) to find N may, therefore, result in "underflow" on the computer. To avoid this, N was found from

$$N = \prod_{i=1}^{b} N_o \prod_{j=1}^{2} b_{jj}^{i} , \tag{5.12}$$

where N_o is a fixed constant of order (K). Like K, N_o is dependent on the problem. For K = 100, N_o = 140 for the channel flow and N_o = 100 for the pipe flow worked very well at all axial locations, Reynolds numbers and frequencies except at $\bar{X} = X/R = 0.0005$ for the pipe flow where N_o was taken as 130.

While using eqn. (5.12), we must make sure that the number of orthonormalizations, b, is the same for every successive iteration to the eigenvalue, or that N_o is used the same number of times during every iteration. If it is not so, proper account must be kept in order to make successive iterations meaningful. In fact, the set of b orthonormalization points may be found for the first iteration and thereafter kept same for the successive iterations.

5.3. Eigenvalue Search Technique

For the pipe flow case, a few eigenvalues of the Hornbeck profile for different R and ω at a given axial location were determined by using the eigenvalue search technique [40]. Although a complicated technique for isolating a number of these eigenvalues simultaneously rather than one at a time has been developed by Delves and Lyness [109], it was not used for the present problem because the main purpose here was not to find a number of stable eigenvalues but to determine the unstable eigenvalue, if any.

The search technique follows directly from the argument principle in complex-variable theory. For a complex function f(z), analytical except for poles in the interior of a closed curve C in the complex z-plane and for f(z) and its first derivative continuous on C, Cauchy's theorem gives

$$N - P = \frac{1}{2\pi i} \int_C \frac{\frac{d}{dz}[f(z)]}{f(z)} dz ,$$

$$\text{or} \qquad N - P = 2\pi i \, M/2\pi i = M , \tag{5.13}$$

where N and P denote respectively the number of zeros and poles of f(z) within the closed region C (counted with their multiplicities) and M is an integer denoting the net multiple of 2π by which the phase angle of f(z) changes as z moves once around on C.

For either flow stability, each element of the determinant D in eqn. (5.1) is a function of the complex eigenvalue k_o, and this function has no poles [40], that is, $P \equiv 0$ in eqn. (5.13) and $N = M$. Thus the problem of finding the number of eigenvalues within a closed region of the k_o-plane is equivalent to counting the net multiples of 2π by which the phase angle of the determinant changes as k_o assumes values on a closed contour in the k_o-plane.

For the stability of the Hornbeck profile in the pipe, some regions of the fourth quadrant on the k_o-plane were examined by the above technique for possible (unstable) eigenvalues at a few selected values of ω, R and X. If an eigenvalue was indicated, it was bracketed by dividing the region into smaller subregions until Muller's iteration converged to the true eigenvalue. For other stability problems, use of this technique was not required as some starting values were available.

5.4. Computational Details

In order to select an appropriate step size for the fourth order Runge-Kutta method some eigenvalues (k_o) were determined for the channel flow at different X, and at each X for a few combinations of R and ω with three step sizes of $\Delta Y = 0.01$, 0.005 and 0.0025. The error in the eigenvalue with the smaller step size was then calculated from [110]

$$\text{error in eigenvalue with the smaller step size} = \frac{(k_o)_{\Delta Y} - (k_o)_{\Delta Y/2}}{2^L - 1}, \qquad (5.14)$$

where L is the order of the integration method and $(k_o)_{\Delta Y}$ and $(k_o)_{\Delta Y/2}$ are the eigenvalues determined with the step sizes ΔY and $\Delta Y/2$, respectively. The error in the eigenvalue with $\Delta Y = 0.0025$ was found to be of the order of 10^{-5} or less in both the real and imaginary parts of k_o. This error was much less than that in the eigenvalue obtained with $\Delta Y = 0.005$. It was also observed that the computation time per iteration was almost doubled as the step size was halved. Therefore, a compromise between computer time and accuracy was made and a step size of 0.0025 was selected. Muller's method [111] was used for iteration to the eigenvalue. It is an iterative procedure for finding the real and complex roots of a polynomial equation whose coefficients may be complex. This procedure selects three arbitrary points as the starting values. The next

approximation to the root is taken to be one of the zeros of the second degree polynomial which passes through the functional values corresponding to three selected points. The iterative procedure is continued by dropping the first point and considering the second point as the first point, the third point as the second point and the new point obtained above as the third point. The advantages of this method are: (i) the complex roots can be obtained; (ii) the iteration requires only the evaluation of functional values and does not include the value of the derivatives of the function; and (iii) after the three initial estimates have been processed, only a single pass through the integration procedure is required for each iteration.

Since the introduction of the factor N_o for maintaining consistency between successive iterations makes the determinant D (eqn. (5.1)) dependent on N_o and hence arbitrary to some extent, the following convergence criterion, instead of making D less than a preassigned value, was used:

$$\frac{|\Delta k_o|}{|k_o|} < \delta \quad , \tag{5.15}$$

where Δk_o is the difference between the eigenvalues of the last two iterations and δ is some preassigned constant. For the accuracy mentioned above, δ was taken as 10^{-6}. In almost all the cases, convergence was achieved in 3-4 iterations. While determining the neutral points, further iteration was terminated when $|k_{oi}|$ became less than 10^{-6}.

While finding the eigenvalues for the Hornbeck profile, the eigenvalue search technique described in Section 5.3 had to be used in a few initial cases since it was not possible to achieve convergence while starting with the values for the Sparrow profile.

For calculating velocity profiles in the entrance region of the channel and pipe by the Sparrow method, eqns. (A.14) and (A.16) respectively were used. The Bessel functions J_o and J_1 for real arguments, appearing in eqns. (A.14) & (A.16), were computed using Garg's programme [112] which was simplified to suit our requirements. The infinite series in eqns. (A.14) or (A.16) was terminated when the ratio of the last term retained to the partial sum of all previous terms became less than 10^{-18}. The velocity gradients were determined by evaluating the relations obtained by differentiating the eqns. (A.14) or (A.16). Fifty values of λ_i were obtained for both the channel and pipe flow by using Muller's root finder [111] for solution of the characteristic eqns. (A.15) and (A.17). These roots are tabulated in Table A1.

For calculating the velocity field at different cross-sections by the finite difference method, eqns. (A.6) through (A.8) were solved with $\Delta Y = 0.0025$ at all cross-sections and $\Delta\bar{X} = 10^{-5}$, 10^{-4}, 5×10^{-4} for $0 < \bar{X} \leq 0.01$, $0.01 < \bar{X} \leq 0.1$ and $0.1 < \bar{X} \leq 0.2$, respectively. This axial spacing was decided on the basis of our efforts to

reproduce the velocity profile given by Hornbeck [113] for both the flow problems. The velocity gradients were determined by use of central differences involving an error of $O(\Delta Y^2)$. For use during the Runge-Kutta integration the velocity at the mid-step points, such as the point Q in Figure 5.1, was determined by taking the average of the velocities at the point Q obtained by quadratic interpolation first from the known velocities at step points A, B and C and then from the known velocities at points B, C and D. This procedure was

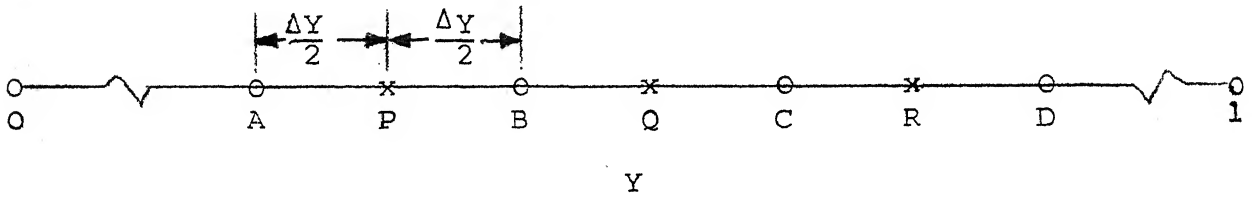

Fig. 5.1 Some step and mid-step points in the range of integration.

adopted after careful numerical experimentation in which velocity at step points like B, D, etc. was calculated while treating them as mid-step points. It was found that the above procedure resulted in values which differed from the actual velocities at these points in the 7th or 8th decimal place. Linear or simple quadratic interpolation resulted in much larger error. However, at the mid-step point $(1 - \Delta Y/2)$, the velocity was determined by simple quadratic interpolation only.

Once k_o, β, and β^* were found, dk_o/dX_1 was calculated from eqn. (3.10) using fifth order composite Newton-Cotes quadrature formula [114] for finding the integrals numerically. The values of $\partial\beta/\partial X_1$ are then given by the integration of eqns. (3.9). It may be noted that for the pipe flow case, the integrands in eqn. (3.6) vanish at Y = 0. Also L'Hospital rule is used to simplify the expressions for A_1 and A_2 at Y = 0 in eqns. (3.9c, d) for starting the integration of eqn. (3.10).

For given ω and R, eqns. (3.12) through (3.14) with (3.16) for channel and (3.17) for pipe case were also solved to yield $k_o(X_1)$, β and its Y derivatives at three axial locations $\bar{X} - \Delta\bar{X}$, $\bar{X}$ and $\bar{X} + \Delta\bar{X}$; $\Delta\bar{X}$ being taken as 10^{-5}. Using central differences involving an error of $O(R^{1/2}\,\Delta\bar{X})^2$, $\delta k_o/\delta X_1$ and $\delta\beta/\delta X_1$ were then obtained. It was found that the values of $\delta k_o/\delta X_1$ and dk_o/dX_1 were in agreement within computational accuracy. Also $\delta\beta/\delta X_1$ and $\partial\beta/\partial X_1$ were in agreement at every point in the flow domain.

Calculations were performed partly on an IBM 7044 computer and partly on a DEC 1090 computer for the channel flow stability and completely on the DEC 1090 computer for the pipe flow stability problem. The computation was done in double precision mode. Both the computers carry 17 digits in this mode. A FORTRAN 10 version of the computer programme for nonparallel pipe flow stability is listed in Appendix D.

Chapter 6

RESULTS AND DISCUSSION

The computation for determining the spatial stability behaviour of the developing flow in a two dimensional parallel plate channel and in a rigid circular pipe was done in three stages, viz., (i) the determination of velocity field at 401 equi-spaced points along the Y direction by the finite difference and linearization methods, (ii) the integration of the continuity and momentum equations for the disturbances superimposed on the developing flow, assumed parallel for this purpose, and (iii) the determination of various growth rates based on different disturbance properties for the actual nonparallel flow. The following sections discuss the results in this order. Since the velocity profiles were computed at some preselected values of $\bar{X}$ instead of X, the growth rates, reported herein, were also obtained at various $\bar{X}$, and hence they are, hereafter, referred to as functions of $\bar{X}$ instead of X; $\bar{X}$ being X/R.

6.1. Parallel Plate Channel

Spatial stability results have been obtained for the B-O profile at several values of $\bar{X}$ and also for the

Sparrow profile at three values of $\bar{X}$ for checking our computer programme and for determining the effect of different velocity profiles on the stability characteristics of the flow.

6.1.1. Developing Velocity Field

Figure 6.1 shows the velocity and its first derivative with Y obtained by the methods suggested by Bodoia and Osterle and by Sparrow et al. at $\bar{X} = 0.00208$ ($X^* = 0.005$) and at $\bar{X} = 0.00408$ ($X^* = 0.009$). It is observed that the two velocity profiles differ more from each other near the boundary layer edge but the maximum difference is within 5% at $\bar{X} = 0.00208$. The velocity gradients also differ considerably near the channel wall and the boundary layer edge; the difference near the boundary layer edge being as much as 100%. The velocity gradient for the B-O profile is larger than that for the Sparrow profile near the channel wall but falls below it mid-way through the boundary layer thickness. These differences decrease with increasing $\bar{X}$. At $\bar{X} = 0.08393$ ($X^* = 0.10$) the two methods give almost the same velocity field. The B-O and Sparrow velocity profiles at some values of $\bar{X}$ are shown in Figure 6.2, and are also tabulated in Tables A3 and A4.

6.1.2. Parallel Flow Instability to Symmetric and Antisymmetric Disturbances

Grohne [94] has shown that for fully developed flows having symmetric velocity distribution, symmetric

disturbances are more unstable. However, it was decided to verify this statement in the case of developing flow through a channel. Therefore, eqns. (3.12) through (3.14) with the boundary conditions (3.16) for symmetric disturbance or (3.17) for antisymmetric disturbance were integrated to get eigenvalues for the unstable modes for different combinations of ω and R at several axial locations. Figures 6.3 and 6.4 show the neutral curves (ω vs. R) and(k_{or} vs. R) at $\bar{X}$ = 0.004, 0.006 and 0.008 for symmetric and antisymmetric disturbances. Tables B1 and B2 give the values of frequency and wavenumber corresponding to the neutral points at different $\bar{X}$ and at each $\bar{X}$ for different Reynolds number for both types of disturbances. It is observed from these tables that at $\bar{X}$ = 0.001 and 0.002 the difference in the neutral point values of ω and k_{or} at any R for symmetric and antisymmetric disturbances is too small to be displayed graphically. As $\bar{X}$ increases the difference in the two neutral curves increases and their lower branches cross each other meaning thereby that there exist some eigenstates which are more unstable for antisymmetric disturbances. However, the critical Reynolds number is smaller at all $\bar{X}$ for the symmetric disturbances. Further, the difference between the critical Reynolds numbers for symmetric and antisymmetric disturbances increases as $\bar{X}$ increases. This is quite evident from Figure 6.5 which

shows the variation of R_c, ω_c and k_{or_c} with $\bar{X}$ for both types of disturbances. It is clear that the difference between critical frequencies and wavenumbers for the two types of disturbances also increases with $\bar{X}$. The critical Reynolds number for symmetric disturbances continues to decrease while that for antisymmetric disturbances passes through a minimum value of about 12100 at $\bar{X}$ = 0.005 and then increases rapidly. It is, therefore, expected that the fully developed flow will be stable to antisymmetric disturbances. It is thus obvious that the developing flow in a channel is more unstable to symmetric disturbances in comparison to antisymmetric disturbances except for a few eigenstates in the near entry region. However, we need consider only the symmetric disturbances so far as our interest is in finding the critical values.

6.1.3. Effect of Velocity Distribution on Parallel Flow Instability – Symmetric Disturbances

The variation of critical Reynolds number with $\bar{X}$ and with X for the present analysis of the B-O profile and for Chen's temporal stability analysis [115] of the Sparrow profile using the finite difference scheme of Thomas [3] is shown in Figures 6.6 and 6.7. It is seen that the critical Reynolds number for the two profiles differ significantly in the region close to the entrance plane where the B-O profile gives a lower critical Reynolds number.

At X = 60 the critical Reynolds number for the B-O profile is about 10900 which is almost half of that for the Sparrow profile. This difference between the R_c values decreases as $\bar{X}$ (or X) increases to $\bar{X} \simeq 0.084$ (or $X \simeq 440$) where the two curves appear to coincide with each other and remain so thereafter. Such a behaviour is to be expected since the two velocity profiles, as noted above, merge into one at $\bar{X} \simeq 0.084$. One, therefore, draws the conclusion that the larger difference in critical Reynolds number in the near entry region is due to the difference in the two velocity profiles. The three points marked ⊙ on Figures 6.6 and 6.7, obtained for the Sparrow profile by the present technique, serve as a very good check for the present method. Chen [115] used several methods including the finite difference method of Thomas [3]. Though Chen himself regarded the finite difference method to be most accurate, it is strange that very few results reported by him were obtained by the finite difference method.

Figure 6.8, where the neutral curves for the present analysis at two values of $\bar{X}$ (both for the B-O and Sparrow profiles) as well as those of Chen obtained from the regular viscous solutions for the full channel profile, i.e., the Sparrow profile, have been brought together, shows further the effects of the difference in the two velocity profiles on the stability characteristics of the

flow. The data for the Sparrow profile are given in Table B3. The neutral curves for the B-O profile encompass more unstable region. Therefore, the flow with the B-O profile is unstable for a wider range of frequencies at a given axial location and Reynolds number. Figure 6.8 also shows the difference in the neutral curves for the same (Sparrow) profile obtained by two different methods. Recalling the above discussion on Figures 6.6 and 6.7, we note that our results, even for the Sparrow profile, are more accurate than those of Chen shown in Figure 6.8. Chen [115] gives several tables of data for the neutral curves obtained by the asymptotic method of Heisenberg [116], viz., the regular viscous and composite solutions for the full channel profile, and for the velocity profile obtained by treating the developing flow as a boundary layer. All of these neutral points are less accurate than those obtained by the present analysis or by the finite difference method used by Chen. Chen's neutral curves obtained from the regular viscous solution for the full channel profile are found to be closest to the present results, and are, therefore, included in Figure 6.8 for comparison. Besides, Chen's analysis is for temporal stability while the present work considers the more realistic spatial stability of the flow. Figure 6.9 shows the neutral curves (k_{or} vs. R) at $\bar{X}$ = 0.00208 and 0.00408 for the B-O and Sparrow profiles

obtained by the present analysis. The same trend as noted for Figure 6.8 is observed.

The neutral curves, (ω vs. R) and (k_{or} vs. R), at various values of $\bar{X}$ are shown in Figures 6.10 and 6.11. It is observed that the Reynolds number, frequency and wavenumber at the critical point and area of the unstable region decrease with increasing $\bar{X}$. The slope of the lower branch of the neutral stability curve is very large at $\bar{X}$ = 0.001 and it decreases with increasing $\bar{X}$ whereas the upper branch of the neutral curve is almost flat at all $\bar{X}$. The critical Reynolds number for the fully developed flow was found to be 3848.1, which agrees very well with the value of 5772.22 reported by Davey [117] and Orszag [5], after multiplying it by the factor of 1.5, since we have used average velocity in place of the maximum velocity as the reference velocity for nondimensionalization. Variation of the critical wavenumber and frequency with $\bar{X}$ is shown in Figure 6.12. One notes that the critical frequency and wavenumber decrease with increasing axial distance in the entrance region and approach asymptotically the corresponding values for the fully developed flow; the two curves being nearly parallel.

Figure 6.13 shows a representative variation of k_{or} vs. ω at $\bar{X}$ = 0.001, 0.002, 0.004 and 0.008 for R = 16000. and at $\bar{X}$ = 0.001 for R = 18000 and 20000. One notes that the different curves are almost parallel. This

behaviour helps a great deal in determining the guess value of k_{or} so that convergence is easily achieved.

Figure 6.14 displays the real and imaginary parts of the eigenfunctions for the streamwise and transverse components of the disturbance velocity at $\bar{X} = 0.001$. These have been normalized with respect to their respective maximum absolute values; the ratio of $|\bar{u}|_{max}$ to $|\bar{v}|_{max}$ being 13.93. It is obvious that the boundary conditions (3.16) are satisfied.

6.1.4. Effects of Nonparallelism of the Flow

Growth rates based on u, ψ and E were obtained at $\bar{X} = 0.001$, 0.002, 0.004, 0.006 and 0.008. Figure 6.15 shows g_ψ, the growth rate based on ψ, as a function of Y for different combinations of $\bar{X}$, R and ω. It is clear that in the region near the channel wall the dependence of g_ψ on Y is quite strong. It is also observed that the maximum growth rate occurs at the centre line of the channel. While g_ψ decreases gradually and uniformly with Y upto the boundary layer edge for all combinations of $\bar{X}$, R and ω, its variation beyond this point depends on the values of $\bar{X}$ and upon the position of the (ω, R) point relative to the neutral curve on the ω - R plot. If the selected combination of R and ω lies close to the neutral curve, g_ψ decreases suddenly near the boundary layer edge and then increases near the channel wall; the magnitude of the depression decreases as

$\bar{X}$ increases or as one goes into the stable region away from the neutral curve. Maximum depression in the growth rate curve at any $\bar{X}$ and R is found to occur at frequencies midway between those corresponding to the upper and lower branches of the neutral curve. The location of this depression shifts with R and ω at a fixed $\bar{X}$.

Since g_ψ is maximum at the centre line, it, $g_\psi\ (\bar{X},0)$, is compared with other growth rates such as that obtained from the parallel flow theory, $-k_{oi}$, that of u at the centre line, $g_u(\bar{X}, 0)$, and that of kinetic energy of the disturbance, $g_E(\bar{X})$, in Figure 6.16 for $\bar{X}$ = 0.001 and R = 16000. It is observed that for any ω, $g_\psi\ (\bar{X}, 0)$ is maximum and is positive for the widest range of frequencies. The growth rates based on ψ and u at the centre line of the channel, on the energy E of the disturbance and on the parallel flow theory for different Reynolds numbers and frequencies, and at different $\bar{X}$ are tabulated in Table B4. Figures 6.17 through 6.21 show variation of these different growth rates with ω at $\bar{X}$ = 0.001, 0.002, 0.004, 0.006 and 0.008 respectively for different Reynolds numbers. One can see that the above conclusion is true for all combinations of $\bar{X}$ and R.

The neutral points corresponding to various disturbance properties can be easily found from Figures 6.17 through 6.21 as they correspond to growth rate being zero. The peaks of the growth rate curves for a disturbance

property at any $\bar{X}$ may be joined; the intersection of such a curve with the ω -axis determines the critical frequency. The critical Reynolds number for the same disturbance property at any $\bar{X}$ is then obtained by plotting its maximum growth rate at that $\bar{X}$ against R (see Figure 6.22) and reading the intercept of the curve with the R-axis. The data corresponding to the neutral and critical points obtained by this procedure are tabulated in Table B5. Figure 6.23 shows the different neutral curves, at different $\bar{X}$, based on (i) g_ψ at the centre line of the channel, (ii) growth of energy of the disturbance and (iii) the parallel-flow theory. Also shown is the neutral curve based on g_u at the centre line of the channel only at $\bar{X} = 0.001$ since it is little different from that corresponding to g_ψ $(\bar{X}, 0)$. It is observed that the neutral curves are different for different flow quantities. However, the difference between the neutral curves corresponding to different disturbance properties decreases as $\bar{X}$ increases. The nonparallel effects make the flow unstable at lower Reynolds number and for a wider range of frequencies compared to those obtained from the parallel flow theory. The actual amount of such an effect depends on the choice of growth rate used for determining the neutral curve. The growth rate g_ψ $(\bar{X}, 0)$ gives the minimum critical Reynolds number at all $\bar{X}$.

Figure 6.24 shows the variation of critical frequency, ω_c, and critical Reynolds number, R_c, as obtained on the basis of g_ψ $(\bar{X}, 0)$, g_E and the parallel flow theory against $\bar{X}$. It is found that at $\bar{X} = 0.001$, the R_c predicted by the parallel flow theory is greater than that corresponding to g_ψ $(\bar{X}, 0)$ by 22.8%, and that corresponding to g_E by 4.5%. At $\bar{X} = 0.008$, these differences reduce to 8.3% and 1.6% respectively. This is to be expected since the nonparallel effects must vanish at large $\bar{X}$. Figure 6.25 exhibits a similar behaviour with the physical coordinate X for the critical Reynolds number based on various growth rates (note that Figure 6.24 is a log-log plot). At X = 20.0 the parallel flow theory overpredicts the critical Reynolds numbers by 24.6% and 6.2% as compared to those corresponding to g_ψ $(\bar{X}, 0)$ and g_E, respectively. These differences reduce to 10.4% and 2.5% at X = 75.

6.2. Rigid Circular Pipe

Assuming the developing flow in the pipe to be parallel, spatial stability results have been obtained for both the Hornbeck and Sparrow profiles. However, nonparallel effects are considered only for the better (Hornbeck) profile. While Huang and Chen [45] do give results for temporal stability of the Sparrow profile on the basis of parallel flow approximation, they cannot be

used directly for comparison since the frequency values of the neutral disturbances are not available in Huang and Chen.

6.2.1. Developing Velocity Field

The variation of the basic flow velocity component U and its gradient in the radial direction obtained for the Hornbeck and Sparrow profiles at $\bar{X} = 0.0014$ ($X^* = 0.003$) and at $\bar{X} = 0.00616$ ($X^* = 0.01$) is shown in Figure 6.26. The differences in the two velocity profiles and their gradients are similar to those for the channel flow (cf. Figure 6.1, Section 6.1.1). Figure 6.27 exhibits the development of the Hornbeck's velocity field as the fluid moves downstream. The velocity data for the Hornbeck and Sparrow velocity profiles at different axial locations are shown in Tables A5 and A6, respectively.

6.2.2. Parallel Flow STABILITY– Central Mode

It is well known that the central mode is the least stable mode for the fully developed flow in a pipe. Therefore, the stability of developing flow was also investigated with respect to the central mode. It was found that for the developing flow also, the central mode tends to approach neutral stability as R increases indefinitely and as ω tends to zero. Also for this mode the two parameters ω and R can be combined into one so that their product ωR governs, in an approximate manner, the values of Rk_o.

For the least stable central mode the variations of Rk_{or} and Rk_{oi} with ωR as the independent variable for different values of $\bar{X}$ are shown in Figures 6.28 and 6.29. Though Rk_{or} and Rk_{oi} vary somewhat with different combinations of ω and R such that ωR is constant, these variations for Rk_{or} are too small to be represented graphically on the scale of Figure 6.28 whereas those for Rk_{oi} are shown by a band I in Figure 6.29. It is observed from these figures that while Rk_{or} may be related to ωR by a power law the relationship between ωR and Rk_{oi} is approximately of exponential type at all values of $\bar{X}$. Also at a given value of ωR, k_{oi} decreases while k_{or} increases as $\bar{X}$ decreases. This implies that though the central mode remains stable, it is less stable for the developing flow than for the fully developed flow. For instability of the developing flow, therefore, we consider only the wall mode in the following sub-sections.

6.2.3. Parallel Flow Stability – Wall Mode

Figures 6.30 and 6.31 show the neutral curves, (ω vs. R) and (k_{or} vs. R), at $\bar{X}$ = 0.0005, 0.001, 0.002, 0.00323, 0.0035, 0.004, 0.005 and 0.00616 for the Hornbeck profile and at X^* = 0.002, 0.003, 0.004, 0.006, 0.007, 0.009 and 0.01 for the Sparrow profile. The data corresponding to these neutral curves are also given in Tables C1 and C2 respectively. Our results in Figure 6.31 for the Sparrow

profile do match very well with the (k_{or} - R) curves of Huang and Chen [45]; the comparison of (ω - R) curves, however, is not possible because Huang and Chen carried out the temporal stability analysis and did not report any frequency values. Comparison of the neutral curves for both the velocity profiles at $\bar{X}$ = 0.00323 (X^* = 0.006) and at $\bar{X}$ = 0.00616 (X^* = 0.01) shows that the instability of the developing flow in a pipe is set in at lower Reynolds number and the area of unstable region encompassed by the neutral curves is larger for the Hornbeck profile. Similar results were obtained for the stability of developing flow in a channel and confirm the fact that the flow instability characteristics are very sensitive to the mainflow velocity field. It is also observed that for both the velocity profiles the slope of the lower branch of the neutral curves is quite large at small $\bar{X}$ and that it decreases as $\bar{X}$ increases. While the area of unstable region, critical frequency and wavenumber decrease with increasing $\bar{X}$, the critical Reynolds number first decreases upto a certain $\bar{X}$ and then increases as $\bar{X}$ continues to increase.

Figure 6.32 shows the variation of critical Reynolds number, critical wavenumber and critical frequency with $\bar{X}$ for the Hornbeck and Sparrow profiles. It also contains some experimental results for R_c obtained by Sarpkaya [48]. It is observed that the minimum critical

Reynolds number is about 11700 for the Hornbeck profile, while it is about 19800 for Sparrow profile; the R_c vs. $\bar{X}$ curve for the Hornbeck profile lying well below that for the Sparrow profile (Huang and Chen [45] report a value of 19900 for the minimum R_c). It is, however, felt that the results reported here are more accurate (cf. Section 5.4, since $\Delta Y = 0.0025$ in the present analysis while Huang and Chen took $\Delta Y = 0.005$ upto $\bar{X} = 0.0014$ and increased it to 0.01 at $\bar{X} = 0.00616$). As $\bar{X}$ increases, the critical Reynolds number passes through a minima for both the velocity profiles and this minima occurs in the vicinity of $\bar{X} = 0.0035$. However, the portion of the curve near the minimum R_c is flatter for the Hornbeck profile. The ratio of the critical Reynolds number for the Sparrow and Hornbeck profiles increases from approximately 1.69 at $\bar{X} = 0.0035$ to about 1.84 at $\bar{X} = 0.001$ and to about 2.21 at $\bar{X} = 0.00616$. This implies that the Sparrow profile tends to become stable quite rapidly in comparison to the Hornbeck profile. In other words, the developing flow in a pipe with the Hornbeck profile will exhibit instability in a greater length of the pipe. This agrees partially with the experimental observations of Sarpkaya [48] that the flow remains unstable further downstream than that predicted by Huang and Chen [45]. We also note from Figure 6.32 that Sarpkaya's experimental results for R_c, though well below the R_c vs. $\bar{X}$ curve for the Hornbeck profile, are

still closer to it than to the R_c vs. $\bar{X}$ curve for the Sparrow profile. Since the flow in the developing region is actually nonparallel, it appears that the parallel flow assumption is not quite valid at least in the near entry region. Sarpkaya found the minimum critical Reynolds number to be about 3800 for $\bar{X}$ in the range $0.012 \leq \bar{X} \leq 0.02$. However, as Sarpkaya himself noted, his critical Reynolds number may be low due to the superposition of some non-axisymmetric disturbances on axisymmetric disturbances as well as due to a higher initial disturbance level than that warranted by the linear theory. In terms of physical length X in the entry region, the first instability of the flow is theoretically found to occur at $X \simeq 37$ for the Hornbeck profile and at $X \simeq 64$ for the Sparrow profile, while Sarpkaya's experimental results yield a range of $45 \leq X \leq 75$ for the same. This is evident from Figure 6.33 which further shows that the Hornbeck profile gives results closer to the experimental ones.

One also notes from Figure 6.32 that the critical frequency and critical wavenumber for the Hornbeck profile are larger than the corresponding values for the Sparrow profile at all $\bar{X}$ and that with increasing $\bar{X}$ both decrease first sharply and then gradually. The dimensionless phase velocity, ω / k_{or}, at the critical point increases from 0.42 and 0.37 at $\bar{X} = 0.001$ for the Hornbeck and Sparrow profiles, respectively, to 0.49 and 0.45 at $\bar{X} = 0.00616$.

However, these values are much lower than that for the fully developed flow for which Garg and Rouleau [40] found the phase velocity to be slightly less than 2.0. One may, therefore, surmise that as the flow develops downstream the critical frequency and wavenumber change so that their ratio increases towards the value for the fully developed flow. Unfortunately, Sarpkaya [48] has not provided experimental results for critical frequency corresponding to an axisymmetric disturbance. However, he does tabulate the experimental values of ω_c for non-axisymmetric disturbances and the theoretical values of ω_c obtained by Huang [102] for the Sparrow profile. It appears from the comparative trend of theoretical values of ω_c for the axisymmetric and non-axisymmetric disturbances for the Sparrow profile that the critical frequencies found here for the Hornbeck profile should compare very well with the experimental values for the axisymmetric disturbance.

Sarpkaya [48] points out that his experimentally observed velocity profile agrees with the Sparrow profile to within 5% whereas Figure 6.26 shows that the Hornbeck profile also agrees with the Sparrow profile to within 5% at sections closer to the entry section. It would have been interesting to compare the experimental and Hornbeck velocity profiles, specially when it is found that the Hornbeck profile gives stability characteristics that are

closer to the experimental ones. Unfortunately, however, Sarpkaya's velocity profiles are not available.

Corresponding to the neutral point for $\omega = 1.0$ and $R = 11779$ at $\bar{X} = 0.0035$, Figure 6.34 displays the real and imaginary parts of the eigenfunctions for the X and Y components of the disturbance velocity. These have been normalised with respect to their respective maximum absolute values; the ratio of $|\bar{v}|_{max}$ to $|\bar{u}|_{max}$ being 0.2432. It is obvious that the boundary conditions (3.17) are satisfied.

Figure 6.35 shows a representative variation of k_{or} vs. ω at $\bar{X} = 0.001$ for $R = 16000$, at $\bar{X} = 0.002$ for $R = 14000$ and 16000 in addition to such variations for $R = 18000$ at $\bar{X} = 0.001$, 0.002, 0.00323, 0.004 and 0.005. It is observed that the k_{or} vs. ω plot is almost a straight line and the slope of the straight lines varies little with $\bar{X}$. It is also observed that the slope of these lines at any $\bar{X}$ increases slowly with Reynolds number. This behaviour helps a great deal in determining the starting value of k_{or} close enough to the actual one so that the convergence is achieved in a few iterations.

6.2.4. Effects of Nonparallelism of the Flow

As noted above the only experimental work on the stability of developing flow in a rigid circular pipe is due to Sarpkaya [48]. Though he mentions that the

streamwise component of the disturbance velocity was measured at different radii, he neither reported the magnitude nor the radii at which measurements were made. Since these details could not be obtained [95], it was decided to compute all the growth rates mentioned earlier. Neutral curves were found on the basis of g_E and the values of g_ψ and g_u at the pipe axis since g_ψ and g_u are functions of Y also. However, it is clear from eqns. (4.4) and (4.6), using appropriate boundary conditions at Y = 0, that $g_u(\bar{X}, 0) = g_\psi(\bar{X}, 0)$.

Growth rates based on u, ψ and E were obtained at $\bar{X}$ = 0.0005, 0.001, 0.002, 0.0035, 0.005 and 0.007. Figure 6.36 shows the growth rate based on ψ as a function of Y for different combination of $\bar{X}$, R and ω. It is observed that the maximum growth rate occurs at the pipe axis and the variation of g_ψ with Y is similar to that in the case of developing flow in a channel (cf. Figure 6.15). Thus remarks made in Section 6.1.4 for Figure 6.15 hold here as well.

Figures 6.37 through 6.42 show the variation of $g_\psi(\bar{X}, 0)$ and $g_E(\bar{X}, 0)$ with ω at $\bar{X}$ = 0.0005, 0.001, 0.002, 0.0035, 0.005 and 0.007, respectively, for different Reynolds numbers. Just as for channel flow, it is observed that for any ω at a given $\bar{X}$ and R, $g_\psi(\bar{X}, 0)$ is greater than g_E and is positive for the widest range of frequencies. One can also obtain the data corresponding to the neutral

and critical points in this case following the method outlined in Section 6.1.4 for the channel flow. Figure 6.43 helps in finding the critical Reynolds number in the present case. The neutral and critical points obtained in this way are tabulated in Table C4. Also Figure 6.44 shows the different neutral curves at various $\bar{X}$, based on (i) $g_{\psi}(\bar{X}, 0)$, (ii) $g_E(\bar{X})$ and (iii) the parallel flow theory. Similar to the channel flow case, it is observed that in comparison to the results for the parallel flow theory, the nonparallel effects make the flow unstable at lower Reynolds number and for a wider range of frequencies. The actual amount of such an effect depends on the choice of the growth rate used for determining the neutral curve. The growth rate $g_{\psi}(\bar{X}, 0)$ gives the minimum critical Reynolds number at all $\bar{X}$.

Figure 6.45 shows the variation of the critical frequency, ω_c, and the critical Reynolds number, R_c, as obtained on the basis of $g_{\psi}(\bar{X}, 0)$, $g_E(\bar{X})$, and the parallel flow theory against $\bar{X}$. It is observed that the variation of ω_c with $\bar{X}$ is similar for various disturbance properties; ω_c corresponding to $g_{\psi}(\bar{X}, 0)$ being maximum and that corresponding to the parallel flow theory being minimum. Also, all the R_c vs. $\bar{X}$ curves pass through a minima. The minimum critical Reynolds number corresponding to $g_{\psi}(\bar{X}, 0)$, to $g_E(\bar{X})$, and to the parallel flow theory are 9700 at $\bar{X} = 0.00325$, 11000 at $\bar{X} = 0.0035$, and 11700 at $\bar{X} = 0.0035$,

respectively. In comparison to the results based on $g_{\psi}(\bar{X}, 0)$ and $g_E(\bar{X})$, the parallel flow theory overpredicts the critical Reynolds number by 29.8% and 3.7% respectively at $\bar{X} = 0.0005$, by 20.0% and 6.4% respectively at $\bar{X} = 0.0035$ and by 26.5% and 12.0% respectively at $\bar{X} = 0.007$. This implies that the R_c vs. $\bar{X}$ curves obtained on the basis of nonparallel flow theory are flatter than those corresponding to the parallel flow theory; R_c does increase beyond $\bar{X} = 0.0035$ but not so sharply as for the parallel flow theory. Physically, it means that the actual developing flow is unstable over a larger inlet length of the pipe than its parallel flow approximate. The first instability of the flow on the basis of $g_{\psi}(\bar{X}, 0)$, $g_E(\bar{X})$, and the parallel flow theory is found to occur at $\bar{X} \simeq 33$, 38, and 37 respectively (see Figure 6.46). The R_c vs. $\bar{X}$ or X curve obtained on the basis of $g_{\psi}(\bar{X}, 0)$ is closest to the experimental data of Sarpkaya [48].

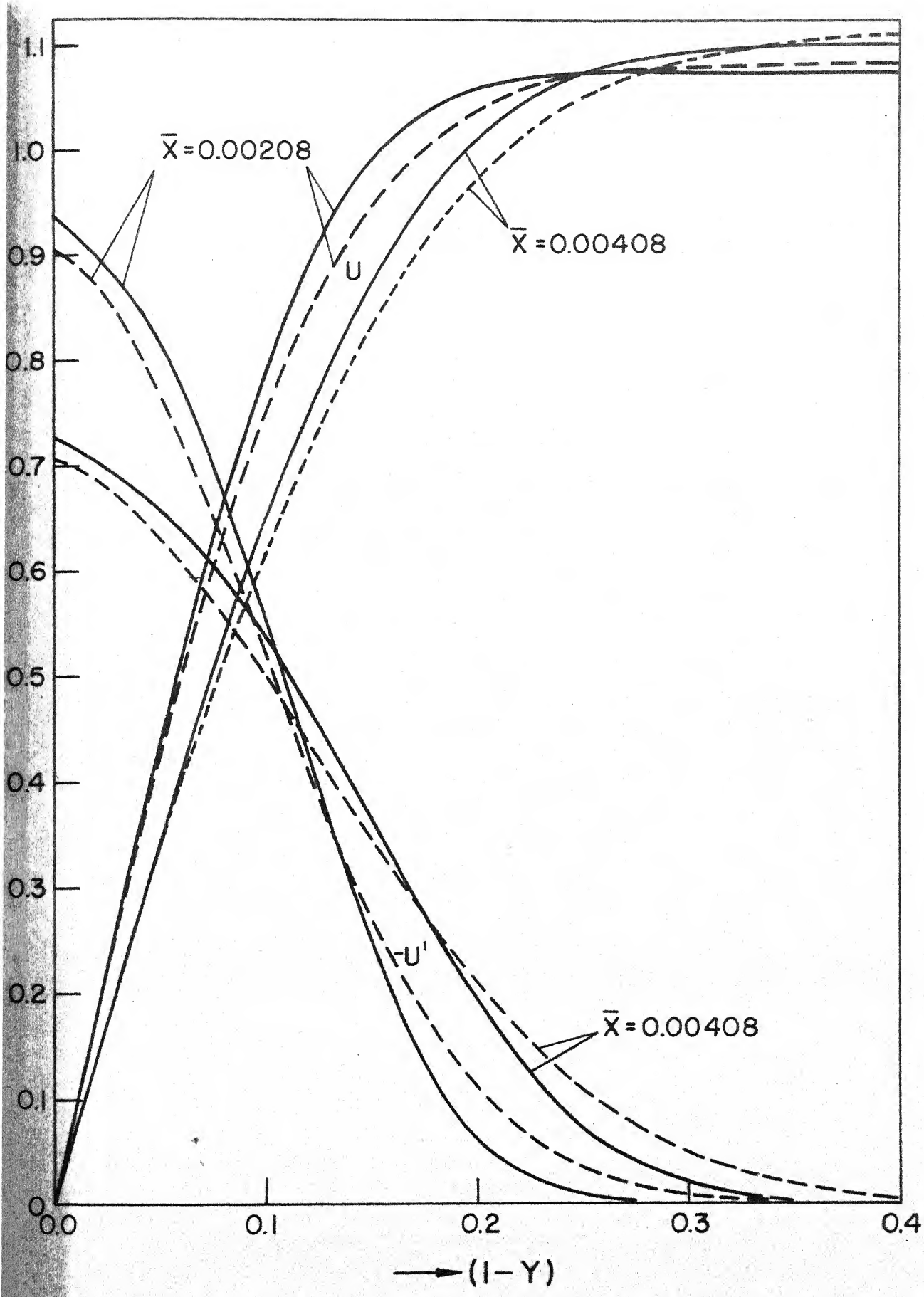

l Developing flow velocity profile and its gradient in a channel at two axial locations.——, present profile; --- Sparrow's profile [19]

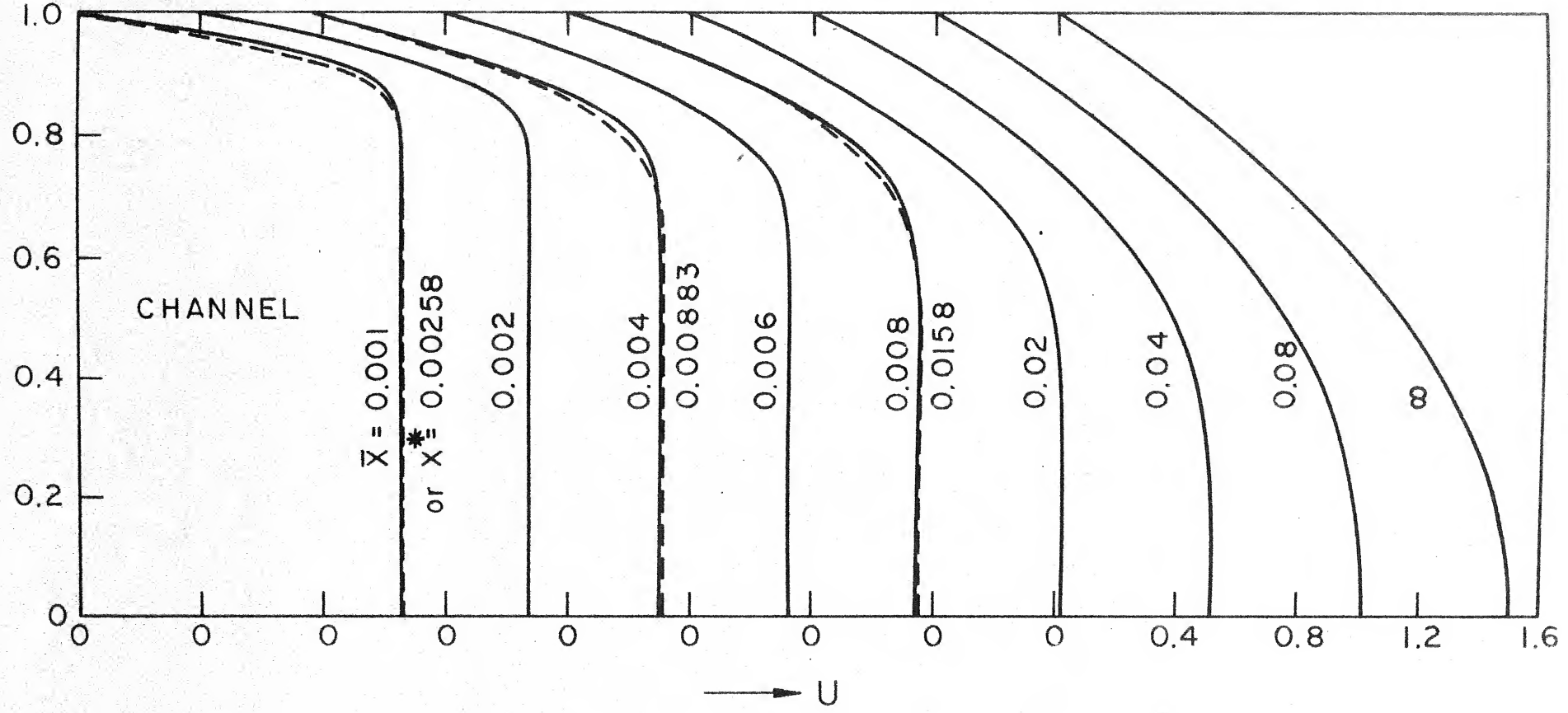

Fig. 6.2 Velocity profiles at several axial locations in a channel. ———, B-O profiles; – – – –, Sparrow's profiles

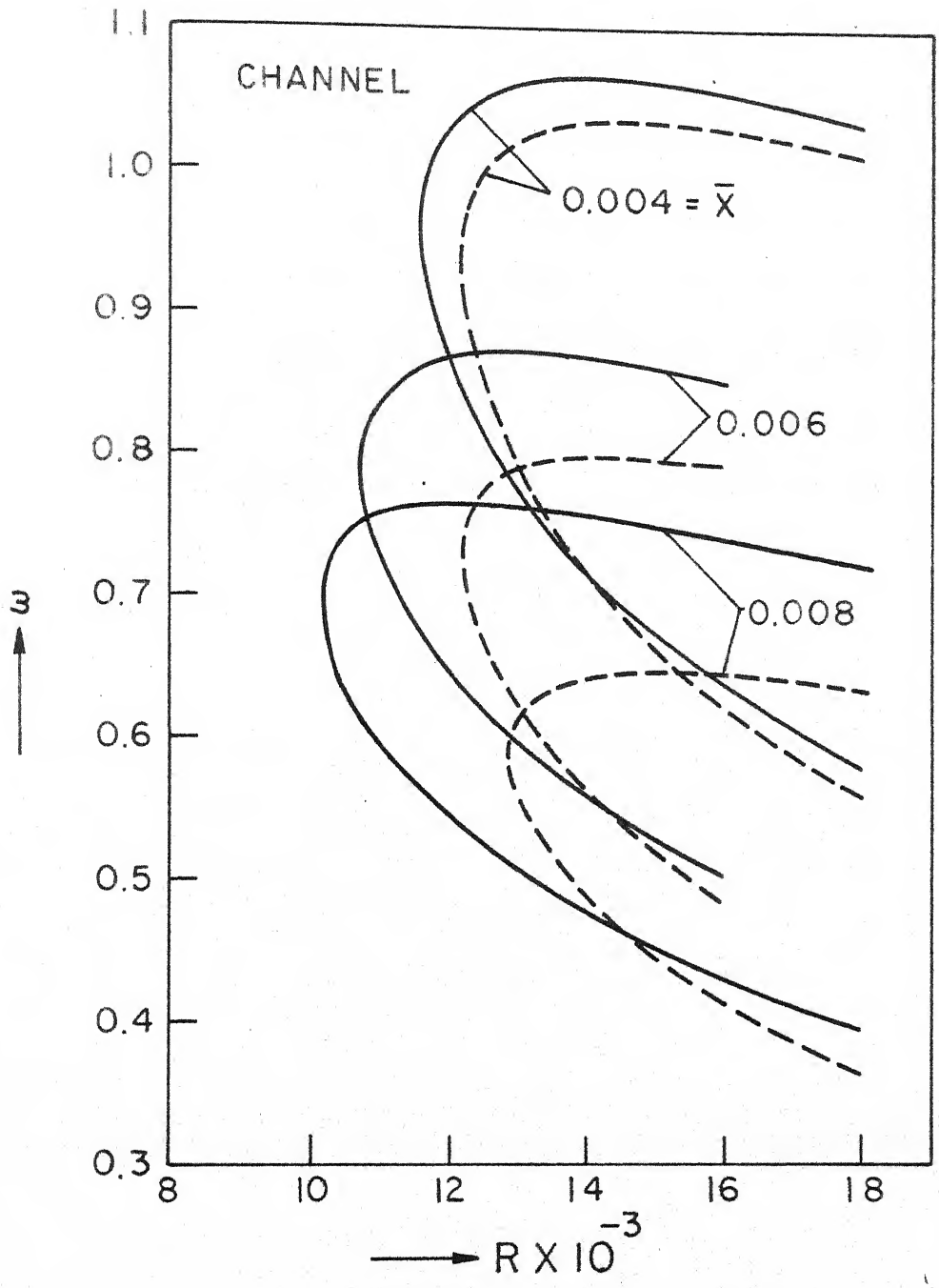

Fig. 6.3 Neutral curves (ω vs R) at several axial locations. ——, symmetric disturbances; - - - -, antisymmetric disturbances.

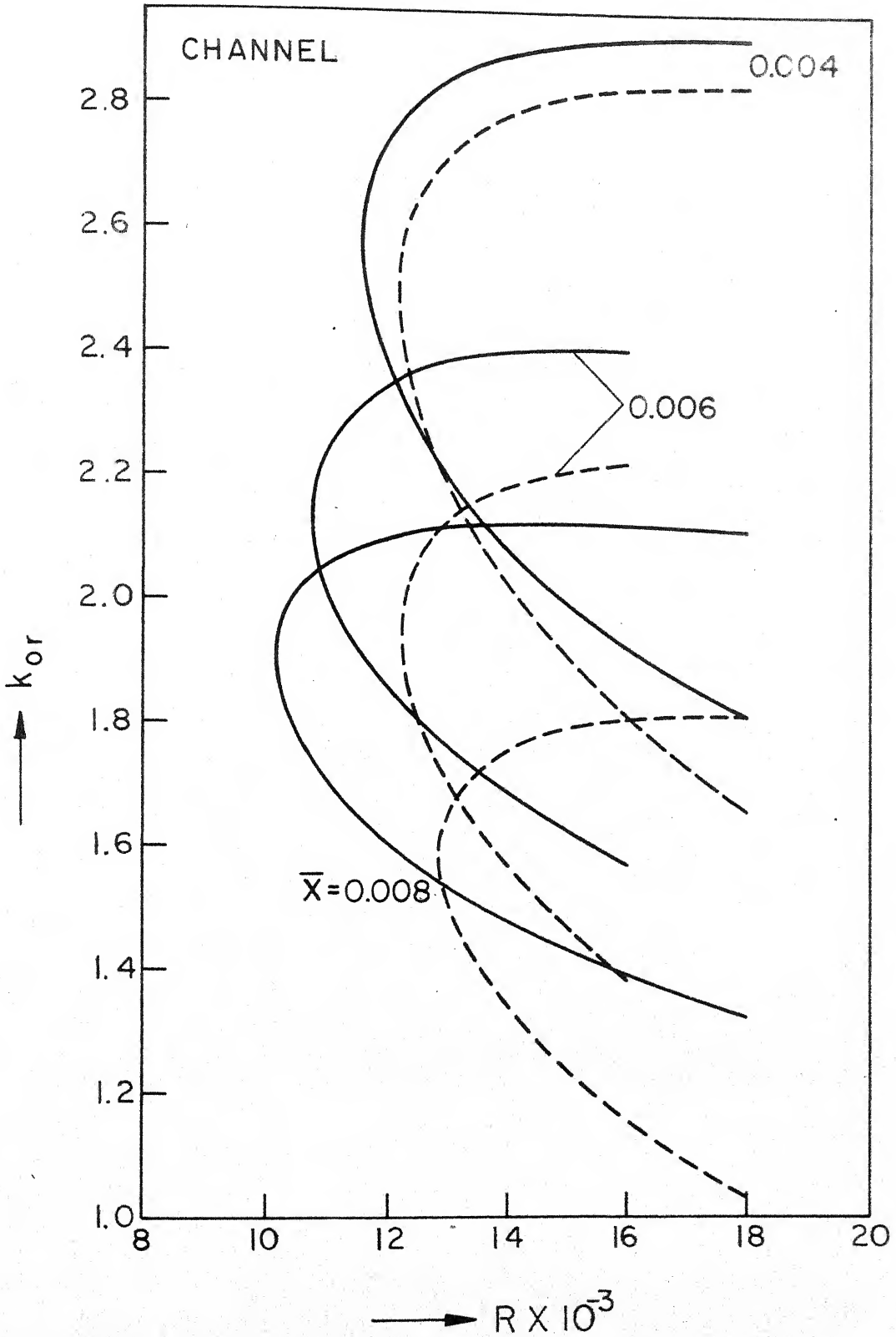

g. 6.4 **Neutral curves (k_{or} vs. R) at various $\bar{X}$. ——, symmetric disturbances; – – – –, antisymmetric disturbances.**

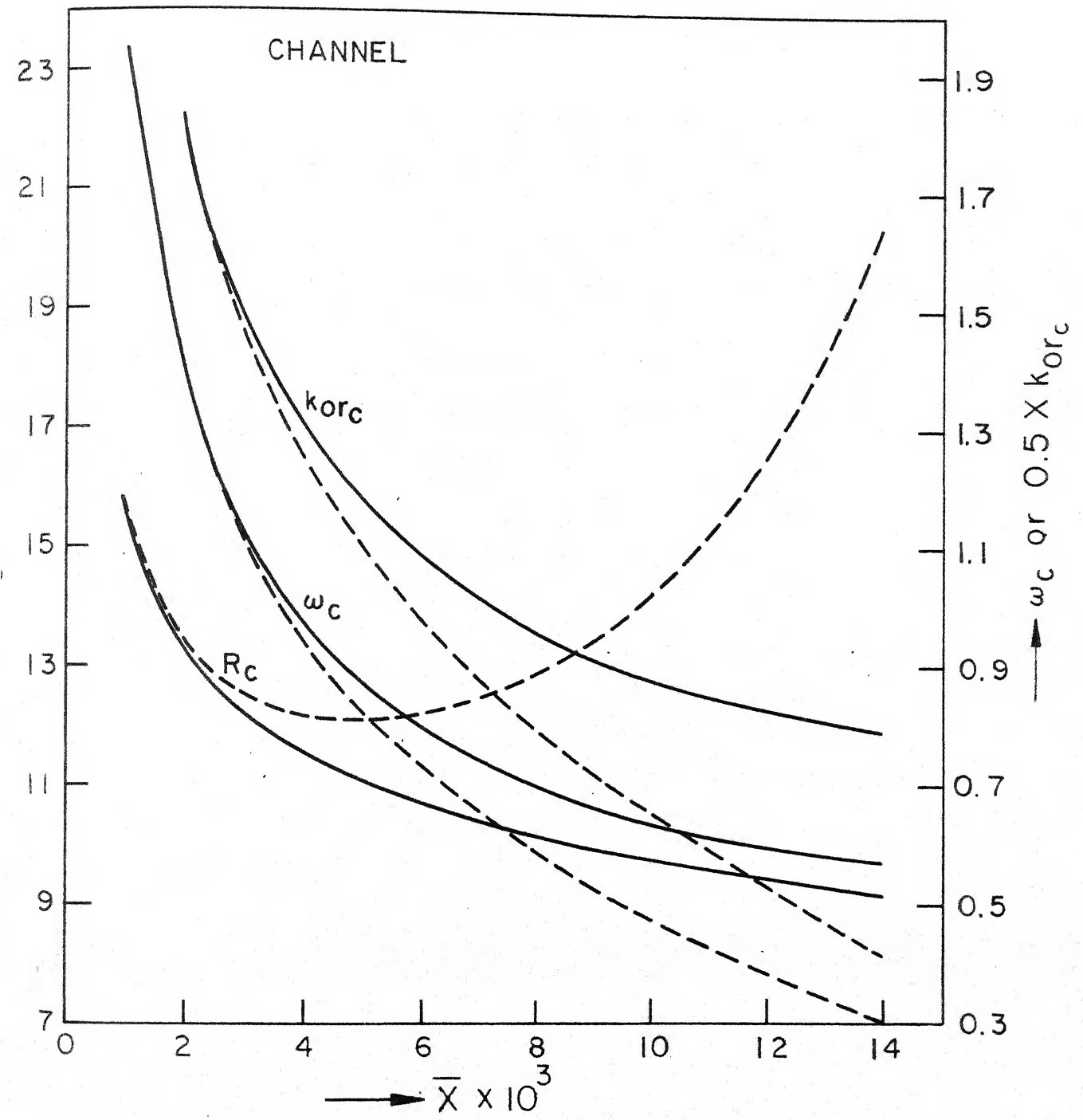

5 Variation of critical Reynolds number, frequency and wavenumber with $\bar{X}$. ——, symmetric disturbances; ----, antisymmetric disturbances.

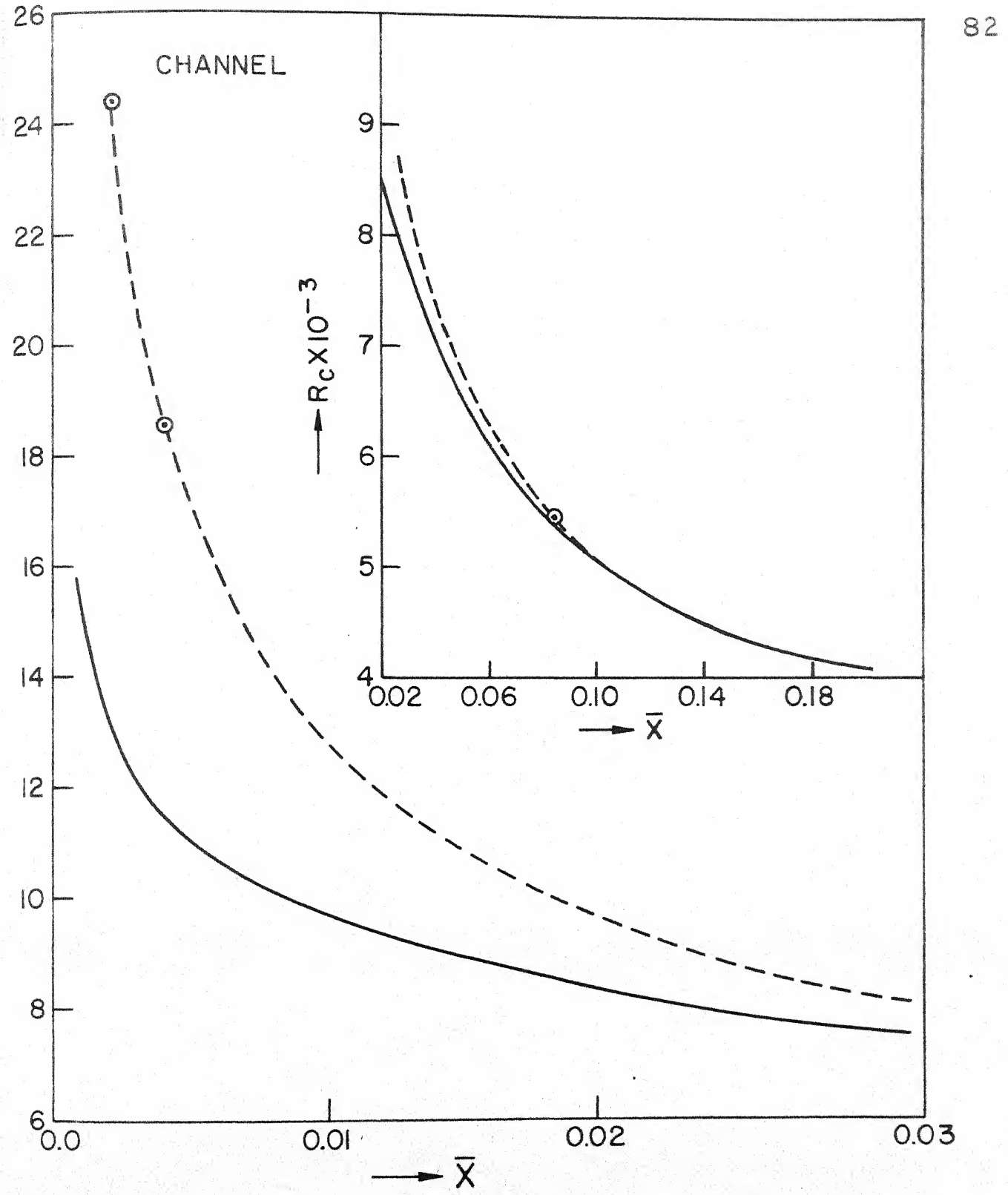

g.6.6 Variation of critical Reynolds number with $\bar{X}$. ——, present work; – – –, Chen's results with finite-difference technique [3]; ⊙ present results for Sparrow's profile [19]

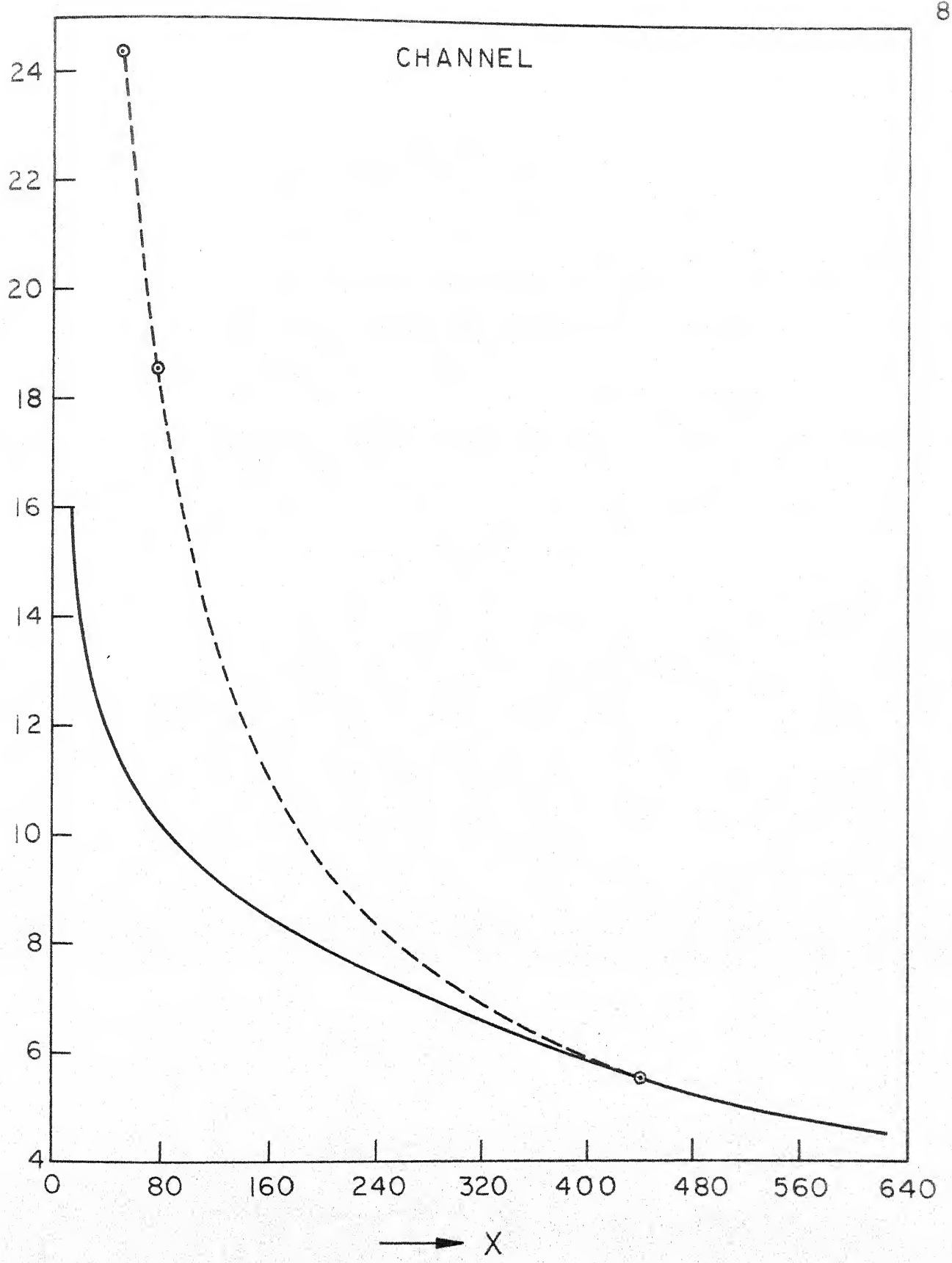

6.7 Variation of critical Reynolds number with X. ——,present work; – – – –,Chen's results with finite difference technique [3]; ⊙ present results for Sparrow's profile [19]

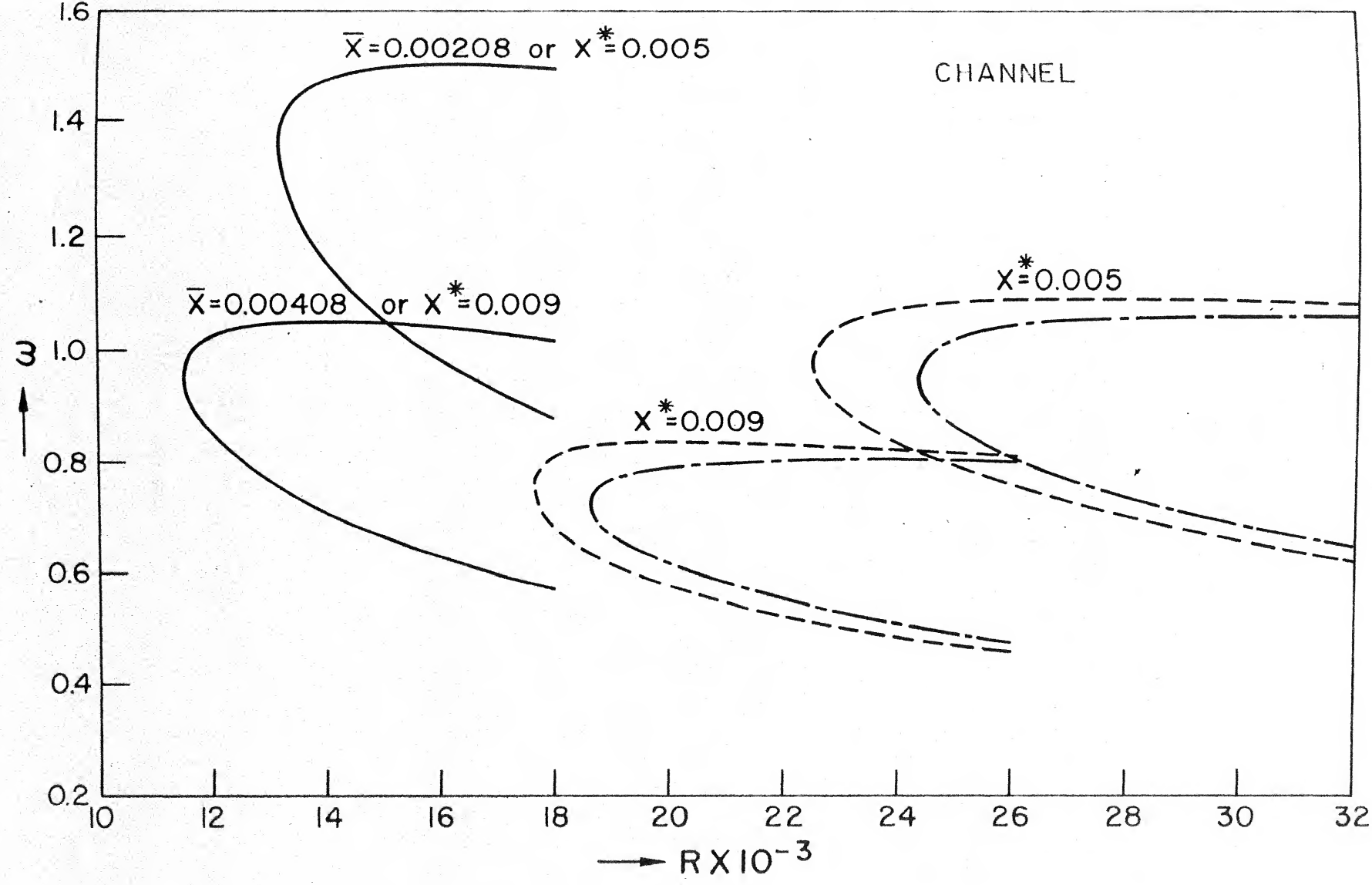

Fig.6.8 Neutral curves at two axial locations. ——, present work; —·—, present results with Sparrow's profile [19]; - - -, Chen's results [115]

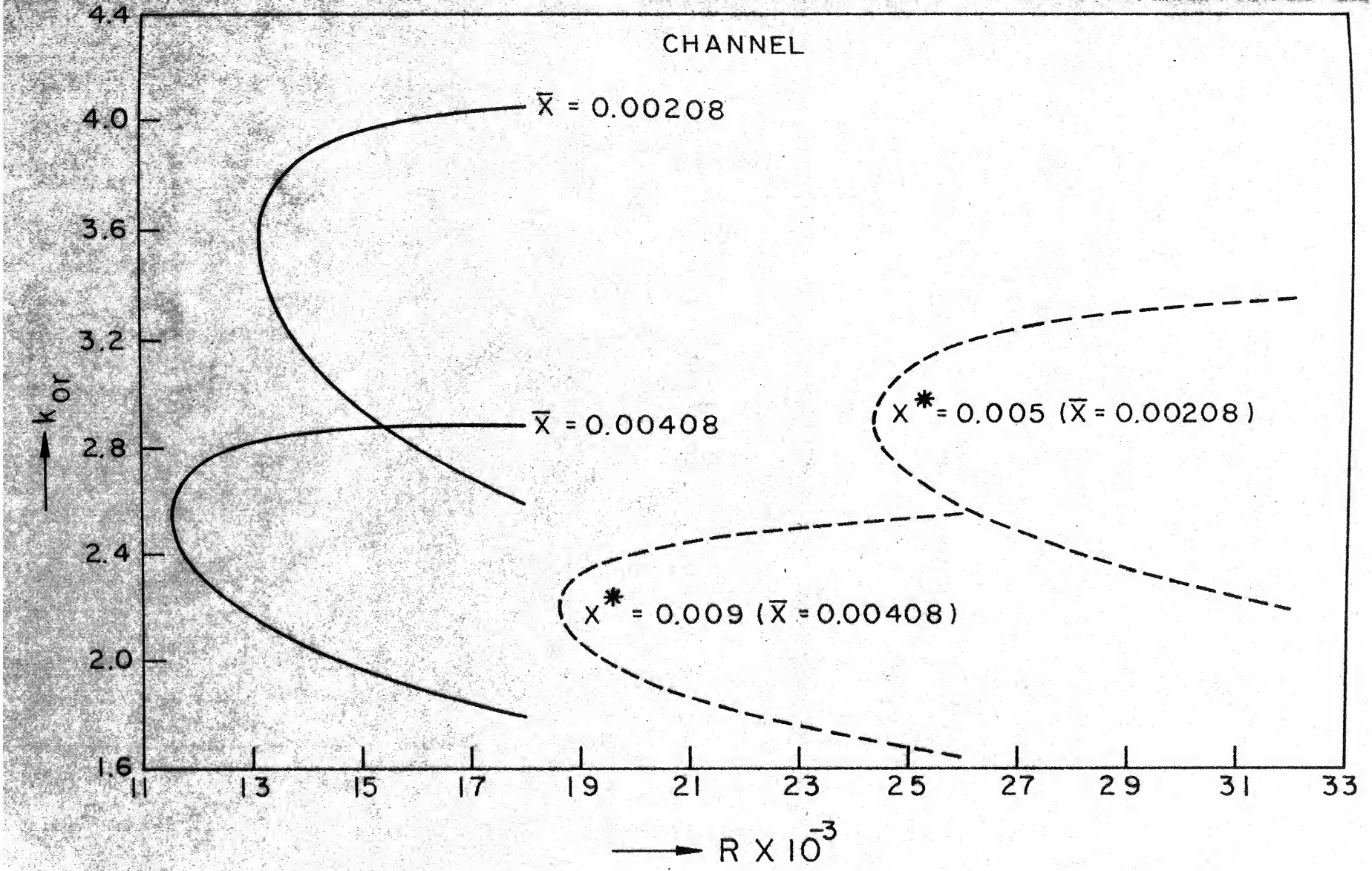

Fig. 6.9 Neutral curves (k_{or} vs. R) at two axial locations. ——, for B-O profile ; ----, for Sparrow's profile

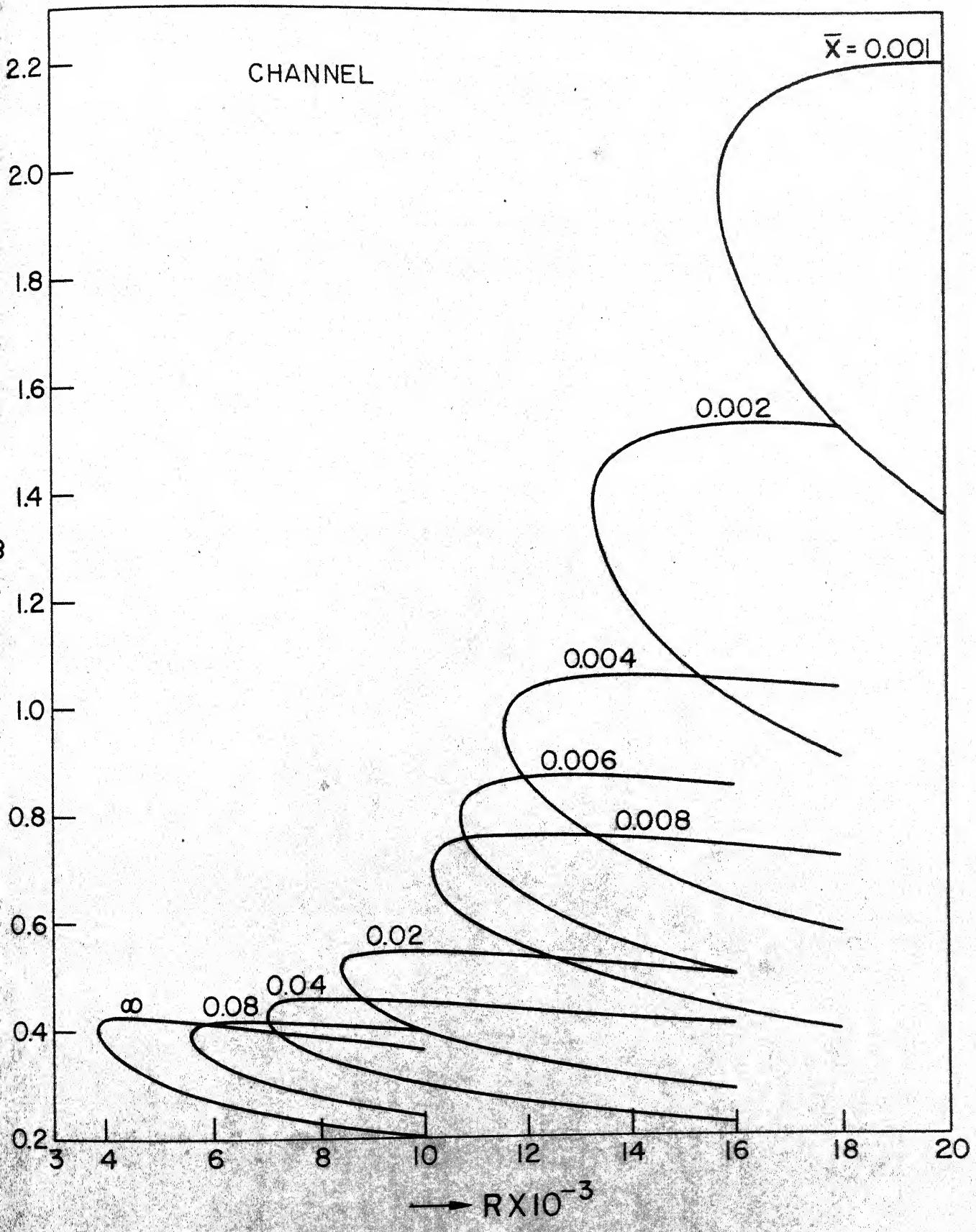

6.10 Neutral curves (ω vs. R) at various axial locations

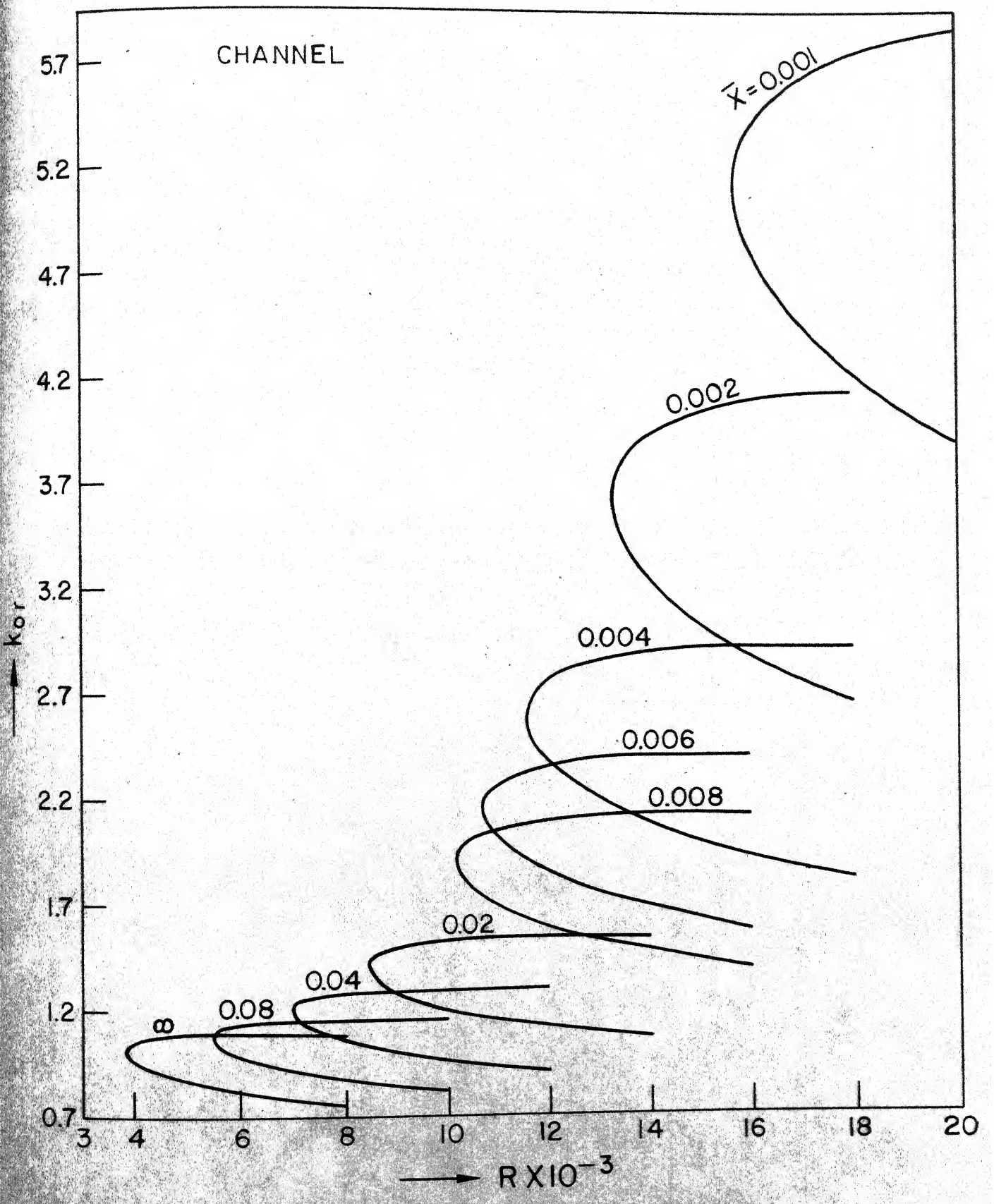

Fig.6.11 Neutral curves (k_{or} vs. R) at various axial locations

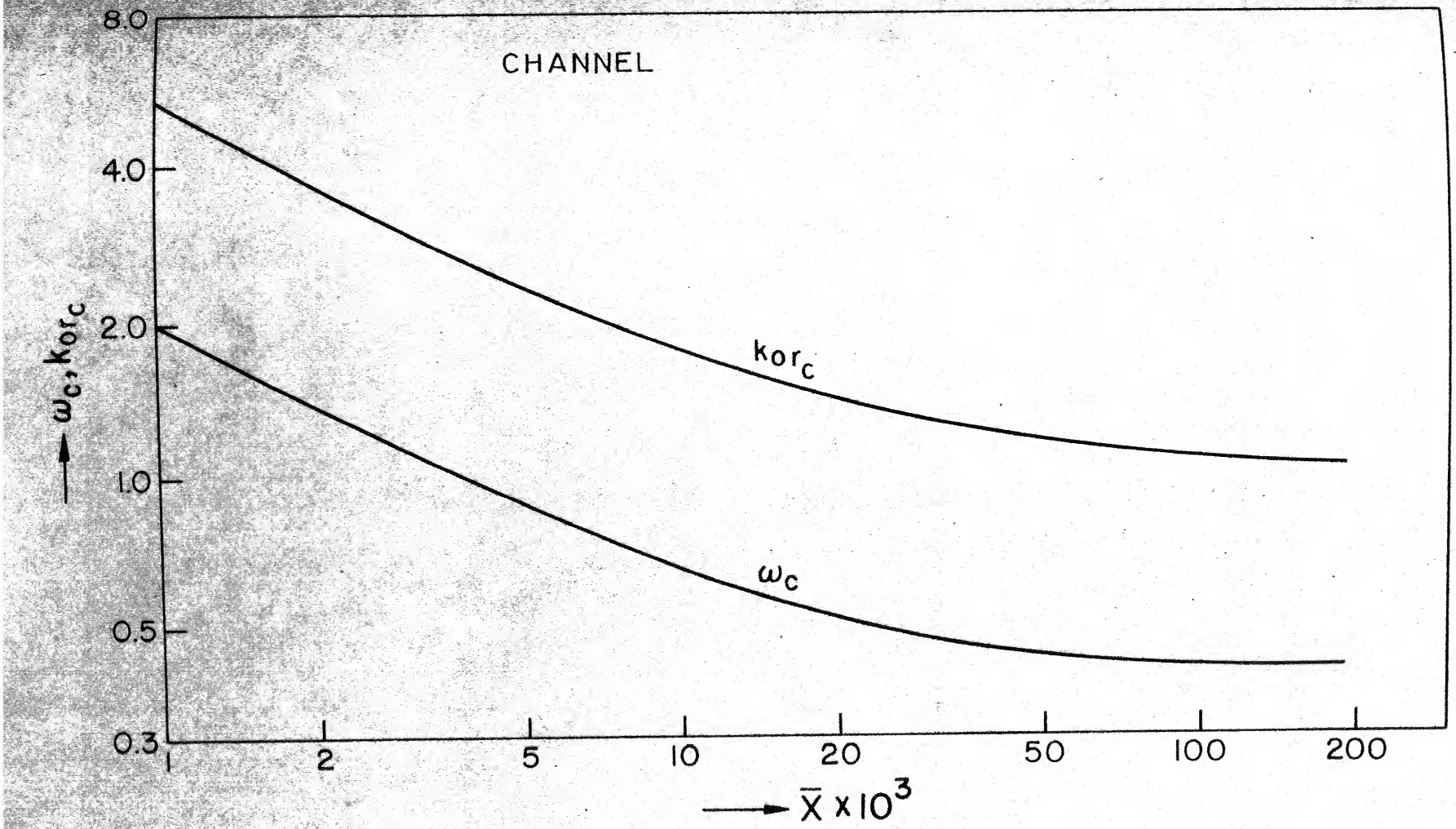

Fig.6.12 Variation of critical frequency and critical wavenumber with $\bar{X}$

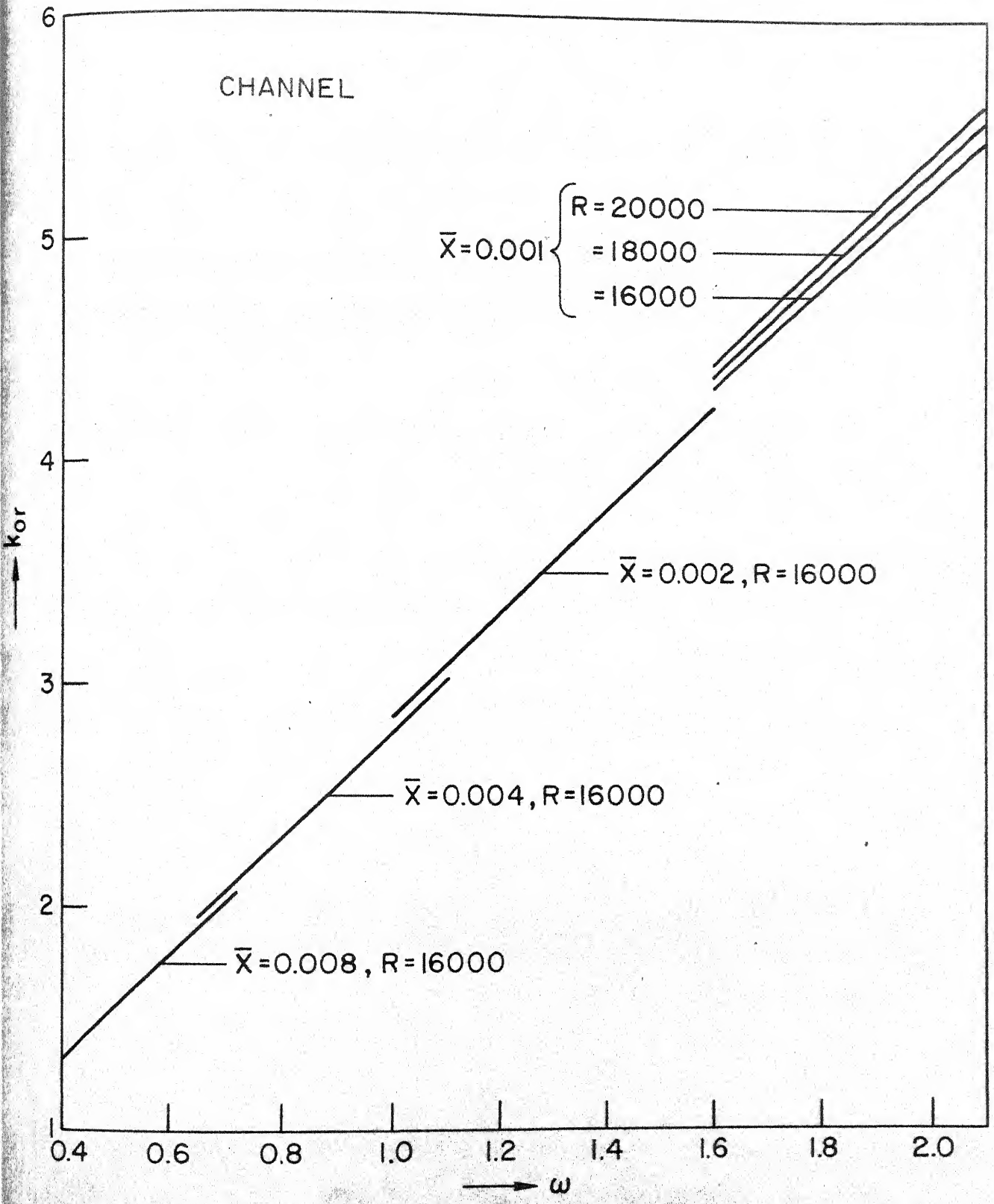

Fig.6.13 Variation of k_{or} with ω for different $\bar{X}$ and R

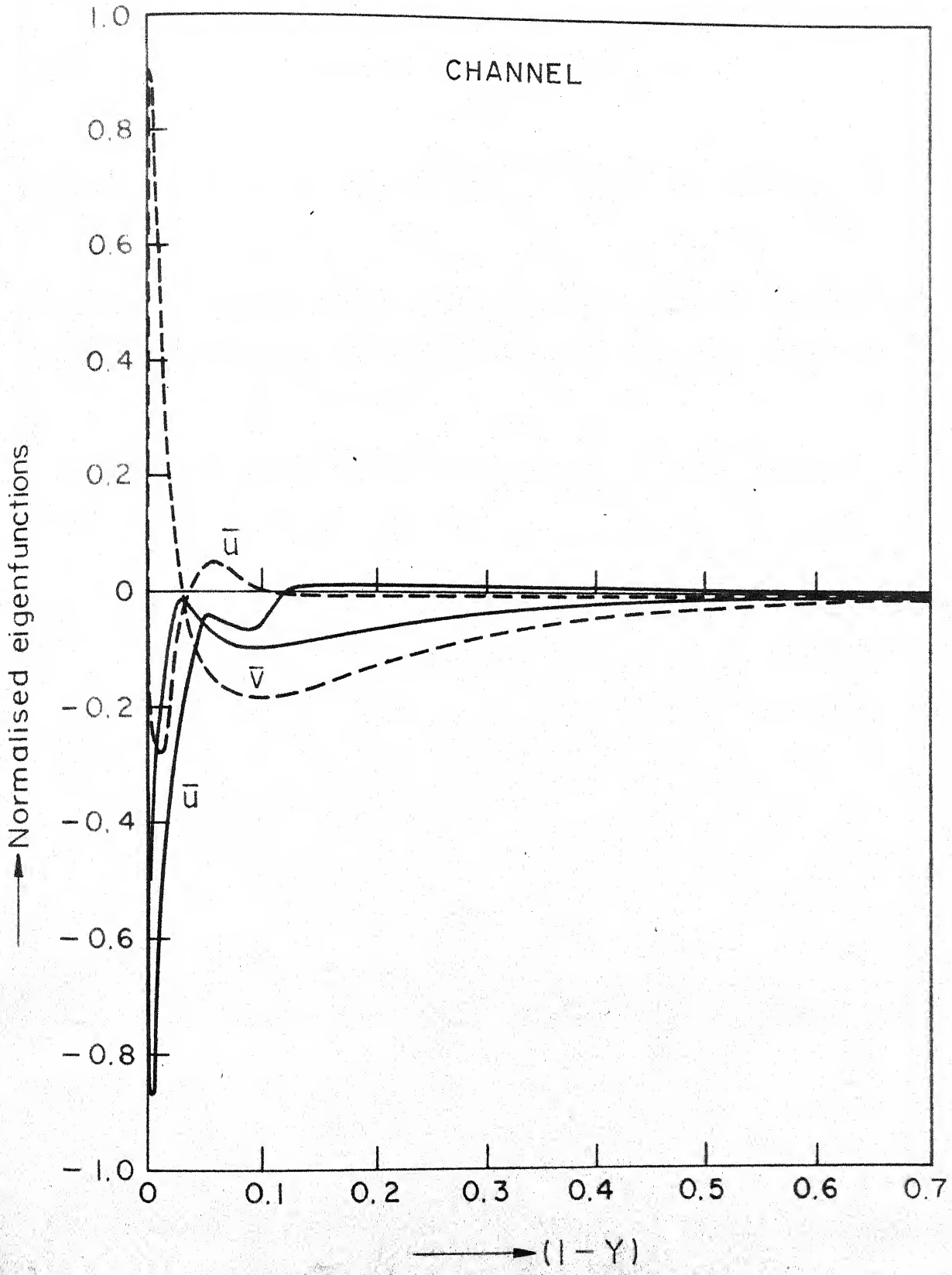

Fig. 6.14 Eigenfunctions $\bar{u}/|\bar{u}|_{max}$ and $\bar{v}/|\bar{v}|_{max}$ for $R = 15778$, $\omega = 1.96$ at $\bar{X} = 0.001$ ($|k_{oi}| \leq 10^{-6}$, $|\bar{u}|_{max}/|\bar{v}|_{max} = 13.93$).——, real part; ----, imaginary part

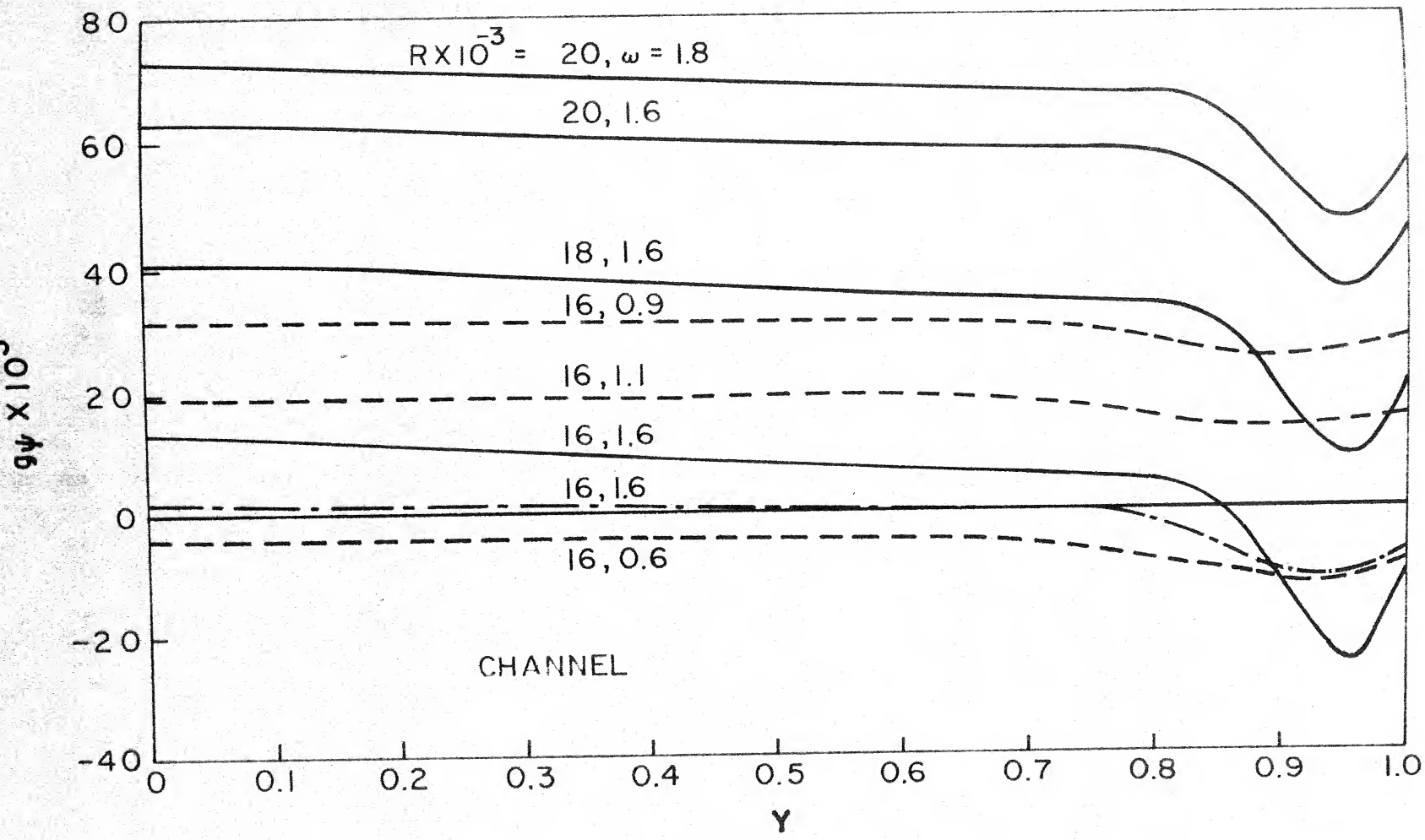

Fig.6.15 Variation of g_ψ with Y for various $\bar{X}$, R and ω. ——, $\bar{X}$ = 0.001; —·—, $\bar{X}$ = 0.002; - - -, $\bar{X}$ = 0.004

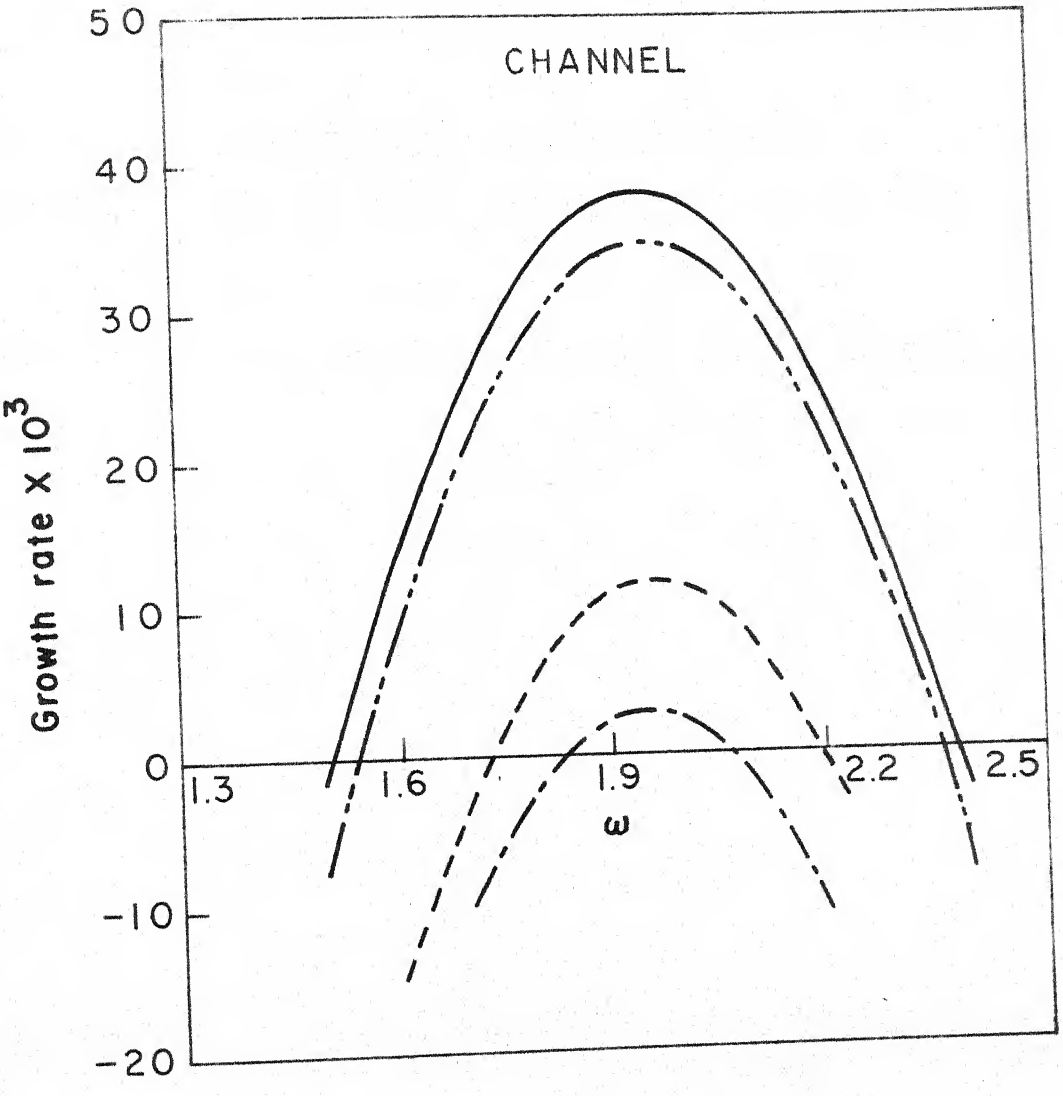

Fig.6.16 Various growth rates for R = 16000 and $\bar{X}$ = 0.001. ——, $g_\psi(\bar{X},0)$; — - - —, $g_u(\bar{X},0)$; - - -, $g_E(\bar{X})$; — — —, $(-k_{oi})$

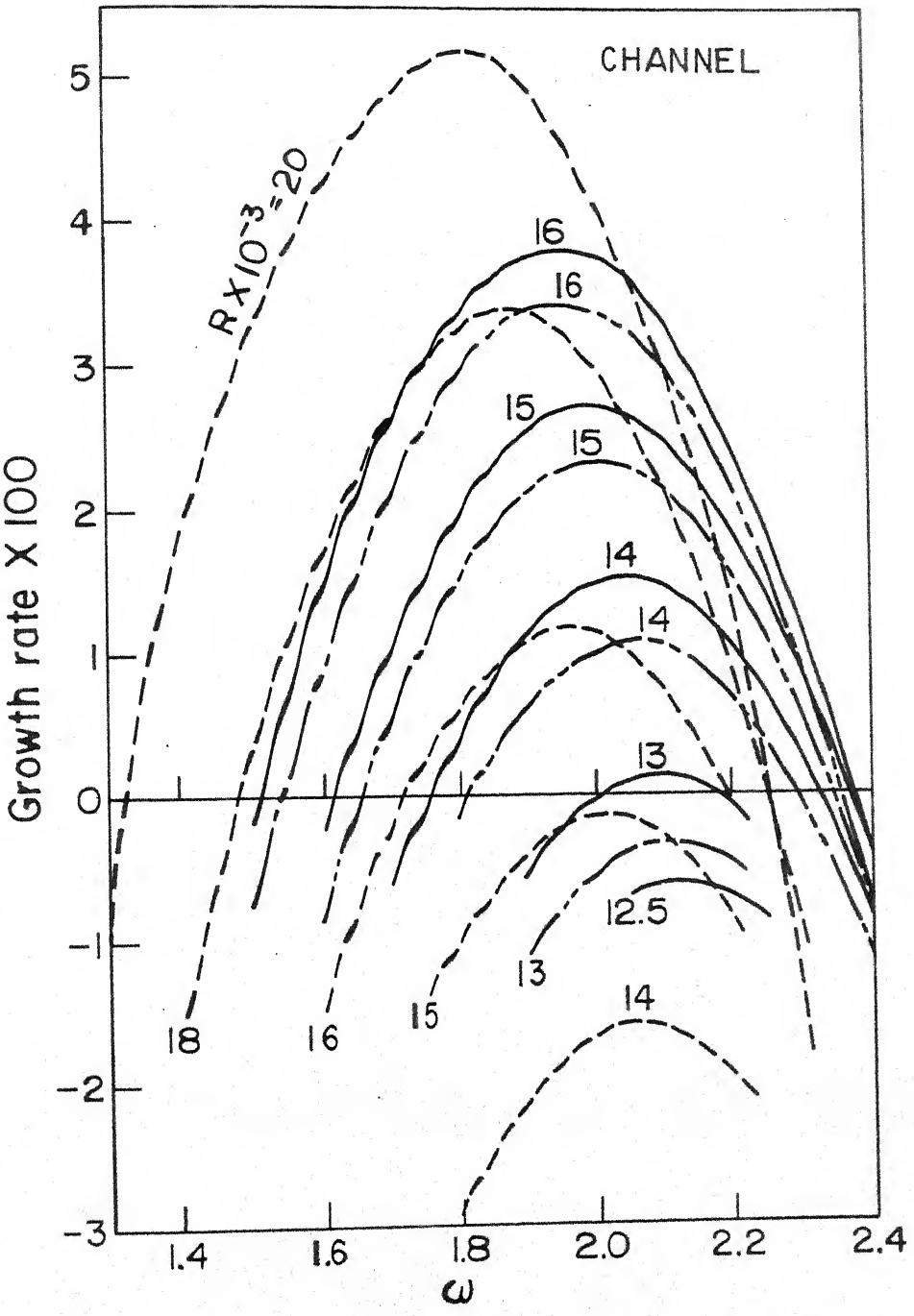

Fig. 6.17 Various growth rates at $\bar{X}=0.001$ and different R. ——, $g_\psi(\bar{X},0)$; —·—·—, $g_u(\bar{X},0)$; ----, g_E

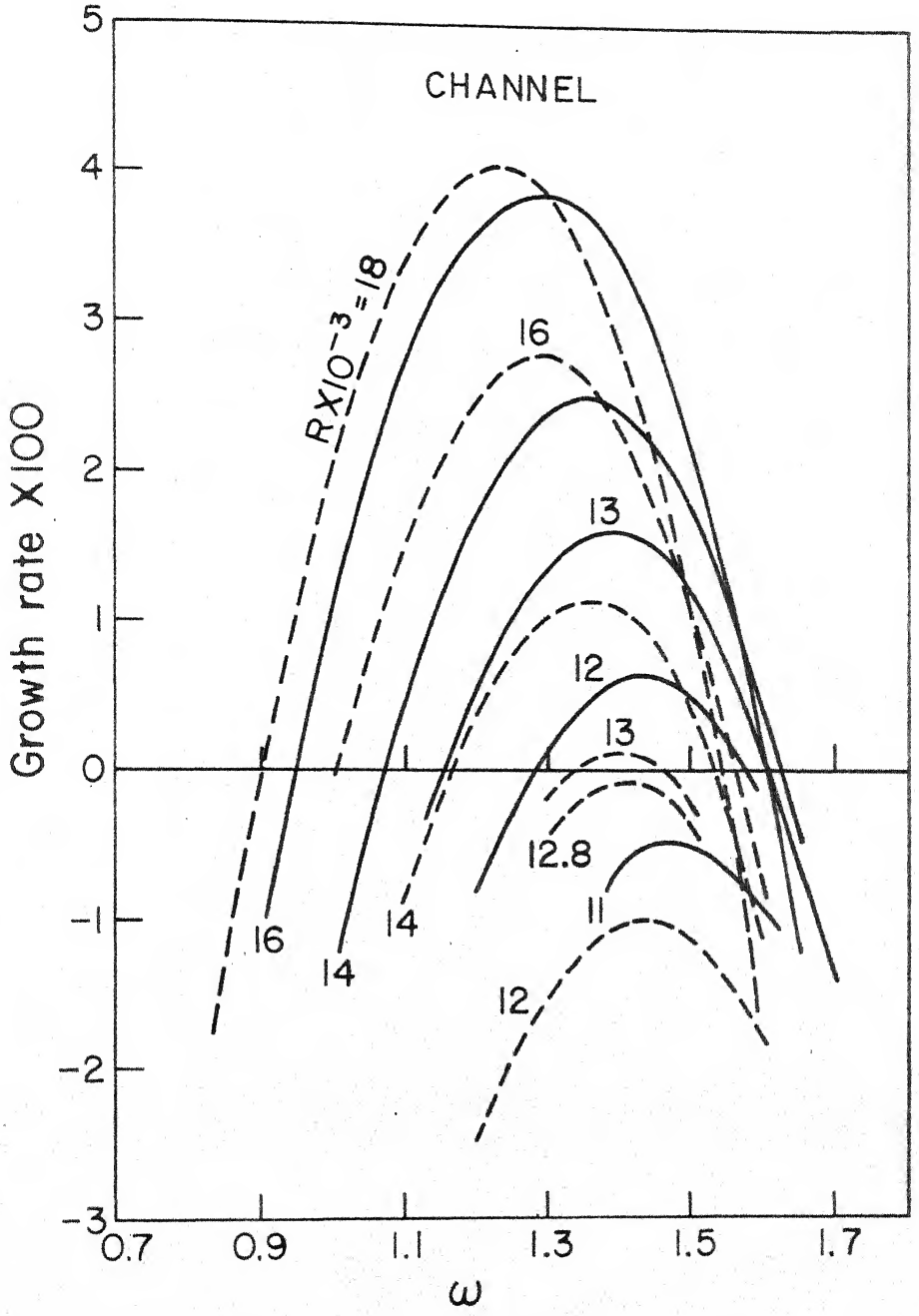

Fig. 6.18 Various growth rates at $\bar{X}=0.002$ and different R. ——, $g_\psi(\bar{X},0)$; ----, g_E

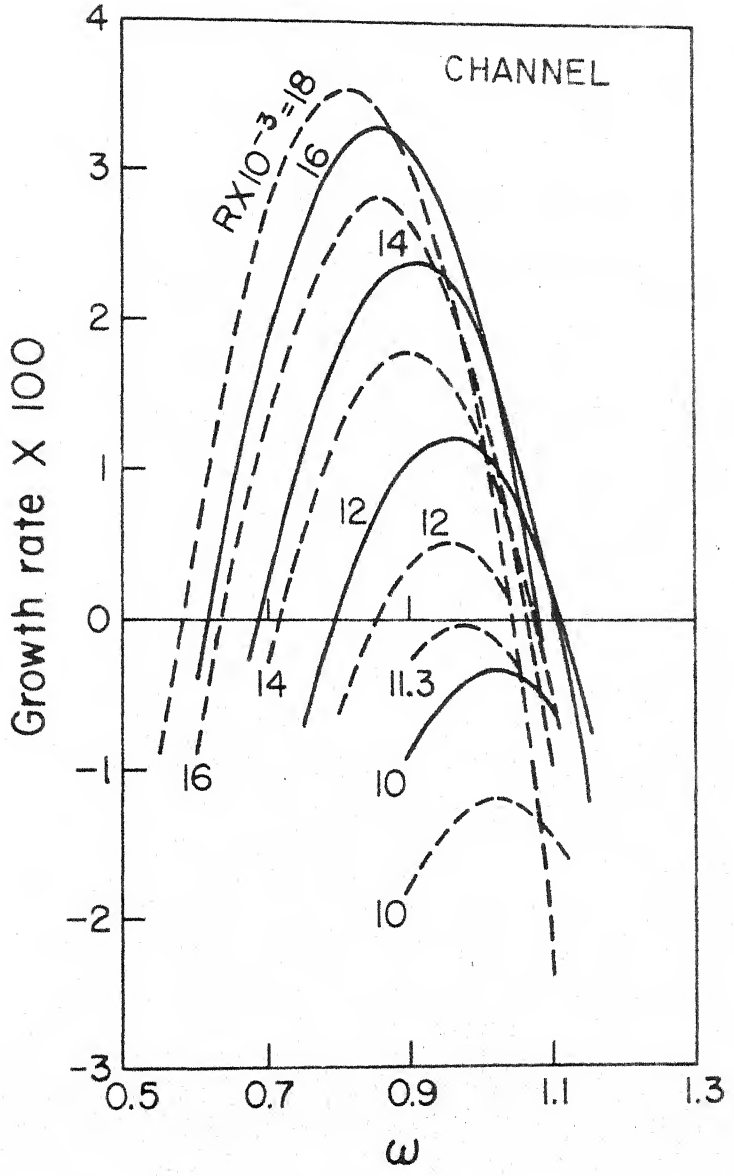

Fig.6.19Various growth rates at $\bar{X}=0.004$ and different R. ——, $g_\psi(\bar{X},0)$;----, g_E

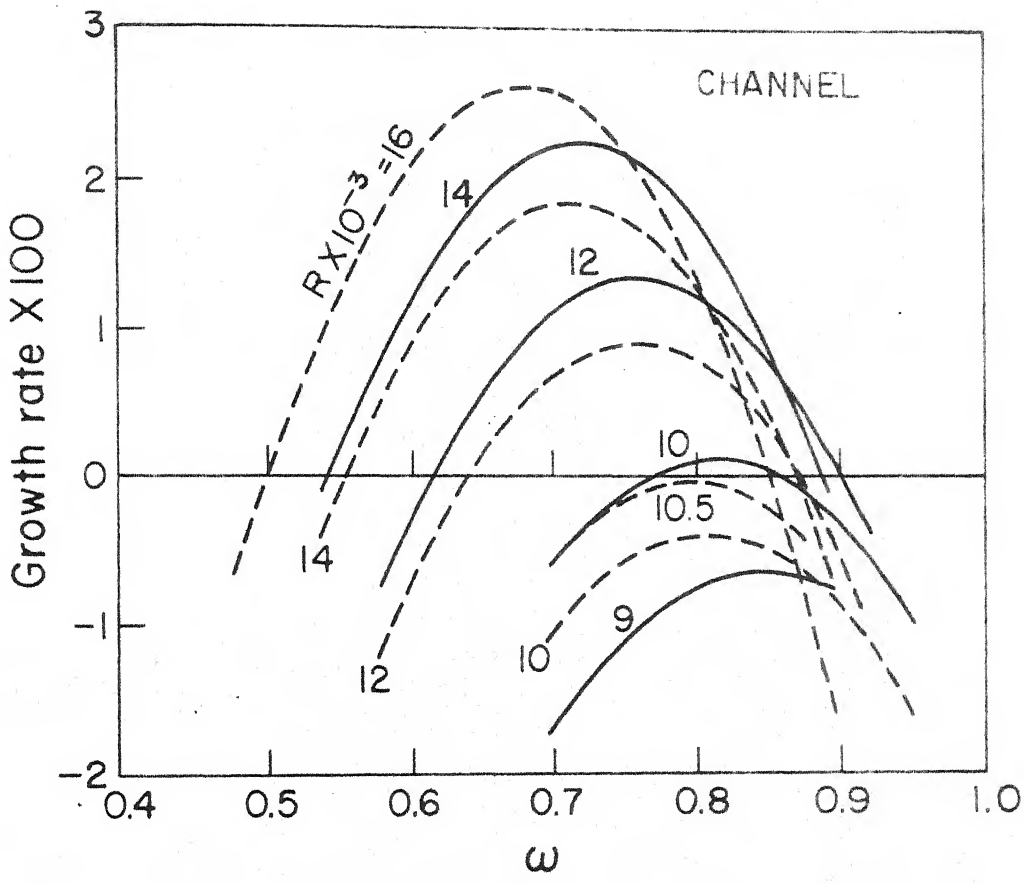

Fig. 6.20 Various growth rates at $\bar{X}=0.006$ and different R.——, $g_\psi(\bar{X},0)$;----, g_E

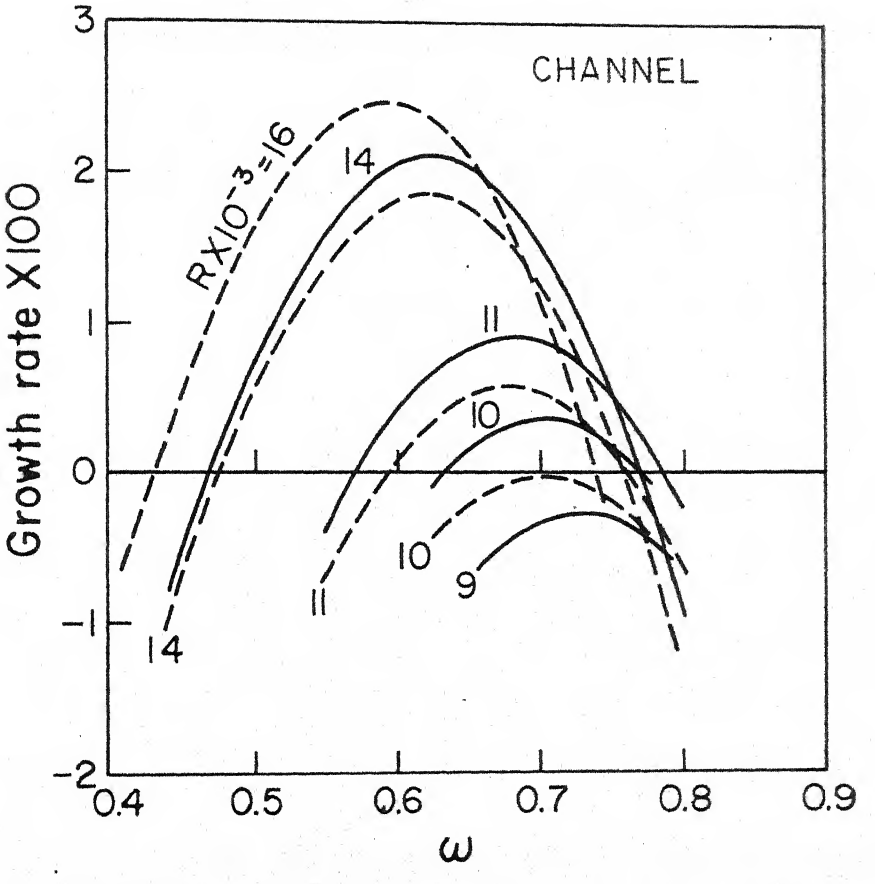

Fig. 6.21 Various growth rates at $\bar{X}=0.008$ and different R. ——, $g_\psi(\bar{X},0)$; ----, g_E

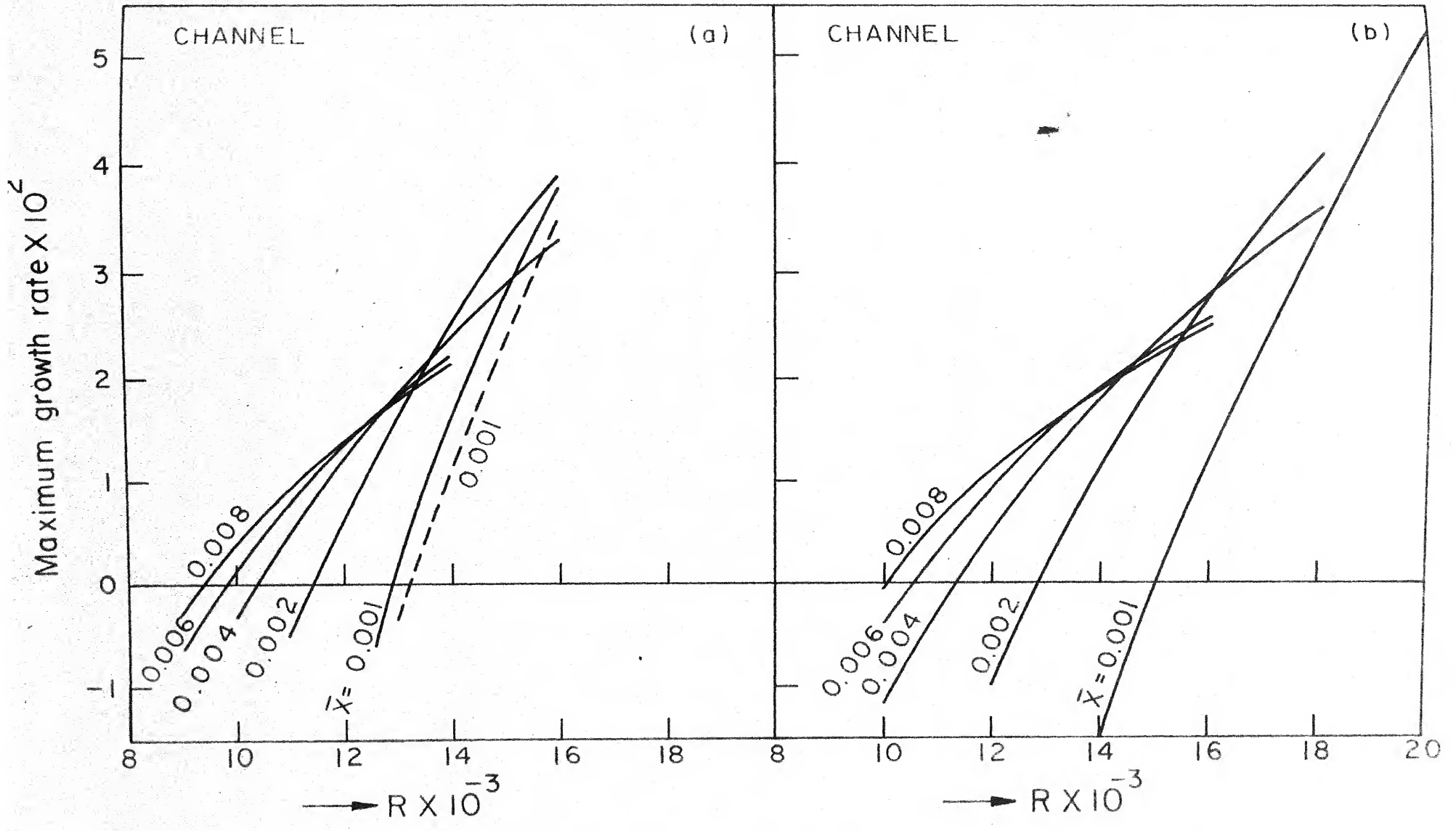

Fig. 6.22 Maximum values of growth rates vs. R at various $\bar{X}$. (a) ——, for $g_\psi(\bar{X}, 0)$; – – – –, for $g_u(\bar{X}, 0)$; (b) for $g_E(\bar{X})$

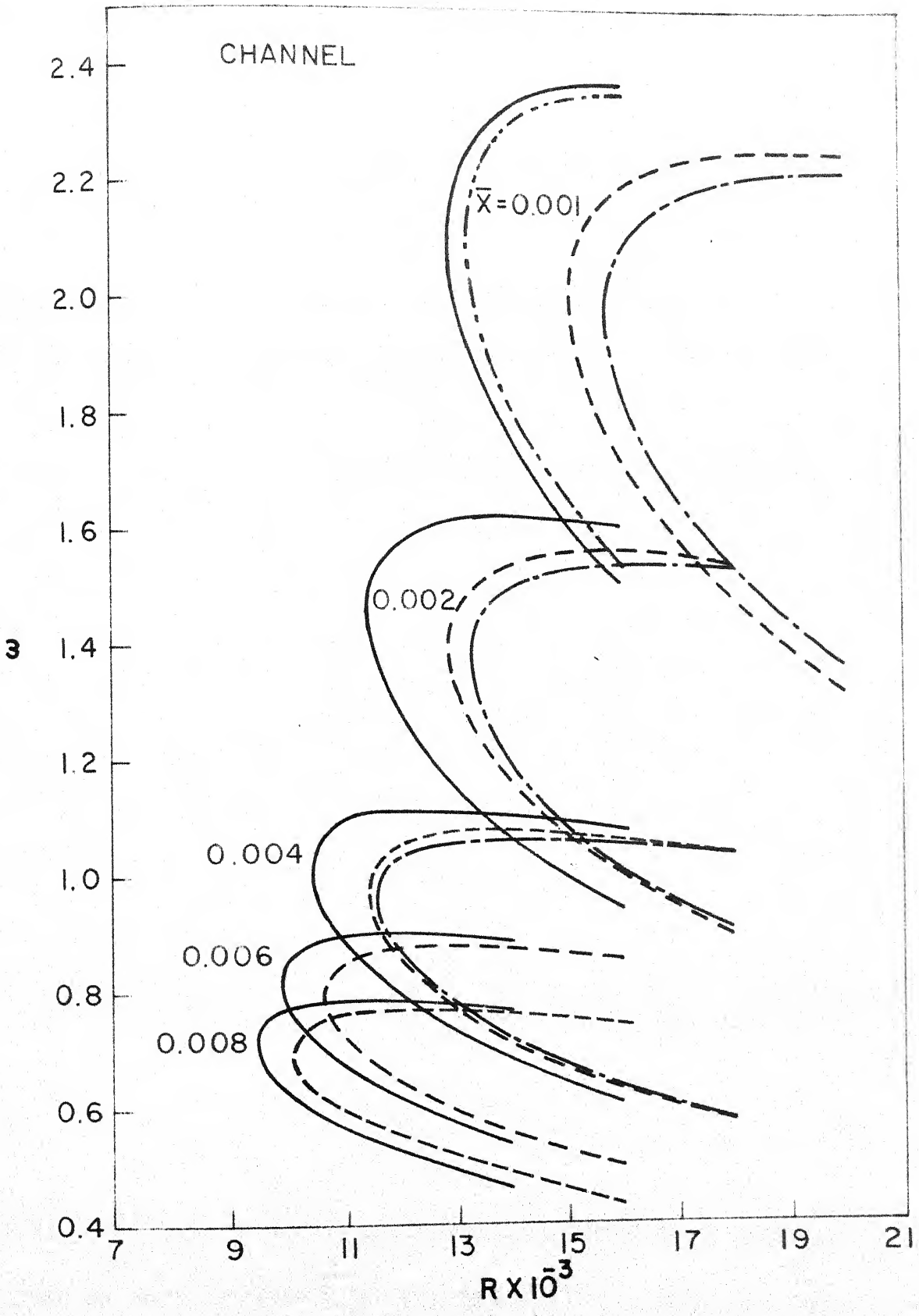

Fig.6.23 Neutral curves at various axial locations. ——, based on $g_\psi(\bar{X},0)$; —·—·—, based on $g_u(\bar{X},0)$; – – –, based on $g_E(\bar{X})$; —– —, based on parallel flow theory

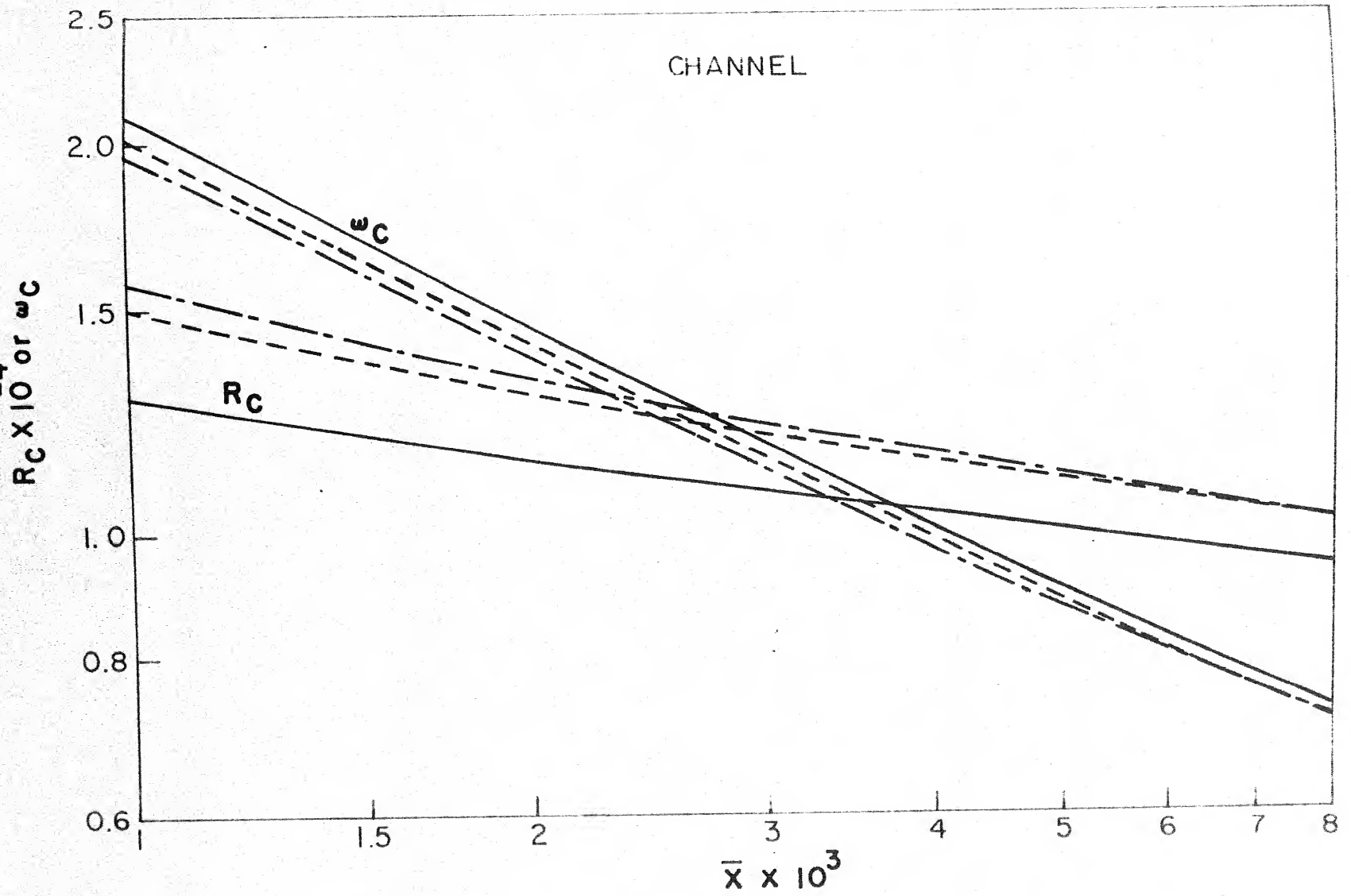

Fig.6.24 Variation of R_c and ω_c with $\bar{X}$. ——, based on $g_\psi(\bar{X},0)$; - - -, based on $g_E(\bar{X})$; ——·——, based on parallel flow theory

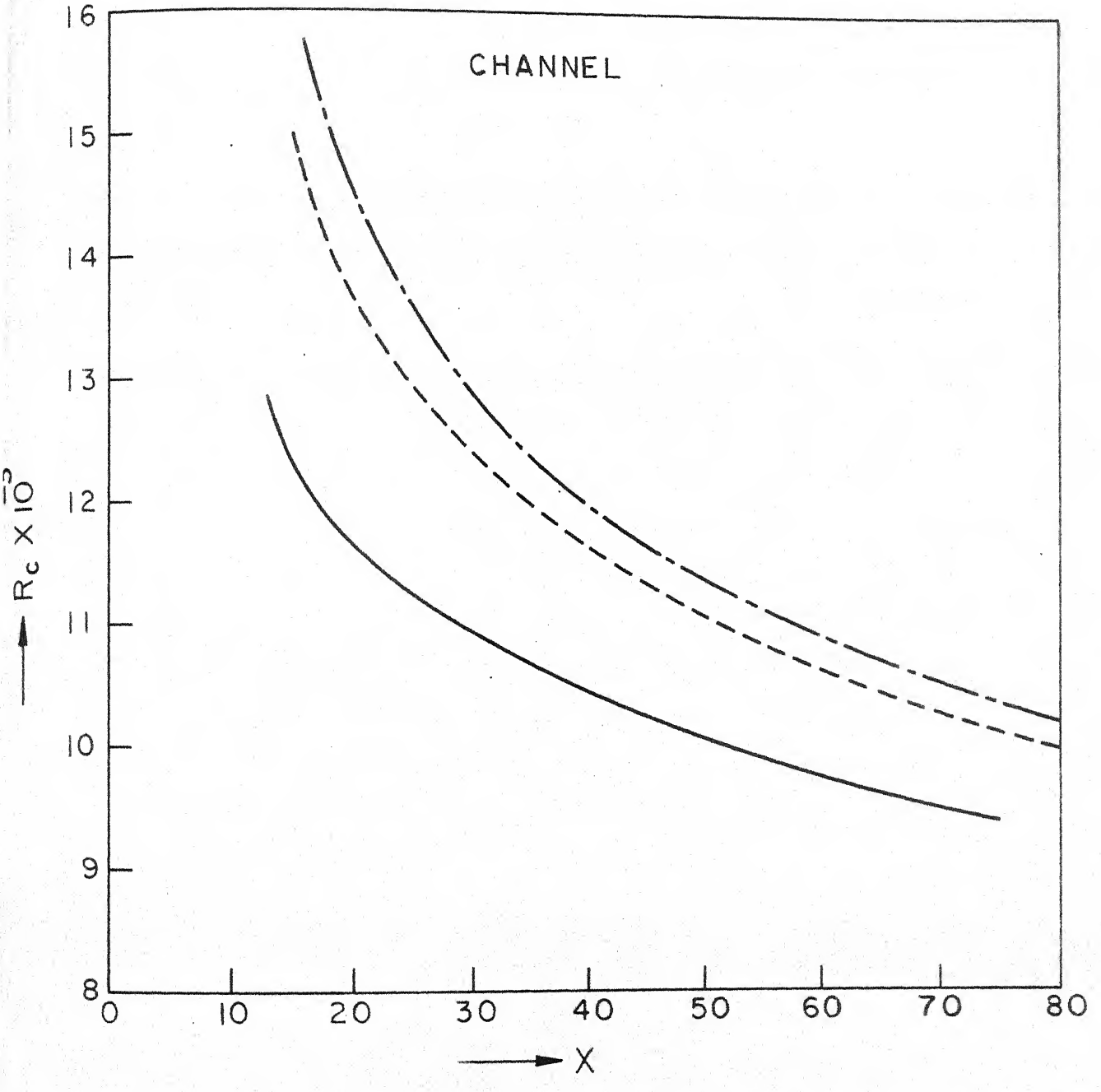

Fig. 6.25 Variation of R_c with X. ——, based on $g_\psi(X,0)$ ----, based on g_E; —·—, based on parallel flow theory

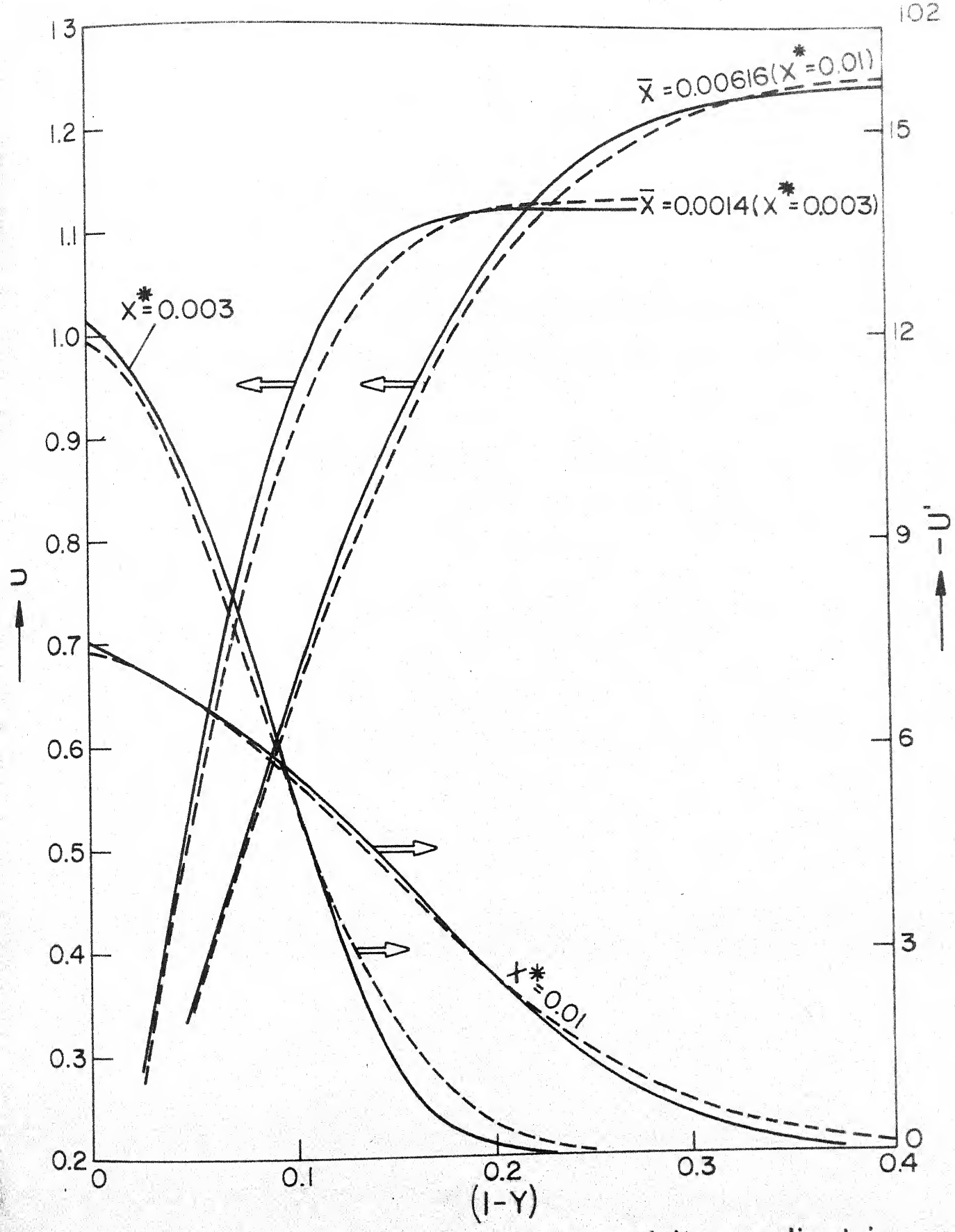

Fig.6.26 Developing flow velocity profile and its gradient in a pipe at two axial locations. ——, Hornbeck's profile [47]; – – –, Sparrow's profile [19].

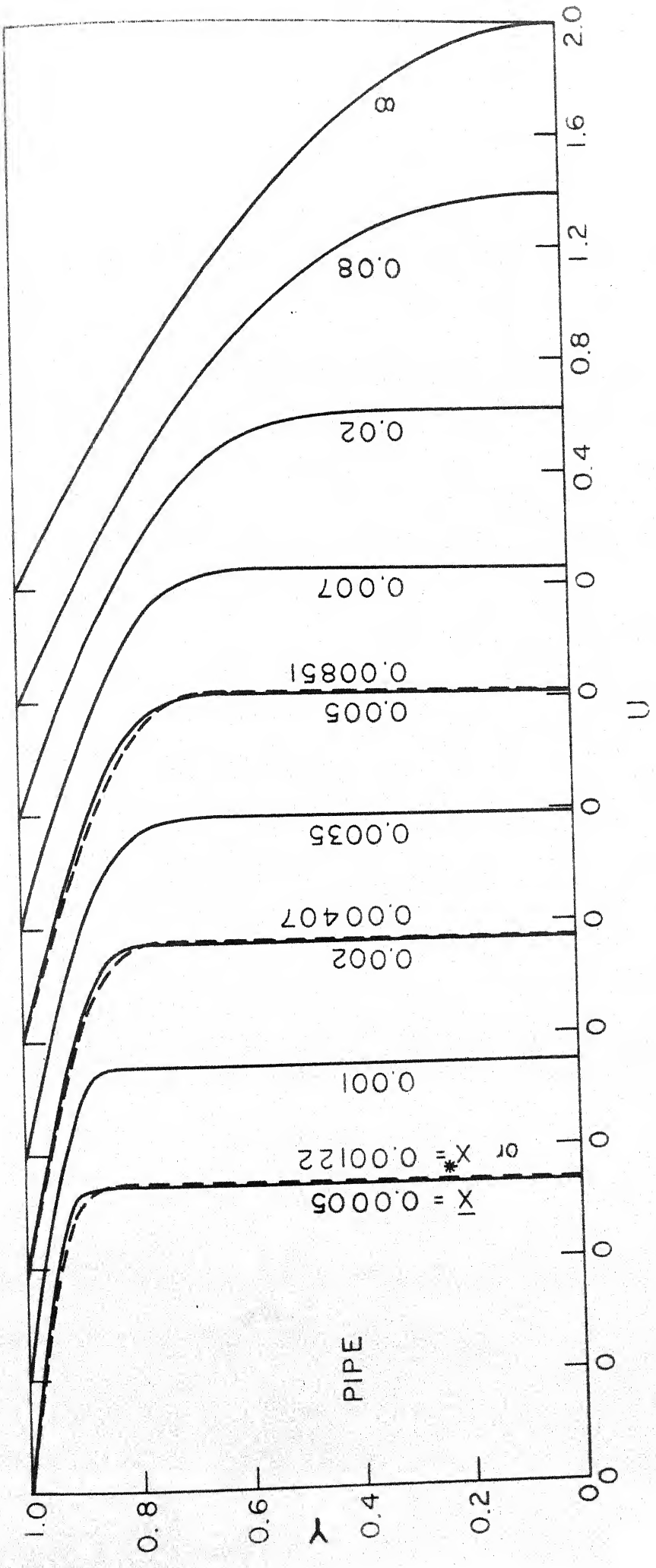

Fig. 6.27 Velocity profiles at several axial locations in a pipe. ——, Hornbeck's profiles; – – – –, Sparrow's profiles

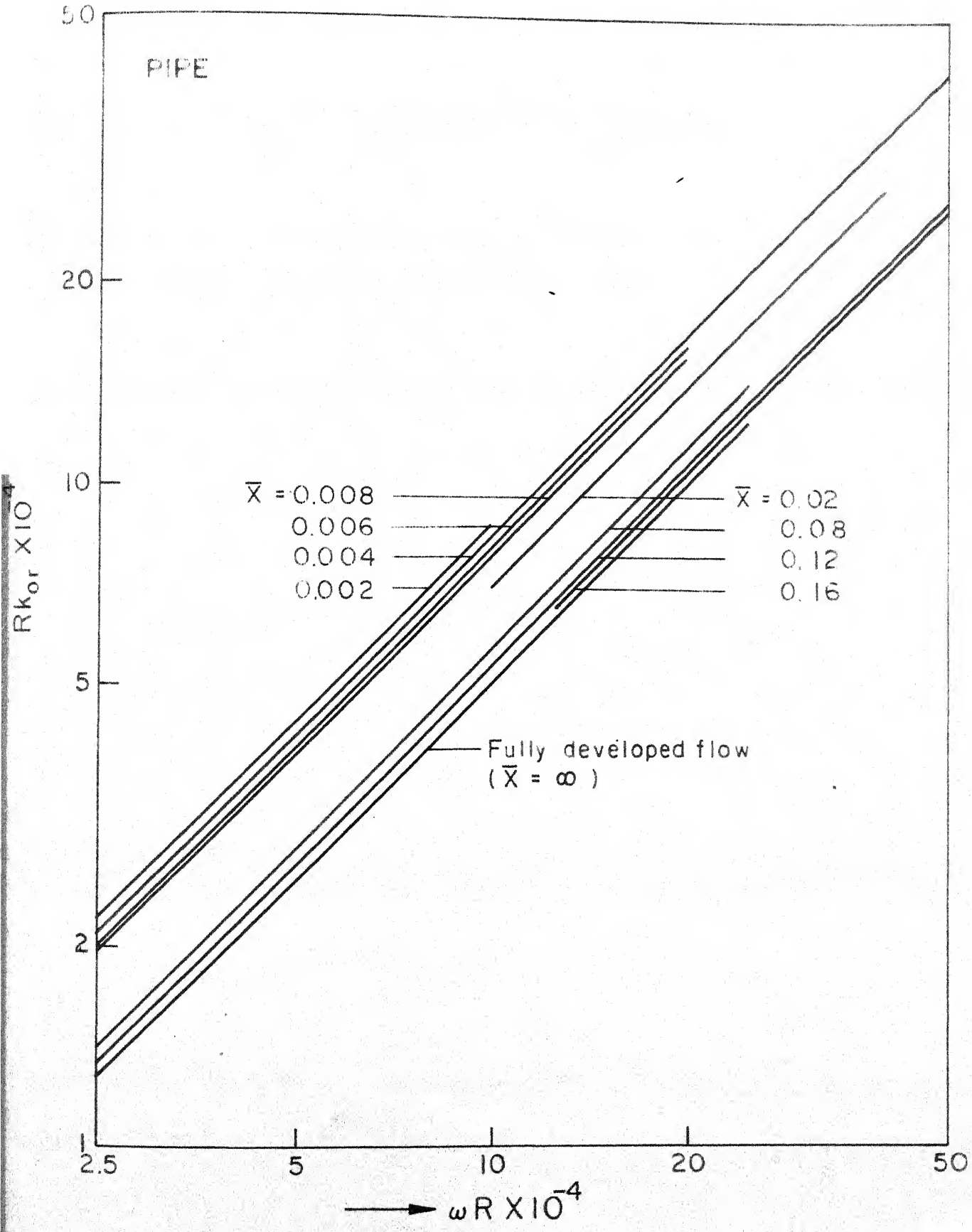

Fig. 6.28 Variation of Rk_{or} with ωR for the least stable central mode at various $\bar{X}$.

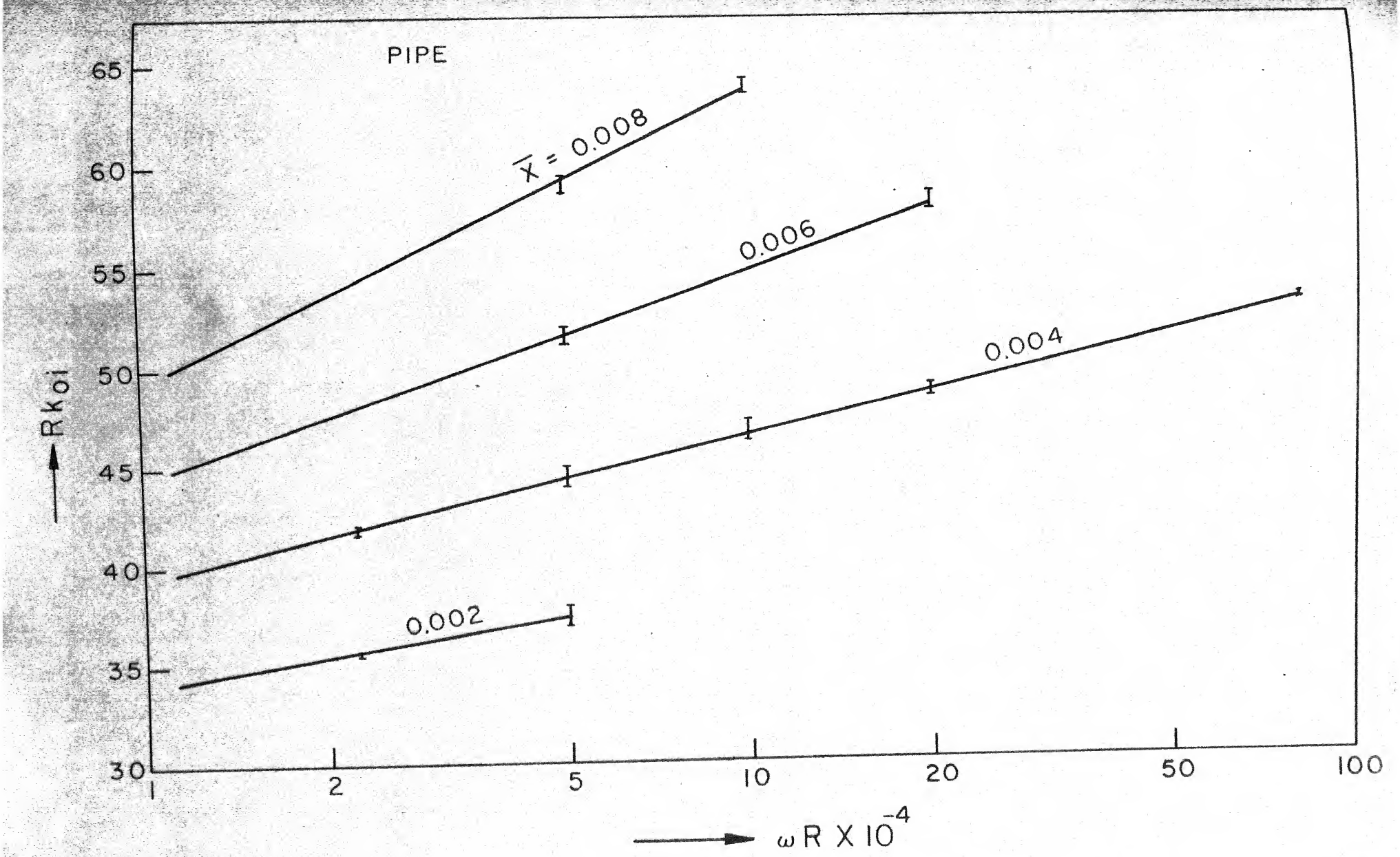

Fig. 6.29 Variation of Rk_{oi} with ωR for the least stable central mode at various $\bar{X}$

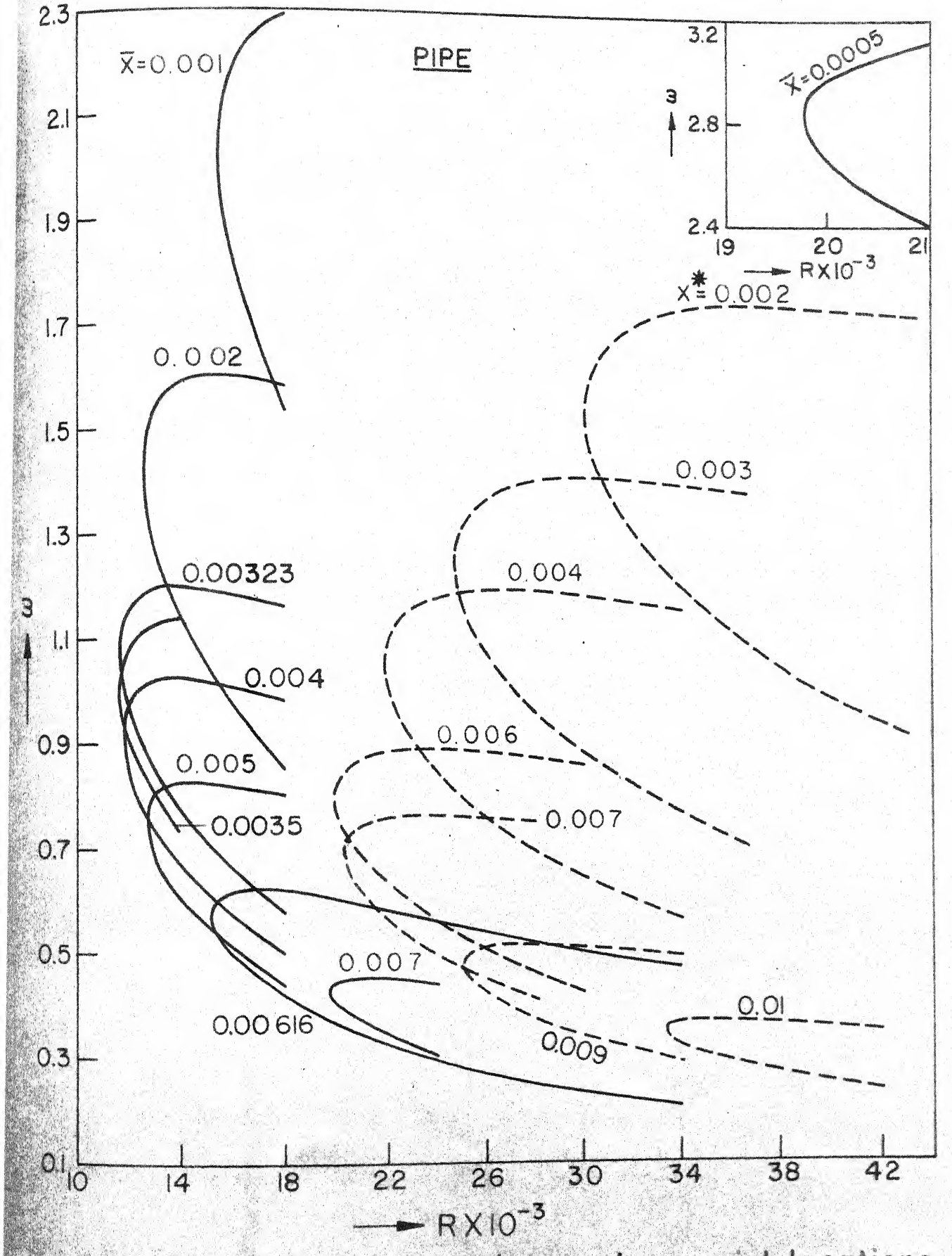

6.30 Neutral curves (ω vs R) at various axial locations
——, Hornbeck's profile; ----, Sparrow's profile

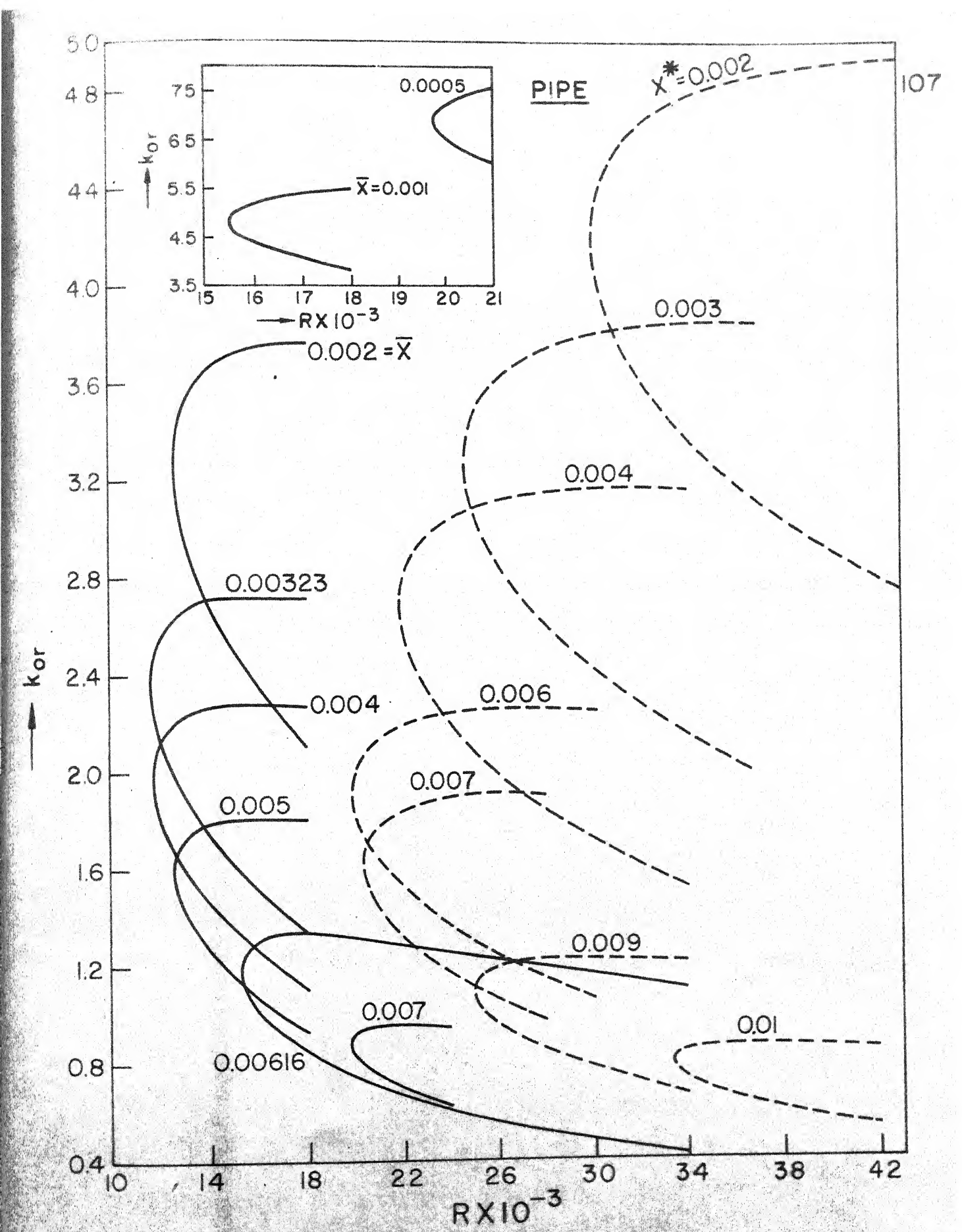

Fig.6.31 Neutral curves (k_{or} vs.R) at various axial locations ——, Hornbeck's profile; ----, Sparrow's profile.

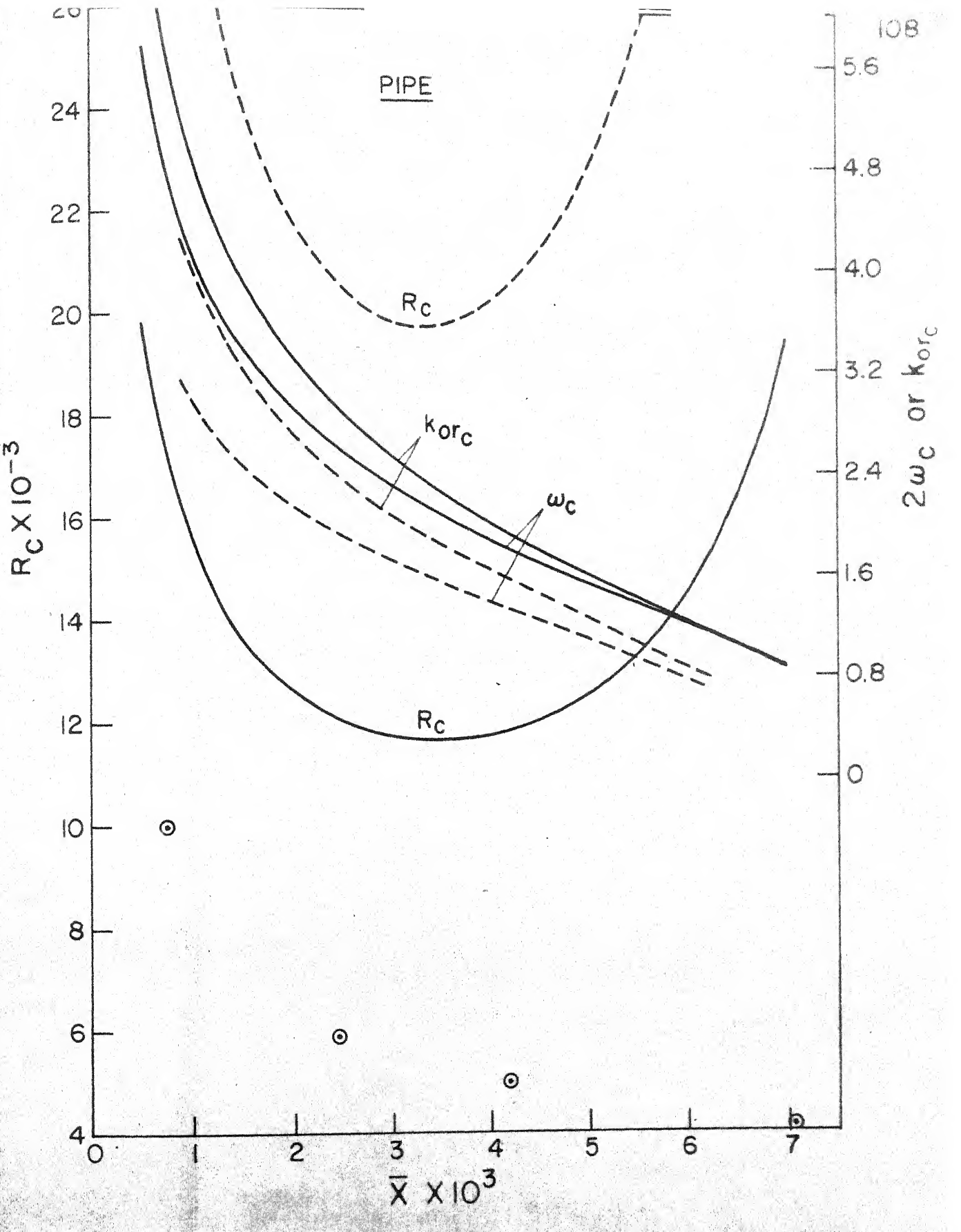

g.6.32 Variation of critical Reynolds number, critical wave-number and critical frequency with $\bar{X}$. ——, Hornbeck's profile; ----, Sparrow's profile; ⊙, experimental data [48] for critical Reynolds number

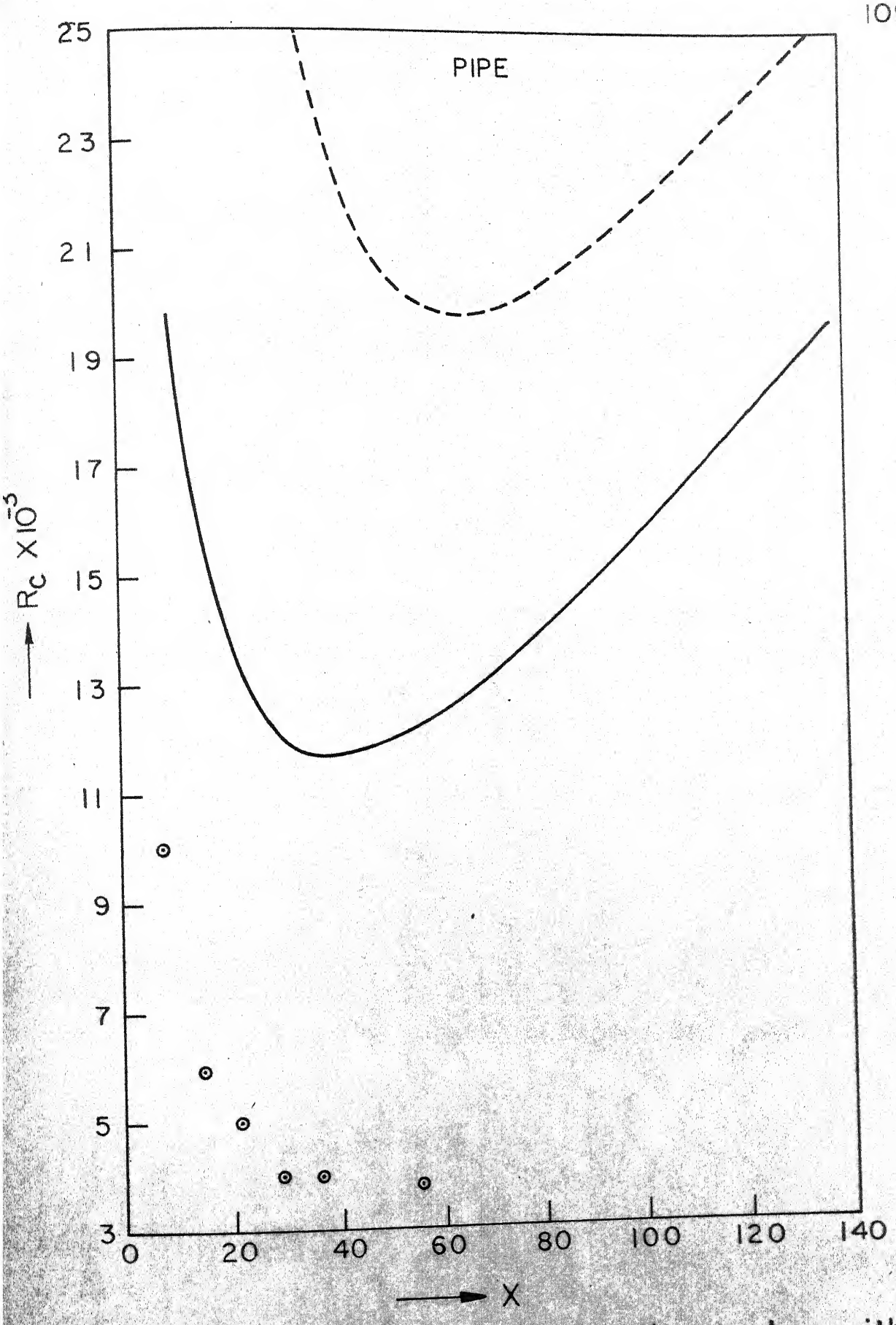

6.33 Variation of critical Reynolds number with X. ——, Hornbeck's profile; – – –, Sparrow's profile; ⊙ experimental data of Sarpkaya [48] for critical Reynolds number

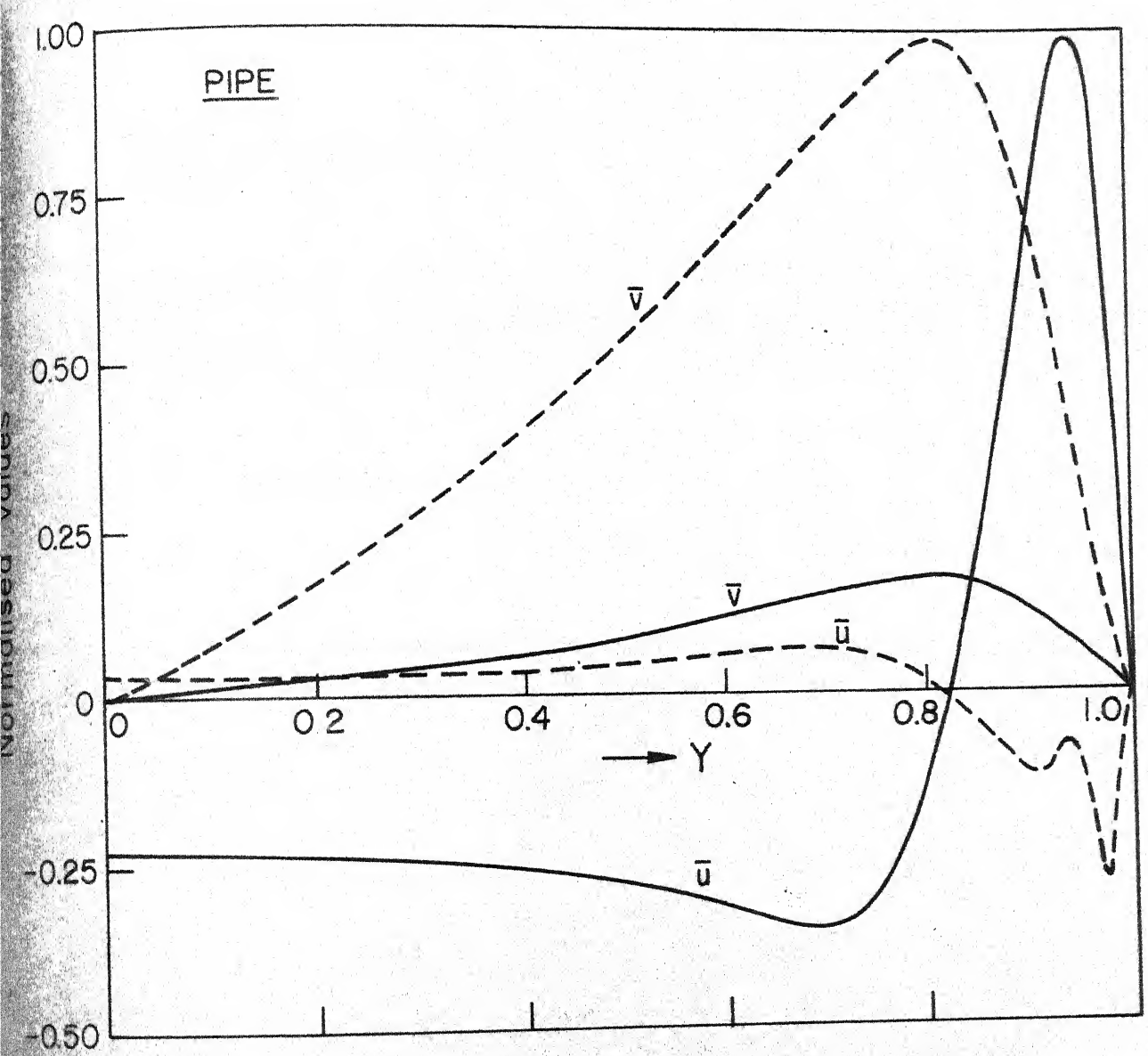

Fig.6.34 Eigenfunctions $\bar{u}/|\bar{u}|_{max}$ and $\bar{v}/|\bar{v}|_{max}$ for $R=11779$, $\omega=1.0$ at $\bar{X}=0.0035$, ($|k_{oi}|<10^{-6}$, $|\bar{v}|_{max}/|\bar{u}|_{max}=0.2432$). ——, real part; ----, imaginary part.

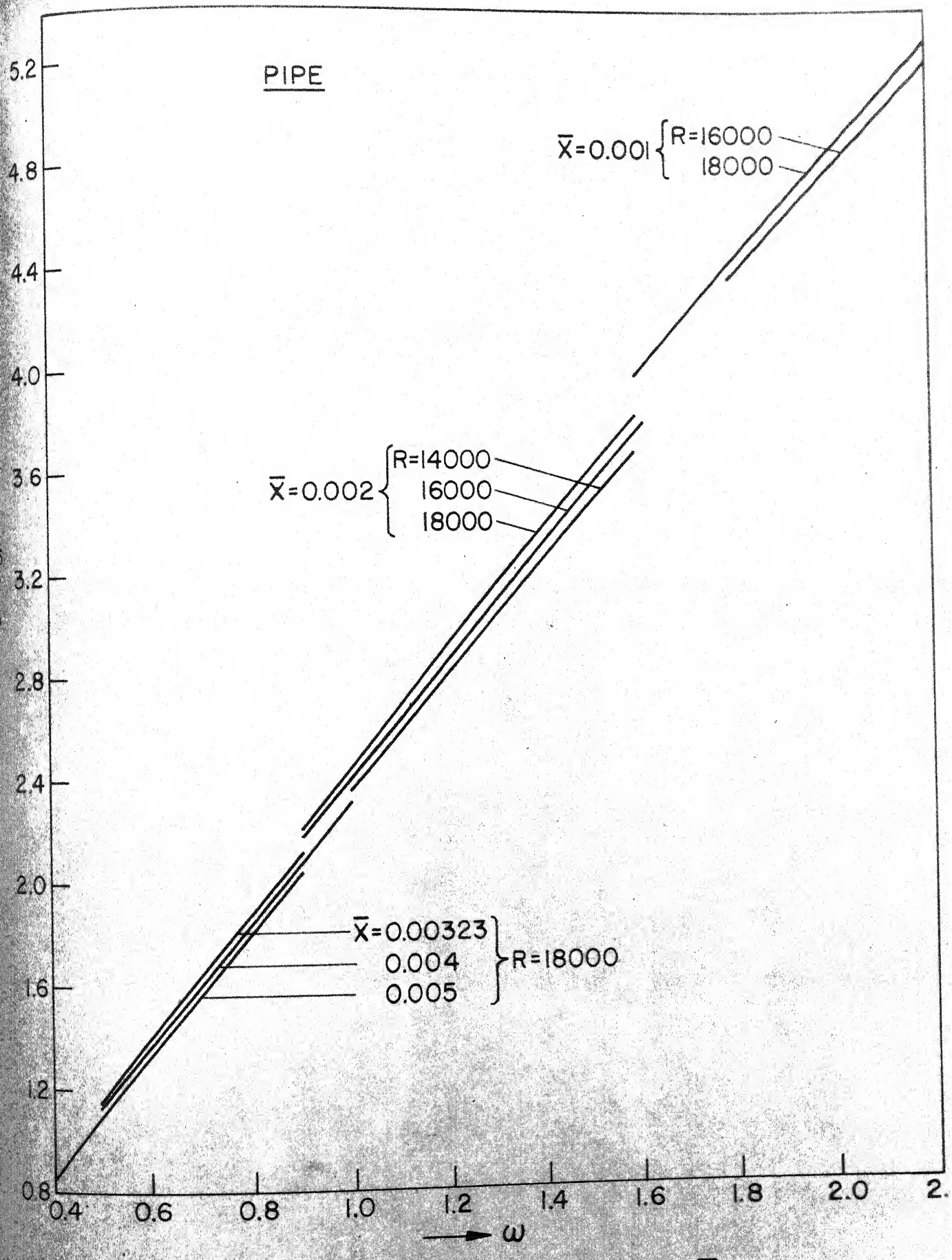

Fig.6.35 Variation of k_{or} with ω for different $\bar{X}$ and R

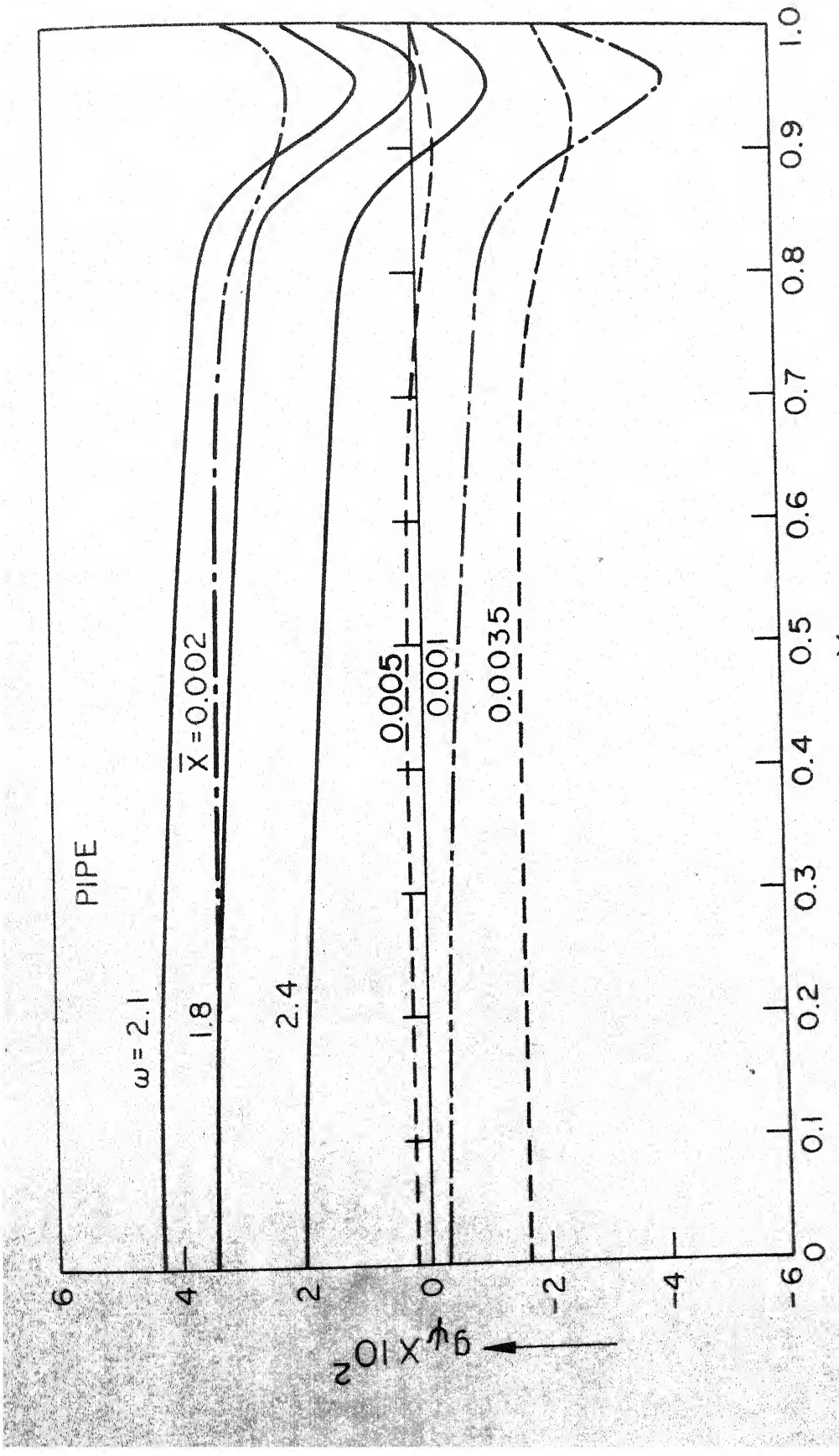

Fig.6.36 Variation of g_ψ with Y for various $\bar{X}$, R and ω. ——, $\bar{X}$ = 0.001, R = 16000; — — —, R = 16000, ω = 1.5; – – – –, R = 13000, ω = 0.6

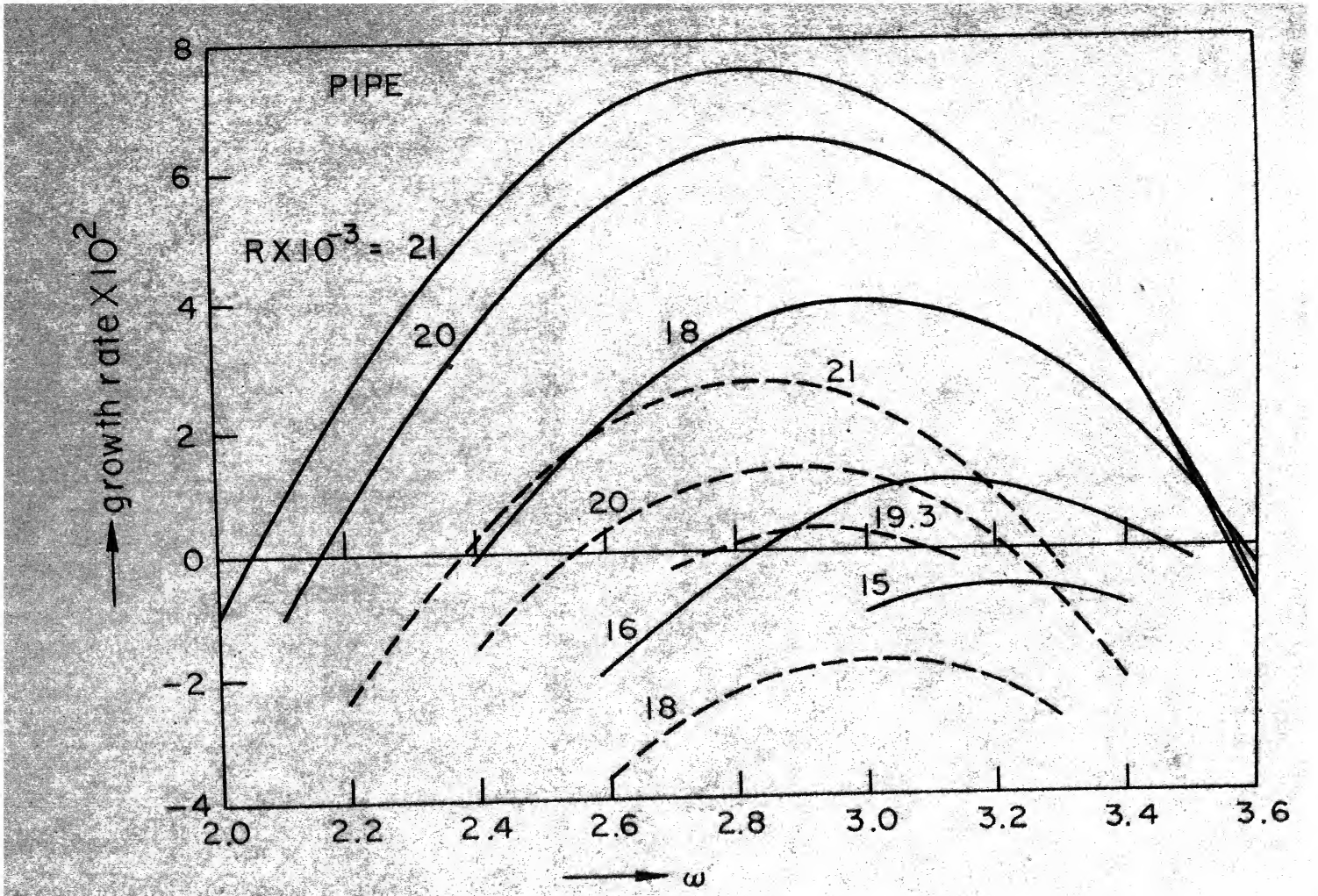

Fig. 6.37 Various growth rates at $\bar{X} = 0.0005$ and different R.——, $g_\psi(\bar{X}, 0)$; ----, g_E

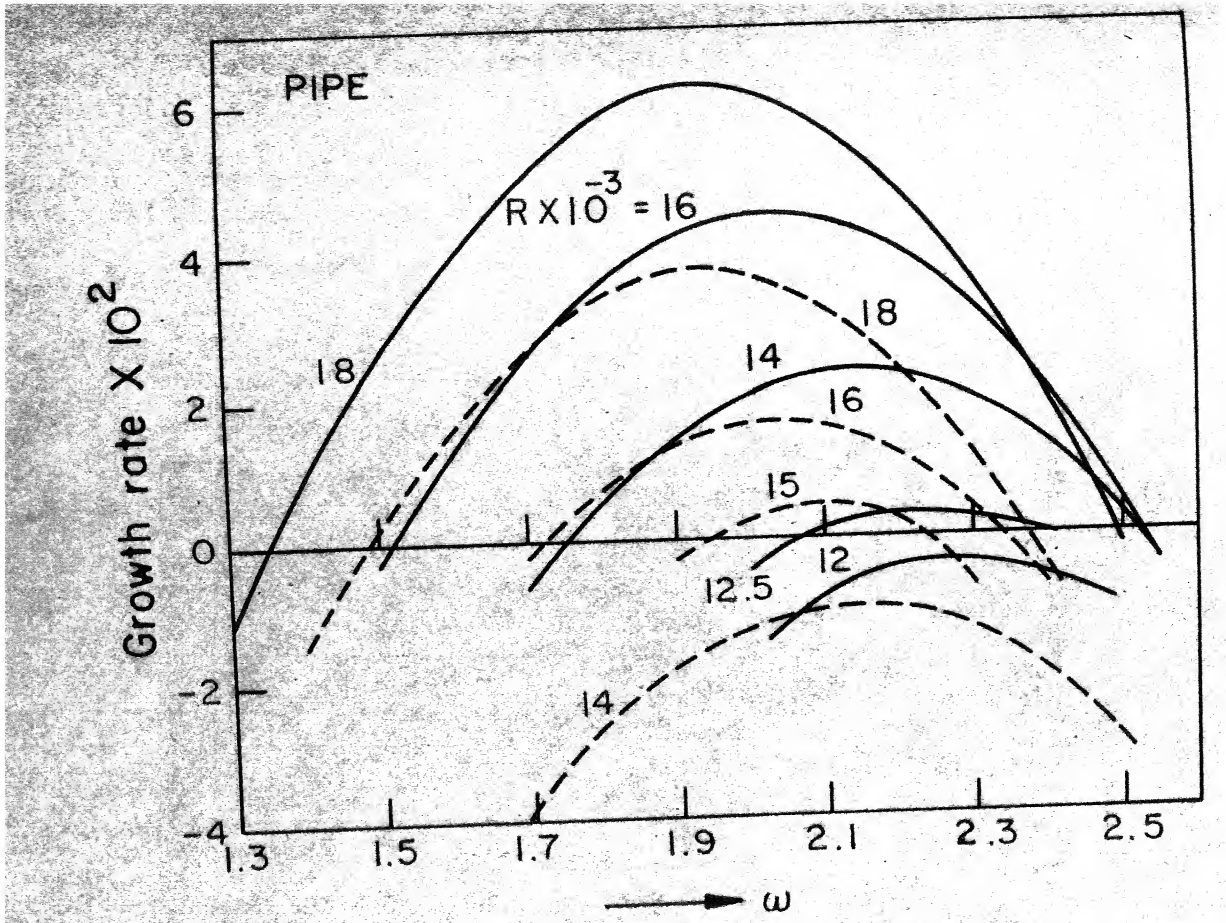

Fig. 6.38 Various growth rates at $\bar{X} = 0.001$ and different R.——, $g_\psi(\bar{X}, 0)$; – – –, g_E

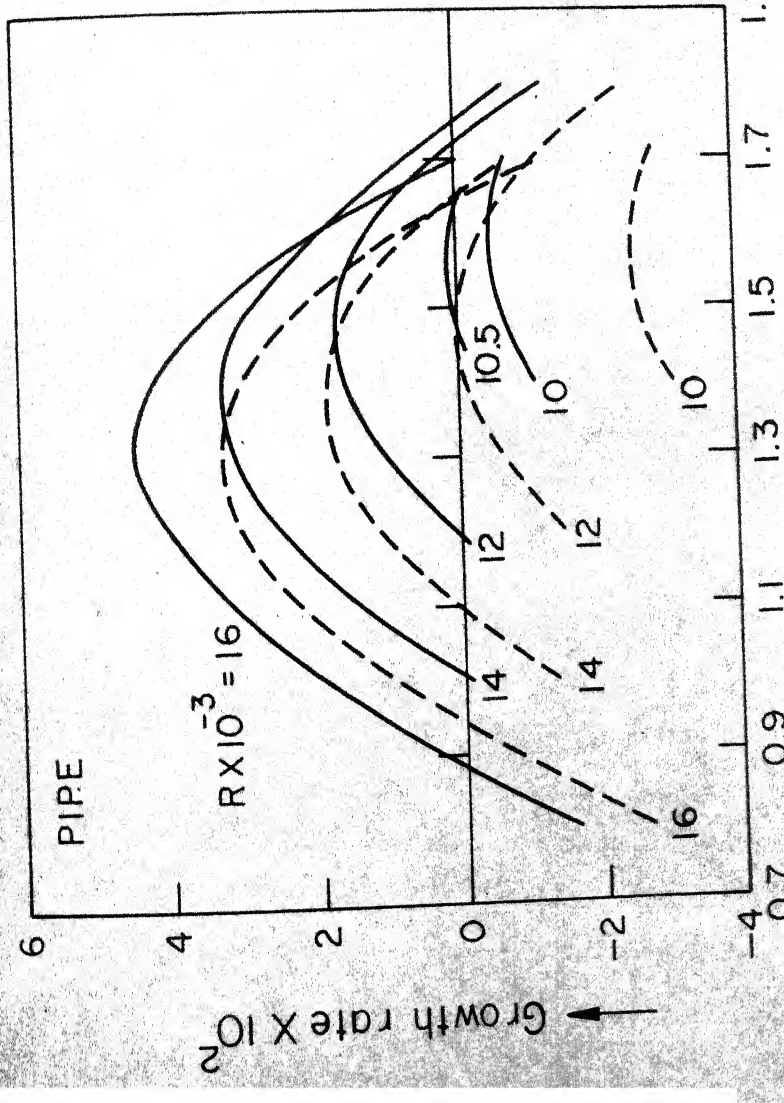

Fig.6.39 Various growth rates at $\overline{X} = 0.002$ and different R. ——, $g_\psi(\overline{X}, 0)$; – – – –, g_E

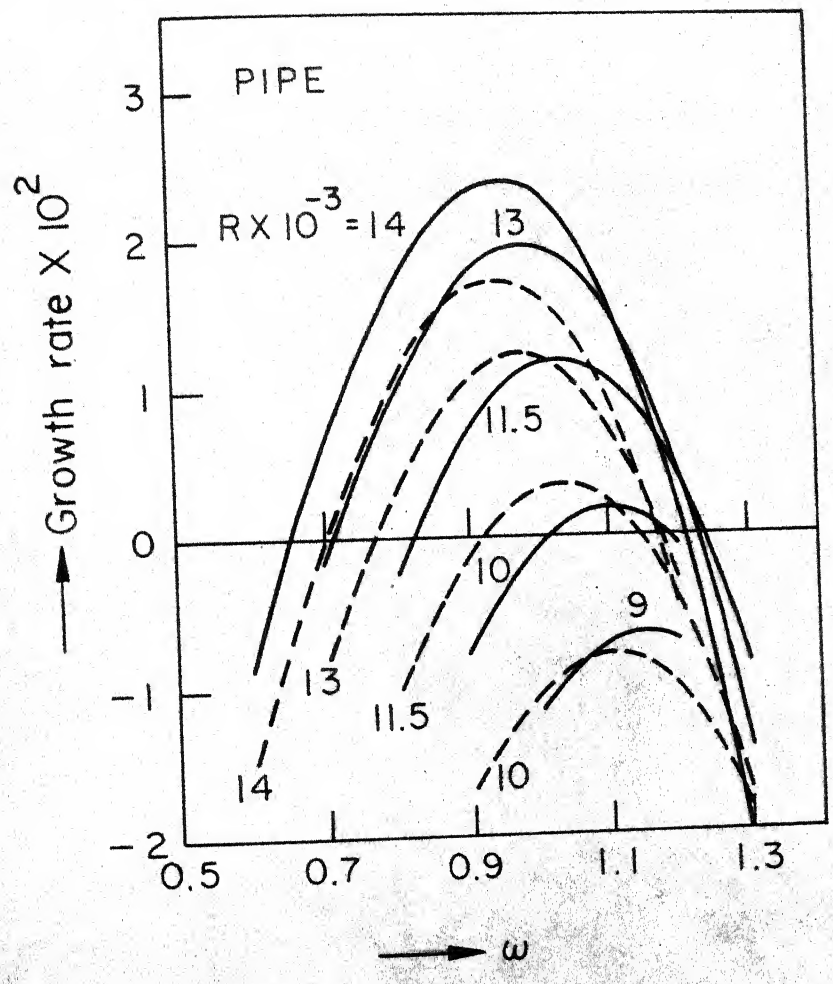

Fig. 6.40 Various growth rates at $\bar{X} = 0.0035$ and different R. ——, $g_\psi(\bar{X},0)$; ----, g_E

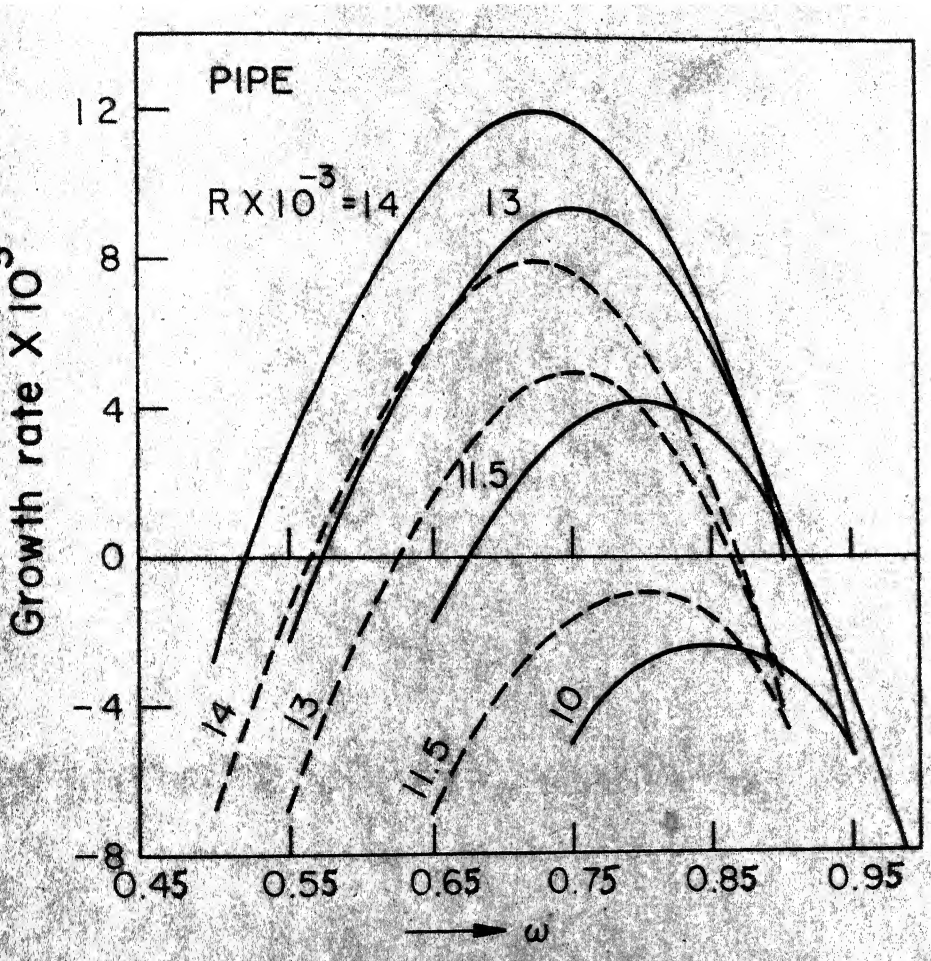

Fig.6.41 Various growth rates at $\bar{X} = 0.005$ and different R. ——, $g_\psi(\bar{X}, 0)$; - - - -, g_E

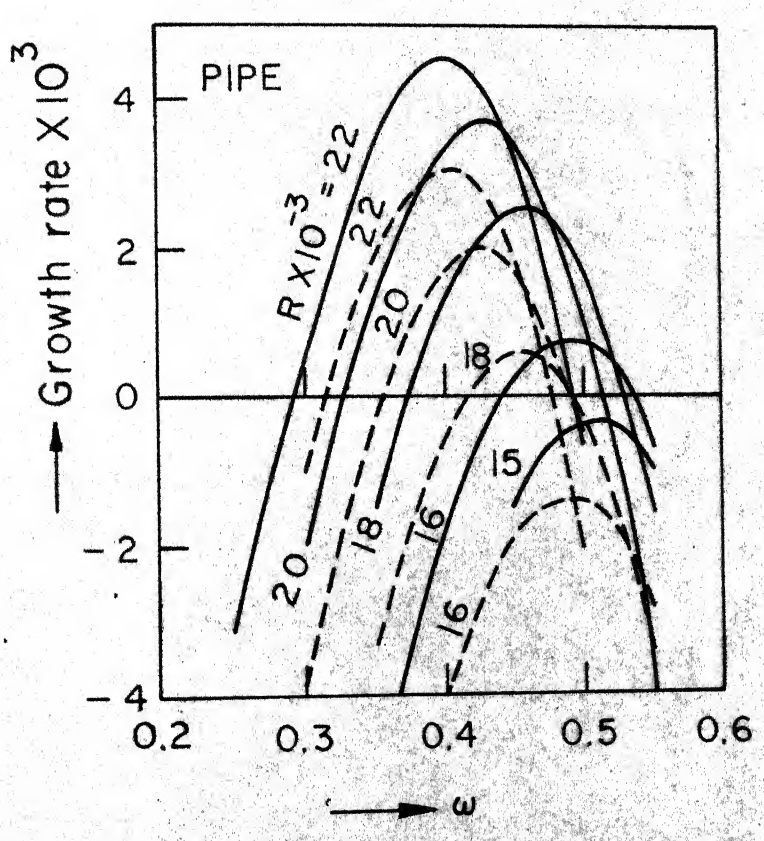

Fig. 6.42 Various growth rates at $\bar{X} = 0.007$ and different R. ——, $g_\psi(\bar{X}, 0)$; ----, g_E

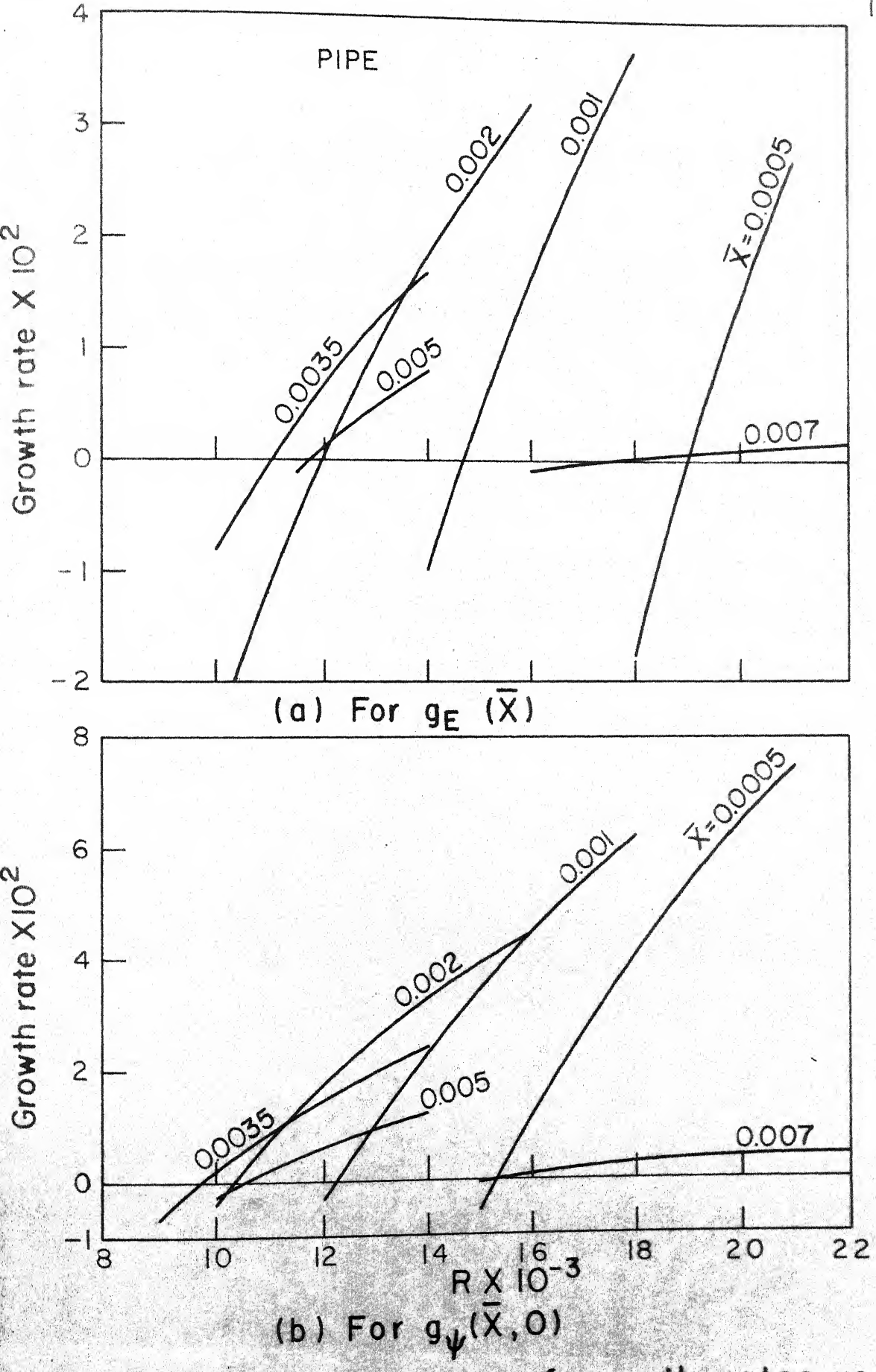

Fig. 6.43 Maximum values of growth rates vs R at various $\bar{X}$

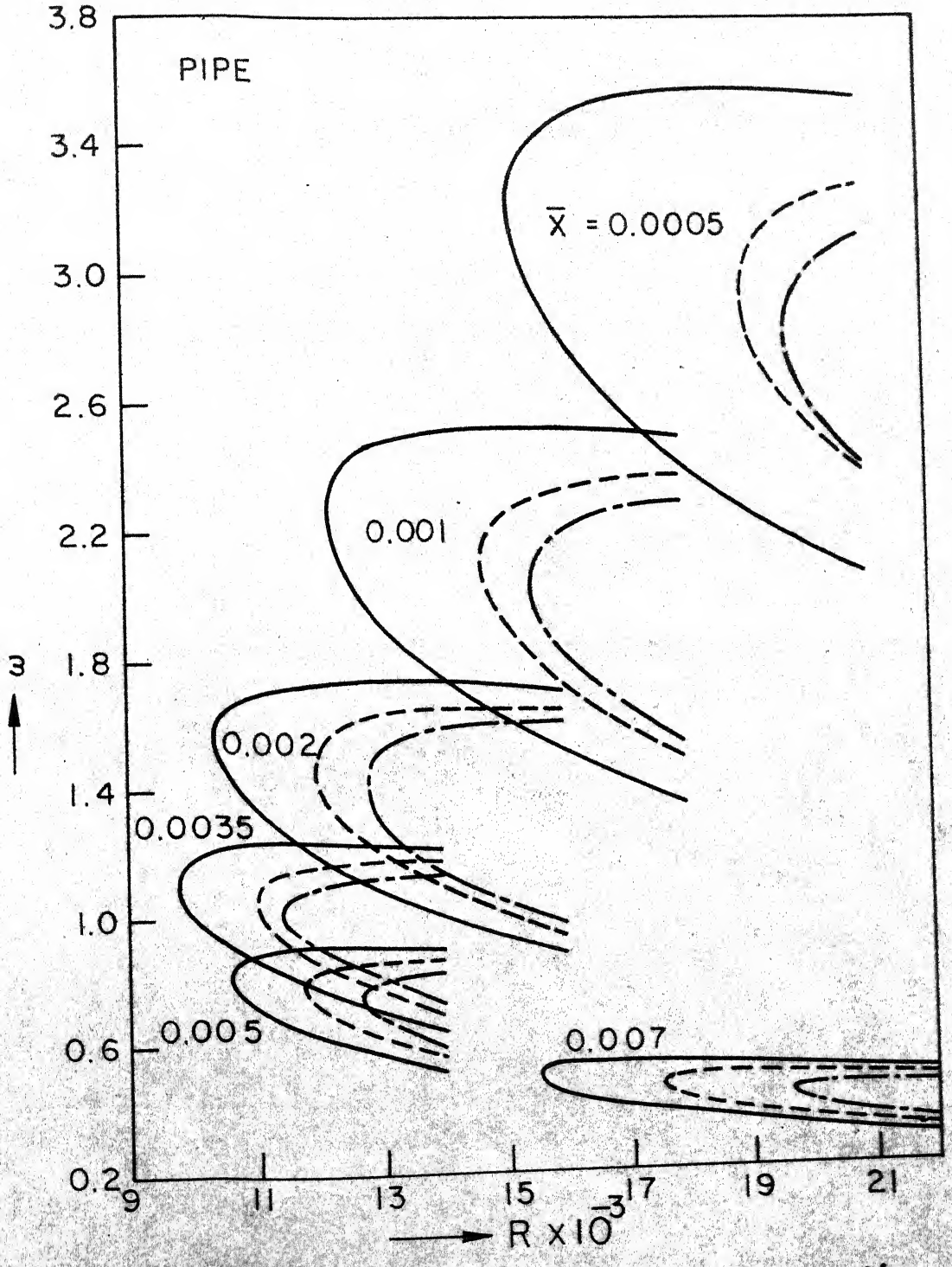

Fig. 6.44 Neutral curves at various axial locations. ——, based on $g_\psi(\bar{X}, 0)$; - - - -, based on g_E; ——- ——, based on parallel flow theory

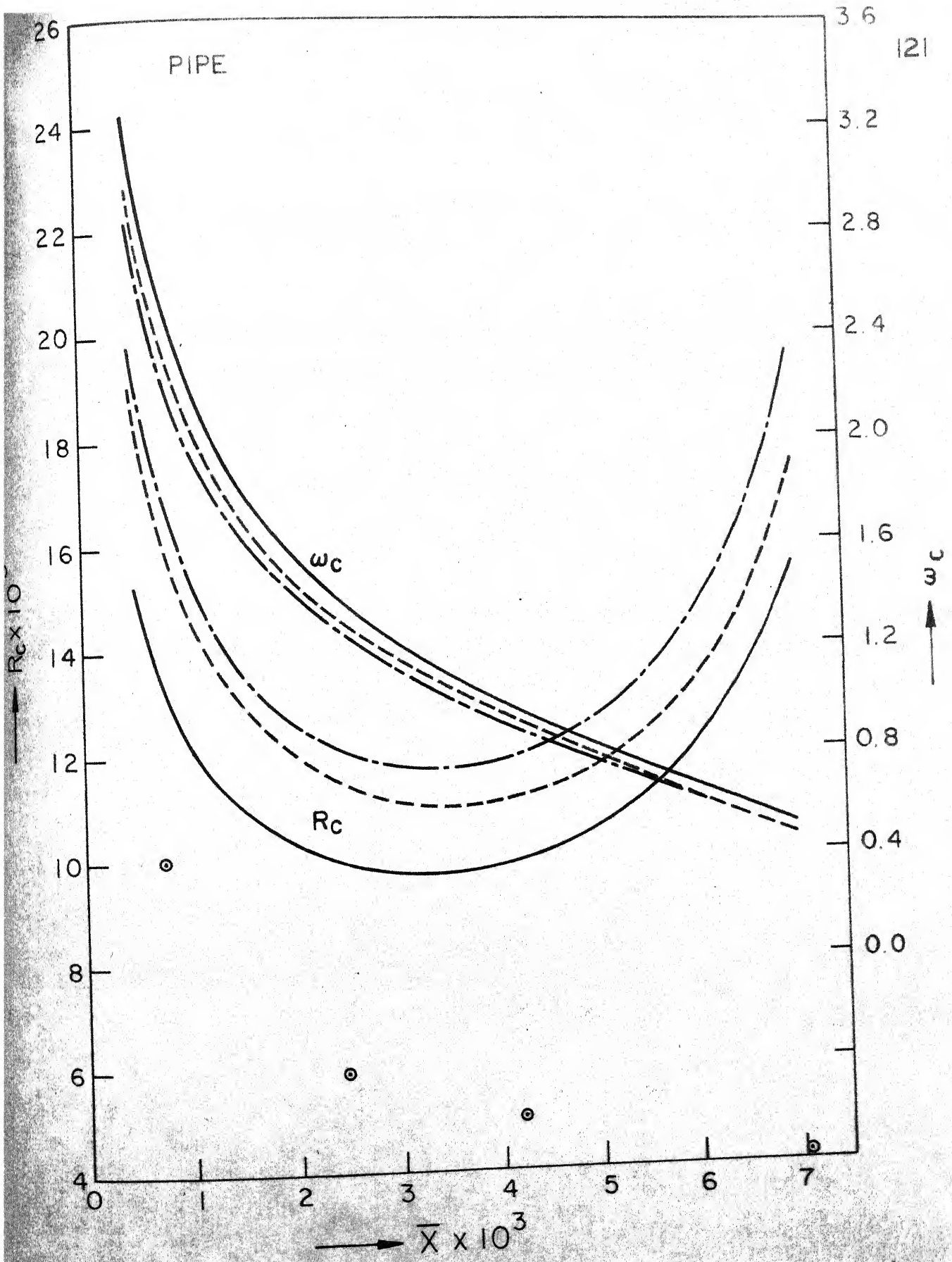

ig.6.45 Variation of R_c and ω_c with $\bar{X}$. ——, based on $g_\psi(\bar{X}, 0)$; – – – –, based on g_E; — – —, based on parallel flow theory ; ⊙ Experimental data [48] for R_c

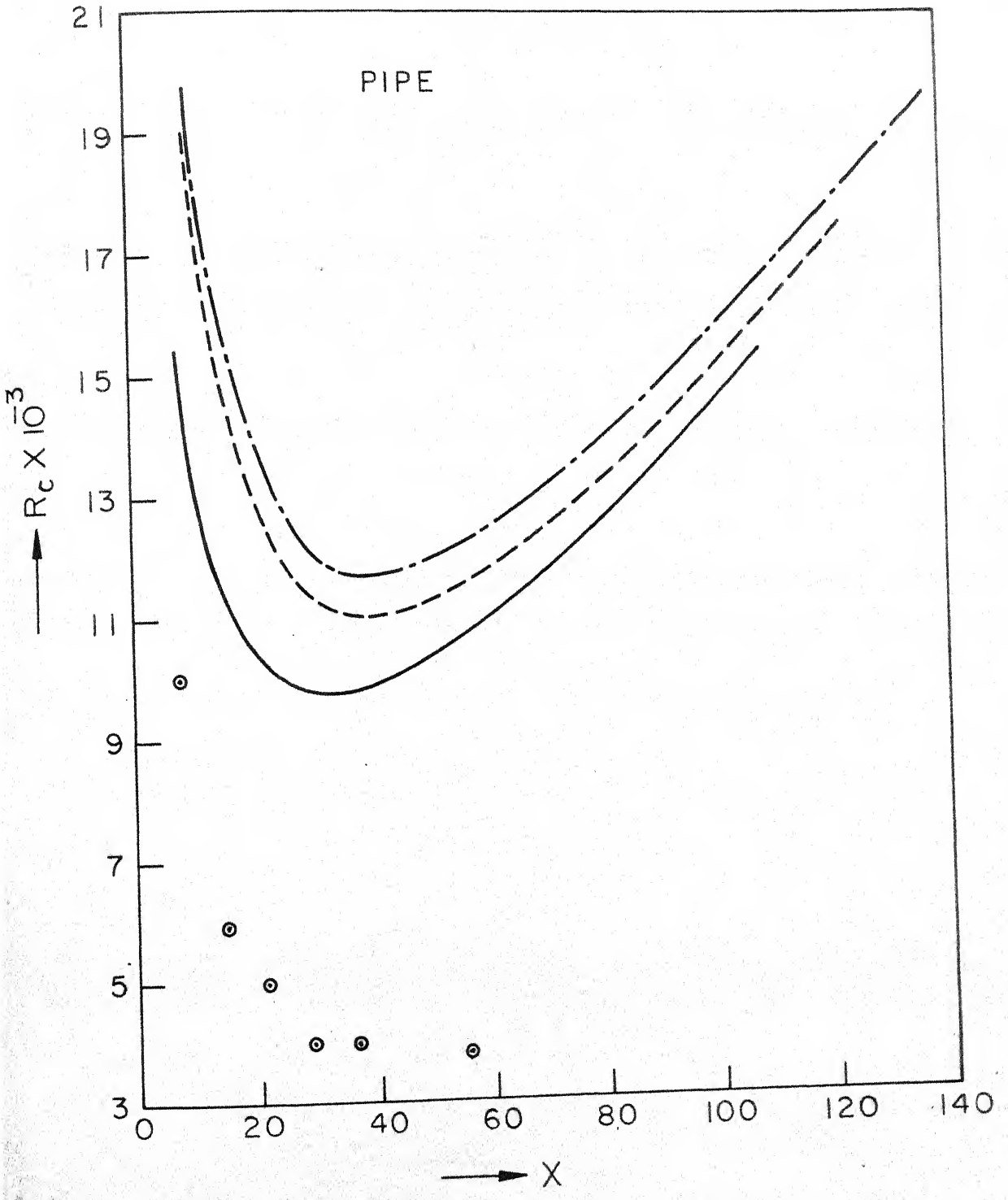

Fig. 6.46 Variation of R_c with X. ——, $g_\psi(X,0)$; - - - -, g_E; —·—, parallel flow theory; ⊙ Sarpkaya's experimental data [48]

Chapter 7

CONCLUSIONS

Spatial stability characteristics of the developing flow in a two dimensional channel and in a rigid circular pipe have been obtained for the actual nonparallel flow as well as for its parallel flow approximate. The developing flow velocity field has been determined by the finite difference method. Considering the developing flow in the channel as a parallel flow, it is found that the symmetric disturbances are more unstable than antisymmetric disturbances. Thus, for most of the analysis, the disturbance is assumed to be symmetric for channel flow, and axisymmetric for pipe flow. Further, only the wall modes have been considered in case of pipe flow stability since they exhibit instability in the developing flow region. The central mode, on the contrary, remains stable. This mode is, however, found to be less stable for the developing flow than for the fully developed flow.

For the parallel flow analysis, results have also been compared with those for the velocity profile given by Sparrow et al.'s linearization method. This comparison reveals that even though the two velocity profiles differ by less than 5% throughout the field of flow in the near-entry region, their stability characteristics

are quite different. Also, the comparative study of the stability characteristics obtained for both geometries of flow on the basis of parallel and nonparallel theories shows that the results are significantly different. The non-parallel effects introduce the following main differences:

(i) The growth rate becomes a function of the streamwise as well as the transverse coordinate. The growth rate of the disturbance stream function, which is maximum at Y = 0, diminishes gradually and uniformly towards the boundary layer edge and changes rapidly in the boundary layer region; the amount of variation of the growth rate in this region is a function of the axial location and frequency of the disturbance.

(ii) The growth rate also becomes a function of the disturbance property involved, that is, the stream function, velocity components, and kinetic energy density of the disturbance have different growth rates. Thus at any point in the flow region some disturbance property may be growing while others may be decaying. This implies that there are different neutral curves and hence different critical Reynolds number and frequency for different disturbance properties.

(iii) The actual developing flow becomes unstable over a wider range of frequencies as compared to its parallel flow approximate; the actual amount of

such an effect depends on the growth rate used for determining the neutral curve. It is found that g_{ψ} $(\bar{X}, 0)$, the growth rate of the disturbance stream function at Y = 0, (a) is the maximum of all growth rates at any frequency for all R and $\bar{X}$, (b) remains positive for the widest range of frequencies, and (c) gives the minimum critical Reynolds number at all $\bar{X}$.

(iv) Like the growth rate, the disturbance wavenumber also becomes a function of the streamwise and transverse coordinates as well as a function of the disturbance property. However, the wavenumber obtained from the parallel flow theory is little affected by the non-parallel effects.

It is found that the step-by-step integration of the continuity and momentum equations separately instead of a single differential equation for the disturbance is more economical as well as accurate. Also, selective application of the Gram-Schmidt orthonormalization procedure is found to be the best way to control the parasitic errors during numerical integration.

The following conclusions apply to the two geometries of flow separately.

7.1. Parallel Plate Channel

When compared with the parallel flow stability results for symmetric disturbances, antisymmetric disturbances are found to be more stable at all $\bar{X}$ except for some eigenstates that lie close to the lower branch of the neutral curve and correspond to Reynolds numbers much greater than the critical value; the critical Reynolds number being lower at all $\bar{X}$ for the symmetric disturbances. The critical Reynolds number for the symmetric disturbance decreases continuously with $\bar{X}$ while for the antisymmetric disturbance it first decreases to about 12100 at $\bar{X} = 0.005$ and then increases rapidly so that the fully developed flow seems to be stable to all antisymmetric disturbances.

For the symmetric disturbances, the developing flow is found to be more stable than the fully developed flow. The critical Reynolds number, wavenumber and frequency decrease with increasing $\bar{X}$ and approach asymptotically the corresponding values of 3848.1, 1.0198 and 0.40369 respectively for the fully developed flow. The comparative study of the stability behaviour of the B-O and the Sparrow velocity profiles for the developing flow considering it as a parallel flow shows that the critical Reynolds numbers are same for both the velocity profiles for $\bar{X} \geq 0.084$ (or $X \geq 440$) but for $\bar{X} < 0.084$, the critical Reynolds number for the B-O profile is less than that for

the Sparrow profile owing to the difference in the two velocity profiles. The critical Reynolds number at $\bar{X} = 60$ for the B-O profile is about 10900, which is almost half of that for the Sparrow profile. This large difference in the critical Reynolds numbers implies that the shape of velocity profile is an important factor for deciding the stability behaviour of the flow. In the absence of any experimental data on the stability characteristics of the developing flow in a channel, it is difficult to determine which velocity profile predicts the stability of the real flow more accurately. However, since the superiority of the B-O profile over the Sparrow profile has been accepted by several research workers [88-93], one has the intuitive feeling that the stability results for the B-O profile should be closer to the actual ones.

The nonparallel theory predicts critical Reynolds numbers which are lower than those obtained from the parallel flow theory. The latter predicts a value which is higher than that corresponding to $g_{\psi}(\bar{X}, 0)$ and to g_E for the nonparallel flow by 22.8% and 4.5% respectively at $\bar{X} = 0.001$. These differences reduce to 8.3% and 1.6%, respectively at $\bar{X} = 0.008$. Moreover, the neutral curves based on different growth rates tend to merge into the neutral curve for the parallel flow theory as $\bar{X}$ increases, implying thereby that the nonparallel effects vanish for large $\bar{X}$ as they should.

7.2. Circular Pipe

Like the fully developed flow, the developing flow is stable to the central mode. However, unlike the fully developed flow, it is unstable to the wall mode. At all axial locations the critical frequency and wavenumber for the wall mode obtained on the parallel flow approximation for the Hornbeck profile have been found to be greater than those for the Sparrow profile. However, reverse is true for the critical Reynolds number. The critical Reynolds numbers at $\bar{X} = 0.0035$ for the Hornbeck and Sparrow velocity profiles are respectively 11700 and 19800. As one moves downstream or upstream of this point, the R_c vs. $\bar{X}$ curve for the Sparrow profile rises more rapidly in comparison to that for the Hornbeck profile implying thereby that the Hornbeck profile is unstable over a larger inlet length of the pipe.

The actual nonparallel flow in the developing flow region of the pipe yields a lower critical Reynolds number. The minimum critical Reynolds number corresponding to $g_\psi(\bar{X}, 0)$ and to $g_E(\bar{X})$ for the Hornbeck profile are 9700 at $\bar{X} = 0.00325$ and 11000 at $\bar{X} = 0.0035$, respectively. The parallel flow theory, in comparison to the results based on $g_\psi(\bar{X}, 0)$ and $g_E(\bar{X})$, overpredicts the critical Reynolds number by 29.8% and 3.7% respectively at $\bar{X} = 0.0005$, by 20% and 6.4% at $\bar{X} = 0.0035$, and by 26.5% and 12.0% respectively at $\bar{X} = 0.007$. The R_c vs. $\bar{X}$ curves obtained

on the basis of nonparallel flow theory are flatter than those obtained from the parallel flow theory. Thus the actual developing flow remains unstable over a larger inlet length of the pipe than its parallel flow approximate. The first instability of the flow, on the basis of $g_{\psi}(\bar{X}, 0)$, $g_{E}(\bar{X})$ and the parallel flow theory, is found to occur at $X \simeq 33$, 38 and 37 respectively. The R_c vs. $\bar{X}$ or X curve obtained on the basis of $g_{\psi}(\bar{X}, 0)$ is closest to the experimental data of Sarpkaya [48].

REFERENCES

1. Reynolds, O., An Experimental Investigation of the Circumstances Which Determine Whether the Motion of Water Shall be Direct or Sinuous and the Law of Resistance in Parallel Channels, in "Scientific Papers", Vol. 2, 1883, pp. 51-105.

2. Lin, C.C., The Theory of Hydrodynamic Stability, Cambridge University Press, 1955.

3. Thomas, L.H., Stability of Plane Poiseuille Flow, Phys. Rev., 91, 1953, pp. 780-783.

4. Hains, F.D., Stability Diagrams for Magnetohydrodynamic Channel Flow, Phys. Fluids, 10, 1967, pp. 2079-2080.

5. Orszag, S.A., Accurate Solution of the Orr-Sommerfeld Stability Equation, J. Fluid Mech., 50, 1971, pp. 689-703.

6. Chock, D.P. and Schechter, R.S., Critical Reynolds Number of the Orr-Sommerfeld Equation, Phys. Fluids, 16, 1973, pp. 329-330.

7. Davey, A., A Simple Numerical Method for Solving Orr-Sommerfeld Problems, Quart. J. of Mech. and Appl. Math., 26, 1973, pp. 401-411.

8. Nishioka, M., Iida, S. and Ichikawa, Y., An Experimental Investigations of the Stability of Plane Poiseuille Flow, J. Fluid Mech., 72, 1975, pp. 731-751.

9. Karnitz, A., Potter, M.C. and Smith, M.C., An Experimental Investigation of Transition of a Plane Poiseuille Flow, ASME Trans., J. Fluids Engg., Paper No. 75-FE-B.

10. Sherlin, G.C., Behaviour of Isolated Disturbances Superimposed on Laminar Flow in a Rectangular Pipe, J. Res. N.B.S. Sec. A, Phys. and Chem., A64, 1960, pp. 281-289.

11. Narayanan, M.A.B. and Narayana, T., Some Studies on Transition from Laminar to Turbulent Flow in a Two-Dimensional Channel, Z. Agnew, Math. Phys., 18, 1967, pp. 642-650.

12. Patel, V.C. and Head, M.R., Some Observation on Skin Friction and Velocity Profiles in Fully Developed Pipe and Channel Flows, J. Fluid Mech., 38, 1969, pp. 181-201.

13. Breslin, J.A., An Experimental Investigation of Laminar-Turbulent Transition in Flow Through a Rectangular Pipe, Lehigh University Tech. Rep., No. 22, 1970.

14. Hahneman, E., Freeman, J.C. and Finston, M., Stability of Boundary Layer and Flow in Entrance Section of Channels, J. Aero. Sc., 15, 1948, pp. 93-96.

15. Chen, T.S. and Sparrow, E.M., Stability of the Developing Laminar Flow in a Parallel Plate Channel, J. Fluid Mech., 30, 1967, pp. 209-224.

16. Lin, C.C., On the Stability of Two-Dimensional Parallel Flows. Parts I-III, Quart. Appl. Math., 3, 1945-46, pp. 117-142, 218-234, and 277-301.

17. Schlichting, H., Boundary Layer Theory, McGraw Hill, 1968, pp. 176-178.

18. Nachtsheim, P.R., An Initial Value Method for the Numerical Treatment of the Orr-Sommerfeld Equation for the Case of Plane Poiseuille Flow, NASA TN-D2414, 1964.

19. Sparrow, E.M., Lin, J.H. and Lundgren, T.S., Flow Development in the Hydrodynamic Entrance Region of Tubes and Ducts, Phys. Fluids, 7, 1964, pp. 338-347.

20. Bodoia, J.R. and Osterle, J.F., Finite Difference Analysis of Plane Poiseuille Flow and Couette Flow Developments, Appl. Sc. Res. (Sec. A), 10, 1961, pp. 265-276.

21. Shen, S.F., Stability of Laminar Flows, Section G in Theory of Laminar Flows, edited by Moore, F.K., Princeton University Press, 1964.

22. Fu, T.S. and Joseph, D.D., Laminar Instability of Asymmetric Flow in Channels, Phys. Fluids, 13, 1970, pp. 217-221.

23. Chen, T.S. and Sparrow, E.M., Stability of Asymmetric Hydrodynamically Developing Channel Flows, Phys. Fluids, 13, 1970, pp. 827-829.

24. Shen, S.F., Some Considerations on the Laminar Stability of Time Dependent Basic Flows, J. Aero. Sc., 28, 1961, pp. 397-404.

25. Schubauer, G.B. and Skramstad, H.K., Laminar Boundary Layer Oscillations and Stability of Laminar Flow, J. Aero. Sc., 14, 1947, pp. 69-78.

26. Ross, J.A., Barnes, F.H., Burns, J.G. and Ross, M.A.S., The Flat Plate Boundary Layer, Part 3, Comparison of Theory with Experiment, J. Fluid Mech., 43, 1970, pp. 819-832.

27. Sexl, T., Uber Dreidimensionale Storungen der Poiseuilleschen Stromung, Annalen Der Physik, 84, 1927, pp. 807-822.

28. Pretsch, T., Uber die Stabiliatat einer Laminarstromung in einem Geraden Rohr mit Kreisformigen Querschnitt, Z. Agnew, Math. Mech., 21, 1941, pp. 204-217.

29. Pekeris, C.L., Stability of a Laminar Flow Through a Straight Pipe of Circular Cross-Section to Infinitesimal Disturbances Which are Symmetrical about the Axis of the Pipe, Proc. Nat. Ac. Sc., U.S., 34, 1948, pp. 285-295.

30. Corcos, G.M. and Sellars, J.R., On the Stability of Fully Developed Flow in a Pipe, J. Fluid Mech., 5, 1959, pp. 97-113.

31. Schensted, I.V., Contributions to the Theory of Hydrodynamical Stability, Ph.D. Thesis, Univ. of Michigan, 1960.

32. Davey, A. and Drazin, P.G., The Stability of Poiseuille Flow in a Pipe, J. Fluid Mech., 36, 1969, pp. 209-218.

33. Lessen, M., Saddler, S.G. and Liu, T.Y., Stability of Pipe Poiseuille Flow, Phys. Fluids, 11, 1968, pp. 1404-1409.

34. Burridge, D.M., The Stability of Poiseuille Pipe Flow to Non-axisymmetric Disturbances, Tech. Rept. No. 34, Florida State University, 1970.

35. Graebel, W.P., The Stability of Pipe Flow, Part 1, Asymptotic Analysis for Small Wavenumbers, J. Fluid Mech., 43, 1970, pp. 279-290.

36. Salwen, H. and Grosch, C.E., The Stability of Poiseuille Flow in a Pipe of Circular Cross-Section, J. Fluid Mech., 54, 1972, pp. 93-112.

37. Gill, A.E., On the Behaviour of Small Disturbances to Poiseuille Flow in a Circular Pipe, J. Fluid Mech., 21, 1965, pp. 145-172.

38. Gill, A.E., The Least Damped Disturbance to Poiseuille Flow in a Circular Pipe, J. Fluid Mech., 61, 1973, pp. 97-107.

39. Leite, R.J., An Experimental Investigation of the Stability of Poiseuille Flow, J. Fluid Mech., 5, 1959, pp. 81-96.

40. Garg, V.K. and Rouleau, W.T., Linear Spatial Stability of Pipe Poiseuille Flow, J. Fluid Mech., 54, 1972, pp. 113-127.

41. Lessen, M., Fox, J.A., Bhat, W.V. and Liu, T., Stability of Hagen-Poiseuille Flow, Phys. Fluids, 7, 1964, pp. 1384-1385.

42. Tatsumi, T., Stability of Laminar Inlet Flow Prior to the Formation of Poiseuille Regime, Part 1, J. Phys. Soc. Japan, 7, 1952, pp. 489-495.

43. Tatsumi, T., Stability of Laminar Inlet-Flow Prior to the Formation of Poiseuille Regime, Part II, J. Phys., Soc. Japan, 7, 1952, pp. 495-502.

44. Chen, B.H.P., Finite Amplitude Disturbances in the Stability of Pipe Poiseuille Flow, Ph.D. Thesis, The University of Rochester, 1969.

45. Huang, L.M. and Chen, T.S., Stability of Developing Laminar Pipe Flow, Phys. Fluids, 17, 1974, pp. 245-247.

46. Huang, L.M. and Chen, T.S., Stability of Developing Pipe Flow Subjected to Non-axisymmetric Disturbances, J. Fluid Mech., 63, 1974, pp. 183-193.

47. Hornbeck, R.W., Laminar Flow in Entrance Region of a Pipe, Appl. Sc. Res. (Sec. A), 13, 1963, pp. 224-232.

48. Sarpkaya, T., A Note on the Stability of Developing Laminar Pipe Flow Subjected to Axisymmetric and Non-axisymmetric Disturbances, J. Fluid Mech., 68, 1975, pp. 345-351.

49. Shen, F.C.T., Chen, T.S. and Huang, L.M., The Effect of Mainflow Radial Velocity on the Stability of Developing Laminar Pipe Flow, J. Appl. Mech., 98, 1976, pp. 209-212.

50. Sato, H. and Sakao, F., An Experimental Investigation of the Instability of a Two-Dimensional Jet at Low Reynolds Numbers, J. Fluid Mech., 20, 1964, pp. 337-352.

51. Scotti, R.S. and Corcos, G.M., An Experiment on the Stability of Small Disturbances in a Stratified Shear Layer, J. Fluid Mech., 52, 1972, pp. 499-528.

52. Mattingly, G.E. and Criminale, W.O., The Stability of an Incompressible Two-Dimensional Wake, J. Fluid Mech., 51, 1972, pp. 233-272.

53. Benney, D.J. and Rosenblat, S., Stability of Spatially Varying and Time-dependent Flows, Phys. Fluids, 7, 1964, pp. 1385-1386.

54. Lanchon, H. and Eckhaus, W., Sur l'analyse de la Stabilite des Ecoulements Faiblement Divergents, J. Mecanique, 3, 1964, pp. 445-459.

55. Barry, M.D.J. and Ross, M.A.S., The Flate Plate Boundary Layer, Part 2, The Effect of Increasing Thickness on Stability, J. Fluid Mech., 43, 1970, pp. 813-818.

56. Boehman, L.I., in Proceedings of the 12th Midwest Mechanics Conference (University of Notre Dame Press, Notre Dame, Indiana), 6, 1971, p. 193.

57. Haaland, S.E., Contribution to Linear Stability Theory of Nearly Parallel Flows, Ph.D. Thesis, University of Minnesota, Minneapolis, 1972.

58. Wazzan, A.R., Okamura, T.T. and Smith, A.M.O., Stability of Laminar Boundary Layer at Separation, Phys. Fluids, 10, 1967, pp. 2540-2545.

59. Bajaj, A.K. and Garg, V.K., Linear Stability of Jet Flows, J. Appl. Mech., 44, 1977, pp. 378-384.

60. Joseph, D.D., Response Function of Pipe-Poiseuille Flow, Appendix: A Perturbation Theory for Nearly Parallel Flows, Advances in Applied Mechanics, Academic Press, Vol. 14, 1974, pp. 268-276.

61. Volodin, A.G., Izv. Sib. Otd. Akad. Nauk SSSR, 2, 1973, p. 13.

62. Ling, C.H. and Reynolds, W.C., Nonparallel Flow Corrections for the Stability of Shear Flows, J. Fluid Mech., 59, 1973, pp. 571-591.

63. Gaster, M., On the Effects of Boundary Layer Growth on Flow Stability, J. Fluid Mech., 66, 1974, pp. 465-480.

64. Bouthier, M., Stabilite Lineaire des Ecoulements Presque Paralleles, J. Mecanique, 11, 1972, pp. 599-621.

65. Bouthier, M., Stabilite Lineaire des Ecoulements Presque Paralleles, II La Couche Limite de Blasius, J. Mecanique, 12, 1973, pp. 75-95.

66. Nayfeh, A.H., Saric, W.S. and Mook, D.T., Stability of Nonparallel Flows, Archives of Mech., 26, 1974, pp. 401-406.

67. Saric, W.S. and Nayfeh, A.H., Nonparallel Stability of Boundary Layer Flows, Phys. Fluids, 18, 1975, pp. 945-950.

68. Smith, F.T., On the Nonparallel Flow Stability of the Blassius Boundary Layer, Proc. Roy. Soc. London, A 366, 1979, pp. 91-109.

69. Drazin, P.G., On a Model of Instability of Slowly Varying Flow, Quart. J. Mech. Appl. Math., 27, 1974, p. 59.

70. Eagles, P.M. and Weissman, M.A., On the Stability of Slowly Varying Flow: The Divergent Channel, J. Fluid Mech., 69, 1975, pp. 241-262.

71. Crighton, D.G. and Gaster, M., Stability of Slowly Diverging Jet Flow, J. Fluid Mech., 77, 1976, pp. 397-413.

72. Eagles, P.M., On the Stability of Slowly Varying Flow Between Concentric Cylinders, Proc. Roy. Soc. London, A 355, 1977, pp. 209-224.

73. Garg, V.K. and Round, G.F., Nonparallel Effects on the Stability of Jet Flows, J. Appl. Mech., 45, 1978, pp. 717-722.

74. Garg, V.K., Spatial Stability of the Nonparallel Bickley Jet (submitted).

75. Brandt, A. and Gillis, J., Magnetohydrodynamic Flow in the Inlet Region of a Straight Channel, Phys. Fluids, 9, 1966, pp. 690-699.

76. Wang, Y.L. and Longwell, P.A., Laminar Flow in the Inlet Section of Parallel Plates, AIChE J., 10, 1964, pp. 323-329.

77. Langhaar, H.L., Steady Flow in Transition Length of a Straight Tube, J. Appl. Mech., 9, 1942, pp. 55-58.

78. Sparrow, E.M., Lundgren, T.S. and Lin, S.H., Slip Flow in the Entrance Region of a Parallel Plate Channel, Proc. Heat Transfer and Fluid Mech. Institute, Stanford, California, 1962, pp. 223-238.

79. Han, L.S., Hydrodynamic Entrance Length for Incompressible Laminar Flow in Rectangular Ducts, J. Appl. Mech., 27, 1960, pp. 403-409.

80. Lundgren, T.S., Sparrow, E.M. and Starr, J.B., Pressure Drop Due to Entrance Region in Ducts of Arbitrary Cross-Section, J. Basic Engg., 86, 1964, pp. 620-626.

81. Schiller, L., Die Entwicklung der laminaren Geschwindigkeitverteilung under ihre Bedentung fur Zahigkeitmessungen, Z. Agnew. Math. Mech., 2, 1922, p. 96.

82. Campbell, W.D. and Slattery, J.C., Flow in the Entrance of a Tube, J. Basic Engg., 85, 1963, pp. 41-46.

83. Garg, V.K., On the Developing Flow in a Channel, J. Phys. Soc. Japan, 46, 1979, pp. 300-302.

84. Mohanty, A.K. and Asthana, S.B.L., Laminar Flow in the Entrance Region of a Smooth Pipe, J. Fluid Mech., 90, 1978, pp. 433-447.

85. Goldstein, S. (Ed.), Modern Developments in Fluid Dynamics, Dover Publications, 1965, p. 309.

86. Roidt, M. and Cess, R.D., An Approximate Analysis of Laminar Magnetohydrodynamic Flow in the Entrance Region of a Flat Duct, J. Appl. Mech., 29, 1962, pp. 171-176.

87. Collins, M. and Schowalter, W.R., Laminar Flow in the Inlet Region of a Straight Channel, Phys. Fluids, 5, 1962, pp. 1122-1124.

88. Crane, C.M. and Burley, D.M., Numerical Studies of Laminar Flow in Ducts and Pipes, J. Comp. Appl. Math., 2, 1976, pp. 95-101.

89. Schmidt, F.W. and Zeldin, B., Laminar Flow in Inlet Section of Tubes and Ducts, AIChE J., 15, 1969, pp. 612-614.

90. Shah, R.K., A Correlation for Laminar Hydrodynamic Entry Length Solutions for Circular and Noncircular Ducts, J. Fluids Engg., 100, 1978, pp. 177-179.

91. van Dyke, M., Entry Flow in a Channel, J. Fluid Mech., 44, 1970, pp. 813-823.

92. Morihara, H. and Cheng, R.T.S., Numerical Solution of the Viscous Flow in the Entrance Region of Parallel Plates, J. Comp. Phys., 11, 1973, pp. 550-572.

93. Shah, R.K. and London, A.L., Laminar Flow Forced Convection in Ducts — A Source Book for Compact Heat Exchanger Analytical Data, Supplement 1 to Advances in Heat Transfer Series, Academic Press, 1978.

94. Grohne, D., On the Spectrum of Natural Oscillations of Two-Dimensional Laminar Flows, NACA TM 1417, 1954.

95. Sarpkaya, T., Private Communication, 1979.

96. Roberts, S.M. and Shipman, J.S., Two Point Boundary Value Problems: Shooting Methods, American Elsevier, 1972.

97. Kaplan, R.E., The Stability of Laminar Incompressible Boundary Layers in the Presence of Compliant Boundaries, M.I.T. Aeroelastic and Structures Research Laboratory Report ASRL TR 116-1, 1964.

98. Godunov, S., On the Numerical Solution of Boundary Value Problems for Systems of Linear Ordinary Differential Equations, Usp. mat. Nauk, 16, 1961, pp. 171-174.

99. Bellman, R.E. and Kalaba, R.E., Quasilinearization and Nonlinear Boundary Value Problems, American Elsevier, 1965.

100. Conte, S.D., The Numerical Solution of Linear Boundary Value Problems, SIAM Rev., 8, 1966, pp. 309-321.

101. Scott, M.R. and Watts, H.A., Computational Solution of Linear Two Point Boundary Value Problems Via Orthonormalization, SIAM J. Numer. Anal., 14, 1977, pp. 40-70.

102. Huang, L., Stability of the Developing Laminar Flow in a Circular Tube, Ph.D. Thesis, University of Missouri-Rolla, 1973.

103. Lee, L.H. and Reynolds, W.C., On the Approximate and Numerical Solutions of Orr-Sommerfeld Problems, Quart. J. Mech. Appl. Math., 20, 1967, pp. 1-22.

104. Garg, V.K., Improved Shooting Techniques for Linear Boundary Value Problems, Comp. Meth. Appl. Mech. Engg., (in press).

105. Sharma, R., Ph.D. Thesis, University of Southampton, 1968.

106. Davey, A. and Nguyen, H.P.G., Finite-Amplitude Stability of Pipe Flow, J. Fluid Mech., 45, 1971, pp. 701-720.

107. Gersting Jr., J.M. and Jankowski, D.F., Numerical Methods for Orr-Sommerfeld Problems, Int. J. Numer. Methods in Engg., 4, 1972, pp. 195-206.

108. Antia, H.M., Finite Difference Method for Generalized Eigenvalue Problem in Ordinary Differential Equations, J. Comp. Phys., 30, 1979, pp. 283-295.

109. Delves, L.M. and Lyness, J.N., A Numerical Method for Locating the Zeros of an Analytic Function, Math. Comp., 21, 1967, pp. 543-560.

110. Collatz, L., The Numerical Treatment of Differential Equations, Springer-Verlag, New York, 1966.

111. Muller, D.E., A Method for Solving Algebraic Equations Using an Automatic Computer, Math. Tables and Other Aides to Comp., 10, 1956, pp. 208-215.

112. Garg, V.K., Computing the Bessel Functions $Y_n(x + iy)$ and $K_n(x + iy)$, The Comp. J., 21, 1978, pp. 272-276.

113. Hornbeck, R.W., Numerical Marching Techniques for Fluid Flows with Heat Transfer, NASA SP-297, 1973.

114. Ralston, A., A First Course in Numerical Analysis, McGraw-Hill Book Co., 1965.

115. Chen, T.S., Hydrodynamic Stability of Developing Flow in a Parallel Plate Channel, Ph.D. Thesis, Univ. of Minnesota, 1966.

116. Heisenberg, W., Uber Stabilitat und Turbulenz von Flussigkeitsstromen, Ann. Phys., 74, 1924, pp. 577-627.

117. Davey, A., Private Communication, 1974.

APPENDIX A

DEVELOPING VELOCITY FIELD IN CHANNEL AND PIPE

A.1. The Finite Difference Method

The finite difference method for determining the velocity field in the flow through a channel was developed by Bodoia and Osterle [20]. Later Hornbeck [47] extended it to the pipe flow case. They took a boundary layer model for the flow in the entrance region and replaced the derivatives by finite difference relations. This results in a set of simultaneous algebraic equations. The solution of these equations determines the velocity field in the flow region. The details of the method for the channel and pipe flow are given below.

For an incompressible, Newtonian fluid, the boundary layer equations for the basic flow, using the non-dimensional variables defined in eqns. (2.9), are

$$Y^m \frac{\partial U}{\partial \bar{X}} + \frac{\partial (\tilde{V} Y^m)}{\partial Y} = 0 , \qquad (A.1)$$

and

$$U \frac{\partial U}{\partial \bar{X}} + \tilde{V} \frac{\partial U}{\partial Y} + \frac{d\tilde{P}}{dX} = \left(\frac{\partial^2 U}{\partial Y^2} + \frac{m}{Y} \frac{\partial U}{\partial Y}\right) , \qquad (A.2)$$

where $m = 0$ for the channel flow and $m = 1$ for the pipe flow. The new nondimensional variables used here are defined as

$$\bar{X} = X/R \,, \qquad \tilde{V} = VR \,,$$

$$\text{and} \qquad \tilde{P} = \frac{\bar{P} - \bar{P}_o}{\rho u_a^2} \,, \tag{A.3}$$

where $\bar{P}_o$ is the pressure at the inlet to the duct. The boundary conditions on $U(\bar{X}, Y)$, etc., are

$$U = \tilde{V} = 0 \qquad \text{at} \quad Y = 1 \quad \text{for all } \bar{X} \geq 0 \,,$$

$$\frac{\partial U}{\partial Y} = \tilde{V} = 0 \qquad \text{at} \quad Y = 0 \quad \text{for all } \bar{X} \geq 0 \tag{A.4}$$

$$\text{and} \quad \tilde{P} = 0 \qquad \text{at} \quad \bar{X} = 0 \quad \text{for all } Y \,.$$

Equations (A.1) and (A.2) with (A.4) are solved using the finite difference method. A grid as shown in Figure A-1 is developed. At any grid point (j, k), using implicit finite difference representation, one can write the finite difference form of the eqn. (A.2), as

$$\left[-\frac{\tilde{V}_{j,k}}{2\,\Delta Y} + \frac{m}{2Y_k\,\Delta Y} - \frac{1}{(\Delta Y)^2}\right] U_{j+1,k-1} + \left[\frac{U_{j,k}}{\Delta \bar{X}} + \frac{2}{(\Delta Y)^2}\right] U_{j+1,k}$$

$$+ \left[\frac{\tilde{V}_{j,k}}{2\,\Delta Y} - \frac{m}{2Y_k\,\Delta Y} - \frac{1}{(\Delta Y)^2}\right] U_{j+1,k+1} + \frac{\tilde{P}_{j+1}}{\Delta \bar{X}} = \frac{\tilde{P}_j + U^2_{j,k}}{\Delta \bar{X}} \,, \tag{A.5}$$

for $k = 1(1)n$, where $(n+2)$ is the number of mesh points along Y at any cross-section j. Also, the finite difference form of eqn. (A.1) is

$$Y_k^m \frac{U_{j+1,k} - U_{j,k}}{2\,\Delta\bar{X}} + Y_{k+1}^m \frac{U_{j+1,k+1} - U_{j,k+1}}{2\,\Delta\bar{X}}$$

$$+ \frac{Y_{k+1}^m \tilde{V}_{j+1,k+1} - Y_k^m \tilde{V}_{j+1,k}}{\Delta Y} = 0 , \qquad (A.6)$$

for k = 1(1)n. Equations similar to (A.5) and (A.6) can be written for k = 0 in case of channel flow invoking the symmetry conditions at the centre line and using the fact that m = 0 in this case. However, in the case of pipe flow, term involving Y in denominator of eqns. (A.1) and (A.2) need to be evaluated at Y = 0 by L'Hospital rule. When eqn. (A.6) is written for k = 0 to n for channel flow or 1 to n for the pipe flow and the resulting equations, including the one obtained from L'Hospital rule in case of pipe flow only, are summed up, we get the following simple equation

$$\left[\frac{U_{j+1,0}}{m+1} + \left(1 + \frac{1}{m+1}\right)U_{j+1,1}\right] \frac{Y_1^m}{2} + \sum_{k=2}^{n} Y_k^m U_{j+1,k}$$

$$= \left[\frac{U_{j,0}}{m+1} + \left(1 + \frac{1}{m+1}\right)U_{j,1}\right] \frac{Y_1^m}{2} + \sum_{k=2}^{n} Y_k^m U_{j,k} . \qquad (A.7)$$

The finite difference form of the resulting equation from the application of L'Hospital rule to eqn. (A.2) is

$$U_{j,0} \frac{U_{j+1,0} - U_{j,0}}{\Delta\bar{X}} = -\frac{\tilde{P}_{j+1} - \tilde{P}_j}{\Delta\bar{X}} + 4\,\frac{U_{j+1,1} - U_{j+1,0}}{(\Delta Y)^2} . \qquad (A.8)$$

Equations (A.5) with k = 0 also and (A.7) for the channel flow or (A.5), (A.7) and (A.8) for the pipe flow give (n+2)

equations in (n+2) unknowns viz., U's at k = O(1)n and $\tilde{P}$ at the cross-section j+1. These equations form a matrix which is of tridiagonal type except for the row corresponding to eqn. (A.7). For solution, this matrix may be partitioned to take advantage of the tridiagonality of the matrix. The Y component of velocity can be obtained from eqn. (A.6).

It is observed that this method is a marching method and therefore requires the values of U, $\tilde{V}$ and $\tilde{P}$ at all the grid points at the entry section. Since the discretization of the duct cross-section, taking $U_{O,k} = 1$ for k = O(1)n, leads to a reduction in the volumetric flow rate because of the no slip condition at the wall, a form factor such as

$$U_{O,k} = 1/(1 - \Delta Y/2) \quad \text{for channel flow ,} \qquad \text{(A.9a)}$$

or $$U_{O,k} = n/(n - 1) \quad \text{for pipe flow ,} \qquad \text{(A.9b)}$$

For k = O(1)n was used [113].

The velocity profiles for the developing flow in the channel and in the pipe are tabulated in Tables A3 and A5 and shown in Figures 6.2 and 6.27, respectively.

A.2. Linearization Method

The linearization method was first proposed by Langhaar [77] and was used later by Sparrow et al. [19] to calculate the velocity distribution in the developing

flow through a channel and a pipe. They recasted the momentum eqn. (A.2) into the form

$$\varepsilon^*(\bar{X})u_a \frac{\partial U}{\partial \bar{X}} = \Lambda(\bar{X}) + \left(\frac{\partial^2 U}{\partial Y^2} + \frac{m}{Y}\frac{\partial U}{\partial Y}\right) , \qquad (A.10)$$

where $\varepsilon^*(\bar{X})$ is a weighting function of $\bar{X}$ to be determined and $\Lambda(\bar{X})$ is another undetermined function which includes the pressure gradient as well as the residual of inertia terms. Finding $\Lambda(\bar{X})$ by integrating eqn. (A.10) over the cross-section while using the continuity equation and introducing the stretched streamwise coordinate X^*, defined by

$$d\bar{X} = \varepsilon^* d X^* , \qquad (A.11)$$

we get the following momentum equation

$$\frac{\partial U}{\partial X^*} = \frac{\partial^2 U}{\partial Y^2} + \frac{m}{Y}\frac{\partial U}{\partial Y} - 2\left(\frac{\partial U}{\partial Y}\right)_{Y=1} . \qquad (A.12)$$

The boundary conditions are

$$U = 0 \quad \text{at} \quad Y = 1, \qquad \frac{\partial U}{\partial Y} = 0 \quad \text{at} \quad Y = 0 , \qquad (A.13)$$

and $U = 1$ at $X^* = 0$.

By expressing the velocity U at any point in the inlet region as the sum of fully developed flow velocity and a difference velocity, Sparrow et al. get a differential equation which has an infinite convergent series solution; the constant of the series being determined by using the orthogonality conditions. Thus they arrive at the following solution.

For Channel:

$$U = 1.5(1 - Y^2) + \sum_{i=1}^{\infty} \frac{2}{\lambda_i^2} \left[\frac{\cos(\lambda_i Y)}{\cos(\lambda_i)} - 1\right] e^{-\lambda_i^2 X^*} , \qquad (A.14)$$

where λ_i are roots of

$$\tan \lambda_i = \lambda_i . \qquad (A.15)$$

For Pipe:

$$U = 2(1 - Y^2) + \sum_{i=1}^{\infty} \frac{4}{\lambda_i^2} \left[\frac{J_o(\lambda_i Y)}{J_o(\lambda_i)} - 1\right] e^{-\lambda_i^2 X^*} , \qquad (A.16)$$

where λ_i are the roots of

$$J_1(\lambda_i) - 0.5\, \lambda_i J_o(\lambda_i) = 0 . \qquad (A.17)$$

The weighting function ε^* for both the flows is given by

$$\varepsilon^* = \frac{\int_o^1 (2U - 1.5\, U^2)(\partial U/\partial X^*)\, Y^m\, dY}{[\partial U/\partial Y]_{Y=1} + \int_o^1 (\partial U/\partial Y)^2\, Y^m\, dY} . \qquad (A.18)$$

The first fifty values of λ for the channel and pipe flow are given in Table A1 while values of $\bar{X}$ corresponding to a few values of X^* for both the flows are given in Table A2. The velocity profiles for the developing flow in the channel and in the pipe are tabulated in Tables A4 and A6 and shown in Figures 6.2 and 6.27, respectively.

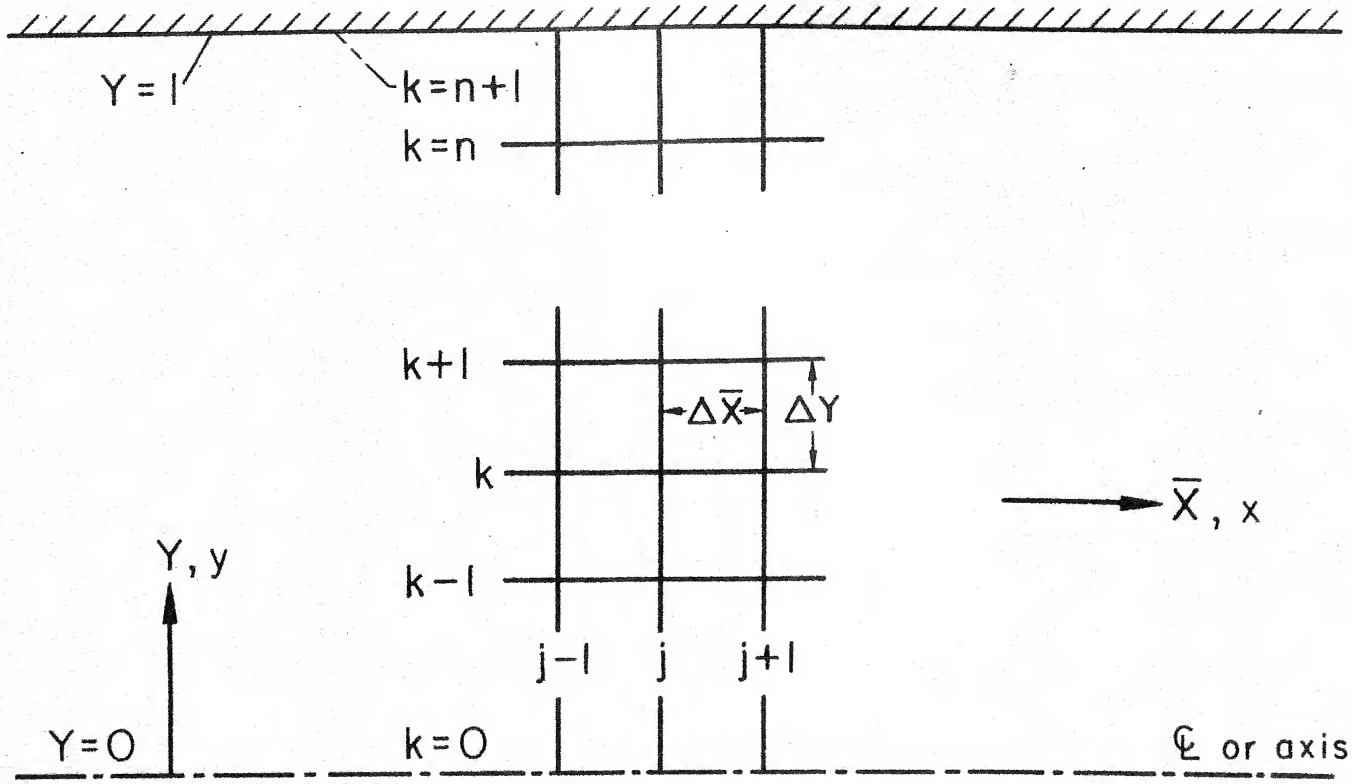

Fig.A-1 Finite difference grid for parallel plate channel or pipe

Table A1 Fifty roots of characteristic equations (A.15) for channel and (A.17) for pipe

N	Channel	Pipe	N	Channel	Pipe
1	4.493409	5.135622	26	83.240192	84.015287
2	7.725252	8.417244	27	86.382222	87.157684
3	10.904122	11.619841	28	89.524221	90.300025
4	14.066194	14.795952	29	92.666192	93.442316
5	17.220755	17.959819	30	95.808139	96.584561
6	20.371303	21.116997	31	98.950063	99.726766
7	23.519452	24.270112	32	102.091966	102.868933
8	26.666054	27.420574	33	105.233852	106.011066
9	29.811599	30.569204	34	108.375720	109.153167
10	32.956389	33.716520	35	111.517572	112.295241
11	36.100622	36.862857	36	114.659411	115.437288
12	39.244422	40.008447	37	117.801236	118.579311
13	42.387914	43.153454	38	120.943049	121.721311
14	45.531134	46.297997	39	124.084851	124.863292
15	48.674144	49.442164	40	127.226643	128.005253
16	51.816982	52.586024	41	130.368425	131.147197
17	54.959678	55.729627	42	133.510198	134.289124
18	58.102255	58.873016	43	136.651963	137.431036
19	61.244730	62.016222	44	139.793720	140.572933
20	64.387120	65.159273	45	142.935470	143.714817
21	67.529435	68.302190	46	146.077213	146.856689
22	70.671686	71.444990	47	149.218950	149.998549
23	73.813881	74.587688	48	152.360680	153.140398
24	76.956026	77.730297	49	155.502406	156.282237
25	80.098129	80.872827	50	158.644126	159.424066

Table A2 Relationship between $\bar{X}$ and X^* for channel and pipe

X^*	$\bar{X}$	
	Channel	Pipe
0	0	0
0.001	0.00038	0.00040
0.002	0.00077	0.00087
0.003	0.00118	0.00140
0.004	0.00162	0.00197
0.005	0.00208	0.00258
0.006	0.00256	0.00323
0.007	0.00305	0.00392
0.008	0.00356	0.00464
0.009	0.00408	0.00539
0.010	0.00462	0.00616
0.015	0.00751	0.01043
0.020	0.01069	0.01527
0.030	0.01780	0.02637
0.040	0.02572	0.03904
0.050	0.03432	0.05297
0.060	0.04349	0.06792
0.080	0.06312	0.10000
0.100	0.08393	0.13396
0.150	0.13852	0.22254
0.200	0.19456	0.31292
0.300	0.30771	0.49472

Table A3 The B-O Profile for channel

$\bar{X}$ =	0.001	0.002	0.004	0.006	0.008	0.02	0.04	0.08
Y	Dimensional Axial Velocity,U							
0.0	1.054201	1.074910	1.103895	1.125908	1.144335	1.223335	1.310295	1.411916
0.1	1.054201	1.074910	1.103895	1.125908	1.144335	1.223319	1.309099	1.404624
0.2	1.054201	1.074910	1.103895	1.125908	1.144335	1.223153	1.303939	1.380975
0.3	1.054201	1.074910	1.103895	1.125908	1.144334	1.221999	1.289491	1.336099
0.4	1.054201	1.074910	1.103895	1.125908	1.144315	1.216051	1.255614	1.263293
0.5	1.054201	1.074910	1.103894	1.125848	1.143795	1.193260	1.187758	1.155778
0.6	1.054201	1.074910	1.103764	1.123955	1.136664	1.128051	1.070450	1.008379
0.7	1.054201	1.074824	1.097564	1.098714	1.086943	0.986636	0.892774	0.818505
0.8	1.053759	1.060709	1.014009	0.955233	0.905566	0.746814	0.651990	0.586091
0.9	0.937307	0.798481	0.651764	0.576296	0.528983	0.411941	0.352323	0.312659
1.0	0.000000	0.000000	0.000000	0.000000	0.000000	0.000000	0.000000	0.000000

Table A4 The Sparrow Profile for channel

X^* =	0.001	0.002	0.004	0.006	0.008	0.01	0.015	0.02
Y	Dimensionless Axial Velocity,U							
0.0	1.036707	1.052532	1.075564	1.093772	1.109497	1.123643	1.154701	1.181922
0.1	1.036707	1.052532	1.075564	1.093772	1.109497	1.123643	1.154701	1.181916
0.2	1.036707	1.052532	1.075564	1.093772	1.109497	1.123643	1.154697	1.181857
0.3	1.036704	1.052531	1.075564	1.093772	1.109497	1.123643	1.154646	1.181433
0.4	1.036704	1.052531	1.075564	1.093772	1.109495	1.123621	1.154145	1.179062
0.5	1.036704	1.052531	1.075564	1.093767	1.109418	1.123222	1.150603	1.168651
0.6	1.036704	1.052531	1.075556	1.093505	1.107876	1.118762	1.132475	1.132780
0.7	1.036700	1.052531	1.074748	1.087391	1.091012	1.087940	1.065187	1.035603
0.8	1.036695	1.050938	1.049405	1.022834	0.989195	0.955675	0.883471	0.828010
0.9	1.010963	0.935538	0.799689	0.709828	0.647388	0.601233	0.524504	0.476499
1.0	0.000000	0.000000	0.000000	0.000000	0.000000	0.000000	0.000000	0.000000

Table A5 The Hornbeck profile for pipe

$\bar{X}$ =	0.0005	0.001	0.002	0.0035	0.005	0.007	0.02	0.08
Y	Dimensionles Axial Velocity,U							
0.0	1.077102	1.105409	1.144957	1.187939	1.221933	1.259739	1.425944	1.793664
0.1	1.077102	1.105409	1.144957	1.187939	1.221933	1.259739	1.425933	1.785587
0.2	1.077102	1.105409	1.144957	1.187939	1.221933	1.259739	1.425820	1.759053
0.3	1.077102	1.105409	1.144957	1.187939	1.221933	1.259739	1.424984	1.707547
0.4	1.077102	1.105409	1.144957	1.187939	1.221933	1.259737	1.420241	1.621635
0.5	1.077102	1.105409	1.144957	1.187939	1.221927	1.259615	1.400097	1.491102
0.6	1.077102	1.105409	1.144957	1.187915	1.221505	1.256670	1.336417	1.307482
0.7	1.077102	1.105409	1.144903	1.185499	1.210013	1.224457	1.185548	1.065978
0.8	1.077101	1.105062	1.133333	1.127141	1.100075	1.060919	0.911069	0.765908
0.9	1.055112	0.996624	0.875844	0.765869	0.700240	0.644086	0.508826	0.409538
1.0	0.000000	0.000000	0.000000	0.000000	0.000000	0.000000	0.000000	0.000000

Table A6 The Sparrow profile for pipe

$X^* =$	0.002	0.003	0.004	0.005	0.006	0.007	0.009	0.01
Y	Dimensionless Axial Velocity,U							
0.0	1.107185	1.133088	1.155474	1.175622	1.194188	1.211560	1.243660	1.258690
0.1	1.107185	1.133088	1.155474	1.175622	1.194188	1.211560	1.243660	1.258690
0.2	1.107185	1.133088	1.155474	1.175622	1.194188	1.211560	1.243660	1.258690
0.3	1.107185	1.133088	1.155474	1.175622	1.194188	1.211560	1.243659	1.258689
0.4	1.107185	1.133088	1.155474	1.175622	1.194188	1.211560	1.243648	1.258653
0.5	1.107185	1.133088	1.155474	1.175622	1.194188	1.211525	1.243386	1.258069
0.6	1.107185	1.133088	1.155466	1.175545	1.193832	1.210564	1.239875	1.252091
0.7	1.107185	1.132972	1.154570	1.172466	1.186286	1.197037	1.211792	1.213622
0.8	1.105602	1.123507	1.127348	1.123814	1.111215	1.099084	1.077736	1.057895
0.9	0.980413	0.909713	0.864415	0.803230	0.764000	0.731240	0.679565	0.658774
1.0	0.000000	0.000000	0.000000	0.000000	0.000000	0.000000	0.000000	0.000000

Appendix B

TABLES OF STABILITY RESULTS FOR THE CHANNEL FLOW

Table B1 The neutral stability results for the B=0 profile and antisymmetric disturbances (parallel flow theory)

$\bar{Y}$	R	ω	k or	R	ω	k or
.001	20000.	1.36115	3.87717	16000.	2.06496	5.36919
.001	18000.	1.52665	4.21493	18000.	2.19319	5.74319
.001	16000.	1.83494	4.85345	20000.	2.20228	5.84482
.001	15810.	2.00000	5.21595			
.002	18000.	0.90242	2.62539	14000.	1.48456	3.89902
.002	16000.	1.01567	2.86183	16000.	1.52856	4.07268
.002	14000.	1.20350	3.25328	18000.	1.51922	4.11720
.002	13396.	1.40000	3.68419			
.004	18000.	0.56066	1.66055	13000.	1.01810	2.71990
.004	16000.	0.62766	1.81212	14000.	1.03317	2.78548
.004	14000.	0.72384	2.02467	16000.	1.02907	2.83023
.004	13000.	0.79625	2.18339	18000.	1.01087	2.83409
.004	12176.	0.95000	2.53327			
.006	16000.	0.48494	1.38593	13000.	0.78860	2.12977
.006	14000.	0.56300	1.56891	14000.	0.80028	2.18370
.006	13000.	0.62183	1.70532	16000.	0.79605	2.21848
.006	12214.	0.72500	1.95114			
.008	18000.	0.36312	1.03272	13000.	0.61103	1.65350
.008	16000.	0.41317	1.15759	14000.	0.64316	1.75876
.008	14000.	0.48867	1.34252	16000.	0.64696	1.80800
.008	13000.	0.56200	1.52373	18000.	0.63645	1.81473
.010	16000.	0.37955	1.04287	15000.	0.52320	1.43749
.010	15000.	0.41750	1.13988	16000.	0.53040	1.47392
.010	14206.	0.48000	1.30447			

Table 62 The neutral stability results for the B=0 profile and symmetric disturbances (parallel flow theory)

$\bar{x}$	R	ω	k or	R	ω	k or
.001	20000.	1.36118	3.88064	16000.	2.06575	5.37124
.001	18000.	1.52625	4.21595	18000.	2.19342	5.74385
.001	16000.	1.83477	4.85373	20000.	2.20244	5.84530
.001	15778.	1.96000	5.12566			
.002	18000.	0.90497	2.65827	14000.	1.49246	3.92067
.002	16000.	1.01451	2.87803	16000.	1.53245	4.08448
.002	14000.	1.19546	3.24536	18000.	1.52232	4.12709
.002	13298.	1.39000	3.66346			
.004	18000.	0.57899	1.81018	11594.	0.97600	2.60900
.004	16000.	0.63668	1.92115	12000.	1.02940	2.74161
.004	14000.	0.71836	2.07958	14000.	1.06439	2.88153
.004	12000.	0.86472	2.37009	16000.	1.05364	2.91056
.004	11584.	0.97000	2.59526	18000.	1.03292	2.90926
.006	16000.	0.50266	1.57708	10742.	0.80000	2.16185
.006	14000.	0.55976	1.68422	12000.	0.86702	2.34599
.006	12000.	0.64853	1.85268	14000.	0.86789	2.39913
.006	10900.	0.74331	2.04029	16000.	0.85196	2.40694
.008	18000.	0.39735	1.32965	11000.	0.75633	2.05375
.008	16000.	0.43149	1.39274	14000.	0.75651	2.12436
.008	14000.	0.47712	1.47666	16000.	0.73955	2.12450
.008	11000.	0.59657	1.69923	18000.	0.72058	2.11415
.008	10181.	0.71000	1.93057			
.020	16000.	0.28542	1.00674	9000.	0.54042	1.49145
.020	14000.	0.31098	1.05189	10000.	0.54538	1.52367
.020	12000.	0.34565	1.11239	11000.	0.54195	1.53620
.020	11000.	0.36864	1.15235	12000.	0.53565	1.54065
.020	10000.	0.39816	1.20382	14000.	0.52024	1.53850
.020	9000.	0.44058	1.27908	16000.	0.50433	1.52975
.020	8433.	0.52000	1.43562			
.040	16000.	0.22273	0.83409	8000.	0.46061	1.27717
.040	12000.	0.26523	0.90739	10000.	0.45209	1.29800
.040	10000.	0.29974	0.96457	12000.	0.43650	1.29607
.040	8000.	0.35538	1.05832	16000.	0.40629	1.27735
.040	7025.	0.44000	1.21370			
.080	10000.	0.24057	0.81750	6000.	0.42177	1.13251
.080	8000.	0.27765	0.87684	8000.	0.41460	1.16177
.080	6000.	0.34777	0.98821	10000.	0.39634	1.15831
.080	5504.	0.41000	1.10004			
∞	10000.	0.20078	0.71509	4000.	0.42377	1.05964
∞	8000.	0.22807	0.75760	5000.	0.42633	1.09437
∞	6000.	0.27187	0.82292	6000.	0.41390	1.09705
∞	5000.	0.30760	0.87474	8000.	0.38742	1.08650
∞	4000.	0.37312	0.97070	10000.	0.36472	1.07156
∞	3852.	0.40000	1.01345			

Table 63 The neutral stability results for the Sparrow profile and symmetric disturbances (parallel flow theory)

x^*	R	ω	k_{or}	R	ω	k_{or}
.005	32000.	0.64674	2.19107	25000.	1.01419	3.10023
.005	28000.	0.73960	2.40351	26000.	1.04025	3.18958
.005	26000.	0.81128	2.57101	28000.	1.05959	3.28301
.005	25000.	0.86547	2.70129	32000.	1.06082	3.35237
.005	24346.	0.95000	2.91615			
.009	26000.	0.47658	1.64107	19000.	0.76873	2.31980
.009	22000.	0.55420	1.80739	20000.	0.79375	2.40300
.009	20000.	0.61739	1.94614	22000.	0.80753	2.47493
.009	19000.	0.66943	0.20649	26000.	0.80129	2.52251

Table 64 Wavenumber and growth rates for the B=0 profile and symmetric disturbances (parallel and nonparallel flow)

$\bar{X}$ =0.001

R	ω	K_{or}	K_{oi}	g_E	$q_\psi(\bar{X},0)$	$q_u(\bar{X},0)$
12500.	2.050	5.17424	0.05462	-0.04398	-0.00704	-0.01243
12500.	2.100	5.28132	0.05362	-0.04273	-0.00616	-0.01130
12500.	2.150	5.38830	0.05487	-0.04232	-0.00611	-0.01102
12500.	2.200	5.49517	0.05424	-0.04276	-0.00690	-0.01160
12500.	2.250	5.60192	0.05589	-0.04407	-0.00856	-0.01306
13000.	1.900	4.87499	0.05109	-0.04134	-0.00535	-0.01107
13000.	2.000	5.09114	0.04567	-0.03555	-0.00026	-0.00548
13000.	2.100	5.30686	0.04376	-0.03314	0.00145	-0.00328
13000.	2.200	5.52215	0.04547	-0.03424	-0.00033	-0.00465
14000.	1.700	4.47934	0.04870	-0.04002	-0.00628	-0.01226
14000.	1.800	4.69921	0.03779	-0.02893	0.00418	-0.00124
14000.	1.800	4.69921	0.03779	-0.02893	0.00418	-0.00124
14000.	1.900	4.91861	0.03040	-0.02123	0.01122	0.00631
14000.	2.000	5.13756	0.02668	-0.01708	0.01471	0.01026
14000.	2.100	5.35605	0.02676	-0.01660	0.01454	0.01050
14000.	2.200	5.57406	0.03074	-0.01992	0.01061	0.00693
14000.	2.300	5.79155	0.03876	-0.02713	0.00283	-0.00055
14000.	2.400	6.00848	0.05091	-0.03835	-0.00891	-0.01202
15000.	1.600	4.29268	0.04154	-0.03353	-0.00225	-0.00802
15000.	1.700	4.51569	0.02823	-0.02012	0.01057	0.00563
15000.	1.800	4.73822	0.01857	-0.01023	0.01985	0.01515
15000.	1.900	4.96028	0.01272	-0.00131	0.02545	0.02120
15000.	2.000	5.18186	0.01080	-0.00162	0.02723	0.02339
15000.	2.100	5.40294	0.01297	-0.00318	0.02508	0.02159
15000.	2.200	5.62348	0.01933	-0.00882	0.01890	0.01571
15000.	2.300	5.84344	0.03001	-0.01864	0.00858	0.00565
15000.	2.400	6.06274	0.04513	-0.03277	-0.00597	-0.00868
16000.	1.500	4.09696	0.03836	-0.03090	-0.00171	-0.00736
16000.	1.600	4.32502	0.02241	-0.01493	0.01373	0.00865
16000.	1.700	4.55056	0.01018	-0.00255	0.02553	0.02097
16000.	1.800	4.77560	0.00188	0.00604	0.03353	0.02943
16000.	1.900	5.00017	-0.00236	0.01067	0.03759	0.03389
16000.	2.000	5.22422	-0.00237	0.01121	0.03756	0.03421
16000.	2.100	5.44772	0.00198	0.00752	0.03334	0.03030
16000.	2.200	5.67062	0.01080	-0.00053	0.02481	0.02203
16000.	2.300	5.89285	0.02424	-0.01306	0.01187	0.00931
16000.	2.400	6.11433	0.04242	-0.03018	-0.00558	-0.00797
18000.	1.400	3.92401	0.02220	-0.01563	0.00977	0.00475
18000.	1.500	4.15532	0.00409	0.00246	0.02737	0.02289
18000.	1.600	4.38609	-0.00997	0.01663	0.04102	0.03702
18000.	1.700	4.61634	-0.01977	0.02666	0.05053	0.04695
18000.	1.800	4.84606	-0.02512	0.03238	0.05572	0.05251
18000.	2.000	5.30377	-0.02184	0.03019	0.05257	0.04996
18000.	2.100	5.53165	-0.01291	0.02200	0.04397	0.04158
18000.	2.200	5.75876	0.00108	0.00889	0.03052	0.02831
18000.	2.300	5.98501	0.02027	-0.00928	0.01211	0.01003
20000.	1.300	3.73606	0.01320	-0.00730	0.01520	0.01060
20000.	1.400	3.97227	-0.00756	0.01337	0.03543	0.03136
20000.	1.500	4.20792	-0.02399	0.02986	0.05145	0.04784
20000.	1.600	4.44301	-0.03586	0.04191	0.06302	0.05981
20000.	1.700	4.67754	-0.04295	0.04931	0.06994	0.06708
20000.	1.800	4.91147	-0.04507	0.05187	0.07205	0.06948
20000.	1.900	5.14474	-0.04206	0.04942	0.06918	0.06686
20000.	2.000	5.37727	-0.03375	0.04179	0.06119	0.05907
20000.	2.200	5.83969	-0.00055	0.01039	0.02932	0.02747
20000.	2.300	6.06931	0.02469	-0.01368	0.00517	0.00339

Contd....

$\bar{x}$ =0.002

σ	ω	k_{or}	k_{oi}	q_{ξ}	$q_{\psi}(\bar{x},0)$	$q_{u}(\bar{x},0)$
11000.	1.400	3.59773	0.02980	-0.02512	-0.00655	-0.00983
11000.	1.500	3.81520	0.02671	-0.02332	-0.00518	-0.00808
11000.	1.600	4.03230	0.03302	-0.02680	-0.00907	-0.01165
12000.	1.200	3.19490	0.02883	-0.02542	-0.00816	-0.01172
12000.	1.300	3.41629	0.01924	-0.01534	0.00156	-0.00156
12000.	1.400	3.63748	0.01504	-0.01051	0.00601	0.00326
12000.	1.500	3.85836	0.00165	-0.01121	0.00492	0.00249
12000.	1.600	4.07877	0.02384	-0.01769	-0.00194	-0.00410
12800.	1.300	3.44395	0.00782	-0.00402	0.01148	0.00874
12800.	1.400	3.66774	0.00535	-0.00090	0.01424	0.01184
12800.	1.500	3.89115	0.00893	-0.00371	0.01107	0.00895
13000.	1.100	3.00129	0.02652	-0.02369	-0.00785	-0.01133
13000.	1.200	3.22604	0.01309	-0.00986	0.00567	0.00263
13000.	1.300	3.45069	0.00521	-0.00143	0.01375	0.01110
13000.	1.400	3.67511	0.00319	0.00125	0.01607	0.01374
13000.	1.500	3.89912	0.00732	-0.00732	0.01237	0.01032
13000.	1.600	4.12257	0.01787	-0.01174	0.00240	0.00057
13000.	1.700	4.34526	0.03510	-0.02792	-0.01407	-0.01572
14000.	1.000	2.80005	0.02935	-0.02700	-0.01234	-0.01582
14000.	1.100	3.02787	0.01165	-0.00899	0.00541	0.00239
14000.	1.250	3.36960	-0.00422	0.00760	0.02152	0.01908
14000.	1.300	3.48343	-0.00647	0.01102	0.02391	0.02163
14000.	1.400	3.71083	-0.00618	0.01055	0.02397	0.02197
14000.	1.500	3.93776	0.00076	0.00443	0.01753	0.01577
14000.	1.600	4.16398	0.01463	-0.00849	0.00433	0.00275
14000.	1.650	4.27676	0.02425	-0.01758	-0.00489	-0.00638
14000.	1.800	4.61338	0.06437	-0.05584	-0.04343	-0.04478
16000.	0.900	2.61080	0.02430	-0.02248	-0.00991	-0.01305
16000.	1.000	2.84416	0.00265	-0.00059	0.01177	0.00908
16000.	1.100	3.07769	-0.01292	0.01537	0.02746	0.02514
16000.	1.300	3.54449	-0.02398	0.02757	0.03908	0.03734
16000.	1.400	3.77730	-0.01874	0.02307	0.03431	0.03278
16000.	1.500	4.00930	-0.00587	0.01108	0.02207	0.02071
16000.	1.600	4.24044	0.01497	-0.00873	0.00207	
16000.	1.650	4.35549	0.02849	-0.02167	-0.01094	-0.01215
18000.	0.800	2.40824	0.02754	-0.02612	-0.01512	-0.01807
18000.	0.900	2.64642	0.00115	0.00043	0.01128	0.00876
18000.	1.000	2.88498	-0.01887	0.02076	0.03139	0.02924
18000.	1.100	3.12370	-0.03190	0.03424	0.04461	0.04278
18000.	1.300	3.60052	-0.03518	0.03874	0.04860	0.04723
18000.	1.440	3.93276	-0.01805	0.02276	0.03233	0.03116
18000.	1.500	4.07449	-0.00550	0.01080	0.02027	0.01916
18000.	1.600	4.30952	0.02271	-0.01629	-0.00691	-0.00796

$\bar{x}$ =0.004

R	ω	K_{cr}	K_{01}	q_E	$q_\psi(\bar{x},0)$	$q_u(\bar{x},0)$
10000.	0.900	2.39382	0.01964	-0.01802	-0.00894	-0.01098
10000.	0.950	2.50261	0.01607	-0.01419	-0.00521	-0.00710
10000.	1.000	2.61152	0.01451	-0.01234	-0.00346	-0.00521
10000.	1.100	2.83009	0.01765	-0.01478	-0.00614	-0.00764
11300.	0.900	2.43073	0.00446	-0.00290	0.00487	0.00326
11300.	0.980	2.60913	0.00234	-0.00033	0.00729	0.00588
11300.	1.050	2.76554	0.00537	-0.00287	0.00460	0.00333
12000.	0.750	2.11287	0.01491	-0.01400	-0.00657	-0.00844
12000.	0.800	2.22476	0.00699	-0.00591	0.00145	-0.00025
12000.	0.900	2.44950	-0.00219	0.00373	0.01093	0.00950
12000.	0.950	2.56226	-0.00329	0.00512	0.01222	0.01090
12000.	1.000	2.67517	-0.00195	0.00410	0.01111	0.00990
12000.	1.100	2.90122	0.00830	-0.00539	0.00142	0.00037
12000.	1.150	3.01421	0.01735	-0.01401	-0.00730	-0.00828
14000.	0.650	1.92285	0.01472	-0.01417	-0.00793	-0.00962
14000.	0.700	2.03741	0.00352	-0.00287	0.00334	0.00180
14000.	0.750	2.15241	-0.00530	0.00612	0.01226	0.01087
14000.	0.900	2.49949	-0.01645	0.01799	0.02390	0.02284
14000.	1.000	2.73186	-0.01020	0.01239	0.01814	0.01724
14000.	1.100	2.96422	0.00780	-0.00479	0.00080	0.00001
14000.	1.150	3.08015	0.02143	-0.01795	-0.01244	-0.01319
16000.	0.600	1.83555	0.00959	-0.00922	-0.00387	-0.00534
16000.	0.650	1.95276	-0.00315	0.00361	0.00892	0.00760
16000.	0.800	2.30710	-0.02513	0.02615	0.03129	0.03031
16000.	0.900	2.54487	-0.02509	0.02666	0.03165	0.03084
16000.	1.000	2.78299	-0.01235	0.01462	0.01948	0.01877
16000.	1.100	3.02056	0.01392	-0.01077	-0.00604	-0.00667
18000.	0.550	1.74094	0.00882	-0.00858	-0.00390	-0.00522
18000.	0.600	1.86045	-0.00582	0.00613	0.01078	0.00960
18000.	0.700	2.10103	-0.02648	0.02708	0.03163	0.03068
18000.	0.800	2.34329	-0.03465	0.03569	0.04012	0.03935
18000.	0.940	2.68371	-0.02331	0.02522	0.02948	0.02886
18000.	1.000	2.82946	-0.00977	0.01214	0.01634	0.01576
18000.	1.100	3.07126	0.02524	-0.02192	-0.01780	-0.01836

Contd....

$\bar{X}$ =0.006

R	ω	k_{or}	k_{oi}	q_E	$\bar{q}_\psi(\bar{X},0)$	$\bar{q}_u(\bar{X},0)$
9000.	0.700	1.90007	0.02422	-0.02346	-0.01715	-0.01880
9000.	0.750	2.00630	0.01832	-0.01739	-0.01112	-0.01264
9000.	0.800	2.11297	0.01488	-0.01372	-0.00752	-0.00891
9000.	0.850	2.22003	0.01399	-0.01256	-0.00644	-0.00771
9000.	0.900	2.32742	0.01574	-0.01401	-0.00796	-0.00914
10000.	0.700	1.92415	0.01231	-0.01161	-0.00605	-0.00741
10000.	0.800	2.14170	0.00547	-0.00433	0.00107	-0.00003
10000.	0.850	2.25106	0.00627	-0.00484	0.00052	-0.00052
10000.	0.900	2.36071	0.01001	-0.00826	-0.00298	-0.00394
10000.	0.950	2.47057	0.01678	-0.01466	-0.00947	-0.01036
10500.	0.725	1.99041	0.00471	-0.00391	0.00129	0.00011
10500.	0.775	2.10028	0.00194	-0.00092	0.00422	0.00314
10500.	0.800	2.15537	0.00166	-0.00051	0.00460	0.00357
10500.	0.825	2.21055	0.00212	-0.00083	0.00424	0.00325
10500.	0.875	2.32113	0.00534	-0.00374	0.00126	0.00035
10900.	0.725	1.99978	0.00116	-0.00037	0.00460	0.00350
10900.	0.775	2.11050	-0.00105	0.00207	0.00698	0.00598
10900.	0.800	2.16601	-0.00102	0.00217	0.00704	0.00606
10900.	0.825	2.22160	-0.00020	0.00150	0.00634	0.00542
10900.	0.875	2.33300	0.00380	-0.00219	0.00258	0.00173
12000.	0.580	1.69975	0.01250	-0.01218	-0.00764	-0.00886
12000.	0.620	1.78689	0.00453	-0.00412	0.00039	-0.00074
12000.	0.660	1.87838	-0.00154	0.00208	0.00655	0.00551
12000.	0.700	1.96820	-0.00564	0.00633	0.01076	0.00980
12000.	0.770	2.12609	-0.00787	0.00888	0.01324	0.01239
12000.	0.840	2.28466	-0.00351	0.00493	0.00920	0.00845
12000.	0.880	2.37547	0.00206	-0.00036	0.00385	0.00315
12000.	0.920	2.46635	0.00993	-0.00794	-0.00379	-0.00445
14000.	0.540	1.63899	0.00465	-0.00446	-0.00066	-0.00168
14000.	0.580	1.73065	-0.00424	0.00452	0.00829	0.00736
14000.	0.650	1.89196	-0.01458	0.01507	0.01879	0.01800
14000.	0.700	2.00781	-0.01768	0.01838	0.02205	0.02134
14000.	0.800	2.24064	-0.01255	0.01379	0.01735	0.01676
14000.	0.850	2.35736	-0.00405	0.00562	0.00912	0.00857
14000.	0.900	2.47411	0.00863	-0.00667	-0.00323	-0.00375
16000.	0.480	1.52407	0.00666	-0.00657	-0.00330	-0.00423
16000.	0.520	1.61774	-0.00461	0.00475	0.00800	0.00717
16000.	0.600	1.80626	-0.02014	0.02048	0.02368	0.02299
16000.	0.650	1.92483	-0.02477	0.02529	0.02845	0.02784
16000.	0.700	2.04385	-0.02530	0.02605	0.02916	0.02861
16000.	0.775	2.22295	-0.01804	0.01920	0.02224	0.02175
16000.	0.800	2.28273	-0.01339	0.01471	0.01772	0.01725
16000.	0.850	2.40225	-0.00060	0.00227	0.00524	0.00480
16000.	0.900	2.52157	0.01702	-0.01493	-0.01200	-0.01244

Contd....

$\bar{Y} = 0.008$

R	ω	K_{or}	K_{oi}	q_F	$q_\psi(\bar{Y},0)$	$q_u(\bar{Y},0)$
9000.	0.650	1.77213	0.01195	-0.01140	-0.00699	-0.00807
9000.	0.700	1.87856	0.00856	-0.00783	-0.00346	-0.00445
9000.	0.750	1.98547	0.00840	-0.00742	-0.00311	-0.00401
9000.	0.800	2.09279	0.01157	-0.01031	-0.00607	-0.00689
10000.	0.625	1.74119	0.00506	-0.00461	-0.00071	-0.00164
10000.	0.675	1.84975	0.00149	-0.00086	0.00300	0.00216
10000.	0.700	1.90421	0.00102	-0.00027	0.00356	0.00276
10000.	0.725	1.95879	0.00143	-0.00056	0.00324	0.00247
10000.	0.775	2.06824	0.00502	-0.00387	-0.00012	-0.00083
11000.	0.550	1.59687	0.00717	-0.00693	-0.00340	-0.00432
11000.	0.600	1.70679	-0.00041	0.00077	0.00427	0.00345
11000.	0.650	1.81727	-0.00436	0.00490	0.00836	0.00762
11000.	0.700	1.92825	-0.00453	0.00530	0.00870	0.00803
11000.	0.750	2.03964	-0.00076	0.00180	0.00515	0.00454
11000.	0.800	2.15132	0.00709	-0.00574	-0.00245	-0.00301
14000.	0.440	1.39182	0.01036	-0.01031	-0.00762	-0.00841
14000.	0.480	1.48326	-0.00071	0.00080	0.00348	0.00277
14000.	0.580	1.71350	-0.01680	0.01713	0.01975	0.01921
14000.	0.650	1.87597	-0.01739	0.01800	0.02057	0.02010
14000.	0.720	2.03914	-0.00855	0.00953	0.01204	0.01162
14000.	0.760	2.13252	-0.00096	0.00027	0.00274	0.00234
14000.	0.800	2.22588	0.01386	-0.01236	-0.00993	-0.01031
16000.	0.400	1.31900	0.01039	-0.01039	-0.00807	-0.00877
16000.	0.450	1.43616	-0.00532	0.00535	0.00765	0.00705
16000.	0.500	1.55391	-0.01659	0.01676	0.01899	0.01847
16000.	0.600	1.79117	-0.02455	0.02499	0.02721	0.02680
16000.	0.650	1.91047	-0.02075	0.02141	0.02360	0.02323
16000.	0.700	2.02996	-0.01145	0.01238	0.01453	0.01419
16000.	0.750	2.14944	0.00365	-0.00239	-0.00028	-0.00061
16000.	0.800	2.26864	0.02487	-0.02362	-0.02115	-0.02147

Table 35 Neutral stability results for B=0 profile and symmetric disturbances(nonparallel flow)

Based on $q_{\psi}(\bar{X},0)$

$\bar{X}$	R	ω	R	ω	R	ω
.001	16000.	1.510	15000.	1.615	14000.	1.755
.001	13300.	2.005	12850.	2.100	13000.	2.185
.001	14000.	2.327	15000.	2.367	16000.	2.375
.002	16000.	0.945	14000.	1.070	13000.	1.150
.002	12000.	1.263	11400.	1.450	12000.	1.575
.002	13000.	1.620	14000.	1.630	16000.	1.610
.004	16000.	0.610	14000.	0.682	12000.	0.790
.004	10350.	1.000	12000.	1.111	14000.	1.100
.004	16000.	1.076				
.006	14000.	0.543	12000.	0.615	10000.	0.772
.006	8850.	0.820	10000.	0.860	12000.	0.903
.006	14000.	0.887				
.008	14000.	0.465	11000.	0.567	10000.	0.630
.008	9400.	0.715	10000.	0.775	11000.	0.787
.008	14000.	0.767				

Based on $q_{u}(\bar{X},0)$

.001	16000.	1.540	15000.	1.660	14000.	1.815
.001	13200.	2.100	14000.	2.293	15000.	2.345
.001	16000.	2.355				

Based on $q_{E}(\bar{X})$

.001	20000.	1.320	18000.	1.482	16000.	1.722
.001	15200.	1.930	15100.	2.015	15200.	2.068
.001	16000.	2.195	18000.	2.255	20000.	2.255
.002	18000.	0.898	16000.	1.005	14000.	1.162
.002	13000.	1.335	12850.	1.408	13000.	1.460
.002	14000.	1.535	16000.	1.565	18000.	1.545
.004	18000.	0.578	16000.	0.630	14000.	0.715
.004	12000.	0.855	11350.	0.975	12000.	1.055
.004	14000.	1.075	16000.	1.065	18000.	1.043
.006	16000.	0.502	14000.	0.557	12000.	0.647
.006	10550.	0.802	12000.	0.877	14000.	0.875
.006	16000.	0.957				
.008	16000.	0.430	14000.	0.475	11000.	0.595
.008	10050.	0.703	11000.	0.767	14000.	0.760
.008	16000.	0.740				

Appendix C

TABLES OF STABILITY RESULTS FOR THE PIPE FLOW

Table C1 The neutral stability results for the Hornbeck profile and axisymmetric disturbances (parallel flow theory)

$\bar{X}$	R	ω	k or
.0005	19788.	2.80000	6.83760
.0005	20000.	2.65917	6.54404
.0005	20000.	2.97288	7.21720
.0005	21000.	2.40546	6.03172
.0005	21000.	3.11545	7.56937
.0010	15517.	2.05000	4.86285
.0010	16000.	1.82569	4.40178
.0010	16000.	2.19562	5.19215
.0010	18000.	1.53324	3.82284
.0010	18000.	2.29176	5.48189
.0020	12737.	1.40000	3.20517
.0020	12862.	1.50000	3.42272
.0020	13000.	1.30534	3.01050
.0020	13000.	1.52389	3.47860
.0020	14000.	1.14846	2.69584
.0020	14000.	1.58791	3.65214
.0020	16000.	0.97177	2.34128
.0020	16000.	1.60197	3.75266
.0020	18000.	0.85507	2.10227
.0020	18000.	1.58036	3.76848
.0035	11784.	1.00000	2.19013
.0035	13000.	0.81085	1.79835
.0035	13000.	1.12768	2.50413
.0035	14000.	0.73311	1.63938
.0035	14000.	1.13447	2.54756
.0050	12669.	0.75000	1.58919
.0050	13000.	0.68340	1.44530
.0050	13000.	0.80474	1.71902
.0050	14000.	0.60047	1.27226
.0050	14000.	0.82817	1.79310
.0050	18000.	0.43752	0.93520
.0050	18000.	0.80169	1.80640
.0070	19719.	0.43000	0.89101
.0070	20000.	0.40135	0.82565
.0070	20000.	0.44418	0.92688
.0070	22000.	0.34137	0.69735
.0070	22000.	0.45043	0.95804
.0070	24000.	0.30452	0.62069
.0070	24000.	0.44023	0.94827

Table C4 The neutral stability results for the Sparrow profile and axisymmetric disturbances (parallel flow theory)

X^*	R	ω	k or	R	ω	k or
.002	30016.	1.55000	4.22193	30100.	1.50070	4.09891
.002	30100.	1.58692	4.31707	33000.	1.72465	4.73194
.002	33000.	1.24667	3.49910	38000.	1.74732	4.89772
.002	38000.	1.04988	3.04463	43000.	0.92309	2.74770
.002	43000.	1.72696	4.94003			
.003	24822.	1.25000	3.28218	25000.	1.15920	3.06140
.003	25000.	1.32356	3.47431	26700.	1.02411	2.74612
.003	26700.	1.38834	3.67429	31700.	1.40988	3.83270
.003	36700.	1.38410	3.85564	36700.	0.70547	2.00243
.004	21633.	1.07000	2.72265	22000.	1.00487	2.56269
.004	22000.	1.10678	2.81783	26000.	0.76099	1.99416
.004	26000.	1.19519	3.12157	30000.	0.64362	1.71924
.004	30000.	1.16475	3.16855	34000.	0.56245	1.52462
.004	34000.	1.15858	3.16468			
.005	23200.	0.69620	1.74840	23200.	1.02858	2.60473
.005	26000.	0.60207	1.52950	26000.	1.02932	2.65701
.006	19900.	0.78141	1.88787	21400.	0.65771	1.59367
.006	21400.	0.88197	2.16755	25000.	0.53099	1.29959
.006	25000.	0.89197	2.25244	19900.	0.81639	1.97604
.006	30000.	0.42960	1.06202	30000.	0.86383	2.24927
.007	20224.	0.70000	1.65934	20400.	0.65427	1.54542
.007	20400.	0.72361	1.72192	24000.	0.49537	1.17275
.007	24000.	0.76877	1.89012	28000.	0.40972	0.97467
.007	28000.	0.75250	1.89921			
.009	24930.	0.46000	1.10422	25600.	0.43513	0.99257
.009	25600.	0.50861	1.18480	30000.	0.34101	0.77270
.009	30000.	0.51463	1.23713	34000.	0.29253	0.66207
.009	34000.	0.49746	1.21941			
.010	33391.	0.36000	0.82778	34000.	0.32179	0.72868
.010	34000.	0.36646	0.84804	38000.	0.27038	0.60378
.010	38000.	0.36634	0.86636	42000.	0.23814	0.53332
.010	42000.	0.35434	0.84997			

Table C3 Wavenumber and growth rates for the Hornbeck profile and axisymmetric disturbances (Parallel and nonparallel flow)

$\bar{X}$= 0.0005

R	ω	k_{or}	k_{oi}	α_E	$q_{\bar{y}}(\bar{X},0)$
21000.0	2.00	5.141017	0.057737	-0.059785	-0.011574
21000.0	2.20	5.581892	0.024511	-0.024152	-0.004074
21000.0	2.40	6.019923	0.000513	0.002579	0.050815
21000.0	2.60	6.455696	-0.013521	0.019966	0.067972
21000.0	2.80	6.889414	-0.017052	0.027238	0.074976
21000.0	3.00	7.321169	-0.009556	0.023717	0.071246
21000.0	3.10	7.536292	-0.001514	0.017729	0.065205
21000.0	3.15	7.643665	0.003611	0.013780	0.061277
21000.0	3.30	7.964985	0.023476	-0.002978	0.044573
21000.0	3.40	8.178480	0.040552	-0.017857	0.029817
20000.0	2.10	5.331597	0.060416	-0.061303	-0.009984
20000.0	2.20	5.549901	0.044383	-0.044410	0.006976
20000.0	2.40	5.984455	0.018916	-0.016189	0.035133
20000.0	2.60	6.416648	0.002841	0.003064	0.054159
20000.0	2.70	6.632051	-0.001447	0.009069	0.060028
20000.0	2.80	6.846946	-0.003196	0.012674	0.063483
20000.0	2.90	7.061373	-0.002310	0.013787	0.064448
20000.0	3.00	7.275321	0.001243	0.012174	0.062716
20000.0	3.20	7.701811	0.016651	0.001051	0.051428
20000.0	3.40	8.126290	0.043478	-0.021538	0.028977
20000.0	3.50	8.337629	0.061283	-0.036975	0.013722
19300.0	2.70	6.602710	0.010379	-0.003102	0.050207
19300.0	2.80	6.816322	0.007729	0.001242	0.054447
19300.0	2.90	7.029521	0.007603	0.003327	0.056356
19300.0	3.00	7.242248	0.010067	0.002842	0.055727
19300.0	3.10	7.454530	0.015188	-0.000118	0.052634
19300.0	3.50	8.298844	0.063143	-0.039489	0.013261
18000.0	2.40	5.909911	0.061525	-0.059702	-0.001055
18000.0	2.50	5.927881	0.041791	-0.026352	-0.001396
18000.0	2.60	6.334639	0.041794	-0.036996	0.021490
18000.0	2.80	6.757473	0.030972	-0.022755	0.035427
18000.0	3.00	7.178487	0.029557	-0.018225	0.039701
18000.0	3.30	7.806959	0.046024	-0.027868	0.029543
18000.0	3.50	8.223723	0.070004	-0.047394	0.009925
18000.0	3.60	8.431377	0.086029	-0.061160	-0.003775
16000.0	2.60	6.246484	0.090524	-0.086653	-0.018676
16000.0	2.80	6.661085	0.075425	-0.070390	-0.002544
16000.0	3.00	7.074019	0.068665	-0.058088	0.009279
16000.0	3.20	7.485446	0.070594	-0.056312	0.010618
16000.0	3.40	7.895345	0.081602	-0.063093	0.003465
15000.0	3.00	7.018517	0.093122	-0.083472	-0.010230
15000.0	3.20	7.425570	0.092028	-0.078632	-0.005845
15000.0	3.40	7.831113	0.099379	-0.082070	-0.009727

Continued...

$\bar{x}$= 0.0010

K	ω	K_{or}	K_{oi}	a_K	$g_\Psi(\bar{x},0)$
12000.0	2.00	4.604580	0.065279	-0.053470	-0.013668
12000.0	2.20	5.010973	0.057380	-0.044302	-0.004357
12000.0	2.40	5.414743	0.060694	-0.045900	-0.005908
12500.0	2.00	4.627859	0.053550	-0.042042	-0.004173
12500.0	2.20	5.036971	0.047260	-0.034406	0.003580
12500.0	2.40	5.443427	0.052673	-0.038043	-0.000012
14000.0	1.70	4.062835	0.048154	-0.038769	-0.006125
14000.0	2.00	4.694209	0.023655	-0.012833	0.020145
14000.0	2.20	5.110953	0.022516	-0.010162	0.022892
14000.0	2.30	5.318258	0.026835	-0.013565	0.019519
14000.0	2.50	5.730811	0.045755	-0.030344	0.002838
14000.0	2.55	5.833515	0.052698	-0.036689	-0.003465
15000.0	1.80	4.311146	0.018236	-0.008941	0.021240
15000.0	1.90	4.523937	0.011279	-0.001438	0.028824
15000.0	2.00	4.735843	0.007515	0.002984	0.033302
15000.0	2.10	4.946938	0.007065	0.004200	0.034557
15000.0	2.20	5.157271	0.010044	0.002085	0.032478
15000.0	2.30	5.366865	0.016561	-0.003468	0.026966
16000.0	1.50	3.694734	0.037709	-0.029828	-0.002338
16000.0	1.70	4.130414	0.010668	-0.002203	0.025619
16000.0	1.80	4.346450	0.001763	0.007187	0.035106
16000.0	1.90	4.561490	-0.003858	0.013408	0.041392
16000.0	2.00	4.775632	-0.006059	0.016315	0.044346
16000.0	2.10	4.988940	-0.004714	0.015776	0.043848
16000.0	2.20	5.201449	0.000298	0.011669	0.039785
16000.0	2.40	5.624088	0.021790	-0.007715	0.020553
16000.0	2.55	5.938893	0.048402	-0.032472	-0.003985
18000.0	1.30	3.298445	0.041036	-0.034224	-0.010735
18000.0	1.40	3.524485	0.021453	-0.014591	0.009150
18000.0	1.50	3.748669	0.004829	0.002240	0.026168
18000.0	1.60	3.971315	-0.008601	0.016015	0.040077
18000.0	1.80	4.412869	-0.025103	0.033564	0.057788
18000.0	2.00	4.850307	-0.026714	0.036638	0.060963
18000.0	2.20	5.284087	-0.012285	0.024062	0.048521
18000.0	2.30	5.499611	0.001282	0.011570	0.036141
18000.0	2.40	5.714176	0.019267	-0.005234	0.019498
18000.0	2.50	5.927717	0.041809	-0.026479	-0.001523

Continued...

$\bar{x}$= 0.0020

k	ω	K_{or}	K_{oi}	q_E	$\bar{q}(\bar{x},0)_\psi$
10000.0	1.40	3.102248	0.039825	-0.031018	-0.010727
10000.0	1.60	3.510662	0.034526	-0.024875	-0.004276
10000.0	1.70	3.712854	0.037602	-0.027341	-0.006624
10500.0	1.45	3.225829	0.028491	-0.019821	-0.000570
10500.0	1.55	3.431593	0.026849	-0.017721	0.001669
10500.0	1.65	3.635982	0.029197	-0.019488	0.000020
12000.0	1.20	2.751973	0.022036	-0.014881	0.001211
12000.0	1.30	2.966502	0.013318	-0.005926	0.010343
12000.0	1.40	3.179094	0.008545	-0.000789	0.015624
12000.0	1.50	3.390004	0.008007	0.000235	0.016769
12000.0	1.60	3.599412	0.011955	-0.003110	0.013531
12000.0	1.80	4.014116	0.034249	-0.023821	-0.006971
13000.0	1.30	2.998950	0.000273	0.006716	0.021548
13000.0	1.40	3.214232	-0.002727	0.010131	0.025089
13000.0	1.50	3.427806	-0.001103	0.009039	0.024107
13000.0	1.60	3.639824	0.005415	0.003174	0.018343
14000.0	1.00	2.363305	0.019548	-0.013530	-0.000404
14000.0	1.10	2.587959	0.005450	0.000655	0.013979
14000.0	1.30	3.029719	-0.010556	0.017224	0.030842
14000.0	1.50	3.463561	-0.007789	0.015490	0.029324
14000.0	1.60	3.677981	0.001402	0.006994	0.020929
14000.0	1.70	3.890830	0.016173	-0.006951	0.007096
14000.0	1.80	4.102098	0.036804	-0.026611	-0.012429
15000.0	0.80	1.938135	0.031876	-0.026542	-0.015668
16000.0	0.90	2.174180	0.012143	-0.006901	0.004201
16000.0	1.10	2.635854	-0.016530	0.022013	0.033460
16000.0	1.30	3.086900	-0.026751	0.032952	0.044637
16000.0	1.40	3.309251	-0.023864	0.030595	0.042379
16000.0	1.50	3.529721	-0.015176	0.022555	0.034439
16000.0	1.60	3.748372	-0.000355	0.008512	0.020509
16000.0	1.70	3.965189	0.020935	-0.011852	0.000264
18000.0	0.70	1.725128	0.033024	-0.028225	-0.018901
18000.0	0.80	1.969517	0.010935	-0.006280	0.003264
18000.0	0.90	2.209697	-0.008102	0.012765	0.022496
18000.0	1.10	2.679780	-0.033251	0.038304	0.048319
18000.0	1.30	3.139136	-0.037110	0.043001	0.053222
18000.0	1.50	3.589753	-0.016132	0.023331	0.033759
18000.0	1.60	3.811943	0.004653	0.003408	0.013972
18000.0	1.70	4.031942	0.032843	-0.023748	-0.013005

Continued...

$\bar{X}$= 0.0035

K	ω	K_{or}	K_{oi}	q_E	$q_\psi(\bar{X},0)$
9000.0	1.00	2.104855	0.029007	-0.022635	-0.011613
9000.0	1.10	2.313298	0.024953	-0.018290	-0.007118
9000.0	1.20	2.519549	0.025344	-0.018276	-0.006976
10000.0	1.00	2.137360	0.016261	-0.010376	-0.000600
10000.0	1.20	2.558903	0.017185	-0.010501	-0.000490
11500.0	0.80	1.741503	0.015081	-0.010216	-0.002132
11500.0	0.90	1.963117	0.006273	-0.001211	0.007009
11500.0	1.00	2.182119	0.002121	0.003240	0.011580
11500.0	1.10	2.398645	0.003352	0.002414	0.010857
11500.0	1.20	2.612820	0.010565	-0.004281	0.004253
11500.0	1.30	2.824721	0.024296	-0.017362	-0.008747
13000.0	0.60	1.313927	0.027287	-0.023083	-0.016292
13000.0	0.70	1.545111	0.012499	-0.008252	-0.001334
13000.0	1.00	2.222851	-0.007376	0.012371	0.019630
13000.0	1.10	2.443494	-0.002537	0.007987	0.015333
13000.0	1.30	2.877211	0.028498	-0.021743	-0.014238
14000.0	0.60	1.328624	0.018538	-0.014644	-0.008394
14000.0	0.80	1.793773	-0.006639	0.010798	0.017280
14000.0	1.20	2.691717	0.010675	-0.004761	0.002074
14000.0	1.30	2.909443	0.033835	-0.027139	-0.020225
16000.0	1.50	3.398998	0.145230	-0.135782	-0.129491

$\bar{X}$= 0.0050

K	ω	K_{or}	K_{oi}	q_E	$q_\psi(\bar{X},0)$
10000.0	0.75	1.530119	0.015450	-0.011072	-0.005053
10000.0	0.85	1.745333	0.013178	-0.008487	-0.002387
10000.0	0.95	1.958616	0.016494	-0.011400	-0.005228
11500.0	0.65	1.342742	0.010428	-0.006710	-0.001649
11500.0	0.70	1.453813	0.007308	-0.003467	0.001629
11500.0	0.80	1.674946	0.004979	-0.000831	0.004333
11500.0	0.90	1.893969	0.006877	-0.002432	0.000894
11500.0	1.00	2.110832	0.020031	-0.014978	-0.009702
13000.0	0.55	1.142201	0.009732	-0.006544	-0.002196
13000.0	0.60	1.255935	0.005120	-0.001833	0.002541
13000.0	0.70	1.482893	-0.000564	0.004107	0.008538
13000.0	0.75	1.595869	-0.001222	0.004924	0.009385
13000.0	0.80	1.708388	-0.000191	0.004072	0.008561
13000.0	0.90	1.931789	0.007550	-0.003233	0.001305
13000.0	0.95	2.042563	0.014537	-0.009958	-0.005399
14000.0	0.50	1.040903	0.009550	-0.006631	-0.002653
14000.0	0.60	1.271181	0.000034	0.003082	0.007102
14000.0	0.70	1.500960	-0.004405	0.007793	0.011866
14000.0	0.80	1.729182	-0.002072	0.005817	0.009941
14000.0	0.90	1.955160	0.008395	-0.004189	-0.000022
18000.0	0.40	0.845718	0.004794	-0.002557	0.000418
18000.0	0.60	1.325340	-0.013001	0.015658	0.018682
18000.0	0.80	1.802410	-0.000282	0.003696	0.006790
18000.0	0.90	2.036809	0.022242	-0.018245	-0.015125

Continued...

$\bar{x}$= 0.0070

K	ω	K_{or}	K_{oi}	q_E	$q_\psi(\bar{x},0)$
18000.0	0.30	0.579961	0.008764	-0.007077	-0.005129
15000.0	0.35	0.671124	0.011827	-0.009796	-0.007413
15000.0	0.45	0.893991	0.005989	-0.003743	-0.001400
15000.0	0.50	1.007067	0.005031	-0.002653	-0.000318
15000.0	0.55	1.120764	0.005845	-0.003316	-0.000987
16000.0	0.35	0.678605	0.009229	-0.007294	-0.005088
16000.0	0.40	0.790688	0.006017	-0.003980	-0.001796
16000.0	0.45	0.904142	0.004043	-0.001885	0.000285
16000.0	0.50	1.018555	0.003694	-0.001400	0.000762
16000.0	0.55	1.133574	0.005322	-0.002872	-0.000716
18000.0	0.35	0.692635	0.005018	-0.003239	-0.001321
18000.0	0.40	0.807205	0.002408	-0.000520	0.001379
18000.0	0.45	0.923158	0.001398	0.000618	0.002504
18000.0	0.50	1.040053	0.002400	-0.000239	0.001637
18000.0	0.55	1.157507	0.005796	-0.003469	-0.001600
19000.0	0.43	0.885115	0.000555	0.001349	0.003121
20000.0	0.30	0.590676	0.005223	-0.003663	-0.001945
20000.0	0.35	0.705608	0.001888	-0.000229	0.001463
20000.0	0.40	0.822466	0.000026	0.001748	0.003423
20000.0	0.41	0.846019	-0.000125	0.001925	0.003596
20000.0	0.43	0.893275	-0.000178	0.002030	0.003696
20000.0	0.45	0.940705	0.000127	0.001780	0.003442
20000.0	0.50	1.059855	0.002635	-0.000574	0.001077
20000.0	0.55	1.179503	0.007965	-0.005726	-0.004085
20000.0	0.60	1.299283	0.016516	-0.014068	-0.012440
22000.0	0.25	0.486252	0.006476	-0.005102	-0.003534
22000.0	0.35	0.717695	-0.000370	0.001933	0.003443
22000.0	0.40	0.836669	-0.001362	0.003046	0.004540
22000.0	0.45	0.957011	-0.000023	0.001847	0.003328
22000.0	0.47	1.005416	0.001274	0.000613	0.002089
22000.0	0.50	1.078220	0.004126	-0.002139	-0.000670
24000.0	0.30	0.610035	0.000270	0.001109	0.002491
24000.0	0.35	0.729024	-0.001905	0.003392	0.004753
24000.0	0.45	0.972250	0.000763	0.000997	0.002328
24000.0	0.50	1.095343	0.006674	-0.004741	-0.003424

Table C4 Neutral stability results for Hornbeck profile and axisymmetric disturbances(nonparallel flow)

Based on $q_\psi(\bar{X},0)$

$\bar{X}$	R	ω	R	ω	R	ω
.0005	21000.	2.055	20000.	2.160	18000.	2.408
.0005	16000.	2.834	15300.	3.230	16000.	3.460
.0005	18000.	3.575	20000.	3.565	21000.	3.555
.0010	18000.	1.350	16000.	1.529	14000.	1.755
.0010	12500.	2.080	12250.	2.260	12500.	2.400
.0010	14000.	2.525	16000.	2.526	18000.	2.493
.0020	16000.	0.877	14000.	1.002	12000.	1.190
.0020	10500.	1.465	10340.	1.570	10500.	1.650
.0020	12000.	1.730	14000.	1.751	16000.	1.700
.0035	14000.	0.65	13000.	0.710	11500.	0.821
.0035	10000.	1.013	9750.	1.115	10000.	1.187
.0035	11500.	1.240	13000.	1.23	14000.	1.210
.0050	14000.	0.470	13000.	0.522	11500.	0.625] increase all ω by 0.05
.0050	10530.	0.782	11500.	0.850	13000.	0.850]
.0050	14000.	0.850				
.0070	22000.	0.291	20000.	0.325	18000.	0.371
.0070	16000.	0.441	15400.	0.500	16000.	0.537
.0070	18000.	0.528	20000.	0.515	22000.	0.493

Based on $q_E(\bar{X})$

.0005	21000.	2.380	20000.	2.555	19300.	2.765
.0005	19050.	2.958	19300.	3.100	20000.	3.210
.0005	21000.	3.273				
.0010	18000.	1.487	16000.	1.725	15000.	1.950
.0010	14700.	2.120	15000.	2.230	16000.	2.377
.0010	18000.	2.370				
.0020	16000.	0.940	14000.	1.095	12000.	1.418
.0020	11900.	1.475	12000.	1.515	14000.	1.655
.0035	14000.	0.700	13000.	0.770	11500.	0.918
.0035	11000.	1.052	11500.	1.147	13000.	1.180
.0035	14000.	1.170				
.0050	14000.	0.563	13000.	0.625	11700.	0.795
.0050	13000.	0.866	14000.	0.870		
.0070	22000.	0.313	20000.	0.355	18000.	0.415
.0070	17450.	0.465	18000.	0.495	20000.	0.492
.0070	22000.	0.468				

COMPUTER PROGRAMME FOR STABILITY OF THE NONPARALLEL DEVELOPING FLOW IN A PIPE

PROGRAMME FOR THE VELOCITY OBTAINED BY HORNBECK'S METHOD

NOMENCLATURE

Stores Newton-Cotes quadrature coefficients
Stores real part of the nondiagonal elements of the matrix B
Stores imaginary part of the nondiagonal elements of the matrix B
Constant K(eqn.(5.9))
Delta used in eqn.(5.15)
Wavenumber obtained from nonparallel flow theory
Growth rate based on the disturbance stream function at pipe axis
GV Growth rates based respectively on streamwise and radial components of the disturbance velocity
Step size used in Runge-Kutta method
Infinitesimal incremental distance along X
Stores imaginary part of the eigenvalue
Stores the real part of the eigenvalue
Spatial growth rate based on parallel flow theory
Wavenumber obtained on the basis of parallel flow theory
Stores the step points at which orthonormalization is being done
Number of solutions
Number of complex eigenfunctions
Number of divisions of the grid along y-direction
Number of mesh points
Radius of any mesh point
Reynolds number based on average flow velocity and radius of pipe
Stores the diagonal elements of the matrix B
Mainflow velocity at the mesh points; stored on the disk
,U2 First and second derivative of mainflow velocity w.r.t.Y; being calculated by central differences
Radial component of mainflow velocity; stored on the disk
,V2 First and second derivatives of V w.r.t.Y; being calculated by central differences
,WT Real and imaginary parts of the frequency of the disturbance.In spatial stability analysis WI=0
Axial location in the inlet region
,YT Store the real and imaginary parts of the current eigenfunctions

SUBROUTINES USED

SDPC Determines absolute value of a complex number
VDPC Determines division of two complex numbers
LT For obtaining simultaneous plot of two functions A&B known at known regular intervals
TGCO Sets the quadrature coefficients
G2G1 Finds K1(SECTION 2.1.2)
LDPC Determines product of two complex numbers
MM Finds maxima and minima of an array and their locations
RTHO Orthonormalizes the solution vectors.It uses Gram-Schmidt Ortho normalization technique(section 5.2.1)
EPCON Repaires the eigenfunctions as per section 5.2.2
INGC Integrates the regular problem(eqns.(3.12) through (3.14))
INGCA Integrates the adjoint problem(eqns.(3.19) through (3.21))
ECANT Uses Muller's method for convergence to eigenvalue
QTDPC Determines squareroot of a complex number
DU1 Knowing velocity at mesh points U apart,it first calculates U at mid-step points using procedure given in section 5.4 and then calculates its first derivative w.r.t.Y using central differences
V2U2 Knowing U&V,it calculates D2U and D2V+DV/Y using central differences

```
      DOUBLE PRECISION BI,BR,EPS,E1,E2,H,H2,H3,KR,KI,AD,DR,DI,DY2,GK
     1,RE,SR,WI,ABSDPC,XX,CR,CI,EP,E3,PR,PI,YR(4,2),YI(4,2),U1(401,2)
     2,CPR(100),CPI(100),RP(2,100),HX,F,A(6),GU(401),V1(401),GV(401),
     4KAR(3),KAI(3),TR(401,3),TI(401,3),GP(401),U0(401,2),U2(401),RSQRI
     5,T0R(401),T0I(401),T1R(401),T1I(401),T2R(401),T2I(401),V(401),
     6Z3R(401),T3I(401),CY,Z3R(401),Z3I(401),DUMI(802),RA(401),V2(401)
      DIMENSION L(101)
      COMMON/A1/U0,U1
      COMMON/A2/YR,YI,CPR,CPI,RP,NCV,NB,L,JP,NFN
      COMMON/A3/N,ND,NN
      COMMON/A4/U2,H3,KR,KI,RE,RA
      COMMON/A5/T0R,T1R,T2R,T3R,V,V1,V2,Z3R,T0I,T1I,T2I,T3I,DUMI,U2,Z3I
      COMMON/A6/TR,TI,KAR,KAI
      COMMON/A7/GP,GU,GV,DR,E2,DI,E3
      DATA NCV,NB/1,2/,WI/0.D0/
      READ 510,ND,N1,N2,NCA,HX,EP
      OPEN(UNIT=15,DEVICE='DSK',FILE='PHK1.DAT',ACCESS='APPEND',
     1RECORD SIZE=132)
      Setting the step size
      N11=N1-1
      N21=N2-1
      NI=ND/5
      N=ND-1
      NN=ND+1
      MT=ND/40
      AD=ND
      H=.1D1/AD
      H2=.5D0*H
      H3=H/6.D0
      DY2=ND*ND
      RA(1)=0
      DO 1 J=1,ND
    1 RA(J+1)=J*H
      CY=ND/2
      Finding quadrature coefficients
      CALL INTGCO(A,H)
      DO 99 NST=1,NCA
      IX=2
      TEXT=A=1
      NFN=2
      READ 520,E1,E2,E3,EPS,NA,CR
      PRINT 610,N11,N21,EPS,E1,E2,E3,EP,H
      OPEN(UNIT=10,DEVICE='DSK',FILE=CR,ACCESS='SEQIN')
    2 READ 525,RE,WR,KR,KI
      VELOCITIES HAVE BEEN DELETED FROM POINTS 1 TO (N1-1) FROM VELOCITY
      DATA FILE,(N1-1) IS THE STEP POINT UPTO WHICH U1=0 AND (N2-1) TS
      THE STEP POINT UPTO WHICH U2=0,
      THE THREE CHOSEN SECTIONS 1,3,2 ARE RESPECTIVELY AT X=X-HX,
      X,AND X+HX,WHERE HX IS DELTA(X)
    4 READ(10,535)XX,(U0(J,1),J=N1,NN)
      CALL U001(CY,N1)
      L(1)=0
      MT=0
      CR=RE*WR
      CI=RE*WI
      IF(N1.EQ.1)GO TO 8
      DO 6 I=1,2
      DO 6 J=1,N11
      U0(J,I)=U0(N1,1)
    6 U1(J,I)=0
```

```
      BR=KR**2-KI**2
      BI=2.D0*KR*KI
      F=1
      JP=1
C     Setting the starting values of YR & YI
      DO 10 J=1,26
      DO 10 I=1,NCV
      YR(I,J)=0
      YI(I,J)=0
      YR(2,1)=1
      YR(4,2)=1
      CALL MULDPC(CR,CI,E3,F,EP,H,NT)
      CALL MULDPC(YR(1,1),YI(1,1),YR(2,2),YI(2,2),DR,DI)
      CALL MULDPC(YR(1,2),YI(1,2),YR(2,1),YI(2,1),PR,PI)
C     DR,DI and AD are real and imaginary parts of the determinant
C     (eqn.(5.1))
C     and its absolute value respectively
C     F represents N in eqn.(5.12)
      DR=(DR-PR)/F
      DI=(DI-PI)/F
      AD=ABSDPC(DR,DI)
      NT=NT+1
      IF(NT.GT.MA) GO TO 60
      CALL SPCANT(KR,KI,DR,DI,AD,EPS,E1,E2,NT,J)
      GO TO(8,16),J
    8 CALL REPCOM
      PRINT 630,XX,RE,WR,KR,KI,AD,EP,F,NT,U0(NN,1),U0(1,1),U1(NN,1)
      KAR(IX)=KR
      KAI(IX)=KI
      DO 20 J=1,NN
   20 CALL DIVDPC(-T0I(J),T0R(J),KR,KI,TR(J,IX),TI(J,IX))
C     GO TO(30,25,34),IX
C     Growth rates at pipe axis and pipe wall are computed separately
   25 GU(1)=ABSDPC(T1R(1),T1I(1))
      GU(NN)=ABSDPC(T2R(NN),T2I(NN))
      GV(NN)=ABSDPC(KR*T2I(NN)+KI*T2R(NN),KI*T2I(NN)-KR*T2R(NN))
      GV(1)=ABSDPC(KR*T1I(1)+KI*T1R(1),KI*T1I(1)-KR*T1R(1))
      IX=1
      K=EP/(E**(1.D0/JP));EP=K
      GK=DATAN2(T1I(1),T1R(1))
      DO 26 K=2,ND
      GU(K)=ABSDPC(T1R(K),T1I(K))
      GV(K)=ABSDPC(T0R(K),T0I(K))
   26 GP(K)=GU(K)*GU(K)
      GO TO 4
   30 GU(1)=GU(1)-ABSDPC(T1R(1),T1I(1))
      GU(NN)=GU(NN)-ABSDPC(T2R(NN),T2I(NN))
      GV(NN)=GV(NN)-ABSDPC(KR*T2I(NN)+KI*T2R(NN),KI*T2I(NN)-KR*T2R(NN))
      GV(1)=GV(1)-ABSDPC(KR*T1I(1)+KI*T1R(1),KI*T1I(1)-KR*T1R(1))
      IX=3
      JP=4
      GK=GK-DATAN2(T1I(1),T1R(1))
      DO 32 I=2,ND
      DR=ABSDPC(T1R(I),T1I(I))
      GP(I)=GP(I)-DR*DR
      GV(I)=GV(I)-ABSDPC(T0R(I),T0I(I))
   32 GU(I)=GU(I)-DR
      IF(IX.EQ.2
      GO TO 2
   34 AD=BX*BB*2.D0
      PRINT 670,JP,(I(I),I=1,JP)
      RSQRT=DSQRT(EP)
      PR=RSQRT/AD
      KAR(3)=(KAR(2)-KAR(1))*PR
      KAI(3)=(KAI(2)-KAI(1))*PR
      K=1
      ND=2
      IX=6
      EPS=KAR(1)**2+KAI(1)**2
      KAR(2)=KAR(2)**2+KAI(2)**2
```

```
      KAI(1)=KR**2+KI**2
      PI=ABSDPC(T1R(1),T1I(1))
      GU(1)=GU(1)/(PI*AD)
      GV(NN)=GV(NN)/(AD*ABSDPC(KR*T2I(NN)+KI*T2R(NN),KI*T2I(NN)-
     1KR*T2R(NN)))
      GV(1)=GV(1)/(AD*ABSDPC(KR*T1I(1)+KI*T1R(1),KI*T1I(1)-KR*T1R(1)))
      PI=ABSDPC(T2R(NN),T2I(NN))
      GU(NN)=GU(NN)/(PI*AD)
      GP(NN)=GU(NN)
      E1=0
      E2=0
      GP(1)=GU(1)
      NI=NI-1
      DO 38 I=1,NI
      DO 36 J=NFN,IX
      K=K+1
      PI=ABSDPC(T1R(J),T1I(J))
      GU(J)=GU(J)/(PI*AD)
      DI=ABSDPC(TR(J,1),TI(J,1))
      KAR(1)=ABSDPC(TR(J,2),TI(J,2))
      DR=ABSDPC(TR(J,3),TI(J,3))
      GV(J)=GV(J)/(AD*ABSDPC(T0R(J),T0I(J)))
      F=A(K)*(KAI(1)*DR*DR+PI*PI)
      KAI(2)=A(K)*(GP(J)+KAR(2)*KAR(1)**2-DI*DI*EPS)
      F1=E1+F*RA(J)
      E2=E2+KAI(2)*RA(J)
      GP(J)=(KAR(1)-DI)/(AD*DR)
      NFN=IX+1
      IX=IX+5
      K=1
      DO 40 J=NFN,ND
      K=K+1
      PI=ABSDPC(T1R(J),T1I(J))
      GU(J)=GU(J)/(PI*AD)
      DI=ABSDPC(TR(J,1),TI(J,1))
      KAR(1)=ABSDPC(TR(J,2),TI(J,2))
      DR=ABSDPC(TR(J,3),TI(J,3))
      GV(J)=GV(J)/(AD*ABSDPC(T0R(J),T0I(J)))
      F=A(K)*(KAI(1)*DR*DR+PI*PI)
      KAI(2)=A(K)*(GP(J)+KAR(1)**2*KAR(2)-DI*DI*EPS)
      E1=E1+F*RA(J)
      E2=E2+KAI(2)*RA(J)
      GP(J)=(KAR(1)-DI)/(AD*DR)
      E1=.5D0*E2/(AD*E1)
      DETERMINATION OF BETA AND ITS DERIVATIVES STARTS.
      Z3R(1)=T1R(1)
      Z3I(1)=T1I(1)
      T3R(1)=0
      T3I(1)=0
      DO 41 I=1,NN,ND
      DO 41 J=1,3
      TR(1,J)=0
      TI(1,J)=0
      DO 42 J=2,ND
      TR(J,1)=(TR(J,2)-TR(J,1))*PR*RA(J)
      TI(J,1)=(TI(J,2)-TI(J,1))*PR*RA(J)
      TR(J,3)=RA(J)*TR(J,3)
      TI(J,3)=RA(J)*TI(J,3)
      TR(J,2)=T1R(J)*RA(J)
2     TI(J,2)=T1I(J)*RA(J)
      DO 43 J=2,NN
      Z3R(J)=T2R(J)*RA(J)+T1R(J)
      Z3I(J)=T2I(J)*RA(J)+T1I(J)
      KAR(1)=GU(J,1)*RE
      DR=BR-KAR(1)*KI+CI
      DI=BI+KAR(1)*KR-CR
      CALL MULDPC(DR,DI,T1R(J),T1I(J),KAR(1),PI)
      CALL MULDPC(-KI,KR,T3R(J),T3I(J),DR,DI)
      E2=RE*U1(J,1)
      T3R(J)=(KAR(1)+DR+E2*T0R(J))*RA(J)+T2R(J)
```

```
      T3I(J)=(PI+D1+E2*T01(J))*RA(J)+T2I(J)
      SETTING INITIAL CONDITIONS FOR ADJOINT PROBLEM
      IX=JP
      NFN=3
      JP=1
      DO 44 J=1,NB
      DO 44 I=1,NCV
      YR(1,J)=0
      YI(1,J)=0
      YR(2,1)=1
      YR(4,2)=1
      F=1
      CALL RUNGCA(BR,BI,CR,CI,E3,F,EP,H)
      CALL MULDPC(YR(1,1),YI(1,1),YR(2,2),YI(2,2),DR,DI)
      CALL MULDPC(YR(1,2),YI(1,2),YR(2,1),YI(2,1),PR,PI)
      F=F/(EP**(JP-IX))
      DR=(DR-PR)/F
      DI=(DI-PI)/F
      PRINT 620,XX,RE,WR,KR,KI,DR,DI,JP
      CALL REPCON
      Finding BETA* and its derivatives(eqns.
      T2R(1)=T1R(1);T2I(1)=T1I(1)
      T1R(1)=0;T1I(1)=0
      DO 45 J=2,NN
      CALL DIVDPC(-T0I(J),T0R(J),KR,KI,T0R(J),T0I(J))
      T0R(J)=RA(J)*T0R(J);T0I(J)=RA(J)*T0I(J)
      T2R(J)=RA(J)*T2R(J)+T1R(J)
      T2I(J)=RA(J)*T2I(J)+T1I(J)
      T1R(J)=RA(J)*T1R(J)
      T1I(J)=RA(J)*T1I(J)
      V2(J) STORES V2(J)+V1(J)/RA(J)
      READ(10,535)(V(J),J=2,NN)
      CALL VV2U2(CY,DY2,N2)
      CALL K1G2G1(WR,WI,BR,BI,A,NI)
      BR=KAR(2)/RSQRT+KR
      BI=KI+KAI(2)/RSQRT
      Final calculation of growth rates and wavenumber
      E1=E1-BI
      DO 50 J=1,NN
      GU(J)=GU(J)-BI
      GV(J)=GV(J)-BI
      GP(J)=GP(J)-BI
      GK=GK/AD+BR
      PRINT 690,KAR(2),KAI(2),KAR(3),KAI(3),BR,BI
      WRITE(15,710)XX,RE,WR,KR,KI,E1,GU(1),GV(1),GK,BR,BI
      CALL MXMN(GP,DR,DI,K,1)
      PR=(K-1)*H;PI=(I-1)*H
      CALL MXMN(GU,CR,CI,K,1)
      BR=(K-1)*H;BI=(I-1)*H
      CALL MXMN(GV,E2,E3,K,1)
      EPS=(K-1)*H;AD=(I-1)*H
      PRINT 640,BR,CR,BI,CI,EPS,E2,AD,E3,PR,DR,PI,DI,E1,GK
      WRITE(15,720)CR,BR,CI,BI,E2,EPS,E3,AD,DR,PR,DI,PI
      CALL PPLT(H,NN)
      GO TO 94
   )  PRINT 570,JP,(U(J),J=1,JP)
      PRINT 580, NA
      IF(IEXTRA.EQ.1) READ 525,RE
   9  CLOSE(UNIT=10)
      CLOSE(UNIT=15)
      STOP
   0  FORMAT(413,2D6.0,A7)
   0  FORMAT(4D6.0,I2,A7)
   5  FORMAT(10X,4D13.0)
   5  FORMAT(D25.0)
   0  FORMAT(/////,1H1,10X,' SPATIAL STABILITY OF HORNBECK*S PROFILE IN
      1 PIPE-COUETE*S THIRD FORMULATION, U1=0 UPTO MESH POINT'I4
      3' AND U2=0 UPTO'I4/6X,'EPS= ',D10.3,3X,'E1 =',D13.6,
      43X4HE2 =D13.6,3X3HE3=D12.5,2X3HEP=D12.5,2X2HH=D10.3/4X'X'7X'RE'5X
      5'WR'10X'KR'10X'KI'12X'AD'9X'EP'10X'F'5X'NT'2X'U(WALL)'3X'U(C.L.)'
      62X'UP(WALL)')
```

```
FORMAT(F8.5,F3.0,F6.3,2D18.10,2D11.3,I3,5X'FROM ADJOINT PROBLEM')
FORMAT(/,F8.5,F6.0,F6.3,2D18.10,3D11.3,I3,D10.2,F9.5,F10.5)
FORMAT(2X'Y='F6.4,2X'GU(MAX)='D13.6,2X'Y='F6.4,2X'GU(MIN)='D13.6,
12X'Y='F6.4,2X'GV(MAX)='D13.6,2X'Y='F6.4,2X'GV(MIN)='D13.6/2X
2'Y='F6.4,2X'GP(MAX)='D13.6,2X'Y='F6.4,2X'GP(MIN)='D13.6
3,2X'GE='D13.6,2X'0 WAVE #='F10.7/85X'Y'8X'GP'10X'GV'10X'GU')
FORMAT(2X13,1X'ORTHONORMALIZATIONS OCCUR AT'2414/(6X,3114))
FORMAT(/,20X,' CASE HAS NOT CONVERGED IN ',I2,' ITERATIONS')
FORMAT(/,6X,'K1=',2(D15.8,2X),'DELK0/DELX1=',
1(D15.8,2X)'K0+EPL*K1='F10.7,D17.8)
FORMAT(F7.4,F8.1,F6.3,F10.7,4D13.6,2F9.6,D13.6)
FORMAT(5(D11.4,F6.4))
END
```

```
DOUBLE PRECISION FUNCTION ABSDPC(A,B)
ABSDPC computes the Absolute value of (A+iB)
DOUBLE PRECISION A,B,C,D
C=DABS(A)
D=DABS(B)
IF(C.GT.D) GOTO 1
ABSDPC=D*DSQRT(1.D0+(C/D)**2)
RETURN
ABSDPC=C*DSQRT(1.D0+(D/C)**2)
RETURN
END
```

```
SUBROUTINE DIVDPC (A,B,C,D,E,F)
DIVDPC divides (A+iB) by (C+iD) to get (E+iF)
DOUBLE PRECISION A,B,C,D,E,F,G,H,DC
IF(DABS(D).GT.DABS(C)) GO TO 1
DC=D/C
G=C+D*DC
H=(A+B*DC)/G
F=(B-A*DC)/G
E=H
RETURN
DC=C/D
G=D+C*DC
H=(B+A*DC)/G
F=(B*DC-A)/G
E=H
RETURN
END
```

```
SUBROUTINE FPLT(H,NN)
DOUBLE PRECISION A(401),B(401),C(2),D(2),H,FMX,FMN,F(401)
DIMENSION E(82),X(82)
COMMON/A7/A,F,B,C,D
DATA N,BL,DOT,SP,UP,BP,AX/82,1H ,1H.,1HS,1HV,1HB,1H+/
FMX=DMAX1(C(1),C(2))
FMN=DMIN1(D(1),D(2))
IF(FMX.LT.0)FMX=0
IF(FMN.GT.0)FMN=0
FMX=(N-2)/(FMX-FMN)
DO 10 J=1,N
X(J)=BL
X(2)=DOT
X(N)=DOT
I=2.D0-FMX*FMN
X(I)=AX
DO 30 J=1,NN,H
Y=H*(J-1)
DO 20 K=1,N
E(K)=X(K)
I=(A(J)-FMN)*FMX+2.D0
E(I)=SP
K=(B(J)-FMN)*FMX+2.D0
E(K)=UP
IF(I.EQ.K) E(I)=BP
PRINT 690,E,Y,A(J),B(J),F(J)
```

```
FORMAT(62A1,F6.2,3D12.4)
RETURN
END
```

```
SUBROUTINE INTGCO(A,H)
DOUBLE PRECISION A(6),H
A(1)=95.D0/288.D0*H
A(3)=25.D0/288.D0*H
A(2)=1.5D0*A(3)
A(4)=A(3)
A(5)=A(2)
A(6)=2.D0*A(1)
RETURN
END
```

```
SUBROUTINE K1G2G1(WR,WI,KSR,KSI,A,NI)
S0R,S0I,S1R,S1I,S2R,S2I are real and imaginary parts resp.
and its first and second derivative w.r.t.Y
Z0R,Z0I,Z1R,Z1I,Z2R,Z2I,Z3R,Z3I are real and imaginary parts respectiv
BETA and its first,second and third derivatives w.r.t.Y
DKR and DKI store real and imaginary parts of DK0/DX1
DZR and DZI store real and imaginary parts of first derivative of BETA
K1R,K1I finally store the real and imaginary parts of K1
DOUBLE PRECISION A(6),AR,AI,B1R,B1I,B2R,B2I,B4,CR,CI,C2R,C2I,C3R,
1C3I,DKR,DKI,KR,KI,KSR,KSI,K1R,K1I,RE,WR,WI,U1(401),U2(401),
2DZR(401),DZI(401),S0R(401),S0I(401),S1R(401),S1I(401),S2R(401),
3S2I(401),D0(401),V(401),V2(401),Z0R(401),D(401),
4Z0I(401),Z1R(401),Z1I(401),Z2R(401),Z2I(401),Z3R(401),Z3I(401)
5,C4R,C4I,C5R,C5I,GS1R,GS1I,GS2R,GS2I,H2,H3,DUMI(802),D2(401)
6,RR,ZR,ZI,RA(401),V1(401)
COMMON/A1/U0,D,U1,D2
COMMON/A3/N,ND,NN
COMMON/A4/H2,H3,KR,KI,RE,RA
COMMON/A5/S0R,S1R,S2R,Z3R,V,V1,V2,Z2R,S0I,S1I,S2I,Z3I,DUMI,U2,Z2I
COMMON/A6/DZR,Z1R,Z0R,DZI,Z1I,Z0I,CR,K1R,DKR,CI,K1I,DKI
GS1R=0
GS1I=0
GS2R=0
GS2I=0
B4=-2.0D0/RE
C2R=-2.D0*B4*KI
C2I=2.D0*B4*KR
C3R=WR+3.D0*B4*KSI
C3I=WI-3.D0*B4*KSR
CR=2.D0*(WR+B4*KSI)
CI=2.D0*(WI-B4*KSR)
CALL MULDPC(KR,KI,CR,CI,CR,CI)
J=2
L=6
DO 25 K=1,NI
I=1
DO 20 J=2,L
RR=1.D0/RA(J)
I=I+1
B1R=CR-3.D0*U0(J)*KSR-U2(J)+U1(J)*RR
B1I=CI-3.D0*U0(J)*KSI
B2R=C2R+U0(J)
ZR=Z2R(J)-RR*Z1R(J)
ZI=Z2I(J)-RR*Z1I(J)
CALL MULDPC(B1R,B1I,Z0R(J),Z0I(J),K1R,K1I)
CALL MULDPC(B2R,C2I,ZR,ZI,AR,AI)
K1R=A(I)*(K1R+AR)
K1I=A(I)*(K1I+AI)
CALL MULDPC(K1R,K1I,S0R(J),S0I(J),C4R,C4I)
GS1R=GS1R+C4R
GS1I=GS1I+C4I
S2R(J)=S2R(J)+RR*(S1R(J)-RR*S0R(J))
```

```
S2I(J)=S2I(J)+RR*(S1T(J)-RR*S0I(J))
CALL MULDPC(B1R+U2(J)+U1(J)*RR,B1I,S0R(J),S0T(J),AR,AI)
CALL MULDPC(B2R,C2I,S2R(J),S2I(J),K1R,K1I)
B1R=2.D0*U1(J)
AR=A2+K1R+B1R*S1R(J)
AI=AT+K1I+B1R*S1I(J)
CALL MULDPC(AR,AI,DZR(J),DZI(J),B1R,B1I)
B2R=C3R-3.D0*U0(J)*KR
B2I=C3I-3.D0*U0(J)*KI
K1R=-V2(J)-(KSR-4.D0*RR*RR)*V(J)
K1I=-V(J)*KSI
CALL MULDPC(B2R,B2I,Z0R(J),Z0I(J),B2R,B2I)
AR=B2R-B1*ZI
AI=B2I+B1+ZR
CALL MULDPC(DKR,DKI,AR,AI,AR,AI)
CALL MULDPC(K1R,K1I,Z1R(J),Z1I(J),K1R,K1I)
B2R=K1R+V(J)*Z3R(J)+AR
B2I=K1I+V(J)*Z3I(J)+AI
CALL MULDPC(KSR,KSI,Z0R,Z0I,AR,AI)
B2R=B2R+V(J)*(2.D0*AR-3.D0*Z2R(J))*RR
B2I=B2I+V(J)*(2.D0*AI-3.D0*Z2I(J))*RR
CALL MULDPC(B2R,B2I,S0R(J),S0I(J),AR,AI)
C5R=A(I)*(B1R+AR)
C5I=A(I)*(B1I+AI)
GS2R=GS2R+C5R
GS2I=GS2I+C5I
J=L+1
L=L+5
GS1R=GS1R-C4R*.5D0
GS1I=GS1I-C4I*.5D0
GS2R=GS2R-C5R*.5D0
GS2I=GS2I-C5I*.5D0
CALL DIVDPC(-GS2I,GS2R,GS1R,GS1I,K1R,K1I)
RETURN
END
C
C
SUBROUTINE MULDPC (A,B,C,D,E,F)
MULDPC multiplies (A+iB) with (C+iD) to get (E+iF)
DOUBLE PRECISION A,B,C,D,E,F,G
G=A*C-B*D
F=A*D+B*C
E=G
RETURN
END
C
C
SUBROUTINE MXMN(ZM,DR,DI,K,I)
DOUBLE PRECISION DR,DI,ZM(401)
COMMON/A3/N,ND,NN
K=1
I=1
DR=ZM(1)
DI=ZM(1)
DO 54 J=2,NN
IF(DI.GT.ZM(J)) GO TO 52
I=J
DI=ZM(J)
GO TO 54
52  IF(DR.GT.ZM(J)) GO TO 54
    DR=ZM(J)
    K=J
54  CONTINUE
    RETURN
    END
C
C
    SUBROUTINE ORTHO(F)
    DOUBLE PRECISION BR,BI,ER,GR,GI,CPR(100),CPI(100),F
    1,YR(4,2),YI(4,2),RP(2,100)
    DIMENSION L(101)
```

```
      COMMON/A2/YR,YI,CPR,CPI,RP,NCV,NB,L,JP,NFN
      ER=0
      DO 11 I=1,NCV
   11 ER=ER+YR(I,1)**2+YI(1,1)**2
      ER=1.D0/DSQRT(ER)
      RP(1,JP)=ER
      DO 12 I=1,NCV
      YR(I,1)=YR(I,1)*ER
   12 YI(I,1)=YI(I,1)*ER
      F=F*ER
      GR=0
      GI=0
      DO 13 I=1,NCV
      CALL MULDPC(YR(I,2),YI(I,2),YR(I,1),-YI(I,1),BR,BI)
      GR=GR+BR
   13 GI=GI+BI
      DO 14 I=1,NCV
      CALL MULDPC(GR,GI,YR(I,1),YI(I,1),BR,BI)
      YR(I,2)=YR(I,2)-BR
   14 YI(I,2)=YI(I,2)-BI
      BR=0
      DO 15 I=1,NCV
   15 BR=BR+YR(I,2)**2+YI(I,2)**2
      BR=1.D0/DSQRT(BR)
      RP(2,JP)=BR
      ER=-BR*ER
      CPR(JP)=ER*GR
      CPI(JP)=ER*GI
      DO 16 I=1,NCV
      YR(I,2)=YR(I,2)*BR
   16 YI(I,2)=YI(I,2)*BR
      F=F*BR
      RETURN
      END
      ------------------------------------------------------------------
      SUBROUTINE REPCON
      DOUBLE PRECISION DR,DI,PR,PI,CPR(100),CPI(100),ER(2),RP(2,100),
     1YR(4,2),YI(4,2),YIR(401,4,2),YII(401,4,2),EI(2)
      DIMENSION L(101)
      COMMON/A2/YR,YI,CPR,CPI,RP,NCV,NB,L,JP,NFN
      COMMON/A3/N,ND,NN
      COMMON/A5/YIR,YII
      M=MAXO(JP,1)
      ER(1)=1
      EI(1)=0
      CALL DIVDPC(-YR(1,1),-YI(1,1),YR(1,2),YI(1,2),ER(2),EI(2))
      IF(NFN.GT.2) GO TO 30
      CALL MULDPC(YR(3,2),YI(3,2),ER(2),EI(2),YR(3,2),YI(3,2))
      YIR(NN,3,1)=YR(3,1)+YR(3,2)
      YII(NN,3,1)=YI(3,1)+YI(3,2)
   30 DO 38 J=1,NN
      I=NN+1-J
      IF(L(M)-I) 36,35,36
   35 CALL MULDPC(CPR(M),CPI(M),ER(2),EI(2),PR,PI)
      ER(1)=RP(1,M)*ER(1)+PR
      EI(1)=RP(1,M)*EI(1)+PI
      ER(2)=RP(2,M)*ER(2)
      EI(2)=RP(2,M)*EI(2)
      M=MAXO(M-1,1)
   36 DO 38 K=1,NFN
      CALL MULDPC(YIR(I,K,1),YII(I,K,1),ER(1),EI(1),PR,PI)
      CALL MULDPC(YIR(I,K,2),YII(I,K,2),ER(2),EI(2),DR,DI)
      YIR(I,K,1)=PR+DR
   38 YII(I,K,1)=PI+DI
      RETURN
      END
      ------------------------------------------------------------------
```

```
      SUBROUTINE RUNGC(BR,BI,CR,CI,E3,F,EP,H,NT)
      DOUBLE PRECISION AR,AI,BR,BI,CR,CI,E3,F,H,H2,H3,KI,KR,EP,U,
     1RE,CPR(100),CPI(100),EI(4),ER(4),FR(4),FI(4),RP(2,100),U0(401,2)
     2,U1(401,2),XR(4),XI(4),YR(4,2),YI(4,2),YIR(401,4,2),YII
     3,RE,RA(401)
      DIMENSION L(101),YII(401,4,2)
      COMMON/A1/U0,U1
      COMMON/A2/YR,YI,CPR,CPI,RP,NCV,NB,L,JP,NFN
      COMMON/A3/N,ND,NN
      COMMON/A4/H2,H3,KR,KI,RE,RA
      COMMON/A5/YIR,YII
      DO 2 I=1,NFN
      DO 2 J=1,NB
      YIR(1,I,J)=YR(I,J)
    2 YII(1,I,J)=YI(I,J)
      M=1
      DO 92 JJ=1,ND
      DO 20 J=1,NB
      I=JJ
      MRK=1
      Calculation of functions at pipe axis being different are handled
      separately
      IF(I.GT.1) GO TO 3
      U=U0(1,1)*RE
      FR(1)=.5D0*KI*YR(2,J)
      FR(2)=0
      FR(3)=.5D0*((BR-U*KI+CI)*YR(2,J)-KI*YR(4,J))
      FR(4)=0
      FI(1)=-.5D0*KR*YR(2,J)
      FI(2)=0
      FI(3)=.5D0*((BI+U*KR-CR)*YR(2,J)+KR*YR(4,J))
      FI(4)=0
      GO TO 8
      Calculation of functions for RA > 0
    3 RR=1.D0/RA(I)
    4 U=U0(1,M)*RE
      AR=BR-U*KI+CI
      AI=BI+U*KR-CR
      U=RE*U1(I,M)
    6 FR(1)=KR*YI(2,J)+KI*YR(2,J)-RR*YR(1,J)
      FR(2)=YR(3,J)
      FR(3)=U*YR(1,J)-KR*YI(4,J)-KI*YR(4,J)-AI*YI(2,J)+AR*YR(2,J)
     1-RR*YR(3,J)
      FR(4)=KR*YI(3,J)+KI*YR(3,J)-AR*YR(1,J)+AI*YI(1,J)
      FI(1)=-KR*YR(2,J)+KI*YI(2,J)-RR*YI(1,J)
      FI(2)=YI(3,J)
      FI(3)=U*YI(1,J)+KR*YR(4,J)-KI*YI(4,J)+AR*YI(2,J)+AI*YR(2,J)
     1-RR*YI(3,J)
      FI(4)=-KR*YR(3,J)+KI*YI(3,J)-AR*YI(1,J)-AI*YR(1,J)
      The Runge-Kutta Method
      GO TO (8,12,16,19),MRK
    8 DO 10 K=1,NCV
      XR(K)=YR(K,J)
      XI(K)=YI(K,J)
      ER(K)=FR(K)
      EI(K)=FI(K)
      YR(K,J)=XR(K)+H2*FR(K)
   10 YI(K,J)=XI(K)+H2*FI(K)
      M=2
      MRK=2
      RR=1.D0/(RA(I)+H2)
      GO TO 4
   12 DO 14 K=1,NCV
      YR(K,J)=XR(K)+H2*FR(K)
      YI(K,J)=XI(K)+H2*FI(K)
      ER(K)=ER(K)+2.D0*FR(K)
   14 EI(K)=EI(K)+2.D0*FI(K)
      MRK=3
```

```
      GO TO 6
      DO 1* K=1,NCV
      YR(K,J)=XR(K)+H*FR(K)
      YI(K,J)=XI(K)+H*FI(K)
      ER(K)=ER(K)+2.D0*FR(K)
      EI(K)=EI(K)+2.D0*FI(K)
      MRK=4
      M=1
      I=I+1
      HH=1.D0/RA(I)
      GO TO 4
      DO 20 K=1,NCV
      YR(K,J)=XR(K)+H3*(FR(K)+ER(K))
      YI(K,J)=XI(K)+H3*(FI(K)+EI(K))
      IF(NT.GT.0) GO TO 26
      Finding the length of vectors for orthonormalization criterion
      (cf. Section 5.2.3)
      DO 23 J=1,NB
      U=0.
      DO 22 K=1,NCV
      U=U+YR(K,J)**2+YI(K,J)**2
      IF(U.GT.E3) GO TO 24
      CONTINUE
      GO TO 26
      Carrying orthonormalizations when necessary
      CALL ORTHO(F)
      L(JP)=JJ
      JP=JP+1
      F=F*FP
      GO TO 26
   3  IF(L(JP).NE.JJ) GO TO 26
      CALL ORTHO(F)
      JP=JP+1
      F=F*FP
   8  DO 92 K=1,NFN
      DO 92 J=1,NB
      YIR(I,K,J)=YR(K,J)
      YII(I,K,J)=YI(K,J)
   2  CONTINUE
      IF(L(JP-1).EQ.ND) GO TO 96
      CALL ORTHO(F)
      F=F*FP
      L(JP)=JJ
      Storing eigenfunctions for later repairs
      DO 94 K=1,NFN
      DO 94 J=1,NB
      YIR(NN,K,J)=YR(K,J)
   94 YII(NN,K,J)=YI(K,J)
      RETURN
   96 JP=JP-1
      RETURN
      END
```

```
      SUBROUTINE RUNGCA(BR,BI,CR,CI,E3,F,EP,H)
      comments made in subroutine RUNGC apply here too
      DOUBLE PRECISION AR,AI,BR,BI,CR,CI,E3,F,H,H2,H3,KI,KR,EP,U,
     1RE,CPR(100),CPI(100),EI(4),ER(4),FR(4),FI(4),RP(2,100),UU(401,2)
     2,UI(401,2),XR(4),XI(4),YR(4,2),YI(4,2),YIR(401,4,2),
     3YII(401,4,2),UU(2),RA(401),RR
      DIMENSION L(101)
      COMMON/A1/UU,UI
      COMMON/A2/YR,YI,CPR,CPI,RP,NCV,NB,L,JP,NFN
      COMMON/A3/N,ND,NN
      COMMON/A4/H2,H3,KR,KI,RE,RA
      COMMON/A5/YIR,YII
      M=1
```

```
      DO 2 I=1,NFR
      DO 2 J=1,JR
      YR(1,I,J)=YR(I,J)
      YI(1,I,J)=YI(I,J)
      DO 92 JJ=1,JD
      DO 20 J=1,JR
      I=IU
      MRK=1
      IF(I.GT.1) GO TO 3
      U=UU(1,1)*RE
      FR(1)=.5D0*KT*YR(2,J)
      FR(2)=0
      FR(3)=.5D0*((BR+BR-U*KI+CI)*YR(2,J)+KI*YR(4,J))
      FR(4)=0
      FI(1)=-.5D0*KR*YR(2,J)
      FI(2)=0
      FI(3)=.5D0*((BI+BI+U*KR-CR)*YR(2,J)-KR*YR(4,J))
      FI(4)=0
      GO TO 8
    3 RR=1.D0/RA(I)
      U=UU(I,1)*RE
      AR=BR-U*KI+CI
      AI=BI+U*KR-CR
      U=RE*UU(I,M)
      UU(1)=AR+BR
      UU(2)=AI+BI
      FR(1)=KR*YI(2,J)+KI*YR(2,J)-RR*YR(1,J)
      FR(2)=YR(3,J)
      FR(3)=UU(1)*YR(2,J)-UU(2)*YI(2,J)+KR*YI(4,J)+KI*YR(4,J)-RR*YR(3,J)
      FR(4)=AR*YR(1,J)-AI*YI(1,J)-U*YR(2,J)
      FI(1)=-KR*YR(2,J)+KI*YI(2,J)-RR*YI(1,J)
      FI(2)=YI(3,J)
      FI(3)=UU(1)*YI(2,J)+UU(2)*YR(2,J)-KR*YR(4,J)+KI*YI(4,J)-RR*YI(3,J)
      FI(4)=AR*YI(1,J)+AI*YR(1,J)-U*YI(2,J)
      GO TO (8,12,16,19),MRK
    8 DO 10 K=1,NCV
      XR(K)=YR(K,J)
      XI(K)=YI(K,J)
      ER(K)=FR(K)
      EI(K)=FI(K)
      YR(K,J)=XR(K)+H2*FR(K)
   10 YI(K,J)=XI(K)+H2*FI(K)
      M=2
      MRK=2
      RR=1.D0/(RA(I)+H2)
      GO TO 4
   12 DO 14 K=1,NCV
      YR(K,J)=XR(K)+H2*FR(K)
      YI(K,J)=XI(K)+H2*FI(K)
      ER(K)=ER(K)+2.D0*FR(K)
   14 EI(K)=EI(K)+2.D0*FI(K)
      MRK=3
      GO TO 6
   16 DO 18 K=1,NCV
      YR(K,J)=XR(K)+H*FR(K)
      YI(K,J)=XI(K)+H*FI(K)
      ER(K)=ER(K)+2.D0*FR(K)
   18 EI(K)=EI(K)+2.D0*FI(K)
      MRK=4
      M=1
      I=I+1
      RR=1.D0/RA(I)
      GO TO 4
   19 DO 20 K=1,NCV
      YR(K,J)=XR(K)+H3*(FR(K)+ER(K))
   20 YI(K,J)=XI(K)+H3*(FI(K)+EI(K))
```

```
      DO 23 J=1,M5
      I=0
      DO 22 K=1,NCV
      U=1+YR(K,J)**2+YI(K,J)**2
      IF(U.GT.E3) GO TO 24
      CONTINUE
      GO TO 26
      CALL OPTNO(P)
      L(JP)=JJ
      JP=JP+1
      P=P*EP
      DO 92 K=1,NEV
      DO 92 J=1,M5
      YR(1,K,J)=YR(K,J)
      YI(1,K,J)=YI(K,J)
      CONTINUE
      IF(L(JP-1).EQ.NN) GO TO 96
      CALL OPTNO(P)
      P=P*EP
      L(JP)=NN
      DO 94 K=1,NEV
      DO 93 J=1,M5
      YR(NN,K,J)=ZR(K,J)
      YI(NN,K,J)=ZI(K,J)
      RETURN
      JP=JP-1
      RETURN
      END
C-----------------------------------------------------------------------
      SUBROUTINE SECANT(ER,EI,DR,DI,TR,E,E1,E2,N,M)
      DOUBLE PRECISION ER,EI,DR,DI,TR,E,E1,E2,AR(2),AI(2),BR(2),BI(2),HR
     1,HI,UR,UI,GR,GI,YR,YI,ABSDPC
      M=2
      IF(N.GT.2 ) GO TO 20
      AR(2)=ER
      AI(2)=EI
      BR(2)=DR
      BI(2)=DI
      IF(N.EQ.1) GO TO 10
      ER=DR/E1
      EI=DI/E2
      GO TO 40
   0  ER=ER*E1*E1
      EI=EI*E2*E2
      GO TO 40
   0  HR=ER-AR(2)
      HI=EI-AI(2)
      TR=ABSDPC(HR,HI)/ABSDPC(ER,EI)
      IF(TR.LE.E) RETURN
      CALL DIVDPC(HR,HI,AR(2)-AR(1),AI(2)-AI(1),UR,UI)
      TR=UR+1.D0
      GR=UR*UR-UI*UI
      GI=2.D0*UR*UI
      YR=TR*TR-UI*UI
      YI=2.D0*TR*UI
      CALL MULDPC(DR,DI,UR+GR,UI+GI,AR(1),AI(1))
      CALL MULDPC(GR,GI,BR(1),BI(1),BR(1),BI(1))
      CALL MULDPC(YR,YI,BR(2),BI(2),YR,YI)
      CALL MULDPC(DR,DI,UR+TR,2.D0*UI,GR,GI)
      GR=GR-YR+BR(1)
      GI=GI-YI+BI(1)
      CALL MULDPC(TR,UI,BR(1),BI(1),BR(1),BI(1))
      CALL MULDPC(UR,UI,YR,YI,YR,YI)
      YR=AR(1)+BR(1)-YR
      YI=AI(1)+BI(1)-YI
      CALL MULDPC(DR,DI,YR,YI,YR,YI)
      YR=GR*GR-GI*GI-4.D0*YR
      YI=2.D0*(GR*GI-2.D0*YI)
      CALL SQTDPC(YR,YI,YR,YI)
      CALL MULDPC(DR,DI,TR,UI,BR(1),BI(1))
```

```
      GR=GP+YR
      GI=GI+YI
      IF(ABSDPC(GR,GI).GT.ABSDPC(GP,GI)) GO TO 30
      GR=GP-YR
      GI=GI-YI
      CALL DIVDPC(PR(1),PI(1),GR,GI,GR,GI)
      CALL MULDPC(GR,GI,HR,HI,HR,HI)
      AR(1)=AR(2)
      AI(1)=AI(2)
      BR(1)=BR(2)
      BI(1)=BI(2)
      AR(2)=ER
      AI(2)=EI
      BR(2)=HR
      BI(2)=HI
      ER=ER+2.D0*HR
      EI=EI+2.D0*HI
      I=1
      RETURN
      END
C-----------------------------------------------------------------------
      SUBROUTINE SQTDPC (AA,BB,C,D)
C SQTDPC takes squareroot of(AA+iBB) to get (C+iD)
      DOUBLE PRECISION C,D,AA,BB,ABSDPC,R,TH
      R=DSQRT(ABSDPC(AA,BB))
      IF(DABS(AA).LE.1.D-28)GO TO 10
      IF(DABS(BB).LE.1.D-28)GO TO 20
      TH=0.5D0*DATAN2(BB,AA)
      C=R*DCOS(TH)
      D=R*DSIN(TH)
      RETURN
10    C=R/1.41421356237309504D0
      D=C
      IF(BB.LT.0.D0) D=-C
      RETURN
20    IF(AA.LT.0.D0) GO TO 40
      C=R
      D=0.D0
      RETURN
40    C=0.D0
      D=R
      IF(BB.LT.0.D0) D=-R
      RETURN
      END
C-----------------------------------------------------------------------
      SUBROUTINE U0U1(CY,N1)
      DOUBLE PRECISION CY,U0(401,2),U1(401,2),A,B,C
      COMMON/A1/U0,U1
      COMMON/A3/N,ND,NM
      U1(1,1)=0
      IF(N1.EQ.1)GO TO 8
      L=N1-1
      DO 2 K=1,L
2     U0(K,1)=U0(N1,1)
8     DO 10 K=N1,N
      T=K+1
      C=U0(K,1)
      A=U0(1,1)-C
      B=U0(K+2,1)-C
      U0(K,2)=.125D0*(6.D0*A-B)+C
10    U1(1,2)=.375D0*(2.D0*A+B)+C
      L=N1+1
      DO 20 K=L,N
20    U0(K,2)=.500*(U0(K,2)+U1(K,2))
      U0(ND,2)=U1(ND,2)
```

```
      DO 30 K=I,M
      J=K+1
      I=K-1
      U1(K,1)=CY*(U0(J,1)-U0(I,1))
      U1(K,2)=CY*(U0(J,2)-U0(I,2))
      U1(ND,1)=CY*(U0(NN,1)-U0(N,1))
      U1(NN,1)=CY*(3.D0*U0(NN,1)-4.D0*U0(ND,1)+U0(N,1))
      U1(NN,2)=.125D0*(6.D0*U1(ND,1)+3.D0*U1(NN,1)-U1(N,1))
      IF(N1.EQ.1)GO TO 50
      I=N1-1
      DO 40 K=1,I
      U0(K,2)=U0(1,1)
      U1(K+1,1)=0
      U1(K,2)=0
      U1(N1,2)=CY*(U0(N1+1,2)-U0(1,1))
      RETURN
   50 U1(1,2)=CY*(U0(2,2)-U0(1,2))
      RETURN
      END
C-----------------------------------------------------------------------
      SUBROUTINE VV2U2(CY,DY2,M2)
      DOUBLE PRECISION DY2,U0(401,2),U1(401,2),U2(401),V(401),V2(401),RE
     1,RA(401),U2,U3,K1,KR,DUMR(1604),V1(401),DUMT(2807),DUM1(401),CY
      COMMON/A1/U0,U1
      COMMON/A3/M,ND,NN
      COMMON/A4/U2,U3,KR,KT,RE,RA
      COMMON/A5/DUMR,V,V1,V2,DUMT,U2,DUM1
      V(1)=0
      DO 9 K=2,ND
    9 V(K)=V(K)/RE
      DO 10 K=2,ND
      I=K+1
      I=K-1
      V2(K)=DY2*(V(J)-2.D0*V(K)+V(I))+CY*(V(J)-V(I))/RA(K)
      IF(DABS(V2(K)).LT.1.D-13) V2(K)=0
   10 CONTINUE
      V2(ND)=DY2*(2.D0*V(NN)-5.D0*V(ND)+4.D0*V(N)-V(N-1))+CY*(3.D0*V(NN)
     1-4.D0*V(ND)+V(N))
      IF(M2.GT.0)GO TO 20
      U2(1)=2.D0*(U0(2,1)-U0(1,1))
      I=2
      GO TO 30
   20 DO 25 K=1,M2
   25 U2(K)=0
      I=M2+1
   30 DO 44 K=I,ND
      J=K+1
   44 U2(K)=DY2*(U0(J,1)-2.D0*U0(K,1)+U0(I,1))
      I=K-1

      U2(NN)=DY2*(2.D0*U0(NN,1)-5.D0*U0(ND,1)+4.D0*U0(N,1)
     1-U0(N-1,1))
      RETURN
      END
C-----------------------------------------------------------------------
```